University of Calgary

PRISM Repository **https://prism.ucalgary.ca**

The Vault Open Theses and Dissertations

2016

Evaluation of Catalytic Steam Cracking Process for Total Acid Number Reduction of Heavy Oils

Moraes Righi, Thiago

Moraes Righi, T. (2016). Evaluation of Catalytic Steam Cracking Process for Total Acid Number Reduction of Heavy Oils (Master's thesis, University of Calgary, Calgary, Canada). Retrieved from https://prism.ucalgary.ca. doi:10.11575/PRISM/25982

http://hdl.handle.net/11023/3186

Downloaded from PRISM Repository, University of Calgary

UNIVERSITY OF CALGARY

Evaluation of Catalytic Steam Cracking Process for Total Acid Number Reduction of Heavy Oils

by

Thiago Moraes Righi

A THESIS

SUBMITTED TO THE FACULTY OF GRADUATE STUDIES

IN PARTIAL FULFILMENT OF THE REQUIREMENTS FOR THE

DEGREE OF MASTER OF SCIENCE

GRADUATE PROGRAM IN CHEMICAL AND PETROLEUM ENGINEERING

CALGARY, ALBERTA

AUGUST, 2016

© Thiago Moraes Righi 2016

Abstract

This study aims to evaluate the performance of different catalysts and conditions in the activity and deactivation patterns of catalytic steam cracking for total acid number reduction in northern Alberta bitumen. Several heavy oil properties relevant for their commercialization were also investigated. The conditions tested varied from 360-390ºC and 800-4,200kPa. The results showed a great activity towards total acid number reduction, further enhanced when using a hydrogenating function containing catalyst. A kinetic study was performed initially excluding the effects of deactivation. The study over extended hours of continuous operation revealed a progressive deactivation. In response to this behavior a guard reactor was implemented. This deactivation was modeled and a regeneration test was successfully performed. Poisoning by metal deposition was found to be negligible over time-on-stream thus deactivation was mainly due to coke deposition. A commercial reaction scheme was proposed and economically evaluated.

Acknowledgements

I would like to leave my sincere appreciation for working with Dr. Pedro Pereira. He always provided me with great guidance and very insightful approaches to my research and professional career. My whole experience working under his supervision shaped the professional I am now and I will carry it throughout my life.

I would also like to thank Dr. Josefina Scott for her support through this journey. Her teaching and guidance gave me the tools that allowed me to grow as a professional. I will always remember our long conversations about matters of research and life that made me learn much about science and about myself.

I would also like to thank Dr. Gerardo Vitale, Mr. Lante Carbognani, and Mrs. Josune Carbognani for all the support over those years. They were always very knowledgeable, available, supportive, and kind when I reached out to them. To the Catalyst for Bitumen Upgrading Group, I would like to thank you all for participating in diverse moments of my personal and professional development pursuing my degree.

Thanks to the Chemical and Petroleum Engineering Department and Cenovus Energy for providing the resources to carry out the project.

I dedicate my thesis to my mother, Maria Aparecida Araujo Moraes Righi; my father, Remo Righi; and my sister, Fernanda Moraes Righi. None of this would be possible without you and I am grateful for the loving and supporting environment I grew up in. And to Keith Knudsen, for being so supportive, encouraging, loving, and caring partner.

Table of Contents

Abstract ii
Acknowledgements iii
Table of Contents iv
List of Tables vii
List of Figures x
List of Symbols xiv
1 Introduction 1
1.1 Economic Overview and Challenges on Heavy Oil Production 1
1.2 Proposed Process 5
1.3 Objectives 6
2 Literature Review 7
2.1 Crude Oil Properties and Composition 7
2.1.1 Elemental Composition and Origin 7
2.1.2 Unconventional Oil 10
2.1.3 Asphaltenes, Resins and Coke 13
2.1.4 Naphthenic Acids 15
2.2 Corrosion in Crude Oil Operations 16
2.3 Traditional Methods for Treating High Acidic Oils 17
2.3.1 Physical Processes 17
2.3.2 Chemical Processes 19
2.4 Catalyst Deactivation 21
2.5 Heavy Oil Upgrading 24
2.5.1 Carbon Rejection Processes 25
2.5.2 Hydrogen Addition Processes 28
2.6 Catalytic Steam Cracking 31
2.7 Supported Catalysts 34
2.7.1 Hydrotalcite 34
2.7.2 MFI Catalyst 35
2.7.3 Molybdenum Carbide 37
3 Experimental Section 39
3.1 Experimental Set-Up 39

3.1.1 Pumping Section 39
3.1.2 Reaction Section 42
3.1.3 Separation and Sampling Section 43
3.2 Experimental Procedure 45
3.2.1 Reactor Filling 45
3.2.2 Catalyst Treatment and Reduction 46
3.2.3 Reaction Start-up 47
3.2.4 Reaction Operation 49
3.2.5 Reactor Cleaning and Catalyst Regeneration 49
3.3 Feedstock 51
3.4 Catalyst Preparation 53
3.5 Sample Analysis 55
3.5.1 Gas Chromatography 55
3.5.2 Total Acid Number (TAN) 56
3.5.3 Viscosity 57
3.5.4 High Temperature Simulated Distillation (SimDist) 57
3.5.5 Oil Density and API Gravity 58
3.5.6 Microcarbon Residue 58
3.5.7 Water Content 59
3.5.8 Bromine Number 59
3.5.9 Metal Content 60
4 TAN Reduction and Catalyst Selection 61
4.1 Thermal Run Results 62
4.1.1 Thermal Kinetics 63
4.1.2 Thermal Reaction Additional Results 69
4.2 Catalytic Condition Screening 74
4.2.1 Catalyst TR1 Temperature Screening 74
4.2.2 Catalyst TR1 Kinetics Modelling 77
4.2.3 Catalyst TR1 First Order Kinetics Assumption 79
4.2.4 Catalyst TR1 Additional Results 81
4.3 Catalyst Screening 87
4.3.1 Total Acid Number Results 88

4.3.2 Gas Composition and Yields 90
5 Deactivation Study on Total Acid Number Reduction for Catalyst TR3 96
5.1 Deactivation Kinetics Model 96
5.2 Base Condition and Duplicate Reactions 99
5.3 Water-to-Oil Ratio Screening 101
5.4 Temperature Screening 105
5.5 Pressure Screening 108
5.6 Metal Deposition Deactivation 111
5.7 Regeneration Study 112
5.8 Additional Results 116
5.8.1 Gas Analysis 116
5.8.2 Additional Oil Properties 118
5.9 Process Economics 121
5.9.1 Catalyst Life Reaction 121
5.9.2 Proposed Reaction Set-up Scheme 123
5.9.3 Total Fixed Capital Cost 124
5.9.4 Operating Costs 126
5.9.5 Gross Profit 126
5.9.6 Cash-Flow 127
6 Final Remarks and Future Work 135
Bibliography 139
Appendix I : Total Capital Investments 145
I.1 Reaction Unit 145
I.2 Heating Unit 150
I.3 Separation Unit 153
Appendix II : Operating Costs 156
Appendix III : Gross Profits 158
Appendix IV : Sensitivity Analysis 162

List of Tables

Table 2-1: Elemental composition ranges for crude oils. 7
Table 2-2: Oil classification in relation to API gravity according to World Petroleum Congress and UNITAR (Huc, 2011). 8
Table 2-3: Oil classification in relation to API gravity according to Canadian Center for Energy (Huc, 2011). 8
Table 2-4: Expected elemental composition of Alberta bitumen (Banerjee, 2012). 11
Table 2-5: Average typical property for Athabasca bitumen (Banerjee, 2012). 12
Table 2-6: Annual corrosion cost in US for different Oil & Gas sectors (Papavinasam, 2014). . 17
Table 3-1: Feedstock properties. 51
Table 3-2: Catalyst components and metal composition. 54
Table 3-3: Standard calibration gas composition. 55
Table 4-1: Products TAN and TAN conversion for thermal reaction (no catalyst) at varying temperature, and space velocity; and constant pressure (2,760kPa), and water-to-oil ratio (5%) 63
Table 4-2: Activation energy and pre-exponential factor for thermal reaction. 68
Table 4-3: Residue content and residue conversion for thermal reaction at different space velocities and temperatures. 69
Table 4-4: Viscosity in cP at 40°C and viscosity reduction for thermal reaction at different space velocities and temperatures. 71
Table 4-5: API gravity and API gravity absolute change for thermal reaction at different space velocities and temperatures. 72
Table 4-6: Products microcarbon and microcarbon increase for thermal reaction at different space velocities and temperatures. 73
Table 4-7: Catalytic and thermal average total acid number reduction for catalyst TR1 at different temperatures. 76
Table 4-8: Catalytic TAN reduction averages for different temperatures for catalyst TR1. 77
Table 4-9: Catalytic TAN reduction averages for different space velocities for catalyst TR1. 80
Table 4-10: Residue conversion for TR1 catalytic reaction at different space velocities and temperatures. 82
Table 4-11: Products viscosity in cP at 40°C and viscosity relative reduction for TR1 catalytic reaction at different space velocities and temperatures. 84
Table 4-12: Products API gravity and API gravity absolute change for TR1 catalytic reaction at different space velocities and temperatures. 85
Table 4-13: Microcarbon relative increase for TR1 catalytic reaction at different space velocities and temperatures. 86
Table 4-14: Products properties for all catalysts at 360°C and 1h^{-1}. 89
Table 4-15: Bromine number increase for different catalysts and thermal reaction. 92

Table 4-16: Henry's law constant for hydrogen and carbon dioxide and calculated concentration on water for 830kPa and 2,760kPa at 25ºC (National Institute of Standards and Technology, 2016a) (National Institute of Standards and Technology, 2016b). 93
Table 5-1: Initial reaction constant rate and deactivation constant for base case and duplicate. 99
Table 5-2: Gas and liquid fraction for reactions at 360ºC and 2,760kPa and different WOR. . 101
Table 5-3: Initial reaction constant rate and deactivation constant for catalyst TR3 with WOR varying from 2.5% to 7.5%. 104
Table 5-4: Initial reaction constant rate and deactivation constant for reaction temperatures of 360ºC and 380ºC. 106
Table 5-5: Pre-exponential factor and activation energy for thermal and catalysts TR1 and TR3. 107
Table 5-6: Gas and liquid fraction for reactions for reaction pressures of 2,760kPa and 4,140kPa. 110
Table 5-7: Initial reaction constant rate and deactivation constant for reaction pressures of 2,760kPa and 4,140kPa. 110
Table 5-8: Metal analysis for Alberta bitumen used on deactivation study. 111
Table 5-9: Demetallization levels after reaction for TR3 catalyst at different temperatures, pressures, and water-to-oil ratios. 111
Table 5-10: Initial reaction constant rate and deactivation constant for reaction at 360ºC, 2,760kPa, 5.0% water and its regenerated version. 114
Table 5-11: Bromine number for reactions using fresh (F) or regenerated (R) TR3 catalyst at different temperatures (360ºC, and 380ºC), water-to-oil ratios (2.5%, 5.0%, and 7.5%), and pressures (2,760kPa, and 4,140kPa). 118
Table 5-12: Products properties for reactions with fresh and regenerated catalyst TR3 at 360ºC and $1h^{-1}$ and its duplicate. 119
Table 5-13: Products properties for reactions with catalyst TR3 at different WOR and pressures. 119
Table 5-14: Averaged products properties for catalytic reactions at 360ºC and 380ºC and its respective thermal reaction values. 120
Table 5-15: Products properties differences at beginning and end of aging reaction for catalyst TR3. 122
Table 5-16: Equipment purchasing costs. 124
Table 5-17: Total fixed capital cost breakdown. 125
Table 5-18: Total operating costs breakdown. 126
Table 5-19: Acidity discount and diluent costs for feedstock and products. 126
Table 5-20: Historical average per year prices of WCS and WTI benchmarks in Canadian dollars (Baytex Energy, 2016). 129
Table I-1: Major assumptions on reactor design for total acid number reduction unit. 145
Table I-2: Enthalpy for molecules and model reactions. 146

Table I-3: Final reactor dimensions. 148
Table I-4: Energy requirements for heating water and oil to reaction set-points. 150
Table I-5: Summary of heat exchangers capacity, surface area, and cost calculation. 152
Table I-6: Final three phase separator dimensions. 155
Table II-1: Total operating costs breakdown. 157
Table III-1: Feedstock, products, diluent, diluted feedstock, and diluted products properties. . 159
Table III-2: Acidity discount and diluent costs for feedstock and products. 161

List of Figures

Figure 1-1: Global oil demand growth per year, for the years 2000-2020, in mb/d, left ordinate, and in percent change, right ordinate (modified from International Energy Agency, 2015b). 1
Figure 1-2: Canadian oil production outlook for 2013-2020 (International Energy Agency, 2015b). 2
Figure 1-3: Common products for Alberta bitumen after upgrading, dilution, or combination of both processes (Banerjee, 2012). 3
Figure 1-4: Proposed schematic representation of field facility for total acid number reduction. 5
Figure 2-1: Idealized average asphaltene structures (Ancheyta et al., 2009)..... 13
Figure 2-2: Naphthenic acids predominant in California crude oil (modified from Speight, 2014a). 15
Figure 2-3: Mechanism for heavy oil hydroprocessing catalyst deactivation (Ancheyta et al., 2009). 21
Figure 2-4: Reaction temperature and catalyst life for hydroprocessing different feedstocks (Ancheyta, 2013)..... 22
Figure 2-5: Cut distribution comparison between extra-heavy oil, synthetic oil, light oil and demand representation (modified from Huc, 2011). 24
Figure 2-6: Schematic diagram of the ROSE process using residuum as feedstock (McHugh et al., 1994). 26
Figure 2-7: Simplified diagram for delayed coking process (Lieberman, 1991). 26
Figure 2-8: Exxon Research and Engineering flexicoking simplified diagram (modified from J. McKetta, 1990). 27
Figure 2-9: Simplified hydrodesulfurization process diagram (Leach, 1983). 29
*Figure 2-10: Example of tar sand bitumen processing sequence (modified from Speight, 2013).*30
Figure 2-11: Mechanism for catalytic steam dealkylation of toluene (Duprez, 1992). 32
Figure 2-12: Schematic representation of hydrotalcite structure (Cantrell et al., 2005). 34
Figure 3-1: P&ID for experimental set-up I. 40
Figure 3-2: P&ID for experimental set-up II. 41
Figure 3-3: Schematic representation of fixed-bed reactor used on experimental set-ups. 43
Figure 3-4: Schematic representation of pre-treatment conditions. 46
Figure 3-5: Schematic diagram of system start-up operation. 48
Figure 3-6: Temperature profile during regeneration for an internal temperature indicator. 50
Figure 3-7: Simulated distillation for the feedstocks used throughout the project. 52
Figure 4-1: Products total acid number conversion (X_{TAN}) for thermal reaction at different temperatures and space velocities. 63
Figure 4-2: First order reaction assumption evaluation through plot of $-\ln(1-X_{TAN})$ versus residence time for temperatures of: ● 360ºC, ▲ 370ºC, and ■ 380ºC. 66
Figure 4-3: Logarithm of kinetic constant versus inverse of temperature for thermal reaction at space velocity of: ● $0.26h^{-1}$, ▲ $0.54h^{-1}$, and ■ for average values. 67

Figure 4-4: Product distribution for feed and products after thermal reaction at different space velocities and temperatures. 69
Figure 4-5: Residue conversion as a function of temperature for thermal reaction at space velocities: ● 0.26h^{-1}, ▲ 0.54h^{-1}, and ■ 1.02h^{-1}. 70
Figure 4-6: Residue conversion in function of space velocity for thermal reaction at temperatures: ● 360°C, ▲ 370°C , and ■ 380°C. 71
Figure 4-7: Temperature screening schematic representation for catalyst TR1 at constant space velocity. 74
Figure 4-8: Temperature (continuous line), thermal (discontinuous line), catalytic TAN, and TAN conversion over time using catalyst TR1 at constant space velocity (1h^{-1}) and temperatures: ● 360°C, ▲ 370°C , ■ 380°C, and ♦ 390°C. 75
Figure 4-9: Schematic representation of catalytic and thermal conversions for catalyst TR1 at constant space velocity (1h^{-1}) and different temperatures. 75
Figure 4-10: Thermal and catalytic total acid number conversion over time for 360°C using catalyst TR1. 76
Figure 4-11: Logarithm of kinetic rate constant versus inverse of temperature for activation energy and pre-exponential factor calculations for catalyst TR1. 78
Figure 4-12: First-order reaction assumption evaluation through plot of –ln(1-X_{TAN}) versus residence time for catalyst TR1. 79
Figure 4-13: Cut distribution for TR1 catalytic reaction at different temperatures. 81
Figure 4-14: Cut distribution for feed and products after TR1 catalytic reaction for different space velocities. 81
Figure 4-15: Products viscosity for TR1 catalytic reaction at different temperatures. 83
Figure 4-16: Logarithm of products-to-feedstock viscosity ratio for TR1 catalytic reaction at different temperatures. 83
Figure 4-17: Logarithm of products viscosity for TR1 catalytic reaction at residue conversions. 84
Figure 4-18: Total acid number over time for catalysts TR1, TR2, TR3, TR4, TR5, and thermal conversion for 360°C and 1.0h^{-1}. 88
Figure 4-19: Gas yield for different gas components for all catalysts tested at 360°C and 1h^{-1}. 90
Figure 4-20: Gas yield for catalyst TR1 tested at different temperatures. 94
Figure 5-1: Logarithm of kinetic rate constant as function of total acid number conversion for residence time equals to 1 hour. 98
Figure 5-2: Total acid number conversion for reaction with catalyst TR3 at 360°C, 2,760kPa, 5% WOR and space velocity 1h^{-1} (base condition reaction); and its duplicate. 99
Figure 5-3: Logarithm of rate constant over time for reaction with catalyst TR3 at 360°C and 1h^{-1} (base condition -▲) and its duplicate (♦). 100
Figure 5-4: Cut distribution and residue conversion for base condition using catalyst TR3. ... 100
Figure 5-5: Total acid number conversion for catalyst TR3 at 360°C, 2,760kPa, space velocity 1h^{-1}, and varying water-to-oil ratios. 103

Figure 5-6: Logarithm of kinetic rate constant over time for catalyst TR3 with WOR of 2.5% (♦), 5.0%(▲), and 7.5% (■). 104
Figure 5-7: Total acid number conversion for catalyst TR3 at 2760kPa, 5% WOR, space velocity $1h^{-1}$ and temperatures of 360°C and 380°C. 105
Figure 5-8: Logarithm of kinetic rate constant over time for reaction temperatures of 360°C (▲) and 380°C (●). 106
Figure 5-9: Temperature effects in coke deposition for hydroprocessing catalyst (Furimsky, 1999). 107
Figure 5-10: Total acid number conversion for catalyst TR3 at 360°C, space velocity of $1h^{-1}$, 5% WOR and pressures at 2,760kPa and 4,140kPa. 108
Figure 5-11: Logarithm of kinetic rate constant over time for catalyst TR3 at 2,760kPa (▲) and 4,140kPa (♦). 109
Figure 5-12: Total acid number conversion over time with fresh and regenerated TR3 catalyst at 360°C, space velocity $1h^{-1}$, 2,760kPa, and 5% WOR. 113
Figure 5-13: Logarithm of kinetic rate constant over time with fresh (▲) and regenerated (♦) catalyst TR3. 114
Figure 5-14: Gas yield for different gas products after1 day for fresh (F), regenerated (R), or duplicate (D) TR3 catalyst reaction at different temperatures (360°C, and 380°C), water-to-oil ratios (2.5%, 5.0%, and 7.5%), and pressures (2,760kPa, and 4,140kPa). 116
Figure 5-15: Total acid number reduction and temperature profile for catalyst TR3 during temperature compensating aging test at space velocity $1h^{-1}$, pressure of 2,760kPa, and 5% WOR. 121
Figure 5-16: Block diagram for A) Proposed reaction, separation and dilution facilities; and B) Current units in heavy-oil production facilities. 124
Figure 5-17: Cash-flow diagram in present value units for total acid number reduction industrial facility over a period of 30 years of operation 127
Figure 5-18: Sensitivity analysis on Western Canadian Select and Edmonton Condensate prices with both WCS and EC varying at the same rate. 128
Figure 5-19: Sensitivity analysis for variations in products viscosity. 130
Figure 5-20: Sensitivity analysis for variations in products total acid number. 131
Figure 5-21: Sensitivity analysis for variations in total investment. 131
Figure 5-22: Tornado chart for internal rate of return for a 30 years investment. 132
Figure 5-23: Tornado chart for payback time. 133
Figure 5-24: Tornado chart for net present value after 30 years of operation. 133
Figure I-1: Heating unit schematic representation composed of two integrated heat exchanger and a furnace. 151
Figure IV-1: Sensitivity analysis on Western Canadian Select and Edmonton Condensate prices with both WCS and EC varying at the same rate. 162
Figure IV-2: Sensitivity analysis for variations in price differential between Edmonton Condensate and Western Canadian Select. 163

Figure IV-3: Sensitivity analysis for variations in products viscosity. 163
Figure IV-4: Sensitivity analysis for variations in products total acid number. 164
Figure IV-5: Sensitivity analysis for variations in catalyst cost. 164
Figure IV-6: Sensitivity analysis for variations in total catalyst life. 165
Figure IV-7: Sensitivity analysis for variations in yearly operating costs. 165
Figure IV-8: Sensitivity analysis for variations in total investment. 166
Figure IV-9: Sensitivity analysis for variations in working capital. 166

List of Symbols

Symbol	Description	Unit
A	Anion, area	n/a, m^2
AGO	Atmospheric gas oil	n/a
AHM	Ammonium heptamolybdate tetra-hydrate	n/a
API	American Petroleum Institute	n/a
AR	Atmospheric residue	n/a
ASTM	American Society for Testing and Materials	n/a
BBV	Bang-bang valve	n/a
BPV	Backpressure valve	n/a
Br	Bromine number	g_{Br2}/100g
C	Carbon monolayer, concentration, cost	g, mol/mL, US$ or CAD$
C_C	Corrosion allowance	M
CCR	Conradson carbon residue	n/a
CEPCI	Chemical Engineering Plant Cost Index	n/a
CRW	Albertan condensate blend	n/a
CSC	Catalytic steam cracking	n/a
D	Diameter	m
d	Days	n/a
DAO	Deasphalted oil	n/a
E_A	Activation energy	kJ/mol
E_j	Joint efficiency	n/a
EC	Edmonton Condensate	n/a
ESMAP	Energy Sector Management Assistance Program	n/a
F	Molar flow, correction factor	mol/h, n/a
f	Factor	n/a
FID	Flame ionization detector	n/a
FCC	Fluid catalytic cracking	n/a
GC	Gas chromatograph	n/a
H	Heat exchanger, enthalpy	n/a, kJ/mol
H/C	Hydrogen to carbon ratio	n/a
HID	Helium ionization detector	n/a
IBP	Initial boiling point	^oC
ISBL	Inside battery limits	$
K	Potassium, adsorption constant, separator constant	n/a, n/a, m/s
k	Kinetic constant	h^{-1}
k_0	Pre-exponential factor	h^{-1}
k_d	Deactivation constant	day^{-1}
k_i	Pre-exponential factor at time zero	h^{-1}

Symbol	Description	Unit
L	Length	M
M, Me	Metal	n/a
MB	Mass balance	n/a
MC	Microcarbon	%wt
MFC	Mass flow controller	n/a
MFI	Mass flow indicator, Modernite Framework Inverted	n/a
MW	Molecular weight	g/mol
n	Integer number, equation coefficient	n/a, n/a
OECD	Organization for Economic Cooperation and Development	n/a
OS	Offsites	$
OSBL	Outside battery limits	$
P	Pump, pressure	n/a, kPa
Q	Volumetric flowrate, heat exchanged	m^3/s, W
R	Hydrocarbon chain, reactor, ideal gas constant, heat exchanger constant, residue content, revenue	n/a, n/a, J/mol.K, n/a, n/a, US$
r	Rate of reaction	$mg_{KOH}/g.h$
R^2	Regression coefficient	n/a
ROSE	Residual Oil Supercritical Extraction	n/a
S	Separator, maximum allowable stress, size, heat exchanger constant	n/a, kPa, kg, multiple units
SAGD	Steam assisted gravity drainage	n/a
SDA	Solvent deasphalting	n/a
SimDist	Simulated Distillation	n/a
SG	Specific gravity	n/a
SV	Space velocity	h^{-1}
T	Temperature	^oC or K
t	Time, thickness	min, m
TAN	Total acid number	mg_{KOH}/g
TCD	Thermal conductivity detector	n/a
TI	Temperature indicator	n/a
TIC	Temperature indicator and controller	n/a
TK	Tank	n/a
TPR	Temperature programmed reduction	n/a
TR1	Silicate I zeotype catalyst	n/a
TR2	Silicate I zeotype and hydrotalcite calcined catalyst	n/a
TR3	Hydrotalcite calcined and molybdenum carbide catalyst	n/a
TR4	Cation-exchanged silicate I zeotype catalyst	n/a

Symbol	Description	Unit
TR5	Silicate I zeotype and hydrotalcite calcined catalyst	n/a
U	Overall heat transfer coefficient	$W/m^2.^oC$
UNITAR	United Nations Institute for Training and Research	n/a
UNDP	United Nations Development Programme	n/a
US	United States of America	n/a
V	Valve, volume	n/a, n/a, m^3
$\dot{V}$	Volumetric flowrate	mL/h, mL/min
Visc	Viscosity	cP
W	Mass or catalyst weight	g, kg
w	Cumulative feed-to-catalyst ratio, weight proportion	n/a
$\dot{w}_0$	Weight flow	g/h
WCS	Western Canadian Select	n/a
WHSV	Weight hourly space velocity	h^{-1}
WOR	Water-oil ratio	n/a
WTI	West Texas Intermediate	n/a
X	Conversion	n/a
x	Molar concentration	n/a
XRD	X-ray diffraction	n/a
ZSM-5	Zeolite Socony Mobil-5	n/a

Greek Letters

α	Empirical coking factor	h^{-1}
Δ	Variation	n/a
δ	Viscosity index	n/a
μ	Viscosity	cP
ρ	Density	g/mL, kg/m^3

Subscripts

b	Blank	n/a
BB	Bang-Bang automated valve related	n/a
c	Consumed	
cat	Catalyst	n/a
CS	Carbon steel	n/a
d	Deactivation, delivery, diluent	n/a
e	Equipment, equipment erection	n/a
es	Electrical systems	n/a
f	Feedstock, furnace, final	n/a
g	Gas	n/a
H	Hold-up	n/a

Symbol	Description	Unit
he	Heat exchanger	n/a
hl	Heavy liquid	n/a
i	Initial	n/a
i	Internal, instrumentation and control	n/a
KOH	Potassium hydroxide	n/a
o	Oil, bitumen	n/a
l	liquids	n/a
ll	Light liquid	n/a
m	Material	n/a
max	Maximum	n/a
ml	Mean logarithm	n/a
p	Products, piping, produced	n/a
r	Regeneration, reactor	n/a
req	Required	n/a
res	Residence	n/a
S	Surge	n/a
s	Service facilities, sample, separator	n/a
sb	Structure and buildings	n/a
sep	Separator	n/a
SS	Stainless steel	n/a
Std. cond.	Standard condition	n/a
T	Temperature, terminal	n/a
TAN	Total acid number	n/a
v	Vapor	n/a
w	Water, steam	n/a
y	Yard improvements	n/a

1 Introduction

1.1 Economic Overview and Challenges on Heavy Oil Production

Crude oil is nowadays one of the main sources of primary energy in the world accounting for almost 40% of all energy produced (International Energy Agency, 2015a). The demand is forecasted to grow in the foreseeable future at a rate around 1.2% year-over-year for the next five years as seen in Figure 1-1 that also shows oil demand growth in the past few years. Although somewhat robust, foreseeable oil demand growth is considered to be weak due to an expected weak global economic growth, increase in fuel efficiencies, and fuel switching out of oil (International Energy Agency, 2015b). However, the unbalanced supply-demand dropped oil prices since late 2014 and low prices could potentially accelerate demand towards oil in the medium term.

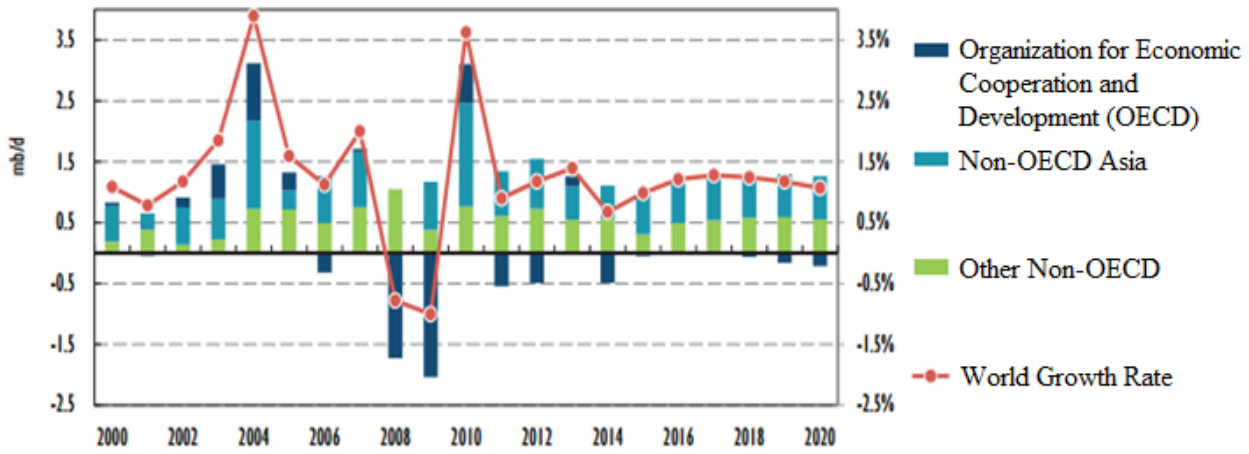

Figure 1-1: Global oil demand growth per year, for the years 2000-2020, in mb/d, left ordinate, and in percent change, right ordinate (modified from International Energy Agency, 2015b).

Canadian oil output is expected to grow steadily over the next five years to just under five million barrel per day, up 810 thousands of barrels per day from 2014 levels as shown in Figure 1-2. It is expected that bitumen and synthetic crude will lead Canadian output growth and the relative proportion of bitumen in Canada's output is expected to reach 60% by 2020. (International Energy Agency, 2015b). Canadian oil production was around 4.3 million barrels per day at the end of 2014, which corresponded to 5.0% of global production, being the 4th largest producer behind United States, Saudi Arabia, and Russia (British Petroleum Global, 2015).

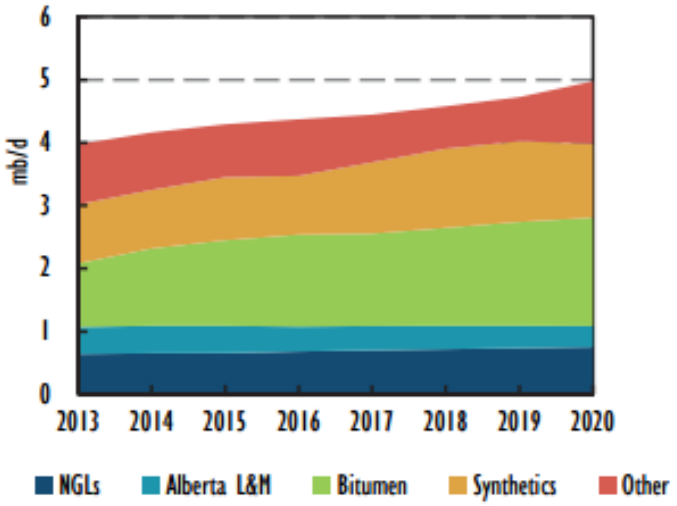

Figure 1-2: Canadian oil production outlook for 2013-2020 (International Energy Agency, 2015b).

In the beginning of oil exploration history, due to low-cost and high-production, conventional oil was primarily explored but high oil demand pushed prices to levels that allowed unconventional oil exploration to be feasible. Heavy oil production has been further enhanced by developments in secondary recovery and enhanced recovery techniques over the past decades. This production comes to take advantage of the large heavy oil and bitumen reservoirs available around the world. By 2013, the global estimated technically recoverable heavy oil and bitumen reserves added up to close to 1.1 trillion barrels which is nearly equal to current remaining conventional oil reserves (Speight, 2013b). Furthermore, it is estimated that oilsands contain around 66% of world total oil reserves, of which ¾ are located in Canada and Venezuela (Papavinasam, 2014).

Alberta unconventional oil is typically explored through mining or steam assisted gravity drainage (SAGD). Because the bitumen produced has high viscosity, around 20,000cSt at 38ºC, and low API gravity, usually 8 to 12, this bitumen needs to be upgraded or diluted to achieve transportable properties through pipelines. The dilution is usually made with naphtha or, most commonly, with natural gas derived condensate that has a higher market price than conventional crude. Dilution costs depend on market price fluctuations and increasing production of unconventional oils in local markets tend to increase diluent costs in the long term due to local high demand. Besides, compatibility between diluent and unconventional oil can be an issue, and therefore, an upgrading alternative is a more stable solution. Upgrading usually takes place in either the wellhead or at an

upgrading facility near production wells and it is an energy-intensive, and expensive process that has its profitability dependent on the heavy oil to conventional oil price differential. Commonly used upgrading processes are thermal cracking, solvent deasphalting, hydrotreating, and hydrocracking (Banerjee, 2012). The use of upgrading, dilution, or a combination of both gives rise to different products that meet transportability criteria, as shown in Figure 1-3.

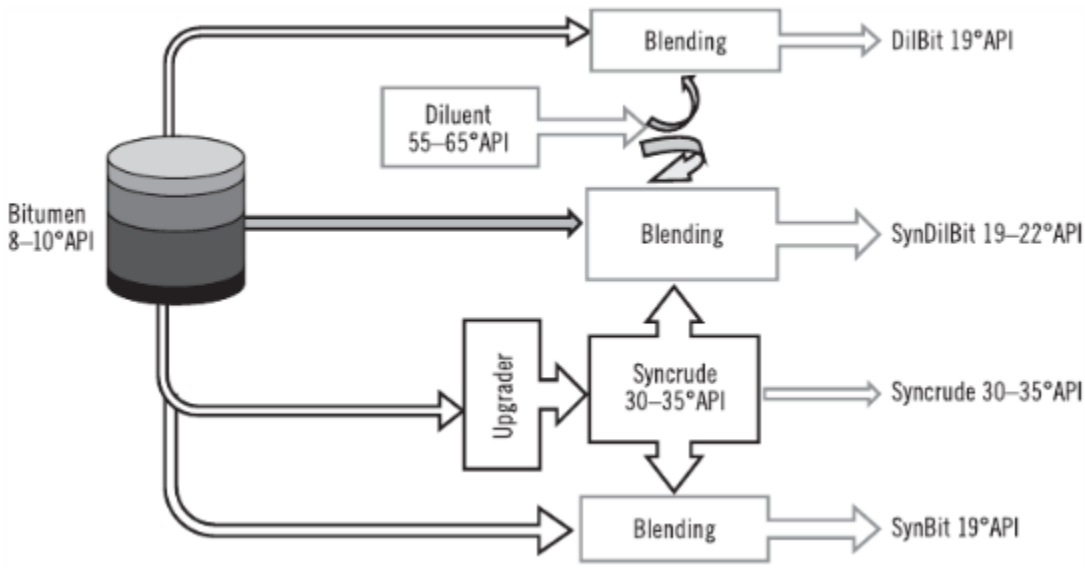

Figure 1-3: Common products for Alberta bitumen after upgrading, dilution, or combination of both processes (Banerjee, 2012).

Acidity is another common issue when dealing with unconventional oil. For Athabascan oil, typical values for total acid number (TAN, a commonly used measurement of acidity) is around 2.5 mg_{KOH}/g (Banerjee, 2012). Oils are only considered non-acidic when their values are below 0.5 (Bacon et al., 2005). Acidity in sour bitumen is generally related to naphthenic acids which are heavy molecules, usually with naphthenic rings and alkyl chains, with one or more carboxylic acids in the structure. Those molecules are responsible for corrosion in major refinery and upgrader equipment, such as distillation units, desalters, and heat exchangers (Speight, 2014b).

To put the size of the corrosion business in perspective, the yearly total cost of corrosion in US oil and gas industry is estimated to be over 25 billion dollars. In refineries only, the yearly cost is estimated to be 1.8B$ in maintenance, 1.4B$ in vessel turnaround, and 0.5M$ in cleaning. For the pipeline sector, the cost of corrosion is around 5.4B$ per year and it is estimated to be responsible

for 24.3% of all pipeline accidents and incidents in the US (Papavinasam, 2014). Corrosion can have sources other than high acidity such as solid particle erosion, and corrosion due to steam, hydrogen, and carbon dioxide (Speight, 2014b).

A few alternatives are commonly taken to manage corrosion issues due to high acidic oils at the industrial level. The most common solution is blending sour with sweet oil. Nevertheless, this is a non-destructive method that could still keep high concentrations of naphthenic acid on certain fractions of the crude. Blend solubility and sweet oil availability can also become issues for blending purpose. Caustic wash, metallurgy upgrading, corrosion inhibitors, and liquid extraction are other methods, which have been used or developed in the past. All those techniques have issues regarding either cost, such as in metallurgy upgrading and corrosion inhibitors, or formation of stable emulsions that are complicated to separate, as in the other two examples (Speight, 2014b). Since acid oil promotes corrosion, fewer refineries and upgraders are able or willing to process it, which lowers its price in the market (Bacon et al., 2005). Thus, a more definitive and cost-efficient solution to oil acidity is necessary for improving oil quality and market price.

1.2 Proposed Process

The process developed in this project has as its main goal to reduce the total acid number of bitumen and diluted bitumen to non-acidic levels, i.e. below 0.5mg_{KOH}/g. Along with it, it is also expected a parallel minor partial upgrading effect by reduction of viscosity, and an increase of API gravity that will tend to reduce the amount of diluent necessary to achieve transportability criteria.

The proposed process consists of an up flow catalytic bed reactor that performs steam cracking at mild conditions. The reactions that take place eliminate naphthenic acids and, thus, it does not leave any fraction of oil with high acidity as in oil blending alternative. The simplicity in the design is key to the process in order to reduce complexities that add much to investment and operational costs. The process was designed to be simple and operated by a minimum number of operators in order to be implemented in an oil producing facility and to be competitive with respect to other total acid number reduction alternatives. Besides bitumen, the only other reactant used in the process during reaction is water, in the form of steam, which is usually already available in SAGD processes and produced as a by-product in oil exploration activities. A simplified schematic design of the proposed field process is shown in Figure 1-4 and it comprehends a natural gas fired furnace, which represents the heating unit; a reaction unit; and a three-phase separator. Since the dilution step is already necessary in an oil producing facility, it is not considered in the scope of this project.

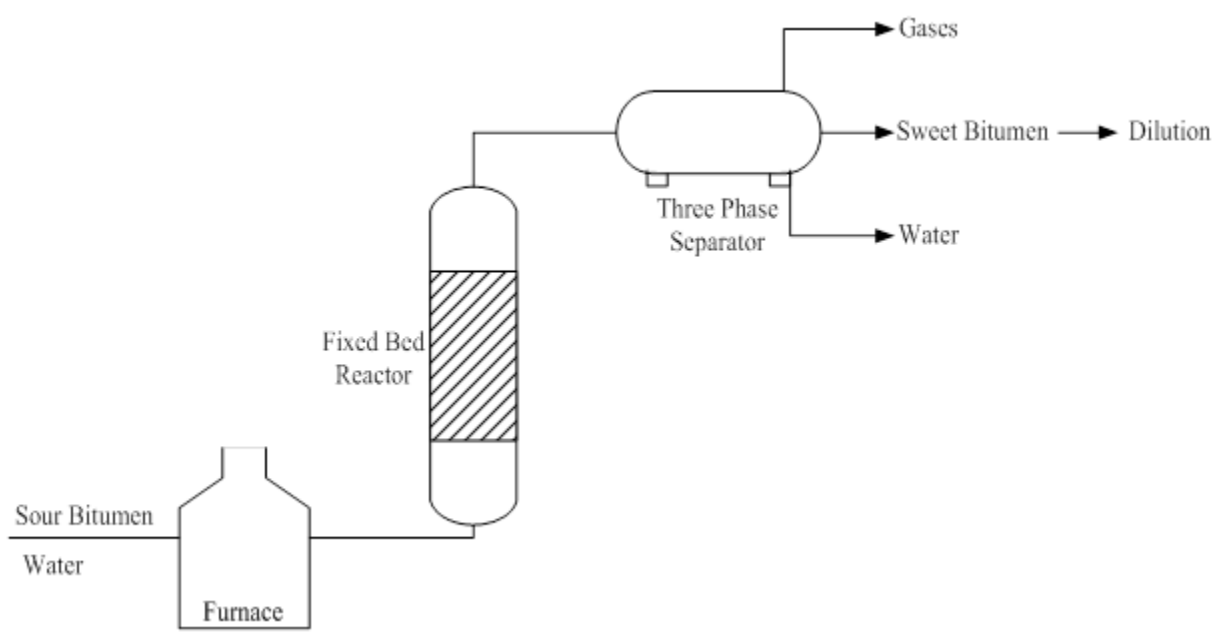

Figure 1-4: Proposed schematic representation of field facility for total acid number reduction.

1.3 Objectives

This thesis is part of a main project in which the objective is to develop a low-cost and easy to operate process for total acid number reduction and partial bitumen upgrading to overcome challenges in the heavy oil producing and refining industry. The research focuses on the studies of different catalysts and conditions, in terms of activity and deactivation rates, on mild severity bitumen catalytic steam cracking processes. Then, identifying catalysts and conditions that improve process reliability, catalyst life, and process economics is the main goal of this project. To achieve such an objective, the scope of this thesis was defined as:

i. Design, build, and commission bench-scale reliable experimental set-ups;
ii. Test and evaluate process performance at different thermal reaction conditions to be used as catalytic process benchmark;
iii. Test and evaluate performance of multiple catalysts at different conditions;
iv. Characterize product and feedstock samples towards total acid number, and other significant properties related to bitumen partial upgrading;
v. Model and calculate activation energies and pre-exponential factors on Arrhenius kinetics equation for both catalytic and thermal reactions;
vi. Identify and choose catalyst and conditions that maximize total acid number reduction with minimum oil degradation to proceed with deactivation tests;
vii. Model and calculate relevant constants related to deactivation kinetics for catalytic reaction at different conditions;
viii. Evaluate catalyst regenerability;
ix. Propose industrial reaction unit based on experimental results, and develop economic evaluation of industrial scale process.

The material related to the objectives listed are organized in six chapters in this thesis. Chapter 1 is the introduction while chapter 2 contains a literature review of the contents related to this field of research. Chapter 3 has a comprehensive explanation of the experimental methodology used throughout the project. Chapter 4 focus on the results related to objectives iii to vi described above. Chapter 5 presents the results related to objectives vii to ix. Finally, chapter 6 contains the conclusions and recommendations of this thesis.

2 Literature Review

2.1 Crude Oil Properties and Composition

Crude oil is one of the major sources of energy nowadays and its production is expected to grow in the foreseeable future (International Energy Agency, 2015b). Strong demand in the past allowed a feasible exploration of both conventional and unconventional oil throughout the world (Speight, 2013b). Both types of crude oils differ in chemical composition, physical properties, and origin. The following sub-sections review and summarize the important differences between different crude oils. Components present in unconventional oils are the focus of this section since it is the feedstock used throughout this project.

2.1.1 Elemental Composition and Origin

Crude oil is generally defined by ASTM International as a liquid hydrocarbon mixture that may also contain sulfur, nitrogen, oxygen, metals and other elements in lower levels (ASTM International, 1995). Speight (1999) defined crude oil as a mixture of gaseous, liquid, and solid hydrocarbon compounds that occur in sedimentary rock reservoirs around the world and comprises small quantities of nitrogen-, oxygen-, and sulfur-containing compounds, and traces of metallic components. Petroleum is one of the most consumed raw materials in modern society and is mainly used as a source of energy and raw material for plastics (Hilyard, 2012). Its physical and chemical characteristics greatly depend on its origin, age and well depth. In terms of elemental composition, different crude oils vary in the ranges highlighted on Table 2-1 (Speight, 1999).

Table 2-1: Elemental composition ranges for crude oils.

Element	Composition Range (wt%)	Composition Range (mol%)
Carbon	83.0-87.0	35.0-38.0
Hydrogen	10.0-14.0	51.0-73.0
Nitrogen	0.1-2.0	0.05-0.80
Oxygen	0.05-1.5	0.02-0.50
Sulfur	0.05-6.0	0.01-0.97
Metals (Ni and V)	<1,000ppm	<100ppm

The formation of oil typically starts in a sedimentary basin in which organic rich sediments from neighboring areas are transported and accumulated over time. Usually, heating and pressure is

induced by burial by overburden rock and, over millions of years, organic matter is converted to oil and gas compounds. The conditions at which the oil is produced determine its maturity and quality. For example, heavy oils are produced at lower temperatures and are commonly considered immature. The hydrocarbons may migrate from the source rock through cracks, faults, fissures, to porous and permeable reservoir rock. To allow commercial exploitation, the reservoir rock must be able to trap and accumulate oil and gas through its geological formation (Hilyard, 2012). This trapping is achieved when reservoir rock is covered by low permeability strata, also known as seal rocks (Hsu et al., 2006). The occurrence of heavy and extra-heavy oils is related to bacterial activity in reservoir that changes the conventional crude oil characteristics. Those alterations are active when temperature in reservoir allows microbial conglomerates to take place (Huc, 2011).

Depending on its physical properties, such as viscosity and density, crude oils can have different classifications. The World Petroleum Congress (1980) and UNITAR (1982), a United Nations autonomous body, defined different oils following Table 2-2. Similarly, the Canadian Center for Energy further separates the extra-heavy oils from bitumen as shown in Table 2-3 (Huc, 2011).

Table 2-2: Oil classification in relation to API gravity according to World Petroleum Congress and UNITAR (Huc, 2011).

Oil Classification	**API gravity**
Conventional Oil	>20°
Heavy Oil	10°-20°
Extra-Heavy Oil and Bitumens	<10°

Table 2-3: Oil classification in relation to API gravity according to Canadian Center for Energy (Huc, 2011).

Oil Classification	**API gravity**	**Viscosity (cP)**
Light Oil	>22.3^{o}	
Heavy Oil	10°-22.3^{o}	
Extra-Heavy Oil	<10°	<10,000
Bitumen	<10°	>10,000

The hydrocarbon molecules in crude oil can be classified into the following categories: paraffins, naphthenes, and aromatics. Paraffins, or alkanes, are saturated carbon chains with the general

formula C_nH_{2n+2}. Carbon chains can be either straight or branched and, thus, a single chemical formula can have different structures that are called isomers. Isomers have different properties, such as melting point, boiling point and octane number (Hsu et al., 2006). Naphthenes are saturated molecules with at least one ring in its structure and, possibly, one or more paraffinic side chains. Finally, aromatics are molecules that contain at least one unsaturated 5 to 6-carbon rings. Those molecules usually form an aromatic nuclei that can be connected to either, or both, paraffinic side chains and naphthenic rings (Hsu et al., 2006).

Crude Oil is a commodity that is commonly sold in the market based on benchmarks that depend on the quality and the region in which the oil is produced. For instance, two of the major global benchmarks are the West Texas Intermediate (WTI), which is a light and non acidic crude oil produced in the United States and sold at the trading hub of Cushing, Oklahoma; and Brent that is related to crude oil produced in the North Sea (Energy Information Administration, 2014). The most commonly used benchmark in west Canada is the Western Canadian Select (WCS), which represents a poor quality and heavy crude oil. Because of its chemical and physical properties, that make WCS hard to process, and because of shipping distance to refineries, WCS is usually traded about $15 to $20 per barrel lower than the American benchmark WTI (Energy Information Administration, 2016).

2.1.2 Unconventional Oil

Most unconventional crude oils have their origin on regular and fluid crude oils that went through one or a combination of some of the following processes: biodegradation, water washing, loss of volatiles, and inorganic oxidation. Those processes tend to decrease the quantities of light molecules and increase quantities of poly-aromatics, resins, asphaltenes, and other heavy molecules, producing a heavy and viscous oil (Tissot et al., 1984).

Some unconventional oils, mobile at reservoir condition, can be produced through conventional methods at low rates and poor recovery. Nevertheless, most heavy oils are immobile at reservoir conditions and need ex-situ mining or in-situ enhanced recovery technologies. A common enhanced recovery technology is steam injection into the reservoirs that heats the heavy oil and decreases its viscosity. In-situ combustion has also been used and consists of injecting air and promoting combustion reaction inside reservoir that promotes cracking and pyrolysis reactions. The products of this process are a lighter oil and coke-type residues (Tissot et al., 1984).

In general, high quality crude oils receive a premium on their price since, when processed, they will yield better quality products that have a higher price in the market. The hard processability of unconventional oils requires a deep-conversion type of refinery that restrains the market for the product and, therefore, decreases its price. Also, as discussed before as one of the reasons for the low price for WCS, the location of production also plays a role in receiving premiums since closer locations avoid high costs with transportation to refineries (Bacon et al., 2005).

Both conventional and unconventional oils are composed of the same types of molecules, i.e. hydrocarbons, resins, and asphaltenes. However, the proportions of those molecules are different and unconventional oil tends to contain less hydrocarbons, mainly alkanes, and more heavy and complex molecules such as sulfur aromatic compounds, resins, and asphaltenes. For instance, asphaltenes and resins together, on average, represent around 54% of heavy oils composition while its proportion in conventional oil is only around 14% (Tissot et al., 1984).

On average, Alberta bitumen is comprised of half un-distillable residue, i.e. molecules with boiling point above 535°C, and half distillable liquids, i.e. with boiling point below 535°C. This bitumen also consists of 20% asphaltenes that is a constituent of the residue fraction. From the low boiling point fraction of the bitumen, one third of it is distillable in an atmospheric distillation unit at

temperatures below 350ºC. This cut is called atmospheric gas oil (AGO). The other two thirds are distillable in a vacuum distillation unit only at temperatures ranging from 350-535ºC and it is called vacuum gas oil (Banerjee, 2012). The elemental composition of bitumen can be seen in Table 2-4, which is mostly within the ranges proposed by Speight (1999) and shown in Table 2-1. The small variations are probably related to the fact that Alberta bitumen is in the low quality end of crude oils.

Table 2-4: Expected elemental composition of Alberta bitumen (Banerjee, 2012).

Element	**Composition Range (wt%)**
Carbon	82.0-83.0
Hydrogen	10.1-10.2
Nitrogen	0.3-0.5
Oxygen	<1.0
Sulfur	4.5-6.0
Vanadium	180-250ppm
Nickel	60-90ppm

Atomic hydrogen to carbon ratio (H/C) is commonly used as an indicator for crude oil quality. The higher this ratio is, the better is the crude quality. For instance, conventional oils commonly have ratios around 1.7-1.8 while asphaltenes usually range between 1.2-1.3. Commonly, bitumen has a low H/C ratio, usually within the 1.4-1.5 range (Banerjee, 2012). The hydrogen deficiency in unconventional oils comes from the large amounts of resins and asphaltenes in its composition (Tissot et al., 1984).

Another indicator of poor quality for bitumen is the high sulfur and nitrogen amounts, the former being a reason for concern in hydrotreating processes, and the latter impacting catalyst activity and environmental emissions. Metals present on bitumen molecules are also poisonous towards the catalyst affecting the activity in processes such as hydroprocessing (Banerjee, 2012). Sulfur, metal, and nitrogen containing compounds are usually related to the amounts of resins and asphaltenes in the oil, which makes unconventional oil prone to have higher amounts of those molecules. Nevertheless, the characteristics of the original crude oil, i.e. before any degradation, also plays a

major role on those molecule content (Tissot et al., 1984). The quantities of metals in Athabasca bitumen and other relevant physical and chemical properties are shown in Table 2-5.

Table 2-5: Average typical property for Athabasca bitumen (Banerjee, 2012).

Property	**Average Value**
API	8.0^{o}API
Sulfur	5.0 wt%
Nitrogen	4,000 ppm
Total Acid Number (TAN)	2.5 mg_{KOH}/g
Ni/V	80 / 220 ppm
Conradson Carbon Residue (CCR)	13.5 wt%
Viscosity at 100°F	20,000 cSt
n-C_5-asphaltenes	15.0 wt%

2.1.3 Asphaltenes, Resins and Coke

Asphaltenes are a class of heavy oil molecules characterized by being large polyaromatic compounds, with molecular weights ranging from 1,000 to around 20,000 g/mol and boiling points higher than 500ºC, thus being a main constituent of residue fraction (Martínez et al., 1997). The most widely used definition for asphaltenes is in terms of their solubility properties since they are not soluble in alkanes but are in aromatic solvents, such as benzene and toluene. Although asphaltenes consist of a complex class of a multitude of molecules, some authors propose that an average asphaltene molecules can be represented by isolated clusters of poly-condensed groups containing 5 to 7 rings bridged with heteroatoms and aliphatic chains. Figure 2-1 shows a representation of idealized asphaltene structures. Alternatively, asphaltenes can be defined as a structure with an aromatic core bearing aliphatic chains with the empirical formula of $C_{80}H_{80}N_2S_2O$, and a molecular weight of 1,150 g/mol (Ancheyta et al., 2009).

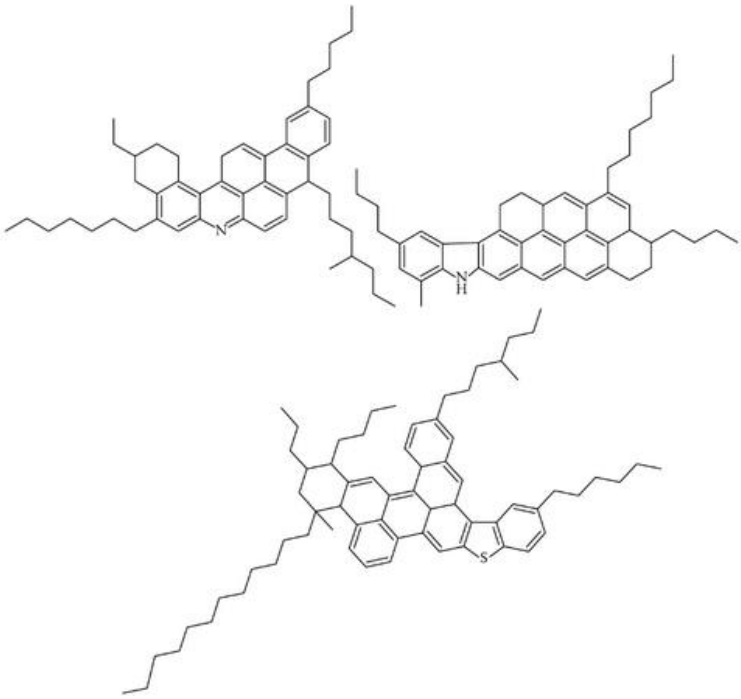

Figure 2-1: Idealized average asphaltene structures (Ancheyta et al., 2009)

Asphaltenes are the major precursors of sludges and sediments and, thus, brings difficulties in heavy oil processing (Ancheyta et al., 2009). In oil exploration, asphaltenes are reportedly responsible for deposition in the porous rock near the wellbore that ultimately reduces the rock permeability and oil production (Duncan, 2010). In oil processing, asphaltenes are responsible for

depositing and growing carbon residues on the surface of catalyst particles that end up blocking access to active sites and pore mouths, which leads to catalyst deactivation. For instance, in hydrotreating, the main sources of coke formation are poly-nuclear aromatics compounds and asphaltenes that adsorb on the catalyst surface due to the presence of nitrogen in those compounds (Ancheyta et al., 2009). Moreover, asphaltene polymerization, that usually takes place at high temperatures, causes plugs in catalyst beds and equipment downstream to reaction units (Martínez et al., 1997).

Resins are another heavy molecule category widely present in unconventional oils. Their classification is also based on solubility since they are soluble in alkanes but not in liquid propane. Asphaltenes conglomerates, also called micelles, are surrounded by resins that act as peptizing agents keeping asphaltenes under colloidal dispersion in the crude oil. The attraction between asphaltenes and resins are mostly due to hydrogen bonding between heteroatoms and dipole-dipole between polar groups. The alignment of polar regions in both molecules keeps the aliphatic regions in resins in the exterior part of the conglomerate, in contact with the bulk of the crude oil. Studies show that, more than the amount of asphaltenes in oil, the ratio of resin to asphaltenes is more important in relation to the crude oil stability, even though the crude oil nature and composition also plays a role on the stability (Ancheyta et al., 2009). Canadian unconventional oil is considered to have an intermediate asphaltene to resin ratio, usually between 0.3 and 1.0 (Tissot et al., 1984).

When processing crude oils, over solid catalysts at high temperatures, production of a heavy, hydrogen-deficient, and non-desorbed co-product, generally named coke, usually results. Coke composition and quantities depend on catalyst type, feedstock, and operating conditions, especially temperature. For processes that take place at high temperatures ($T>350^{o}C$), the coke may become a highly polyaromatic compound if low pressure of hydrogen is predominant in the medium. Though, for low temperature processes ($T<200^{o}C$), there is no polyaromaticity on the produced coke. Processing in intermediate temperatures tends to show a mix of both types of coke (Guisnet et al., 2001). Coke usually remains adsorbed on the catalyst surface blocking access to active sites and pore mouths and, consequently, promoting deactivation. The rate at which deactivation takes place depends on the studied catalytic system, i.e. catalyst and operating conditions. For instance, in reforming, 1 out of 200,000 carbon atoms that are activated by the active site is transformed into coke, while in heavy oil cracking, the ratio goes to 1:20 (Guisnet et al., 1989).

2.1.4 Naphthenic Acids

One important sub-class of molecules on the oxygen-containing species in crude oils is the naphthenic acids. This term is typically used to describe a mixture of carboxylic acids that contains at least one saturated alicyclic ring. Naphthenic acids naturally occur in crude oils and have the general formula RCOOH, in which R represents the naphthenic component consisting of 5- to 6-carbon rings derivatives and any acyclic aliphatic acids. Another general way of describing naphthenic acids is by using the general formula $C_nH_{2n+Z}O_2$ in which Z is a negative number that represents hydrogen deficiencies (Clemente et al., 2005). Naphthenic acids could also include phenol derivatives even though they are less present in crude oils. Figure 2-2 shows examples of naphthenic acid molecules that are common in Californian crude oils (Speight, 2014a). Naphthenic acids are natural components of petroleum that are non-volatile, stable, and act as surfactants. These molecules are originated from catagenesis or bacterial biodegradation. Characterization of naphthenic acids in Californian crude oil shows that 85% of these molecules contain other heteroatoms besides the two oxygens in the carboxyl-group (Clemente et al., 2005).

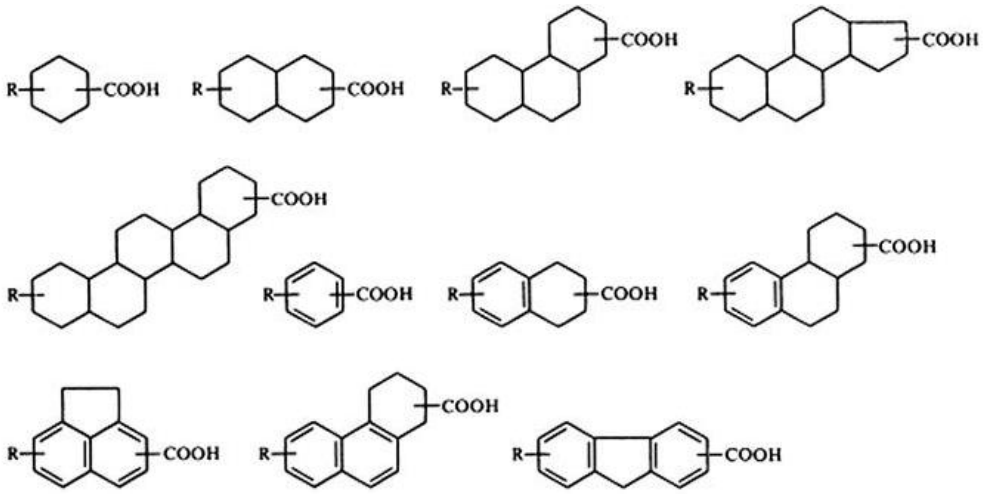

Figure 2-2: Naphthenic acids predominant in California crude oil (modified from Speight, 2014a).

The naphthenic acid content on a crude oil is defined as total acid number (TAN) and it is the amount of potassium hydroxide (KOH) in miligrams necessary to neutralize a gram of crude oil sample. TAN values range between 0.1 and 10 mg_{KOH}/g but it is more commonly found between 0.1 and 3.5 (Javaherdashti et al., 2013). The current method for TAN determination is ASTM D664 and it is based on the crude oil titration with potassium hydroxide. It is important to highlight that,

although ASTM D664 is a well-established and accepted method, it has issues such as: it does not differentiate strong from weak acids and therefore it cannot be directly used to indicate strength of corrosion; and it does not differentiate between naphthenic acids, phenols, carbon dioxide, hydrogen sulfide, mercaptans, and other acidic compounds present in the oil (Speight, 2014a).

Naphthenic acids are related to different issues on oil production and processing. Mainly, it is related to corrosion at mild conditions, especially at temperatures between 220-400°C. A more extensive review of corrosion effects due to naphthenic acids can be found in 2.2. Furthermore, bitumen production in Alberta also releases naphthenic acids into tailing ponds reaching concentrations around 20-120 mg/L in these ponds. Those concentrations may become an important issue when turning tailing ponds into natural habitats after oil operations (Clemente et al., 2005).

2.2 Corrosion in Crude Oil Operations

Speight (2014) made an extensive study on all types of corrosion that oil and gas facilities are susceptible to. According to the author, there are several different corrosion agents present in the crude oil, its products, byproducts, and other common reactants. For example, naphthenic acids, sulfur compounds, hydrogen, carbon dioxide, and ammonia could all lead to corrosion in different processes in a refinery. More related to the focus of this project, naphthenic acids corrosion depends on the process conditions and acid concentration. In fact, experiments in carbon steel show that naphthenic acid corrosive effects can only be observed at temperatures above 180-220°C. Its corrosiveness increases with temperature until it achieves its maximum rate between 280-385°C (Dettman et al., 2009). Yu et al., (2009) tested temperatures from 220-400°C on carbon steel, and stainless steel grades 304 and 316 and found that all of them present some rate of corrosion for the temperature range tested. Also, the reported corrosion rate followed an Arrhenius type of kinetics with activation energies ranging from 23kJ/mol (SS316) to 34kJ/mol (CS).

Highly acidic oils can promote corrosion in major equipment in a refinery. For instance, distillation units are one of the equipment mostly corroded due to its range of operating temperature that much increases naphthenic acid corrosion rate. Furthermore, acidic oils usually also contain high amounts of other corrosive components, such as: sediments, salts, and organic chlorides. Since these components are difficult to separate in desalters, they may also reach distillation units and other equipment downstream (Speight, 2014b).

Corrosion prevention and remediation can become very costly for oil producing, transportation, and processing facilities. Table 2-6 shows a breakdown of the annual cost of corrosion for US per sector (Papavinasam, 2014). The total cost of corrosion is estimated to be over 26 billion US dollars per year of which over ¼ is related to the pipeline sector and over ¼ is related to storage.

Table 2-6: Annual corrosion cost in US for different Oil & Gas sectors (Papavinasam, 2014).

Sector	**Cost with Corrosion (M$/year)**
Convention oil production	1,372
Pipeline transmission	6,973
Tanker transportation (Global)	2,734
Storage	7,000
Refining	3,692
Distribution	5,000

2.3 Traditional Methods for Treating High Acidic Oils

Naphthenic acid promotes corrosion in major refinery equipment, pipelines, and storage tanks causing great costs for prevention and remediation. To prevent this type of corrosion, a few methods have been used and developed so far. Those methods can be classified into physical processes and chemical processes, and a review of the commonly used processes can be seen in the following sub-sections.

2.3.1 Physical Processes

A physical method for dealing with high acidic crude oils is called blending. In this process, a high TAN oil is blended with a low TAN oil until a manageable TAN level is achieved, i.e. a level in which corrosion is negligible. That level is commonly accepted to be at $0.5 mg_{KOH}/g_{oil}$. This method is the most common solution for processing high TAN crudes (Speight, 2014a). However, there are some issues related to this method. Especially when dealing with very high TANs, the amount of low TAN oil to balance its acidity increases proportionally. In those cases, supply and cost of the low TAN oil can become a limitation. Also, compatibility between oils or oil streams can be a restriction since heavy crude constituents, such as asphaltenes, commonly have solubility issues. Finally, other properties limits, such as sulfur content, can restrain the blending. For example, a

low TAN but high sulfur content oil might not be suitable for blending purpose. It is also important to highlight that blending does not eliminate acidic compounds and, hence, it does not eradicate the chances of naphthenic acid corrosion in equipment that process specific cuts. For instance, different trays in distillation units might have liquid-vapor equilibrium in a range of temperature in which a high concentration of naphthenic molecules are present since blending oil could be considerably lighter than sour heavy-oil (Speight, 2014a).

One effective but also nondestructive way of separating naphthenic acids from crude oils is liquid-liquid extraction, especially when using ammonia or alkali alcoholic solutions. Removal of up to 94% from crude oils has been reported (Gaikar et al., 1996). This process usually promotes very stable water-crude oil emulsions that could prevent naphthenic acids separation (Speight, 2014a).

Another alternative for a nondestructive method to separate naphthenic acids is adsorption. So far, zeolites, aluminosilicates, and silica gels have been successfully tested for this method and recovery of naphthanates from spent aqueous alkali solutions can be achieved with strongly basic ion-exchange resins (Gaikar et al., 1996). This method of adsorption, though, may only be applied with light crudes and light distillation fractions. Viability of technologies involving ionic liquids in refineries still needs to be proven since economical, technological, operational, and environmental feasibility of large scale processes have not been addressed yet (Speight, 2014a).

Corrosion can also have its rate slowed by upgrading the alloys of pipes and equipment that process acidic crudes. Stainless steels 316/317 contain molybdenum and are significantly more resistant to naphthenic acid corrosion than other alloys such as carbon steel. This method for corrosion prevention involves large capital investments and long turnaround for execution (Speight, 2014a). Furthermore, stainless steel equipment is more expensive than carbon steel and usually makes the total investment around 30% higher (Towler et al., 2013).

2.3.2 Chemical Processes

A chemical method to deal with acid crude oils is the addition of small amounts of diluted caustic solutions into the acidic crude oil. However, this method produces naphthenic salts that are responsible for corrosion on furnace tubes. Furthermore, hydrocracking catalysts are also susceptible to deactivation due to compounds generated by caustic wash (Gao et al., 2008). This process also results in the formation of stabilized emulsions that become difficult to separate (Speight, 2014a).

The use of corrosion inhibitors is another method of mitigating naphthenic corrosion by layering a protective barrier on the metal surface of equipment in a refinery. Usually, inhibitors are organic compounds, which mainly contain oxygen, sulfur, nitrogen, or phosphorus. There are numerous patents for different inhibitors and a wide range of temperature applications, and a compilation of the latest patents can be found in the work of Duan et al. (2012). Although phosphorus containing corrosion inhibitors were found to be particularly effective for naphthenic acid corrosion, its use is limited since excess amounts can act as a catalyst poison in downstream refinery operations (Duan et al., 2012). This method becomes economically attractive when high acid crudes are only occasionally processed in the refinery since it could prevent the capital intensive alloy upgrade (Speight, 2014a).

Thermal or catalytic decarboxylation of naphthenic acids is another alternative for processing acidic crude oils. The decarboxylation can be achieved by esterification reactions, amidification, or direct removal of carboxyl radicals. Those reactions are exemplified by, respectively, Equation 2-1, Equation 2-2, and Equation 2-3. Naphthenic acids are found to react with alkanols to produce corresponding esters. Commonly used alkanols are methanol, ethanol, and mixtures in different proportions of both. Usually alkanol to naphthenic acids ratios are between 0.5 to 20 and it can be carried in the presence or absence of catalyst at temperatures of 250ºC and higher (Sartori et al., 2001).

$$R_1COOH + R_2OH \rightarrow R_1 - COOR_2 + H_2O \qquad \text{Equation 2-1}$$

$$R_1COOH + R_2R_3NH \rightarrow R_1 - CNR_2R_3 + H_2O \qquad \text{Equation 2-2}$$

$$R_1COOH \rightarrow R_1 - H + CO_2 \qquad \text{Equation 2-3}$$

Similarly, the amidification reaction, uses organic amines as a reactant and a catalyst that can be, for example, potassium hydroxide, sulphate, molybdate, and phosphate. The decarboxylation

reaction can be thermally achieved at temperatures higher than 400°C. There are several patented thermal processes that claim to be able to reduce crude oil acidity in temperatures ranging from 350-500°C, relatively low pressures (up to 1.0 MPa) and residence times up to 120 minutes. Decarboxylation can also be achieved by catalytic methods and there are several patented processes that claim to perform decarboxylation at temperatures as low as 200°C by using catalysts such as group IA metal oxide and an inorganic salt of group IIA metal (Duan et al., 2012). Those technologies though have several issues such as requiring other reactants such as oxides, requiring long contact times, or even large ratios between catalyst and oil.

Some technologies claim to perform decarboxylation at low temperature, however, in most cases, there are concerns about regenerability of catalyst during reaction. For example, in the work of Zhang et al. (2006), different types of metal oxides are used to react with naphthenic acids. In that work, most metal oxides were able to decrease the total acidity. All but one reaction produced carbon dioxide as the decarboxylation reaction, represented by Equation 2-3. Therefore, it is expected that either a metal naphtenate is being produced, or a metal carbonate, or both. Equation 2-4, and Equation 2-5 represent the chemical reactions that would produce those species without production of carbon dioxide. For the case in which carbon dioxide is produced, it remains unknown if metal carbonate or naphthanate is produced and to what extent.

$$2R_1COOH + MeO \rightarrow (R_1COO)_2Me + H_2O \qquad \text{Equation 2-4}$$

$$R_1COOH + MeO \rightarrow R_1H + CO_2 + MeO \rightarrow R_1H + MeCO_3 \qquad \text{Equation 2-5}$$

US Patent number 6,251,305 proposes a technology to reduce total acid number by reacting naphthenic acids with alcohols to form esters, as shown in Equation 2-1. The reactions were found to happen using alkanols and alkane diols at temperatures ranging from 250-350°C, naphthenic acids to alcohol ratios were preferably from 1:1 to 1:10, and contact times could go up to hours (Sartori et al., 2001). The long contact times and high consumption of alcohols become a challenge in making this technology feasible economically. A similar type of research has been done using a catalyst based on SnO and Al_2O_3. Similarly, acid to alcohol ratios were around 1:5 to 1:10 and temperatures from 140-320°C (Wang et al., 2007).

2.4 Catalyst Deactivation

In common oil-processing facilities, such as hydrotreating, catalyst deactivation happens as an effect of carbon and metal deposition that leaves active sites inaccessible. Traditionally, coke deposition is considered responsible for deactivation on the initial hours of reaction while metal deposition deactivation takes place gradually with time on stream. Finally, the combined effect of metal and carbon deposition decreases support porosity and leads to diffusion limitations and pore access blockage that quickly drops catalyst activity.

A common method for dealing with catalyst deactivation on fixed-bed hydroprocessing units is to increase the bed temperature to compensate for deactivation. Usually, this temperature is increased until a limit that is due to product quality or metallurgical constraints. This methodology is illustrated by Figure 2-3 and it also shows the deactivation mechanisms through the catalyst life. The deactivation due to carbon deposition can usually be recovered but metal deposition is permanent (Ancheyta et al., 2009).

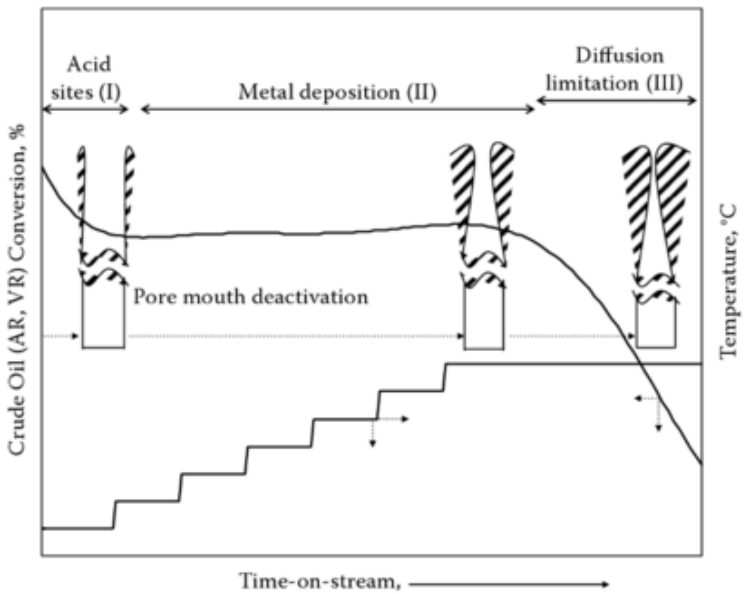

Figure 2-3: Mechanism for heavy oil hydroprocessing catalyst deactivation (Ancheyta et al., 2009).

In the initial stages of catalyst deactivation, represented by phase I in Figure 2-3, nitrogen rich carbon deposits on pore mouths, bulk phase, and/or uniformly on the surface depending on the nature of pores and reaction conditions. Regardless of the type of coke deposition, the coking

process proceeds to plug access to pores which leads to a major loss of available surface area (Ancheyta et al., 2009).

For phase II in Figure 2-3, nitrogen-, sulfur-, and metal-containing compounds deactivate hydroprocessing catalysts by strongly adsorbing on active sites. Due to their basic nature, those compounds will preferentially adsorb on acidic sites and such adsorption could be either reversible or irreversible depending on reaction conditions. Hydrodenitrogenation occurs at more severe conditions than other reactions for different heteroatoms and requires a higher partial pressure of hydrogen (Furimsky, 1999). Sulfur compounds and hydrogen sulfide are both known to reversibly adsorb on catalyst, acting as inhibitors.

The type of oil being processed plays an important role on the deactivation of the catalyst. For instance, when processing oils with high asphaltene content, it is expected to observe more asphaltene precipitation on the catalyst surface, more catalyst pore blockage, more coke formation since asphaltenes act as coke precursors, and more metal deposition since most heavy metals are concentrated in asphaltenes. Figure 2-4 represents the effects of oil quality on reaction severity and deactivation. It can be seen that lighter oils are expected to have several times longer catalyst life than heavier oils (Ancheyta, 2013).

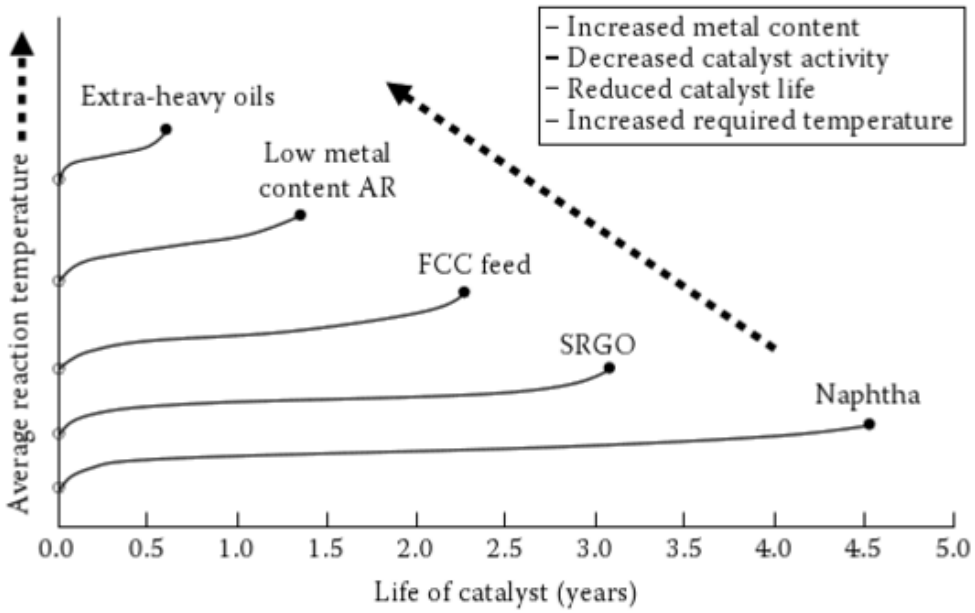

Figure 2-4: Reaction temperature and catalyst life for hydroprocessing different feedstocks (Ancheyta, 2013).

Deactivation can also be caused by changes in catalyst structure due to temperature and duration of exposure. Changes in catalyst phase are usually very slow and require high temperatures to take place. In any case, those changes tend to be irreversible, causing permanent loss of activity. For instance, the active phase can diffuse to the support or suffer recrystallization. Another example is when metals in the feed interact with promoters on the catalyst that will be less available for the active sites (Furimsky, 1999). Sintering of metals on supported catalysts, which results in the agglomeration of metal particles, is another source of deactivation on catalytic process. It is usually related to the long exposure of active sites to high temperatures that allows metal particles to diffuse and spread over the support (Ghorpadkar, 1993).

When metal poisons are not present in a crude oil, most of the catalyst activity can be recovered through regeneration. The regeneration comes from the combustion of coke particles that prevent the access to active sites and pore mouths. Regeneration processes can be complicated since metal sintering could become an issue since it happens at high temperatures (Guichard et al., 2009).

In a hydrotreating study involving several spent, regenerated, and resulfided $NiMoP/Al_2O_3$ and $CoMoP/Al_2O_3$ catalysts, it was found that almost all catalysts tested were able to recover activity after regeneration. XPS analysis shows that some of the catalysts go through some active site loss after reaction. The catalyst activity was measured by toluene hydrogenation reactions at 350°C and 6MPa while the regeneration was done with air at temperatures that went up to 500°C (Guichard et al., 2009).

2.5 Heavy Oil Upgrading

Global oil demand has increased steadily throughout the past decades but little increase to refinery capacity has happened in the same time period, which makes refineries work close to full capacity in recent years. Also, when crude oil prices are high, heavy and extra heavy oils exploitation becomes financially profitable and politically important to meet fuel demand. Heavy (and extra heavy) oil production requires that those feedstocks are upgraded and transformed into synthetic crude oils by deep (and ultra-deep) conversion to achieve product quality close to refinery requirements. These synthetic crude oils have both a cut composition and bulk characteristics, such as viscosity, API gravity, and sulfur content, closer to market requirements. Figure 2-5 represents the cut distribution differences between an extra-heavy oil, a synthetic oil, a light oil, and a representation of crude oil demand (Huc, 2011).

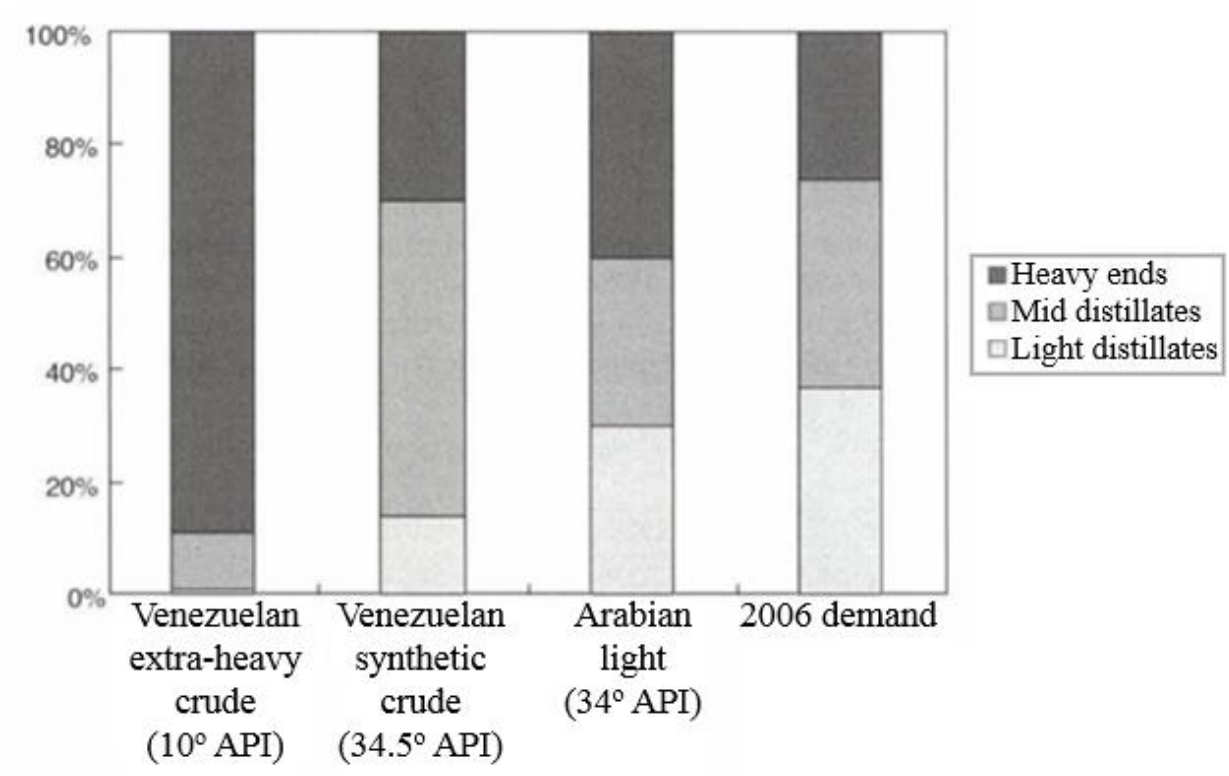

Figure 2-5: Cut distribution comparison between extra-heavy oil, synthetic oil, light oil and demand representation (modified from Huc, 2011).

The first upgrading process to be introduced was desulfurization, that later evolved to also incorporate partial conversion of heavy molecules in up to 30%. Since then, upgrading evolved to different processes that can be categorized into thermal cracking, catalytic cracking, and

hydroconversion. The goal of upgrading processes is to increase the hydrogen to carbon ratio in the valuable product, and to achieve that, those processes may have two different principles of operation, i.e., carbon rejection and hydrogen addition. In carbon rejection processes, there is a redistribution of hydrogen amongst different components that lead to a low and a high hydrogen content fraction. On the other hand, hydrogen addition processes react feedstock with a hydrogen source to increase hydrogen to carbon ratios (Speight, 2013a).

2.5.1 Carbon Rejection Processes

Solvent de-asphalting (SDA) is a very flexible process, on the family of carbon rejection technology, which uses paraffinic solvents to destabilize and precipitate asphaltene-resin aggregates. As asphaltenes and resins are rich in sulfur, nitrogen, and metal, and have high molecular weights, the resulting deasphalted oil is lighter, and has lower metal, sulfur, and nitrogen content than the original oil (Huc, 2011). The heavy product can be used to produce asphalt or as blend stock or visbreaker feedstock for low-grade fuel oil while the light product can proceed to be refined and converted on a fluid catalytic cracking unit. The main drawbacks from the process are the generation of the low value heavy product and the fact that the quality of products depends on the quality of the feedstock since there is no conversion involved. (Speight, 2013a).

The Residual Oil Supercritical Extraction (ROSE) is the most widely used commercial SDA process. In this process, a first separator is used at subcritical conditions to separate precipitated solids. In a second separator that is operated at supercritical conditions, solvent is recovered and recirculated. The depth of separation is related to the process conditions, such as pressure, temperature, and solvent (that is usually an alkane from C_3 to C_6 for SDA processes) (Banerjee, 2012). A diagram of the ROSE process is shown in Figure 2-6.

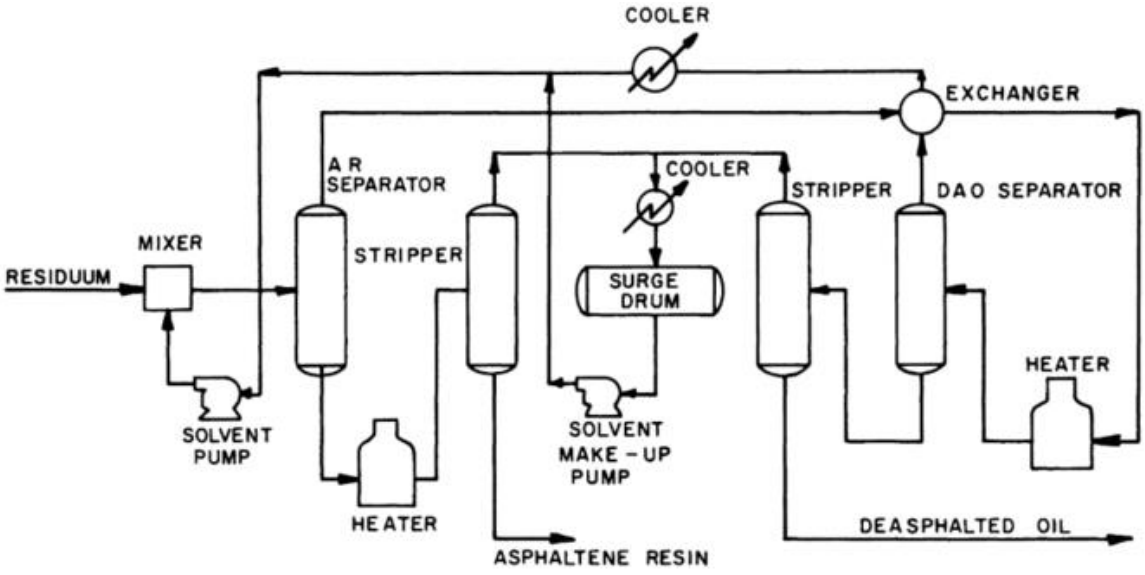

Figure 2-6: Schematic diagram of the ROSE process using residuum as feedstock (McHugh et al., 1994).

Delayed coking is another process based on carbon rejection and it uses severe conditions to produce a hydrogen rich distillate and a hydrogen poor solid that also contains the metals and good proportion of sulfur and nitrogen compounds. Figure 2-7 shows a simplified representation of the process.

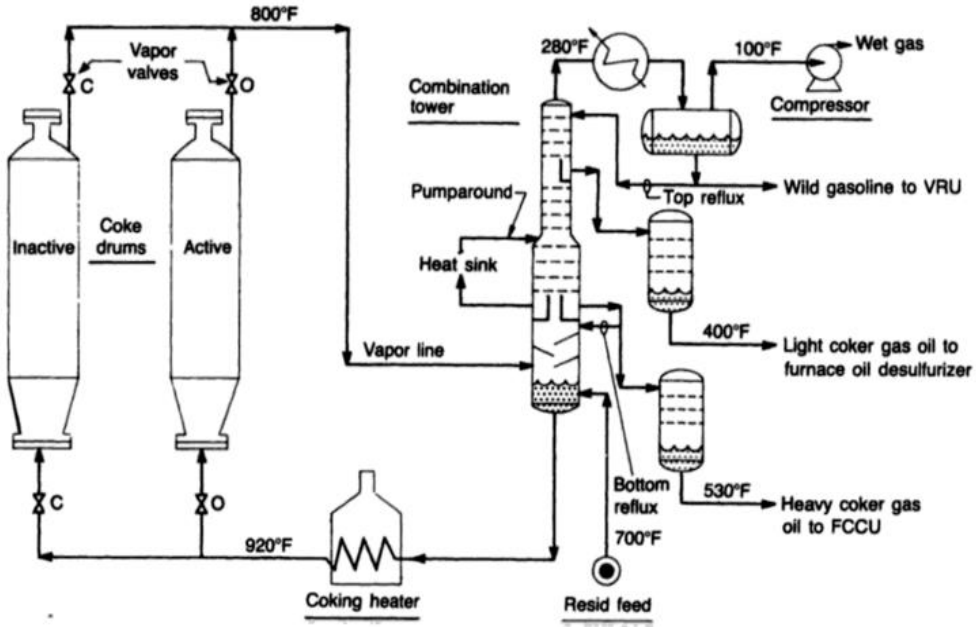

Figure 2-7: Simplified diagram for delayed coking process (Lieberman, 1991).

This thermal upgrading technology produces a poor quality distillate product that still needs further treatment to achieve market specifications for olefins, nitrogen, sulfur, and aromatic content (Huc, 2011). Typically, the distillate product will be formed by 50 vol% gas oil, 20 vol% middle distillates, and 30 vol% naphtha. About one third of all carbon fed to the process is converted into low-value poor-quality coke. One advantage of this process is that coke retains about 50% of sulfur, 60% of nitrogen and 90% of metals in the feed with no need of using hydrogen to eliminate them. Delayed coking is the most widely used technology for bitumen upgrading due to its simplicity and economic viability (Banerjee, 2012).

In delayed coking, the feedstock, usually the vacuum residue of a fractionator, is heated on a furnace to temperature around 500°C and fed to a coker drum in which residence times are around 10-12 hours and temperatures are around 430-450°C. At this stage, coke is produced and accumulated in the drum. Later the coke produced is removed and retrieved from the drum. The system usually operates with two drums in parallel with 24-hour long cycles.

Fluidcoking and flexicoking are processes derived from delayed coking and targeting higher liquid and lower coke yields. Figure 2-8 has a representation of a simplified flexicoking process diagram.

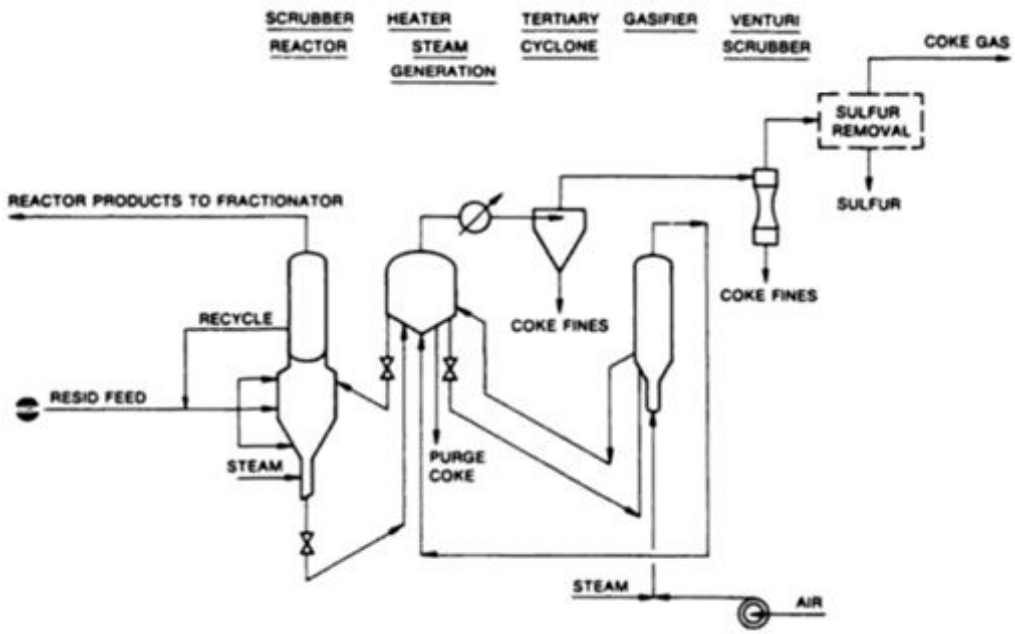

Figure 2-8: Exxon Research and Engineering flexicoking simplified diagram (modified from J. McKetta, 1990).

In fluidcoking, the use of a fluidized bed allows for higher temperatures and lower residence times having the effect of promoting the cracking of very high molecular weight molecules while allowing less time for polycondensation to take place. On top of fluidcoking process, flexicoking also gasifies the coke that is produced. The main challenge of the fluidized bed processes is the control of coke particle agglomeration and settling inside the reactor that may lead to a process shutdown (Banerjee, 2012).

Visbreaking is a thermal, carbon rejecting process that uses steam injection to crack heavy molecules into lighter ones under mild conditions, usually between 430-500°C, and contact times between 1-8 minutes. The thermal cracking reduces the viscosity of the products but, at the same time, it promotes asphaltene aromatization and light saturate formation that potentially can cause asphaltenes to precipitate. Another challenge in this process is determining reaction conditions in such a way as to keep both coke and gas yields low, and to reach high viscosity reduction (Huc, 2011). Commercial processes usually operate at 20-30% residue conversion since product instability usually prohibits an increase in severity (Banerjee, 2012).

2.5.2 Hydrogen Addition Processes

On the hydrogen-addition processes, hydroprocessing is a family of processes using hydrogen to improve hydrogen-to-carbon ratios and to reduce heteroatom content in heavy oils (Banerjee, 2012). For instance, hydrotreating is used prior to catalytic cracking processes to reduce sulfur content and improve products yield. Due to the wide range of process feedstock and conversion targets, there are different catalysts and process flow schemes that are commercially used. Although cobalt-molybdenum catalysts are the most widely used, catalysts such as tungsten-nickel sulfide, cobalt-molybdenum-alumina, nickel oxide-silica-alumina, and platinum-alumina are also commercially employed. The temperatures in hydrotreating processes range between 290-445°C, and hydrogen pressures up to 21,000kPa. Low temperatures and hydrogen partial pressures are used when cracking reactions are to be avoided (Speight, 2013a). The low severity process is commonly referred to as hydrotreating. Depending on the heteroatom target of the hydroprocessing, the process can be also referred to as hydrodesulfurization, hydrodenitrogenation, or hydrodemetalization (Huc, 2011). Alternatively, hydrocracking is the recognized term when more severe conditions are used to promote cracking. Hydrocracking is one of the major hydrogen addition processes and when it catalytically cracks high molecular weight

molecules, it creates free radicals that are capped by hydrogen, which prevents polymerization reactions (Banerjee, 2012).

From the process point of view, hydroprocessing reactors are commonly downflow plug flow reactors with a catalytic fixed bed. Due to its high exothermicity, the reaction mixture can be quenched with cold recycled gas at intermediate points in the reactor, and the reactor can be treated as a series of catalytic beds. The first bed in the series is severely poisoned by vanadium and nickel and it is usually an inexpensive catalyst, being named guard catalyst. As the catalyst proceeds to become poisoned and deactivated, overall catalytic bed temperature is increased to compensate for losses in activation until the catalyst regeneration is required. After regeneration, the guard catalyst is commonly discarded and replaced by fresh guard catalyst prior to restarting the reaction. Some other process variations, such as up-flow expanded bed reactor, are also available commercially. The latter is used when commonly dealing with heavy, high metal, and particulate content feedstocks. The bed expansion allows particulates to flow between catalytic bed without plugging it (Speight, 2013a). Figure 2-9 shows a diagram representation of a hydrodesulfurization plant in which one guard reactor is used together with two major reactor beds. The oil is recovered after going through two flash drums and a stripper while hydrogen is further separated and recycled to the reaction unit.

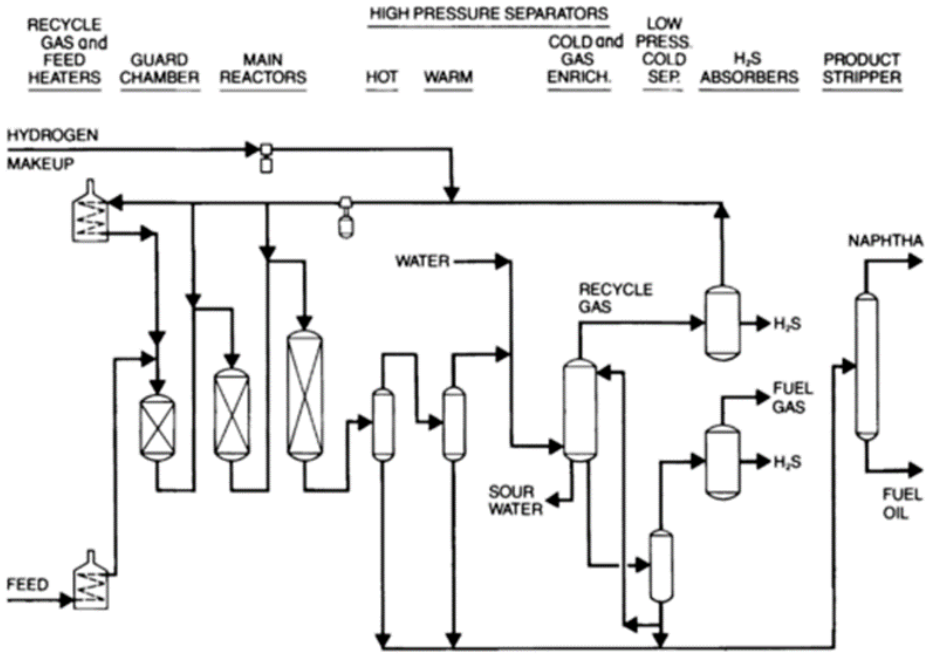

Figure 2-9: Simplified hydrodesulfurization process diagram (Leach, 1983).

To address the issues related to poor-quality bitumen, upgraders use different combinations, configurations, and variations of the previously discussed processes. Also, new and different technologies from the ones discussed in the literature review have been used commercially. The choice between varieties of upgrader configurations can be made based on feedstock properties, quality, and existing facilities.

Figure 2-10 shows an example of upgrader configuration for bitumen processing. In this diagram, delayed or fluid coking can be used as the primary conversion step followed by hydrotreating of the products that can be further combined to produce synthetic crude that could be shipped to a conventional refinery for further processing (Speight, 2013a).

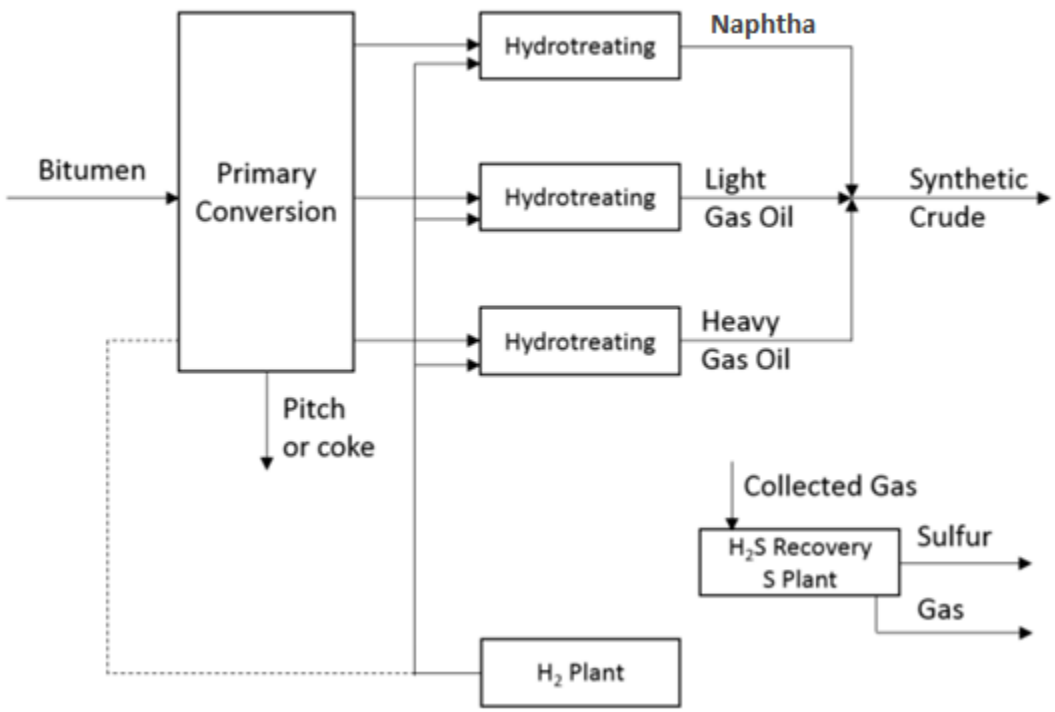

Figure 2-10: Example of tar sand bitumen processing sequence (modified from Speight, 2013).

2.6 Catalytic Steam Cracking

Many upgrading and refining facilities carry out heavy oil processing through thermal technologies such as delayed coking and visbreaking due to proven reliability and economic feasibility. Yet, such processes produce large amounts of low quality byproducts, such as coke. Alternatives for thermal processes are mainly hydrotreating and deasphalting processes as discussed in section 2.5. Hydrotreating consumes large amounts of expensive high pressure hydrogen while deasphalting uses precipitant solvents that are subject to losses during the process (Fathi et al., 2011). An alternative that has been explored in the recent years to heavy oil upgrading is catalytic steam cracking (CSC). This process can be defined as a moderate-conversion process for unconventional oil or heavy cuts that catalytically produces hydrogen through steam dissociation while, in parallel, it cracks heavy molecules both thermally and catalytically (Trujillo, 2008). Because of those characteristics, CSC processes can be considered as both hydrogen adding and carbon rejecting technology. When using a catalyst able to perform water splitting, hydrogen can be produced in the reactor and used to hydrogenate heavy molecules. At the same time, cracking reactions also take place.

Catalytic steam cracking can be considered as a combination of steam reforming and thermal, or catalytic, cracking. Steam reforming is an industrial technology that produces hydrogen gas from methane or higher molecular weight alkanes, such as the ones present in naphtha. The general chemical reaction for complete steam reforming is given by Equation 2-6 (Duprez, 1992). If n=1 and x=4, Equation 2-6 becomes the methane steam reforming reaction. Since the maximum value of x is 2n+2 for alkanes, the maximum hydrogen yield is 3n+1 for a production of n molecules of CO_2. Then, the ratio H_2:CO_2 is maximized for methane and it is 4:1. For other alkanes, this ratio varies from 3:1 to 4:1 while cyclic molecules, aromatics, and alkenes can have values below 3:1.

$$C_nH_x + 2n\ H_2O \rightarrow n\ CO_2 + (2n + x/2)\ H_2 \qquad \text{Equation 2-6}$$

Steam reforming can also happen partially and, in that situation, steam dealkylation, i.e. cracking of specific carbon-carbon bonds, take place first in the reaction. The chemical reactions for toluene under steam dealkylation are given by Equation 2-7, and Equation 2-8 (Duprez, 1992).

$$C_6H_5 - CH_3 + \ H_2O \rightarrow C_6H_6 + CO + 2\ H_2 \qquad \text{Equation 2-7}$$

$$C_6H_5 - CH_3 + \ 2H_2O \rightarrow C_6H_6 + CO_2 + 3\ H_2 \qquad \text{Equation 2-8}$$

Extensive studies on catalytic steam cracking show that Group VIII metal catalysts have good activity towards the reaction with rhodium and ruthenium being more active. It has been shown that the nature of the support is very relevant in the overall activity. It is believed that this dependence is related to the bifunctionality effect in which the metal is the site responsible for dissociative chemisorption of hydrocarbons while water activation in hydroxyl groups happens on the support. A proposed mechanism for toluene steam dealkylation is represented on Figure 2-11. Toluene adsorbs and splits on the support producing a phenyl and methyl group. The latter transfers a hydrogen atom to the former, which produces a benzene molecule that is quickly desorbed. The remaining compound continues to hydrogenate or react with oxygen compounds transferred from the support, where water splitting takes place (Duprez, 1992). An alternative and generic mechanism for catalytic steam cracking is represented by Equation 2-9 to Equation 2-12, and summarized by Equation 2-13 (modified from Fathi et al., 2011).

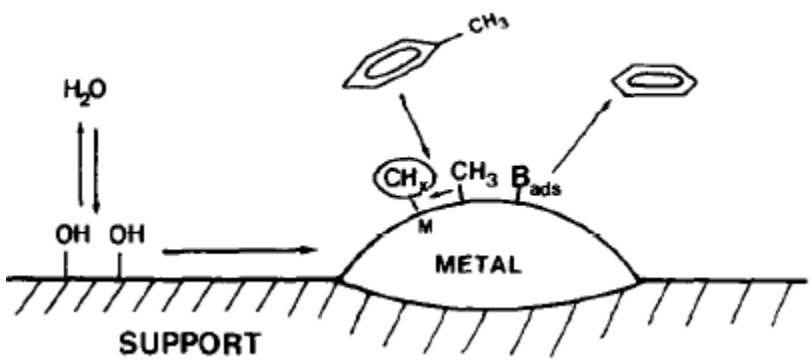

Figure 2-11: Mechanism for catalytic steam dealkylation of toluene (Duprez, 1992).

$$2H_2O \rightarrow 2H^* + 2OH^* \qquad \text{Equation 2-9}$$

$$R - CH_2 - R_n \rightarrow R^* + R_n - CH_2^* \qquad \text{Equation 2-10}$$

$$R^* + H^* \rightarrow RH \qquad \text{Equation 2-11}$$

$$2OH^* + R_n - CH_2^* + H^* \rightarrow CO_2 + 2H_2 + R_nH \qquad \text{Equation 2-12}$$

$$R - CH_2 - R_n + 2H_2O \rightarrow RH + CO_2 + 2H_2 + R_nH \qquad \text{Equation 2-13}$$

Equation 2-9 and Equation 2-10 represent, respectively, water splitting and organic molecule cracking into different radicals. Equation 2-11 shows the reaction of an organic radical with a hydrogen radical to produce stable hydrocarbon molecules. Equation 2-12 represents the reaction between an OH radical with a hydrocarbon radical to produce carbon dioxide, hydrogen, and a stable hydrocarbon molecule.

Interest in catalytic steam cracking is on the rise on the past few years and a number of patents have been issued on oil upgrading. Pereira et al. proposed a scheme to upgrade heavy oil consisting of a separation unit, a solvent deasphalting (SDA) unit, and a catalytic steam cracker (CSC) unit that uses a nano-catalyst. In this process, heavy oil is split into a light stream and a topped heavy oil stream. The latter goes through the SDA unit and the produced deasphalted oil is processed on the CSC unit to yield gases and light products. Finally, upgraded oil can be formed by mixing different streams while the asphaltene-rich stream can be disposed of, used for fuel or used as feedstock in other processes (Pereira-Almao et al., 2013). The dissertation of Garcia-Hubner (2015), applies a similar concept as the Pereira-Almao et al.'s patent but using a supported catalyst to react deasphalted oil (Garcia-Hubner, 2015). Wrisberg et al. patented a CSC process that reacts saturated hydrocarbons, especially low weight molecules and aromatics, into unsaturated molecules at high conversions and no coke deposits. This process uses high temperatures, commonly 500-800°C, and pressures in the range 0.1-50 atm (Wrisberg et al., 1973). Kondh et al. conducted experiments with bitumen and superheated steam with a series of fixed-bed oxide catalysts. The conditions used were weight hourly space velocities (WHSV) of 2.5 h^{-1}, weight water to oil ratios of 2, temperatures of 470°C, and atmospheric pressure. The experiments resulted in yields of gasoline and kerosene going up to 40% but, at the same time, yields of coke reaching over 20%. Considerable quantities of hydrogen were also produce for some of the catalysts tested which shows the potential for water splitting (Kondoh et al., 2016). In another study developed by the same research group, a CeO_2-ZrO_2-Al_2O_3-FeO_x catalyst was used under 350-420°C, pressures of 19MPa, WHSV of 0.25 h^{-1}, and water to bitumen ratios of 20. The results represent an improvement from the previous research, although most conditions are much more severe. Coke yields never passed 10%, and light oil yields, i.e. VGO and lighter cuts, were up to 70%. Also, hydrogen yields for this experiment were several times smaller than previous reactions reported, which is most likely related to hydrogenating of oil molecules. After six hours of reaction, the catalyst was calcined with air at 500°C for 2 hours and both the XRD pattern and the products yield showed a good recovery of activity (Kondoh et al., 2016).

Catalytic steam cracking has proved to be able to generate hydrogen during reaction and upgrade deasphalted oil or light olefins and aromatics. The process represents an advantage in relation to hydrotreating due to the lack of high cost reactants, such as hydrogen. Moving catalytic steam cracking towards whole heavy oils could potentially eliminate the use of a solvent deasphalting

unit. Although that was implemented by Kondoh et al. (2016), low coke yields were only obtained when using high pressures and water-to-oil ratios. Thus, there is a potential for operating condition optimization and catalyst screening that could produce a feasible industrial process. The simplicity of the process would allow it to be placed on oil producing facilities.

2.7 Supported Catalysts

The type of catalysts used throughout the course of this project have been designed for fixed bed reactor configuration. These are supported catalysts or catalysts that contain a core or support and have active phases on top (supported). In this case the active phases are one or a combination of the following solid types: hydrotalcite-type precursor containing Ni, Ce, Mg, and Al; metal-doped silicate MFI-type structure also containing Ni and Ce inside the network structure; and molybdenum carbide. Those type of catalysts are reviewed in the following sub-sections.

2.7.1 Hydrotalcite

Hydrotalcite is a precursor structure that has been successfully used to give good metal dispersion of the active phase (Zurita et al., 2015). Its acid/basic properties can be easily manipulated by changing its composition. Its general chemical formula is $[M^{2+}_{(1-x)}\ M^{3+}_{x}(OH)_2]^{x+}(A_{x/n})^{n-}.yH_2O$ and its structure is composed by layers of double brucite-like octahedrically-coordinated M^{2+} and M^{3+} hydroxides. The hydrotalcite layer has a net positive charge that is balance by anions A^{n-} that are encountered in the interlayer space (Cantrell et al., 2005). Figure 2-12 shows a schematic representation of a hydrotalcite structure.

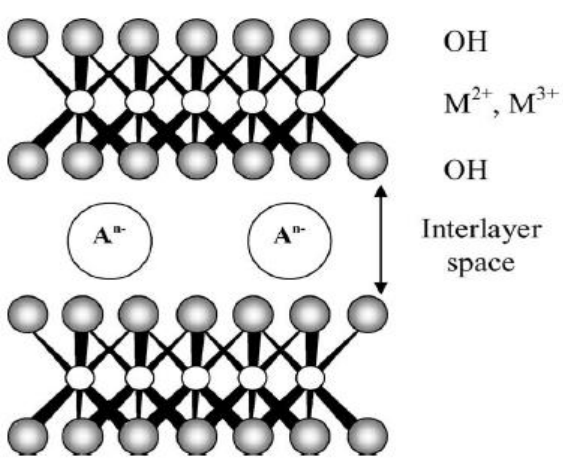

Figure 2-12: Schematic representation of hydrotalcite structure (Cantrell et al., 2005).

When submitted to thermal decomposition, hydrotalcite produces structures with highly dispersed mixed oxides and, therefore, it can be used as precursor for catalyst in applications such as methane steam reforming (Resini et al., 2009). Hydrotalcite has been successfully tested on catalytic reforming and steam cracking. Perez Zurita et al. conducted a study on toluene catalytic steam cracking over catalysts prepared with hydrotalcite-type solids as precursor. Regarding metal substitution on the hydrotalcite structure, their method proved to be successful when partially exchanging Mg^{2+} for Ni^{2+} and Al^{3+} for Ce^{3+}. Nevertheless, it was found that Ce^{3+} precipitated as crystalline nano-CeO_2. The catalyst developed proved to be active towards toluene cracking. Furthermore, cerium was found to improve catalyst activity and resistance towards carbon deposition. A high hydrogen yield was obtained during the conducted research which implies that the developed catalyst is able to perform water splitting (Zurita et al., 2015).

2.7.2 MFI Catalyst

Crystalline silicates have been used to produce different materials for catalytic purposes. Of particular interest to this project is the metal-doped silicate material having the Modernite Framework Inverted (MFI) structure (Ni-Ce-Silicalite-I). Those MFI structures have a combination of sinusoidal and straight interconnected channel systems that result in defined tortuous and porous pathways (Diaz et al., 2004) of diameters around 0.50 to 0.55nm.

Some of the metals that have been successfully doped into the silicalite I (with the MFI structure) in the past are: zirconium (Rakshe et al., 1997), aluminum, gallium, indium (Cejka et al., 1994), and iron (Dumitriu et al., 1999). The metal-doping process creates solids with different properties like acid strength, that make them suitable to specific reactions (Dumitriu et al., 1999). For instance, iron-containing silicalites have been studied since 1988 due to their role in benzene oxidation to phenol (Ferretti et al., 2002).

The preparation of metal containing zeolitic catalysts is well known and used. For instance, nickel impregnated ZSM-5 (the most used solid of the MFI family) catalysts have been used for hydrogenation, isomerization, dehydrogenation, oxidation, aromatization, hydrogen production, carbon nanotube preparation, NO_x reduction, and hydrocracking reactions. The activity, stability and selectivity of this type of catalyst are very dependent on the conditions and methodology used to incorporate nickel on the catalyst surface. Some of the methodologies that have been used so far for preparation of nickel-containing catalysts are: precipitation, impregnation and ion-exchange

processes, chemical vapor deposition, mechanical mixing, solid-state reactions, and nickel precursor introduction during support synthesis. For zeolitic-type catalysts, nickel incorporation is done mostly through impregnation or ion exchange (Vitale et al., 2013).

In the Vitale et al. (2013) work, nickel incorporation was performed by adding a nickel precursor during the zeolite preparation step and, later on, anchoring it during the crystallization step. This preparation method also includes a calcination step to remove the organic template, and ion exchange step to produce the acid form of the nickel-incorporated zeolite. This methodology effectively incorporates the metal in the framework since X-ray diffraction (XRD) does not indicate any other crystalline phase. The produced catalyst showed good nickel dispersion, high activity in relation to hydrogenation, good physical-chemical properties, and good tolerance to sulfur (Vitale et al., 2013).

The incorporation of transition metals into zeolite and zeolite-like structures, that has the effect of adding extra functionalities, has been widely used to enhance the properties of materials that already have versatile microporous channels and cavities with adjustable acidities. Under controlled synthesis conditions and methodologies, it is possible to produce numerous transition metal incorporated zeolites into their frame work, i.e. the tetrahedral coordinated sites of parent silica or aluminum ions. However, incorporation of large atoms into the framework can distort the zeolite structure (Gu et al., 2013). Cerium has been incorporated into different solid catalysts and it has shown the capability of reducing coke formation in the following reactions: gasification, isomerization, and steam reforming. In the family of MFI structures, a preparation of a HZSM-5 catalyst with cerium incorporated in the framework has been reported to show good selectivity towards catalytic fast pyrolysis and low coking yields (Neumann et al., 2012).

For the present work, a doped Ni-Ce-silicate with the MFI structure was prepared following the synthesis procedure reported by Vitale et al. (2013), where aluminum was replaced by cerium in the synthesis gel and the crystallization incorporated both, Ni and Ce into the produced material. A thermal treatment was performed to remove the template and no ion exchange procedures were carried out. Binding the zeolite powder with silica and activation in hydrogen were used as post-modification methods to produce and activate the structured catalysts for testing in the pilot plant unit.

2.7.3 Molybdenum Carbide

Molybdenum carbide is a transition metal containing catalyst that, similarly to tungsten carbide, is known for its hardness, thermal stability and activity in heterogeneous reactions (Liu, 2015). Molybdenum carbide has been treated as a potential substitute to noble metal catalyst, especially ruthenium (Lee et al., 1991). Experiments on low-temperature benzene hydrogenation showed that molybdenum carbide had a higher activity than Ru and Pt catalysts but it undergoes severe deactivation over a few hours of reaction. The deactivation rates were found to be more severe at higher temperatures but the mechanisms of deactivation are still to be understood (Lee et al., 1991). This deactivation is less commonly seen during processing of other molecules. A study on toluene hydrogenation showed that toluene conversion up to 98% could be achieved at 473K with no evident deactivation on the first 1000 hours of reaction (Frauwallner et al., 2011). Furthermore, molybdenum carbide has shown activity towards several other reactions, such as oxidation of hydrocarbons, water gas shift, alcohol synthesis, hydrazine decomposition, reforming, and hydrotreating (Vitale et al., 2011).

One of the most common methods of preparation of molybdenum carbide catalysts was developed by Lee et al. and it consists of a temperature-programmed reaction of low specific surface MoO_3 with a methane and hydrogen gas mixture. This method uses very high temperatures that can exceed 1000 K in the preparation and produces hexagonal molybdenum carbide unsupported powders with specific surface areas between 50 to 100 m^2/g (Lee et al., 1987). Other new methodologies for molybdenum carbide preparation have been explored ever since, such as the methodology described by Frauwallner et al. that uses toluene as a carbon source and temperatures up to 673K (Frauwallner et al., 2011). The work developed by Vitale et al. shows a novel methodology that uses ammonium heptamolybdate tetra-hydrate (AHM) and sucrose as precursors to obtaining cubic molybdenum carbide. The preparation method had final temperatures of 673K and the catalyst showed high activity towards toluene hydrogenation, especially when prepared with molybdenum vacancies (Vitale et al., 2011).

Garcia-Hubner prepared a catalyst combining molybdenum carbide prepared using the methodology reported by Vitale et al. and a Ni and Ce catalyst prepared using a hydrotalcite precursor (Garcia-Hubner, 2015). The catalyst produced had $117m^2/g$ of surface area and was used to process deasphalted oil in a catalytic steam cracking reactor. This catalyst was tested at different

temperatures and pressures and showed a considerable higher activity than other catalysts in which Mo_2C was not used, especially at higher temperatures and pressures. In fact, for 370^oC and 2,760kPa, residue conversion was around 45%, in comparison with 22% of thermal reaction. The improvements under high pressure were attributed to the higher hydrogen partial pressure, which improves hydrogenating reactions, and reactant diffusion. No considerable improvement towards total acid number reduction was observed from the different pressure runs. A labelled water experiment conducted in the Garcia-Hubner work using a catalyst prepared solely with the Ni and Ce hydrotalcite precursor phase showed a high activity towards water splitting (Garcia-Hubner, 2015).

This thesis explore catalytic steam cracking as a technology for reducing acidity in heavy oils. The catalysts used throughout the project are combinations of the ones listed in this section. Chapter 3 contains a detailed explanation of the composition of each one of the catalyst. Also, it contains a description of the methodology used during the experiments.

3 Experimental Section

In this section, a description of materials, experimental set-ups, characterization methods, and procedures applied throughout this project are given. The description of the experimental set-up is given in section 3.1 and its sub-sections while the methodology applied to run the experiments is given in section 3.2. A summary of the feedstocks and catalysts used are given in sections 3.3 and 3.4 respectively. The methodologies used on the samples characterization are given in section 3.5.

3.1 Experimental Set-Up

Two different experimental set-ups were used for the development of the project and they mainly differ on sampling methodology and reactor configuration. The set-ups are represented by Figure 3-1 (set-up I) and Figure 3-2 (set-up II), and are composed by a pumping section (section 100 for oil, and 200 for water and gases in the diagram), reaction section (300), and separation section (400). Chronologically, the set-ups represent advances and improvements on the process and a detailed explanation of all set-ups is done in the following sections. The software LabVIEW was used for controlling, recording, and monitoring the system throughout all its operation.

3.1.1 Pumping Section

In this section of the plant, oil, water, and gases are set to the desired flow rates and transported towards the reaction section. The gases, i.e., nitrogen and hydrogen, are kept in separate pressurized cylinders (TK-201 and TK-202, respectively in Figure 3-1, and Figure 3-2), and connected to mass flow controllers MFC-201-Brooks 5850S and MFC-202-Brooks Delta II, respectively.

Water is a reactant that was continuously pumped through the system during regular operation. In set-up I, this pumping was done by an Eldex reciprocating pump model 1LMP (P-201) that was fed by a 500 mL stainless steel water reservoir (TK-203). In set-up II, the pumping was improved to a more reliable syringe-type pump model Teledyne ISCO pump 500D, also represented by P-201 in Figure 3-2. Since pump P-201 is a syringe-pump, it requires filling prior to reaction and, when necessary, during reaction. The same stainless steel water reservoir (TK-203) was used for refilling. Heating tapes were wrapped around lines downstream to the pump to vaporize water and ramp its temperature to reaction set-point values.

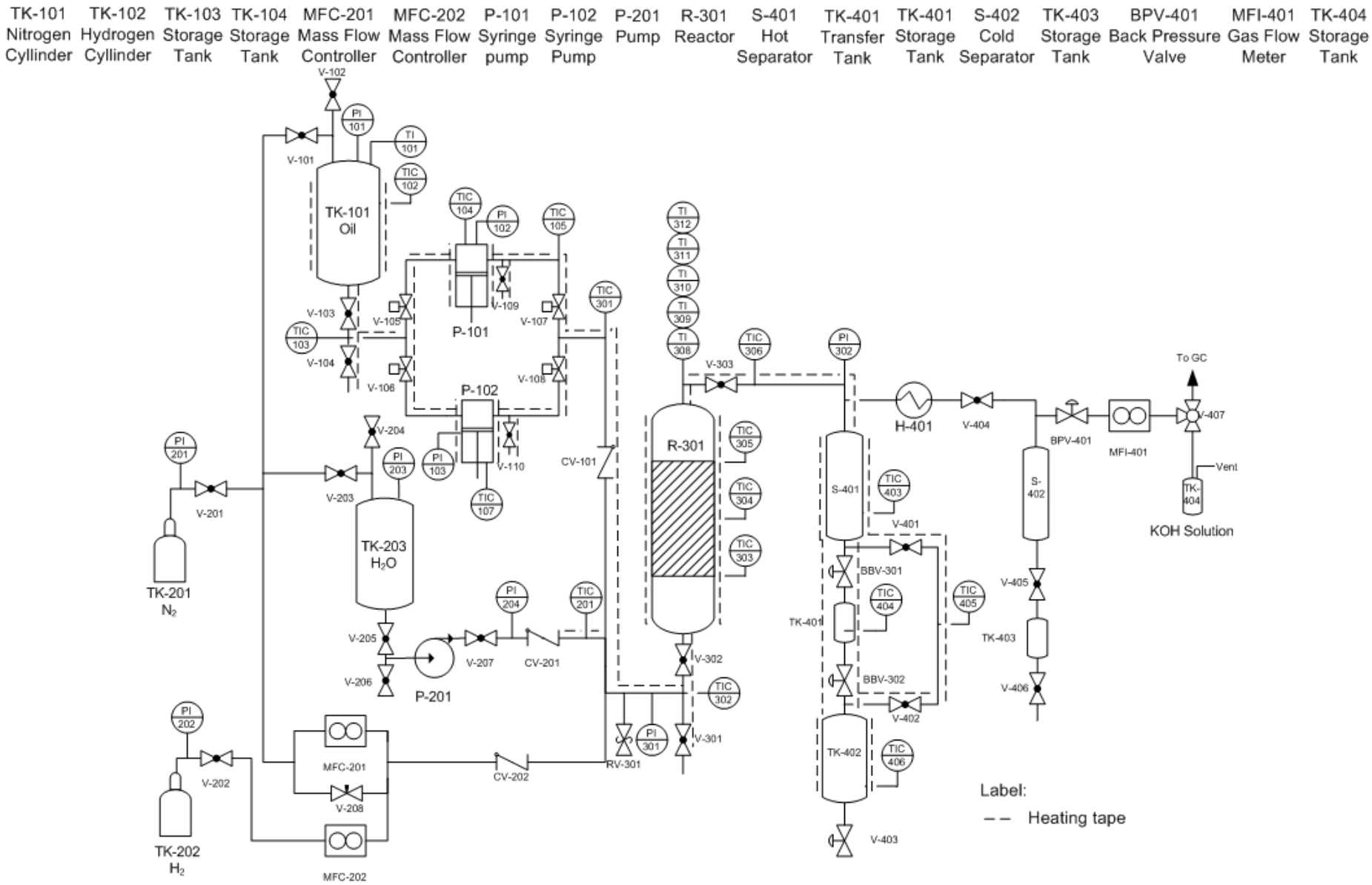

Figure 3-1: P&ID for experimental set-up I.

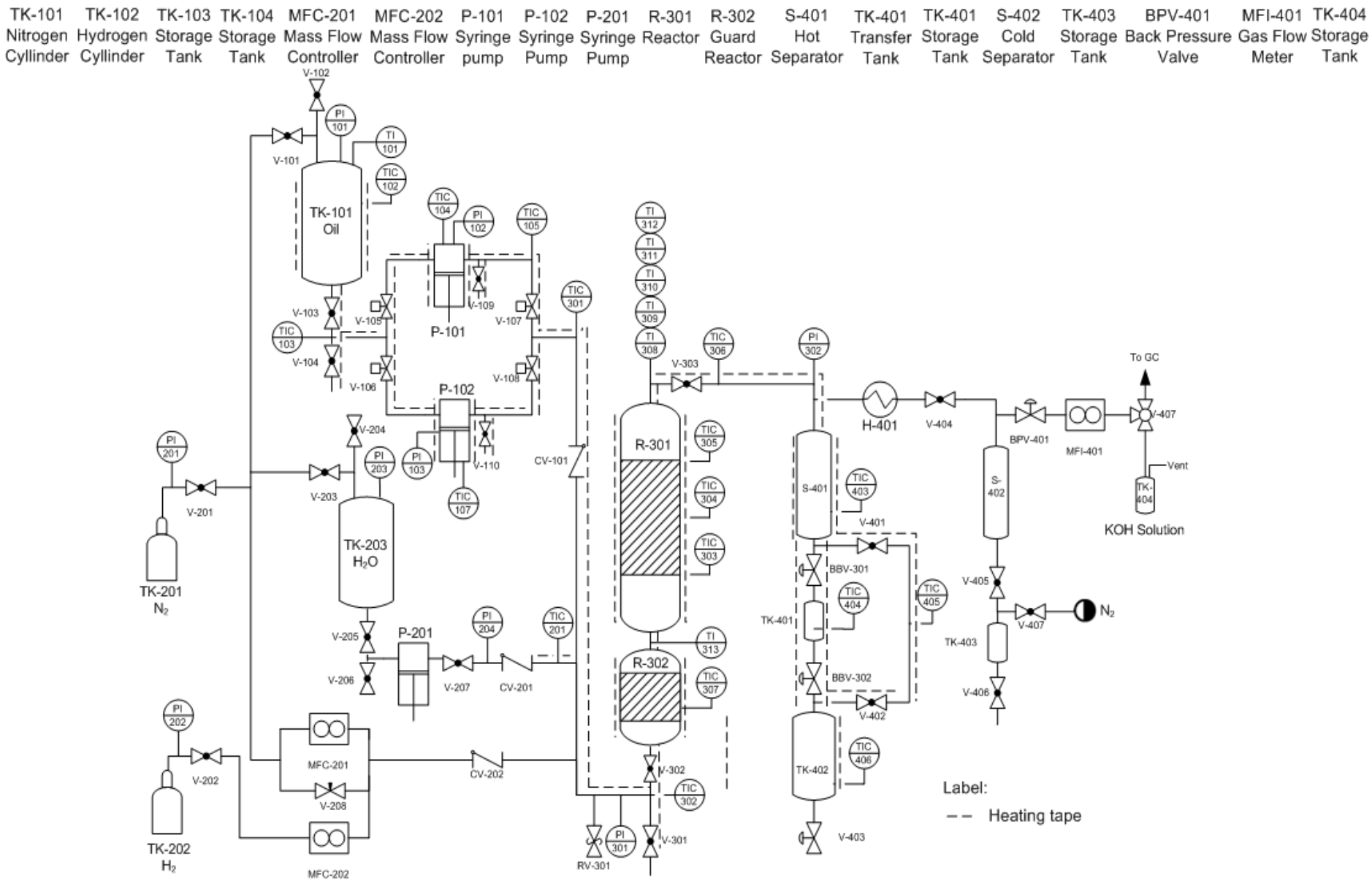

Figure 3-2: P&ID for experimental set-up II.

Heavy oils, such as the bitumen and diluted bitumen further described in section 3.3, are the other reactant that was also continuously pumped to the system. Because both set-ups were designed for long and high space velocity runs, oil was pumped through two Teledyne ISCO pump 500D working in parallel (P-101 and P-102). A set of four pneumatic automated valves (V-105 to V-108) operated the pair of pumps by continuously pumping and refilling them in alternate cycles. The pumps were connected one way to a 3-gallon tank (TK-101) where oil was kept for refilling, and the other way to the reaction system. Heating tapes were wrapped around lines and pumps to provide heating when necessary, i.e., when high viscosity oils were being used during operation. Similar heating elements on the lines towards the reactor were also used to increase bitumen temperature to reaction set-points.

3.1.2 Reaction Section

The reaction section was based on an up flow fixed-bed catalytic reactor. The reactor tube had 32cm of length, 1.91cm (3/4”) of external diameter, and 1.72cm of internal diameter and is represented by unit R-301 in Figure 3-1 and Figure 3-2. The total length of the reactor was filled with catalyst pellets. Five internal temperature indicators were located 6 cm apart from each other, and they are represented by TI-308, 309, 310, 311, and 312 in both diagrams. The internal temperature indicator closer to the bottom was located 4 cm above the reactor inlet. Three temperature controllers were used on this experimental set-up and their external temperature indicators (TIC-303, 304, and 305) were located right outside from the bottom, medium, and top internal temperature indicators, i.e. TI-308, 310, and 312. Three heating tapes, one for each external temperature indicator, were used to control the reaction temperature. The reactor is schematically represented by Figure 3-3.

In addition to the catalytic reactor (R-301), experimental set-up II also had a guard reactor that is represented by the unit R-302 in Figure 3-2. This guard reactor always carried a different, inexpensive formulation of a catalyst as further described in section 3.4. Its goal was to trap poisonous components in the feedstock that could potentially deactivate the main catalyst. The guard reactor length was 10 cm and it was fully filled with the material of choice. The guard reactor had one heating tape, one internal, and one external temperature indicator (respectively, TI-313 and TIC-307). The guard reactor was placed right at the bottom, or entrance, of the catalytic reactor.

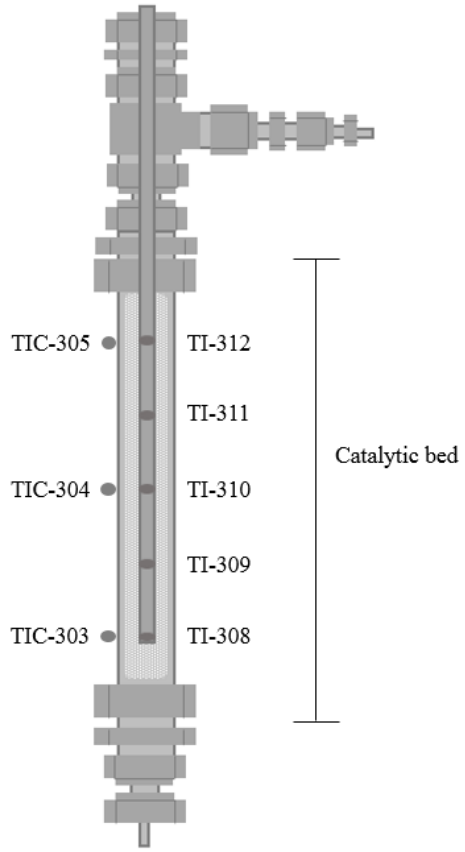

Figure 3-3: Schematic representation of fixed-bed reactor used on experimental set-ups.

3.1.3 Separation and Sampling Section

The product separation was performed in two steps in both experimental configurations. The first stage, called a hot-separator, was composed of a heated cylindrical reservoir that was kept at temperatures above the boiling point of water for the system pressure. On all diagrams, this separator is represented by unit S-401. On that separator, water, light oil fractions, and gases were separated from heavy oil fractions. The second separation step was performed by the cold-separator (S-402), which was kept at room temperature. It consisted of a cylindrical reservoir that separated water and light hydrocarbon products from gases. Gases proceeded to an Omega mass flow meter model FMA 4306 (MFI-401) and gas chromatograph (GC) for further composition analysis. The GC used was an SRI model 8610C built with a TCD detector for the analysis of gaseous products. Lights and water were separated by freezing water in an external refrigerator. Light oil fractions were mixed with heavy products to obtain the final oil product.

An automatic sampling system (Bang-Bang) was used for collecting the heavy hydrocarbons. The Bang-Bang system worked with two valves in series and a fixed volume between them. The valves were operated in such a way that it allowed sample transfer from the hot separator to a storage tank from time-to-time while it simultaneously isolated storage tanks from the main process. This operation ensured that pressure drops during sampling were minimized during sample collection. The Bang-Bang system is represented by the Bang-Bang valves (BBV-301 and BBV-302), a 125mL transfer tank (TK-401), and a 2-gallon storage tank (TK-402) on Figure 3-1 and Figure 3-2. The cold separator had a similar but manual system composed by manual valves (V-405 and V-406), and an intermediate volume of 20mL. Set-up II differed from set-up I on the cold separator system since it allowed re-pressurization of the cold separator (S-402) through a manual valve (V-407) after sampling. That procedure was necessary to keep reaction conditions when high pressure reactions took place.

Set-ups I and II also used a heat exchanger (H-401) to cool down the stream coming out of the hot separator and into the cold separator. The heat exchanger was a counter-current double-pipe heat exchanger that used cool water at 4°C as a cooling agent going through the external pipe. The cool water was provided by a VWR model 1180S chiller.

The experimental plant described in this section was used for the experiments in this project. Section 3.2 has a description of the experimental procedure used during reaction preparation and pilot plant operation.

3.2 Experimental Procedure

The experimental units described in section 3.1 were used to test different catalyst and conditions through this project. In section 3.2.1, a description of the procedure to prepare and mount the reactor is shown while, in section 3.2.2, catalyst treatment and reduction steps are described. The methodologies used to start-up and operate the reaction are given by sections 3.2.3 and 3.2.4, respectively. Finally, section 3.2.5 describes cleaning and regeneration procedures. It will be pointed out in the following sections whenever there is a considerable difference between procedures for different experimental set-ups.

3.2.1 Reactor Filling

A representation of the packed bed reactor (R-301) used on the experiments can be seen on Figure 3-3. To pack the reactor, the reactor exit (upper end) fittings, containing the thermocouple, were closed and attached to reactor empty tubing. The reactor was positioned upside down and glass wool was introduced through the tubing and placed on the exit (upper end) of the empty reactor. Using a funnel, the catalyst was loaded from the bottom of the reactor and vibration was applied to ensure particles were well packed. Another layer of glass wool was placed at the end of the catalyst bed. These glass wool layers ensured catalyst particles would not leave the reactor by backflow mixing or by being carried away in the stream. Finally, entrance fittings were closed and the reactor was placed on the system for leak testing. For set-up II, a guard bed reactor (R-302) is also used and the filling of this reactor followed the same procedure as the main reactor (R-301).

Leak tests were performed in the reactor to ensure fittings were properly closed and all leakages were identified and corrected prior to reaction. This procedure consisted of placing the reactor in the experimental set-up and pressurizing it with nitrogen to reaction pressures. Valves V-302 and V-303 in Figure 3-1 and Figure 3-2 were closed to isolate the reactor from the system. The reactor pressure was taken at different times for a minimum duration of two hours. The maximum acceptable pressure drop over the two hour period was 1% and, if the limit was not met, further measurements to stop leaks were taken until pressure drop limits were achieved.

3.2.2 Catalyst Treatment and Reduction

Most of the catalysts used in this project went through a calcination step done in an oven outside the experimental plant. Catalyst TR3, described in section 3.4, though, cannot be calcined due to reactivity between oxygen and the molybdenum carbide phase. For that reason, when TR3 was used on reactions, the catalyst passed through a thermal treatment, in which a nitrogen flow was set at 60mL/min, and the temperature was ramped to 500ºC at a rate of 10ºC/min. After reaching the set-point, external temperatures were adjusted in order to ensure that all five internal temperatures, i.e. TI 308-312, were on the set-point. The temperature was then maintained for five hours, after which it was returned to room temperature and nitrogen flow set to zero. Note that atmospheric pressure was used throughout this procedure.

All the tested catalysts also passed through a reduction step prior to the reaction. This step was necessary to ensure, when applicable, that metals in the catalyst were in their reduced form during the reaction. The reduction temperature was obtained by a temperature programmed reduction (TPR) experiment. The minimum reduction temperature varies from catalyst to catalyst but 500ºC proved to be a suitable temperature for all catalysts used during this project and, for that reason, the reduction temperature was kept constant. Reduction consisted of setting the hydrogen flow to 60mL/min and ramping the reactor temperature to 500ºC at a rate of 10ºC/min. After reaching the set-point, the temperature was maintained for 5 hours, after which it was returned to room temperature and hydrogen flow set to zero. Note that atmospheric pressure was used throughout the procedure. A schematic representation of both steps is shown in Figure 3-4.

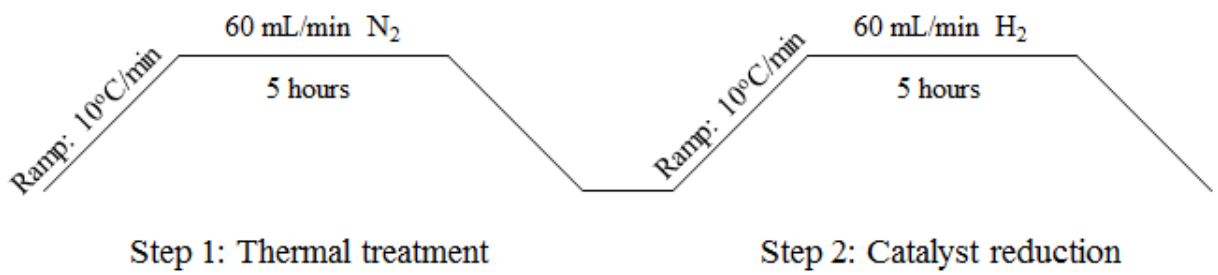

Figure 3-4: Schematic representation of pre-treatment conditions.

3.2.3 Reaction Start-up

Reaction start-up is a procedure that took place after reduction and with the goal of starting the plant operation and bringing all process variables to reaction conditions in a smooth manner. The first step on reaction start-up was to flush the remaining hydrogen in the system from the reduction step with nitrogen. For doing so, nitrogen was set to flow through the system at 60mL/min for, at least, one hour. Gas chromatography was used as a quantitative analysis to ensure that the gas at the system exit was purely nitrogen. While the system was being flushed with nitrogen, the temperatures in the pumping and separation sections lines were increased to the regular operation set-point.

After flushing the system with nitrogen, the pressure was increased to reaction conditions. This was done by manually closing the backpressure located at the exit of the system (BPV-401). The backpressure constrained the gas flow at the exit until pressure built up to the set-point value. A bypass valve located at the entrance of the system (V-208) was used to carefully increase system pressure to the set-point. After the system was fully pressurized, nitrogen flow rates were set to reaction levels and reactor temperatures were steadily increased to 10°C above the boiling point of water at reaction pressure. In set-up II, this same temperature was used in the guard reactor during this procedure step. For all experiments performed during this project, the reaction nitrogen flow rate was 5mL/min. Note that nitrogen is an inert gas for the reactions that take place and it ensures pressure stability in the system. Nitrogen flushing and system pressurization are schematically represented by step 1 in Figure 3-5.

The second step was to flow water through the reactor. At reactor start-up conditions, water was in the steam phase and the goal of this stage was to ensure that catalyst pores were well filled with steam. The procedure for doing so was to first pump water at 0.45mL/min for 20 minutes so all the lines leading to the reactor were filled with water/steam. Then, the water flowrate was changed so steam residence time in the reactor was one hour. Steam was left passing through the reactor for a total of 60 minutes, i.e. one residence time. This water treatment step can be visualized in step 2 in Figure 3-5.

Keeping the steam flowrate constant, oil was flowed through the system at 1mL/min for 10 minutes to allow the lines leading to the reactor to be filled. Then, oil flow rate was changed so its residence time in the reactor was one hour. Oil was left passing through the reactor for a total of 60 minutes,

i.e. one residence time. By the end of this step, both oil and water flow rates were set to the reaction flow rate. The oil flow rate was calculated based on the mass of catalyst, desired weight hourly space velocity (WHSV), and oil density as shown in Equation 3-1. The water flow rate was based on desired water-to-oil ratios (WOR) and it was calculated according to Equation 3-2. Common values for WOR used on this project were between 2.5 and 7.5%. This step is represented in Figure 3-5 by step 3.

$$\dot{V}_o = \frac{W_{cat} \times WHSV}{\rho_{oil}} \qquad \text{Equation 3-1}$$

$$\dot{V}_w = \dot{V}_o \times WOR \qquad \text{Equation 3-2}$$

The last step of the reaction start-up was to increase temperature to reaction condition. The heating rate used on this step was 10°C/min and external temperatures were adjusted in such a way that all five internal temperatures had minimal differences between them. In set-up II, the guard reactor final temperature set-point was 350°C throughout all reactions. Such a temperature was used to minimize thermal reactions and their effects on the results from catalytic reaction. The time zero for reaction was considered to be the time at which internal temperatures achieved the reaction set-point temperature.

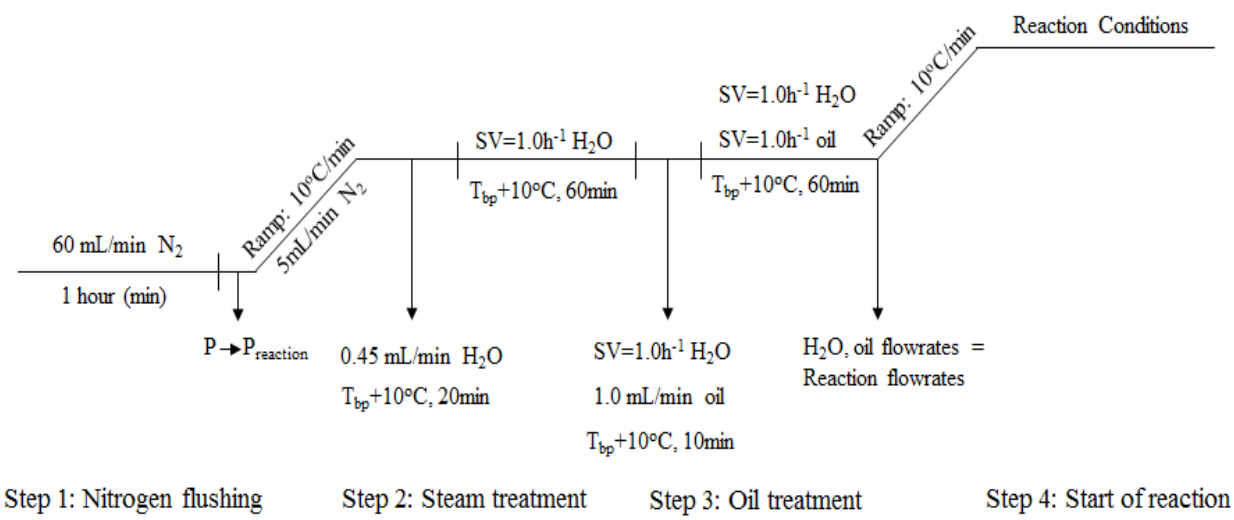

Figure 3-5: Schematic diagram of system start-up operation.

3.2.4 Reaction Operation

An automated sampling system (Bang-Bang) transferred hot separator contents to a storage tank that was drained to obtain hydrocarbon samples. Its operation is described in details in section 3.1.3. When closing a mass balance, sampling from the cold separator was done at the same time as a transfer from the hot separator to the products tank. The Bang-Bang valve cycle time (t_{BB}) in the automated sampling system was calculated from Equation 3-3, in which 125mL is the volume of the cylinder between the hot separator and the products tank.

$$t_{BB} = \frac{125mL}{\dot{V}_o} \qquad \text{Equation 3-3}$$

3.2.5 Reactor Cleaning and Catalyst Regeneration

After determining the end of reaction, all reactors went through a cleaning step that consisted of contacting catalyst with gasoline for 15 minutes at room temperature. To do so, all lines were cooled down to room temperature by shutting-off heating tapes. Gasoline was pumped to the system and kept in contact with catalyst by keeping valve V-303 closed. After 15 minutes, gasoline was allowed to proceed to hot-separator and removed from the system through the Bang-Bang valve system. Gasoline was used for being a solvent that could dissolve most of remaining hydrocarbons from the lines and reactor. When no further reaction was planned with the catalyst, the protocol of shut-off was conducted by turning off all pumps and closing LabView software. The reactor could then be withdrawn from the pilot plant and the catalyst recovered from its interior by opening the connection in the entrance and exit of the reactor and manually removing the spent catalyst.

In some cases catalyst regeneration was also performed after cleaning by burning the coke and remaining oil in the reactor in the presence of air. The regeneration was executed by passing air through the catalyst bed at 60mL/min and 430ºC. To reach this condition, the temperature was ramped at a rate of 10ºC/min. Since combustion reactions are exothermic, the extent of reaction could be followed by observing the variations in the internal temperatures inside the reactor and by monitoring with the gas chromatograph the amounts of CO_2 produced and O_2 spent. Since external temperatures were kept constant, when combustion reactions were taking place nearby an internal temperature indicator, its temperature increased. After all coke was burned in this reactor section, this temperature decreased back to its previous level. This cycle is exemplified by Figure

3-6, in which some temperatures were controlled during regeneration in order to avoid reaching too high temperatures that could have damaged the catalyst structure. For instance, the temperature profile of TI-308 has two temperature adjustments, one around 20h of regeneration and the other around 30h of regeneration. When all internal temperature indicators had passed through an increase and decrease of temperature and CO_2 was not detectable anymore by gas chromatography, the regeneration was completed. After regeneration, the described reduction and start-up of the reaction were performed. The nitrogen pre-treatment was not necessary at this stage.

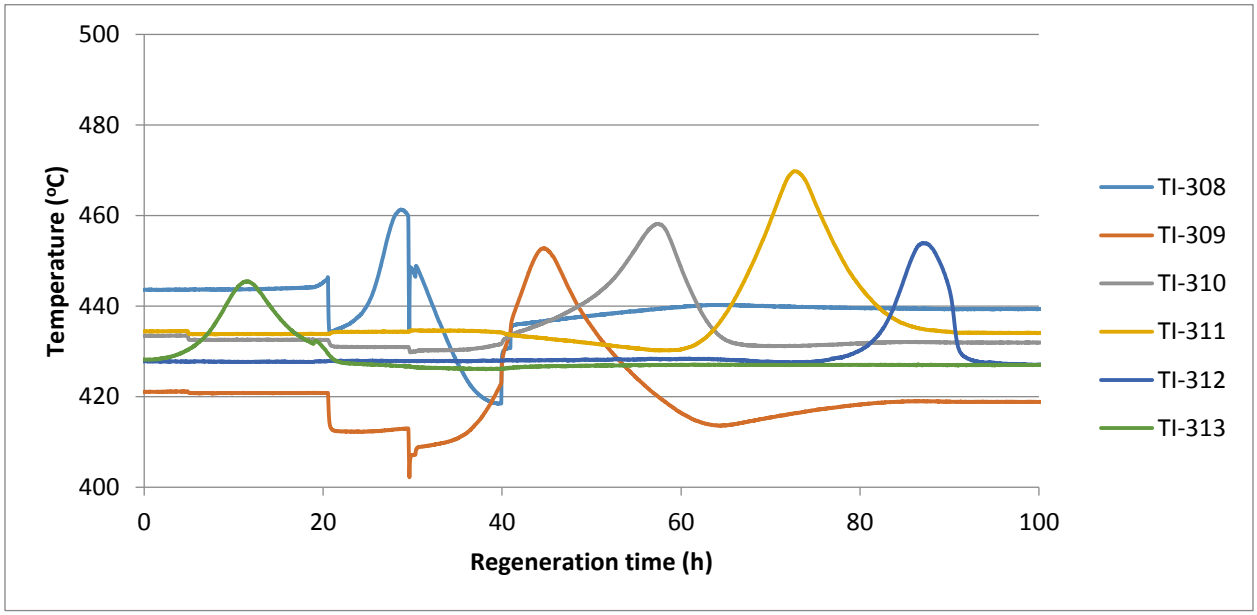

Figure 3-6: Temperature profile during regeneration for an internal temperature indicator.

The procedures described in this section were used in the experiments throughout this project. Section 3.3 contains a description of the feedstocks used in these experiments.

3.3 Feedstock

Two different feedstocks, both of them provided by Cenovus Energy, were used in this project. The first, a Cenovus Energy bitumen that was sent to a third party company for cutting. The nominal value of the cut was 220°C+, which means that it did not contain the lighter fractions of bitumen that have boiling point below 220°C. The other feedstock was Cenovus Energy partially diluted bitumen (dilbit). Table 3-1 has the main properties for both feedstocks while Figure 3-7 has the simulated distillation profile of the feedstocks. Section 3.5 has a review of the techniques used to obtain the properties reported in Table 3-1. Note that the nominal cut values for the bitumen cuts do not necessarily imply that the initial boiling point (IBP) is the given value. In fact, the cut 220+ has an IBP of 160.9^{o}C, which just reflects typical difficulties and inaccuracy of properly cutting bitumen fractions in industrial set-ups. Table 3-2 contains the feedstock used for every catalyst tested during the project. An analysis of Table 3-1 values shows that both feedstocks have very similar properties and, thus, they can be used for comparison of different catalysts and conditions. The only value that differs considerably between both feeds is their viscosity.

Table 3-1: Feedstock properties.

Property	**Bitumen 220+**	**Diluted Bitumen**
^{o}API	8.9	11.8
Total Acid Number (mg_{KOH}/g)	1.75	1.70
Microcarbon	13.1	12.8
Viscosity (cP at 40°C)	18,500	3,300
Bromine Number ($g_{Br2}/100g$)	13.4	17.1
Cut Distribution:		
Naphta (IBP-190°C)	0.9%	2.6%
Kerosene (190-260°C)	3.1%	3.4%
Diesel (260-343°C)	10.4%	9.9%
Distillates (343-545°C)	34.7%	32.4%
Residue (>545°C)	50.9%	51.7%

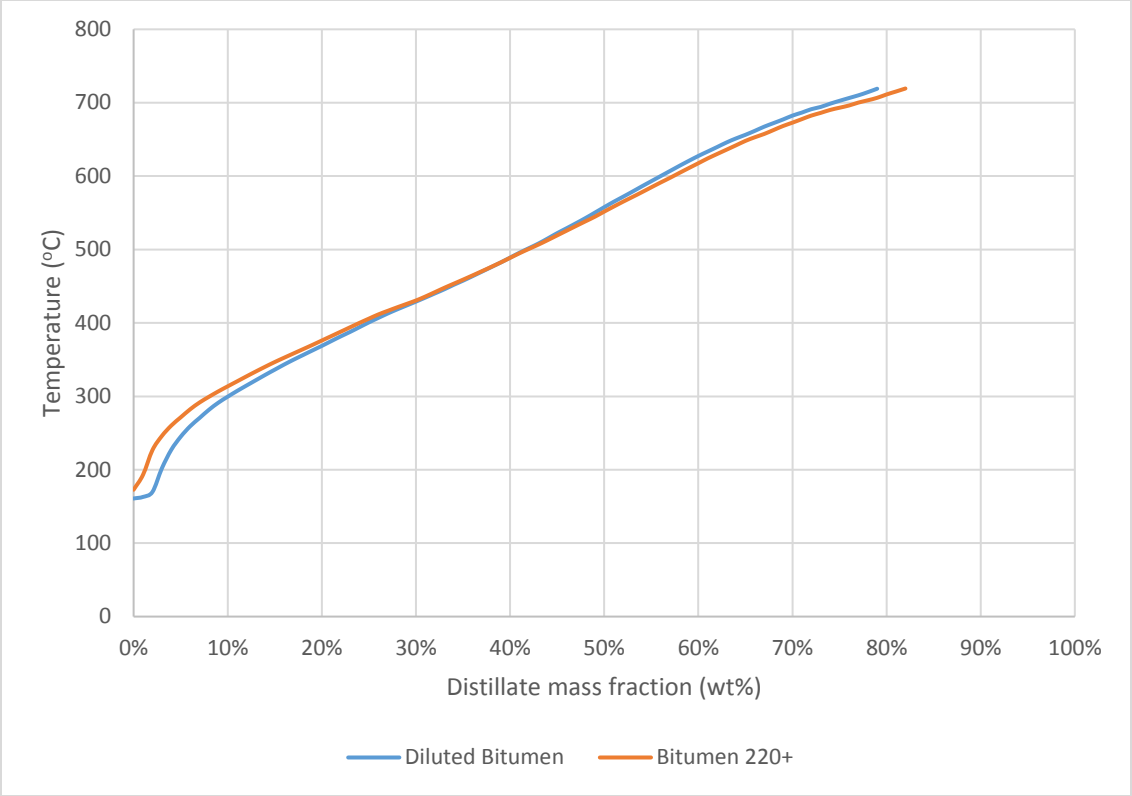

Figure 3-7: Simulated distillation for the feedstocks used throughout the project.

The feedstock described in this section went through catalytic steam cracking experiments that took place in the pilot plant described in section 3.1 and that was operated using the procedures shown in section 3.2. Section 3.4 has a description of the catalysts used in these experiments.

3.4 Catalyst Preparation

During the course of this project, the tested catalysts were prepared and provided by postdoctoral fellow Dr. Gerardo Vitale. The catalyst formulations used in this project contained a combination between the phases discussed in this thesis literature review (refer to section 2.7, page 34, for more information). Table 3-2 summarizes the metal loading and catalytic phases on each one of the catalysts used in this project.

Catalyst TR1 uses a silicalite-I zeotype material to support active sites. The silicate material has silicon and oxygen as only building blocks and has the MFI structure. This structure is doped with metals and has no aluminum in its composition. This type of structure limits the amount of active sites that can be effectively loaded to the structure, thus catalyst TR1 is the one with the lowest metal content. Section 2.7.2 contains a literature review about the material and preparation of this type of catalyst. This catalyst also contains a binder which is a material commonly used on catalyst preparation for shaping and enhancing mechanical properties.

Catalyst TR2 has two different precursors in its formulation. The first one, the silicalite-I zeotype material, identical to the one used for catalyst TR1. The second structure is a calcined hydrotalcite structure that allows the production of a supported catalyst with good metal dispersion. This type of structure allows a higher metal loading thus being a good material for complementing the silicate based catalyst. It also acts as a binder, enhancing its mechanical properties. Section 2.7.1 contains a literature review about the material and preparation of this type of catalyst.

Catalyst TR3 is a combination of the supported catalyst made out of the calcined hydrotalcite structure used on catalyst TR2 and molybdenum carbide. The intent of this combination is to take advantage of the high amounts of hydrogen produced on the catalytic reactions to upgrade the products since molybdenum carbide catalysts are well known to be able to perform hydrogenating reactions. Section 2.7.3 has a literature review about the material and preparation of this type of catalyst.

Catalyst TR4 is a similar catalyst to TR1 but contains a larger amount of metals doped on its structure. Furthermore, the silicalite-I structure preparation was further developed by cation exchanging sodium ions with proton ions (H^+) to avoid sodium washing in the catalyst during reaction.

Finally, catalyst TR5 is similar to catalyst TR2 but contains a silicalite-I structure doped with a higher amount of metals. The supported catalyst made from calcined hydrotalcite structure is also the same as used in catalyst TR2.

Table 3-2: Catalyst components and metal composition.

Catalyst	**TR1**	**TR2**	**TR3**	**TR4**	**TR5**	**Guard**
Component Content						
Silicalite-I (wt%)	75	75	0	75	75	0
Hydrotalcite (wt%)	0	25	63	0	25	10
Molybenum carbide (wt%)	0	0	6	0	0	0
Binder 1 (wt%)	0	0	22	0	0	72
Binder 2 (wt%)	25	0	9	25	0	15
Other (wt%)	0	0	0	0	0	3
Total Metal load						
%wt Ni	2.1	6.0	9.8	2.2	6.8	1.5
%wt Ce	1.7	7.4	13.9	1.9	8.5	2.4
%wt Mo	0	0	5.2	0	0	0
%wt Na	1.1	1.1	0.5	0.2	0.9	0
%wt Fe	0	0	0	0	0	1.7
%wt Mg	0	2.9	10.5	0	2.9	1.2
Feedstock	Cut 220°C+	Cut 220°C+	Dilbit	Dilbit	Dilbit	Dilbit
Experimental Set-Up	I	I	II	II	II	II

The products from the catalytic steam cracking experiments that used the catalysts described in this section were analyzed in order to evaluate their physical and chemical properties. Section 3.5 has a description of the methodologies and analytical procedures used throughout this thesis.

3.5 Sample Analysis

The liquid and gas samples obtained during the experiments in this project were analyzed to fully characterize their properties. In this section, the analysis used to obtain oil and gas properties are listed and explained.

3.5.1 Gas Chromatography

Gas chromatography (GC) was the main gas analysis done during the course of the project. GC gives a molar (or volumetric) composition of the gases that elutes through its columns. Standard calibration gases were used to calibrate TCD signals and their composition, and measurement error can be seen in Table 3-3.

Table 3-3: Standard calibration gas composition.

Gas	**Standard 1 %mol**	**Standard 2 %mol**	**Average Relative Error (%)**
Hydrogen (H_2)	13.6%	10.0%	3.4%
Carbon monoxide (CO)	0.00%	15.0%	0.6%
Carbon dioxide (CO_2)	3.99%	10.0%	0.9%
Methane (CH_4)	3.99%	5.00%	0.5%
Ethane (C_2H_6)	15.9%	5.00%	0.8%
Ethylene (C_2H_4)	1.50%	0.00%	1.4%
Propane (C_3H_8)	8.21%	0.00%	0.9%
Propylene (C_3H_6)	3.10%	0.00%	1.0%
n-Butane (n-C_4H_{10})	2.60%	0.00%	1.3%
iso-Butane (i-C_4H_{10})	1.00%	0.00%	1.4%
1-Butene (1-C_4H_8)	2.39%	0.00%	1.5%
iso-Pentane (i- C_5H_{12})	0.10%	0.00%	6.5%
Nitrogen (N_2)	0.00%	5.00%	0.8%
Helium	Balance	0.00%	n/a
Argon	0.00%	Balance	n/a

The GC used was an SRI model 8610C that contains one thermal conductivity detectors (TCD), one flame ionization detector (FID), and one helium ionization detector (HID). The TCD was the detector most commonly used during the experiments and its principle of operation is based on the

differences in thermal conductivity in the carrier and analyzed gases. Since every compound has its characteristic thermal conductivity, they can be detected and measured by a TCD. The carrier gas used for the experiments was helium, which is the most commonly used gas for this purpose. TCD is mainly a Wheatstone bridge which obtains an analog signal that is acquired by current unbalancing due to thermal conductivity differences in sample and carrier gas (SRI-Instruments, 2005).

3.5.2 Total Acid Number (TAN)

The acidity of the samples was measured by following the titration methodology described by the norm ASTM D664. In ASTM D664, the titrant is an alcoholic potassium hydroxide solution (KOH) with a concentration of 0.1 mol/L. The solvent solution is used to dilute the oil sample and is volumetrically composed by 50.0% toluene, 49.5% iso-propanol, and 0.5% water. The solution blank value is always measured prior to sample determination so its acidity is not double counted (ASTM-International, 2011). For this technique, the repeatability is reported to be around 0.12mg_{KOH}/g for the common values of feedstock used in this project, while reproducibility is around 0.20 mg_{KOH}/g (Nadkarni, 2007). The apparatus used for total acid number measurement was a Metler-Toledo T50 Titration Excellence. A minimum of 1 gram of oil sample is measured on a titration vessel, diluted using 60mL of solvent, and placed on an auto-sampler tray. Electrode, titration solution dispenser, and mixer are placed inside titration vessel for measurements. The titration is potentiometrically monitored with the electrode and the inflection point determines the solution acidity. Final total acid number also depends on blank value and mass of oil inserted. The TAN for a sample (TAN_s) can be determined using the titrant volumes used for sample and blank (V_s and V_b, in mL), the concentration of titrant solution (C_{KOH}, in mol/L), and KOH molecular weight (M_{KOH}, in g/mol), as shown in Equation 3-4. The TAN conversion (X_{TAN}) can be calculated by Equation 3-5, using the TAN of the sample and feed.

$$TAN_s = \frac{(V_s - V_b) \times C_{KOH} \times M_{KOH}}{W_s} \qquad \text{Equation 3-4}$$

$$X_{TAN} = 1 - \frac{TAN_s}{TAN_f} \qquad \text{Equation 3-5}$$

3.5.3 Viscosity

The viscosity of different oil samples was determined using a Brookfield model RVDV-II+PRO viscometer that allows viscosity measurements over a wide range of temperatures. A Brookfield TC-502 bath is used to set the temperature for the viscosity measurement. For the viscosity measurement procedure, a layer of sample is placed on a cup in order to cover the face of a selected spindle. After reaching the desired temperature, spindle rotation is then applied and manipulated until a torque around 30-70% of the maximum 0.7187N/m is achieved. When this is achieved, viscosity can be read right from the viscometer. Errors for this method are around 5%. Due to the high viscosity of feedstocks and products processed on this project, the temperature of 40ºC was selected for all viscosity measurements. Viscosity reduction was calculated throughout this thesis using Equation 3-6.

$$Viscosity\ Reduction = 1 - \frac{\mu_s}{\mu_f} \qquad \text{Equation 3-6}$$

3.5.4 High Temperature Simulated Distillation (SimDist)

SimDist is a laboratory scale technique used to determine the boiling point profile of an oil sample and it allows each oil fraction percentage to be calculated. The profile is obtained by the software Simdist Expert after analyzing signals provided by Agilent Technologies Gas Chromatograph model 7890A. The conditions and methodology followed norm ASTM D7169 from 2005. In this technique, a solution is made out of 0.15g of oil sample and 20mL of CS_2. 1µl of this solution is then injected into a temperature-programmed chromatograph column. The operation is based on a steady increase in temperature that gradually vaporizes and elutes part of the hydrocarbons, depending on their boiling point. Those molecules are flown into a detector that measures the amounts of sample eluted in a given time and temperature (Banerjee, 2012). The gas chromatograph is calibrated using a range of different molecular weight alkanes at given concentrations. It has been found that HTSD is able to determine fraction boiling points up to 3ºC errors and is able to reproduce fraction yields with standard deviations around 0.5% (Raia et al., 2000). Alternatively, it has also been reported errors of 1% for samples with boiling point below 550ºC and of 4% for heavier fractions (Rodriguez-DeVecchis et al., 2015). Examples of SimDist curves can be seen on Figure 3-7 where all feedstocks used are represented. Through a SimDist curve, the cut composition of an oil can be determine and, throughout this thesis, the oil fractions

and respective boiling point followed the ranges shown in Table 3-1. The calculations of residue conversions (X_R) were also based on SimDist data and followed Equation 3-7, in which R is the residue content of a sample, i.e. the oil fraction with boiling point above 545°C.

$$X_R = 1 - \frac{R_s}{R_f} \qquad \text{Equation 3-7}$$

3.5.5 Oil Density and API Gravity

Oil density is an important property used to measure oil quality. This measurement was performed in this project by a Rudolph Research Analytical density meter model DDM 2911 that measures density based on standard method D1250-08. This equipment is capable of measuring densities ranging from 0-3 g/cm^3 with an accuracy of 0.0001g/cm^3. Due to the difficulties related to the high levels of viscosity of samples used, the samples needed to be diluted in a solvent prior to measurement. The solutions consisted of the sample in toluene at 0.5 wt% and 1.0 wt%. The measurements were based on oscillatory frequency of a U-tube filled with the solution containing the sample. The frequency varies proportionally with the mass inside the constant volume U-tube. The sample gravity was obtained by extrapolation of values to 100 wt% concentration of sample. The API gravity can be calculated according to Equation 3-8, in which SG is the oil specific gravity. The API gravity absolute increase or decrease is commonly reported throughout this thesis and was calculated by Equation 3-9.

$$^{o}API = \frac{141.5}{SG} - 131.5 \qquad \text{Equation 3-8}$$

$$^{o}API\,Absolute\ Change = API_s - API_f \qquad \text{Equation 3-9}$$

3.5.6 Microcarbon Residue

Carbon residue values are an important quality parameter for oils since they give the tendency of the amounts of carbonaceous material deposition under degradation conditions similar to those used at the test condition (Nadkarni, 2007). For instance, residues under delayed-coking processing usually produce 1.5-2.0 times more coke than their Conradson carbon value while, for fluid coking and flexicoking, the range is 1.1-1.4 (Le Page et al., 1992). For the range of values used in this project, repeatability is reported to be around 3%, while reproducibility is around 10% (Nadkarni, 2007). The analytical method consists in submitting a certain amount of sample to heating for a determined amount of time under an inert atmosphere. The carbonaceous residue can be weighted

and proportionally compared to the initial amount of sample to give the microcarbon residue content of a sample. During this project, 20 mg of samples were submitted to temperatures of 520ºC for 20 minutes under a nitrogen atmosphere for microcarbon determination. Equation 3-10 shows how to obtain the final microcarbon value (MC). Microcarbon relative increase or decrease is commonly reported throughout this thesis and it is calculated through Equation 3-11.

$$MC_s = \frac{W_{residual}}{W_s} \times 100\% \qquad \text{Equation 3-10}$$

$$\%Microcarbon\ Relative\ Change = \frac{MC_s}{MC_f} - 1 \qquad \text{Equation 3-11}$$

3.5.7 Water Content

Although a separator was used on the system to separate water from heavy oil products, this separation was not fully completed and, therefore, a measurement of water content in oil samples was necessary. For this measurement, a Mettler-Toledo Titrator model C20 was used to perform Karl-Fisher Water Determination method. This method uses the coulometric anode solution Coulmat A, produced by Aquastar®, and contains methanol, chloroform, imidazole, and iodine that reacts with water and in which the reaction extension can be measured coulometrically to determine the amount of water consumed. The samples were dissolved in tetrahydrofuran (THF) prior to titration and blank measurement was performed to ensure water in solvent was not being taken into account.

3.5.8 Bromine Number

The level of unsaturation in an oil sample is an important property to keep track of since it is related to the tendency of that oil to foul the catalyst. The olefin content in a sample can be determined by the bromine number that can be measured by method ASTM D1159. The method is accurate when dealing with light oil fractions but the presence of resins in whole crudes can lead to erroneous results. Bromine numbers are given in grams of bromine (Br_2) necessary to saturate 100 grams of sample (Banerjee, 2012). The solvent used was a mixture of glacial acetic acid, dichloromethane, methanol, and sulfuric acid and the titrant was a solution composed by potassium bromate and potassium bromine at 0.1 N. A Mettler-Toledo T50 Titration Excellence was used to perform the low temperatures titration (below 4ºC) that is monitored potentiometrically. Low temperatures were used to avoid side reactions with heterocycles and aromatic molecules. The relative increase

or decrease of the bromine number is commonly reported throughout this thesis and it is calculated as shown in Equation 3-12, in which Br represents the bromine number of a sample.

$$Bromine\ Number\ Relative\ Change = \frac{Br_s}{Br_f} - 1 \qquad \text{Equation 3-12}$$

3.5.9 Metal Content

Another major fouling component for catalytic applications that is present in heavy oils is metal compounds. The amount of metals on a material can be determined by inductively coupled plasma (ICP). The equipment used for this analysis was an IRIS Intrepid optical emission spectrometer-ICP developed by Thermo Electron Corp. The error of this technique is 1% in the concentration of each one of the metals present (Rodriguez-DeVecchis et al., 2015). Prior to ICP analysis, the sample was mixed with nitric acid (HNO_3) and phosphoric acid (H_3PO_4) or hydrochloric acid (HCl) and the solution was digested in a CEM Mars 6 microwave digester. The acid addition step was necessary to transform metals in the oil sample into water soluble material. Note that this technique can also be used to determine metal content in solids such as the catalyst used in the project. This methodology was used to determine the total metal loading of the catalyst presented on Table 3-2.

The experimental plant, methodologies, and analytical procedures described in this chapter were used in the experimental section in chapter 4. In section 4.1, thermal reaction, i.e., with no catalyst, is evaluated towards TAN reduction and other relevant oil properties. In section 4.2, the catalytic reaction is evaluated and compared to thermal reaction. This section also contains a kinetic evaluation of the catalyst. Finally, section 4.3 contains a comparison between different catalysts for the selection of the best performing catalyst towards TAN reduction.

4 TAN Reduction and Catalyst Selection

The pilot plant, procedure, and sample characterization methodologies described in chapter 3 of this thesis were used in order to evaluate thermal and catalytic reactions towards total acid number reduction.

In this section, the results obtained are presented and discussed. The catalytic experiments were performed using five different catalysts and results were analyzed in order to identify the catalyst able to reduce acidity at the least severe conditions. A thermal reaction was carried out in order to compare and understand the effects of catalytic behavior on product quality.

Crude oils are a complex mixture of hydrocarbons, as discussed in section 2.1 of this thesis. Thus, a very complex system of reactions takes place when temperature, pressure, and other reactants are contacted with the feedstock. Some of the reactions that are expected to take place thermally or catalytically in the reactor were discussed in section 2.6, and includes: hydrocarbon steam reforming (Equation 4-1), water splitting (Equation 4-2), and steam cracking (Equation 4-3).

$$\mathrm{C_nH_x + 2n\ H_2O \rightarrow n\ CO_2 + (2n + x/2)\ H_2} \qquad \text{Equation 4-1}$$

$$\mathrm{2H_2O \rightarrow 2H^* + 2OH^*} \qquad \text{Equation 4-2}$$

$$\mathrm{R - CH_2 - R_n + 2H_2O \rightarrow RH + CO_2 + 2H_2 + R_nH} \qquad \text{Equation 4-3}$$

In addition, partial steam cracking (Equation 4-4), incomplete partial steam cracking (Equation 4-5), thermal dehydrogenation (Equation 4-6), catalytic hydrogenation (Equation 4-7), and naphthenic acid steam decarboxylation (Equation 4-8) reactions are also all part of the set of reactions that are expected to take place.

$$R - CH_3 + 2H_2O \rightarrow RH + CO_2 + 3H_2 \qquad \text{Equation 4-4}$$

$$R - CH_3 + H_2O \rightarrow RH + CO + 2H_2 \qquad \text{Equation 4-5}$$

$$R_1 - CH_2 - CH_2 - R_2 \rightarrow R_1 - CH = CH - R_2 + H_2 \qquad \text{Equation 4-6}$$

$$R_1 - CH = CH - R_2 + H_2 \rightarrow R_1 - CH_2 - CH_2 - R_2 \qquad \text{Equation 4-7}$$

$$R - CH_2 - COOH + 2H_2O \rightarrow RH + 2CO_2 + 3H_2 \qquad \text{Equation 4-8}$$

However, those reactions do not include the totality of reactions that take place. For instance, polymerization and condensation reactions are not shown, neither are desulfurization, denitrogenation, and demetallation reactions that can take place in the presence of hydrogen.

For complex mixtures of hydrocarbons such as those found in heavy oils, desirable reactions are hard to specify and track and, for that reason, physical and chemical properties of the products are used to understand the effectiveness of a reaction. For instance, the decarboxylation of naphthenic acids on oil can be tracked by measuring the total acid number reduction on the products in relation to the feedstock. In addition, heavy molecule cracking reactions can be assessed by tracking vacuum residue conversion, API gravity, and viscosity, which are properties related to the level of upgrading. Microcarbon indicates changes in the tendency to form carbonaceous material when products are submitted to further processing. A comprehensive understanding of the products properties on catalytic and thermal reactions is imperative to understand the benefits of using a selected process.

4.1 Thermal Run Results

In order to properly evaluate the performance of a catalyst, the purely thermal effects of a reaction must be understood and used for comparison. The thermal effects are related to the capability of molecules to react without the use of active sites in a catalyst to promote the reaction. Possible improvements related to the use of a catalyst are: higher product yields, better product quality, and smaller undesirable side reaction yields.

The thermal reaction was performed by entirely filling the reactor shown in Figure 3-3 with carburundum. This material was pre-washed in an acid solution in order to dissolve any metals attached to it that could present catalytic activity during reaction. The addition of carburundum was necessary in order to ensure that flow patterns were similar to the catalytic experiments. The thermal reaction followed the same pre-treatment procedure as in catalytic experiments.

4.1.1 Thermal Kinetics

The thermal reaction, i.e. with no catalyst, was performed in three different temperatures and space velocities in order to analyze the effects of different variables on the process. Each condition was left for a minimum of 24 hours and it was comprised of three mass balances. The results shown in this section are average values for the three mass balances. Table 4-1 shows the conversions for total acid number and Figure 4-1 shows a graphical representation of the same data.

Table 4-1: Products TAN and TAN conversion for thermal reaction (no catalyst) at varying temperature, and space velocity; and constant pressure (2,760kPa), and water-to-oil ratio (5%) .

	Space Velocity (h^{-1})	**Temperature (ºC)**		
		360	**370**	**380**
TAN (mg_{KOH}/g)	0.26	1.48	1.28	1.12
	0.52	1.58	1.48	1.31
	1.04	1.60	1.54	1.53
	Feedstock		1.75	
TAN conv.	0.26	15.6%	27.0%	35.7%
	0.52	9.5%	15.3%	25.3%
	1.04	8.8%	12.1%	12.3%

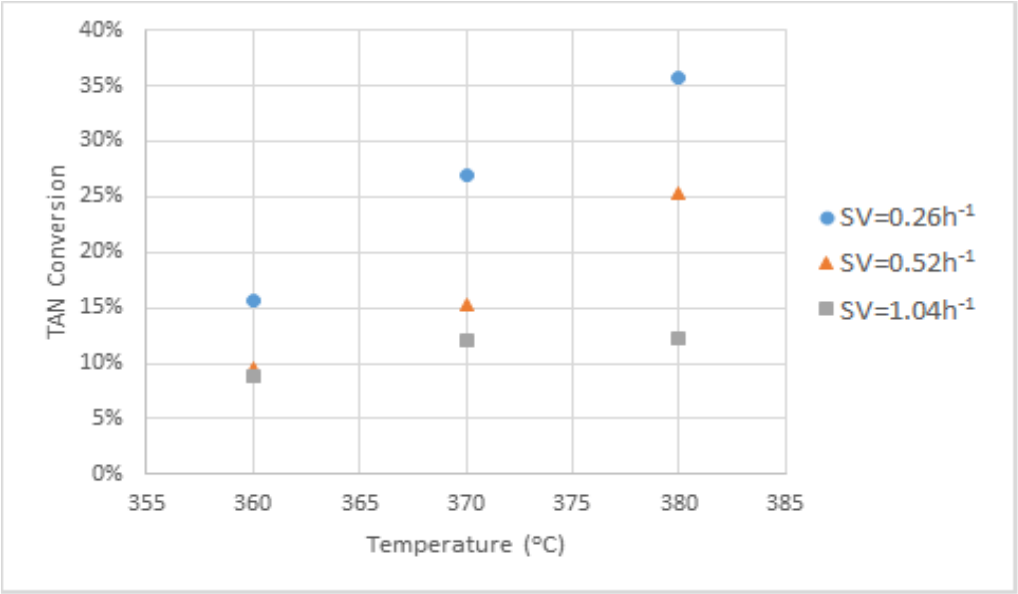

Figure 4-1: Products total acid number conversion (X_{TAN}) for thermal reaction at different temperatures and space velocities.

Using the results from Table 4-1, the activation energy and pre-exponential factor for the thermal reaction were calculated. A first order model, following the Arrhenius equation, was used to describe the reaction. In a similar study involving decarboxylation of naphthenic acids using supercritical water and no catalyst, it was found that a first-order reaction was suitable for the kinetics mechanism (Mandal et al., 2012). That is an indication that reactions involving naphthenic acids and water reactions tend to involve first-order kinetics. Verification of such an assumption was done later on in this section. The kinetics equation is shown in Equation 4-9 while the Arrhenius law for the kinetic constant is shown in Equation 4-10.

$$-r_{TAN} = k \times TAN \qquad \text{Equation 4-9}$$

$$k = k_0 \times exp\left(\frac{-E_A}{RT}\right) \qquad \text{Equation 4-10}$$

In Equation 4-9, the rate of reaction (r) is related to the reaction kinetic constant (k) and the total acid number of the reactants (TAN). Recall that the TAN is a measurement of concentration of acid sites per gram of hydrocarbon. Equation 4-10 gives a relationship in which the kinetic constant (k) changes with temperature through its pre-exponential factor (k_0) and activation energy (E_A). The kinetics model developed considers a non-dependence in relation to the water content. This is so, since for each gram of bitumen, approximately $3x10^{-5}$ moles of carboxyl groups are present if a TAN value of $1.7mg_{KOH}/g$ is used. Considering the flowrate proportions between water and oil, for the same one gram of bitumen, a total of 0.052 grams of water are available, which roughly represents $3x10^{-3}$ moles of water. Thus, water was in excess of 100 times in relation to carboxyl groups and its proportion varied little during the total acid number reaction, which allowed water partial pressure to be omitted from the kinetics equation. As a result, water was consistently recovered mostly unreacted during reaction on the cold separator. The water mass balance, i.e. the ratio between the amount of water recovered and the amount of water fed to the system, was consistently above 80% even with all losses through gases or liquid sampling.

Equation 4-10 can be linearized by taking logarithms on both side of the equation as shown in Equation 4-11.

$$\ln k = \ln k_0 - \frac{E_A}{RT} \qquad \text{Equation 4-11}$$

Thus, a plot of the kinetic constant logarithm versus the inverse of temperature allowed the calculation of the pre-exponential factor and activation energy. Equation 4-9 can also be used to

allow the calculation of the reaction kinetic constant using experimental values. This calculation can be seen through equations 4-12 to 4-21. Equation 4-12 substitutes TAN as a function of the feedstock TAN (TAN_f) and TAN conversion (X_{TAN}).

$$-r_{TAN} = k \times TAN = k \times TAN_f(1 - X_{TAN}) \qquad \text{Equation 4-12}$$

Equation 4-13 is the packed-bed plug flow reactor kinetics equation derived from the general mole balance equation (Fogler, 2006), and it introduces the catalyst weight (W) and the molar flow of acidic molecules (F_{TANf}).

$$F_{TAN_f}\frac{dX_{TAN}}{dW} = -r_{TAN} \qquad \text{Equation 4-13}$$

Equation 4-14 is the substitution and re-arrangement of Equation 4-12 combined with Equation 4-13.

$$\frac{dX_{TAN}}{(1 - X_{TAN})} = \frac{k \times TAN_f}{F_{TAN_f}}dW \qquad \text{Equation 4-14}$$

Equation 4-15 is the integral solution of the left hand side of Equation 4-14, while Equation 4-16 is the solution of the right hand side.

$$\int_0^{X_{TAN}} \frac{dX_{TAN}}{(1 - X_{TAN})} = -\ln(1 - X_{TAN}) \qquad \text{Equation 4-15}$$

$$k\frac{TAN_f}{F_{TAN_f}}\int_0^W dW = k\frac{TAN_f}{F_{TAN_f}}W = k\frac{TAN_f}{TAN_f\dot{w}_0}W = k\frac{W}{\dot{w}_0} = kt_{res} \qquad \text{Equation 4-16}$$

Note that in Equation 4-16, F_{TANf} can be substituted by the acidic molecules concentration per mass of feedstock (TAN_f) and the oil weight flowrate (w_0). Furthermore, the ratio between catalyst weight and weight flowrate was defined as the residence time (t_{res}). Note that for the thermal reaction there was no catalyst being used, thus the weight flowrate used was the same as in the catalytic reaction for a given residence time.

Equation 4-17 recalls and defines the concept of total acid number conversion (X_{TAN}) and Equation 4-18 combines Equations 4-14, 4-15, and 4-16.

$$X_{TAN} = 1 - \frac{TAN_p}{TAN_f} \qquad \text{Equation 4-17}$$

$$\ln(1 - X_{TAN}) = -kt_{res} \qquad \text{Equation 4-18}$$

Equation 4-19 makes a mathematical manipulation of Equation 4-18 to allow kinetic constant calculation based on residence time and TAN conversion.

$$k = \frac{-\ln(1 - X_{TAN})}{t_{res}} \qquad \text{Equation 4-19}$$

Finally, Equation 4-20 represents the relationship between weight hourly space velocity (WHSV) and residence time while Equation 4-21 applies this concept into Equation 4-19.

$$WHSV = \frac{1}{t_{res}} \qquad \text{Equation 4-20}$$

$$k = -WHSV \times \ln(1 - X_{TAN}) \qquad \text{Equation 4-21}$$

The assumption of a first order reaction can be evaluated using Equation 4-22, which is a modified version of Equation 4-18.

$$-\ln(1 - X_{TAN}) = k t_{res} \qquad \text{Equation 4-22}$$

According to this equation, for a constant k, a plot of $-\ln(1-X_{TAN})$ versus different residence times should give a straight line with intercept at the origin. Through Equation 4-10, one can see that kinetic constant is only a function of temperature and therefore, reaction values for the same temperature, but different space velocities, can be used for first order reaction evaluation. The plot suggested by Equation 4-22 at different temperatures can be seen in Figure 4-2.

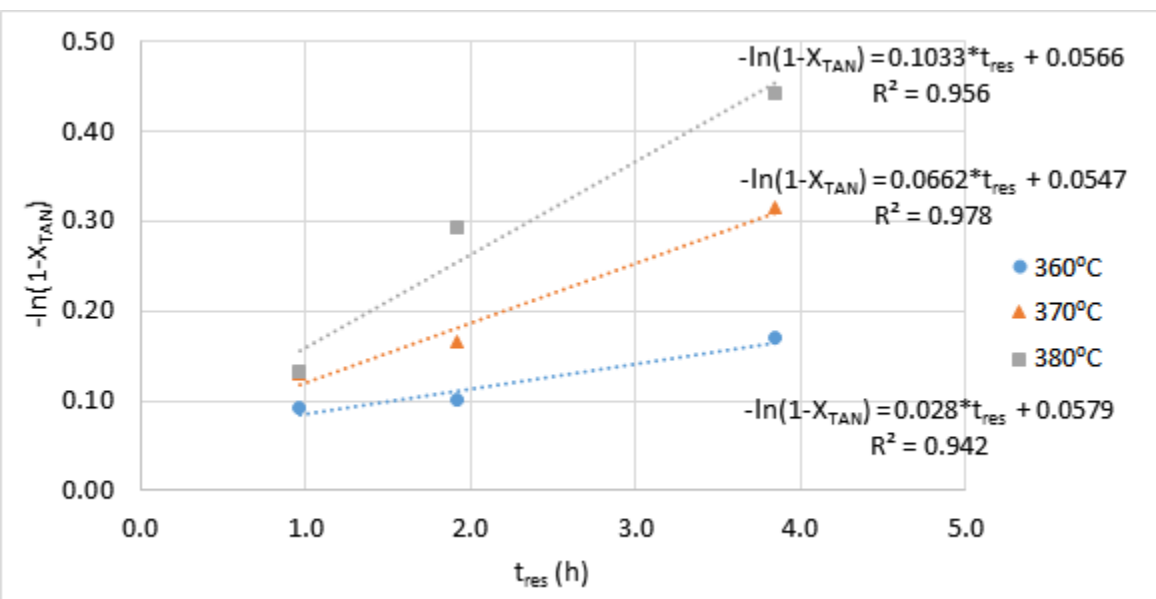

Figure 4-2: First order reaction assumption evaluation through plot of $-\ln(1-X_{TAN})$ versus residence time for temperatures of: ● 360°C, ▲ 370°C, and ■ 380°C.

Besides the small amount of points used in the regression, Figure 4-2 reveals an agreement between the proposed model, i.e. first order kinetics, and the experimental data as evidenced by the high values of the regression constant. The model proposed by Equation 4-22 suggests no intercept should be present in the plot in Figure 4-2. For all three different temperatures tested, a small value was obtained. If the intercept values are used to calculate a TAN conversion for residence time equals to zero, the calculated conversion would be around 5.5% for all three values while no conversion should be obtained when residence time is zero. This error is still within analytical errors and, thus, for the range of temperatures and space velocities used, a first order kinetics seems to deliver a reasonable estimation for the reaction system.

Figure 4-3 shows the results from the linearization shown in Equation 4-11 for the thermal results obtained in order to calculate the activation energy and the pre-exponential factor.

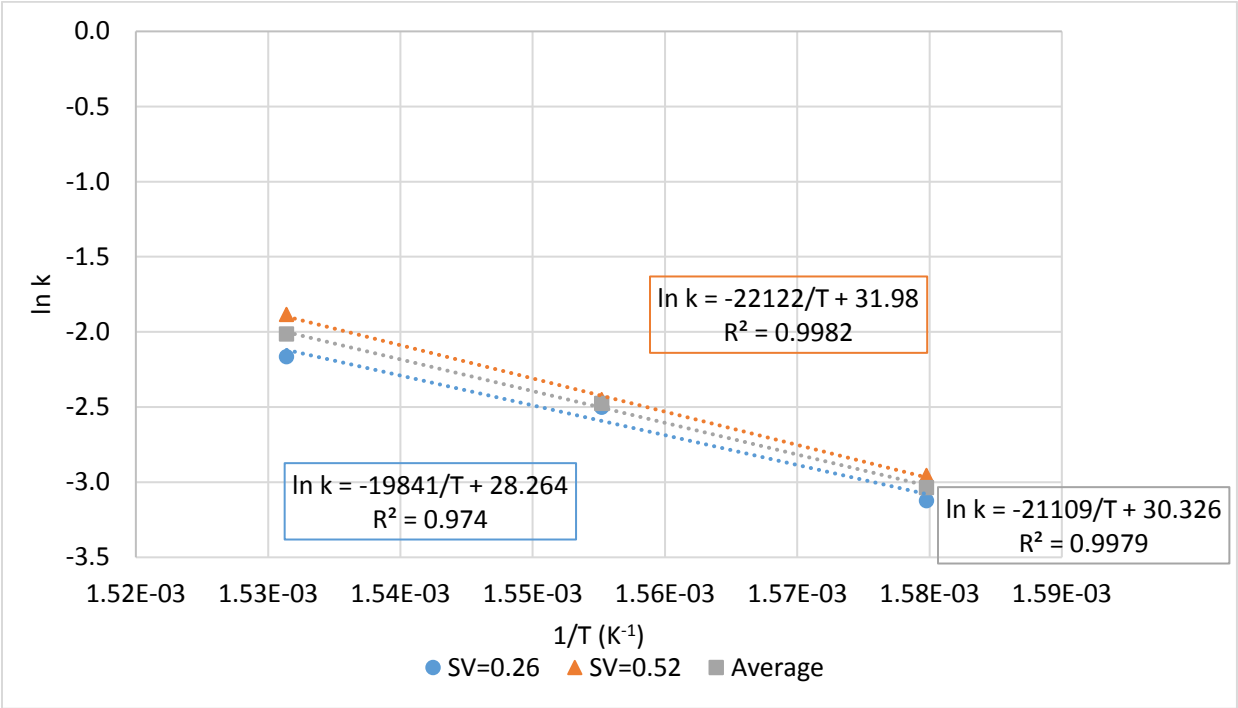

Figure 4-3: Logarithm of kinetic constant versus inverse of temperature for thermal reaction at space velocity of: ● 0.26h^{-1}, ▲ 0.54h^{-1}, and ■ for average values.

In Figure 4-3, only reactions with space velocity equal to 0.26h^{1} and 0.52h^{-1} were used since conversions at space velocity 1.04h^{-1} were too low, i.e. around 10%, so it hardly changed at different temperatures. Considering the error in the TAN measurement, it becomes pointless to evaluate the activation energy and the pre-exponential factor out of that data. For the lower space

velocities, conversions on the range of 10-36% are encountered which allows for a smaller effect of the analytic errors on the estimated data. The values of the activation energy and the pre-exponential factor can be calculated using the intercept and slope of the curves in Figure 4-3 and the results can be seen in Table 4-2. Since the activation energy and the pre-exponential factor do not depend on space velocity, but only on temperature, the average values for k for different space velocities were used in order to estimate the overall kinetic constants.

Table 4-2: Activation energy and pre-exponential factor for thermal reaction.

Space Velocity (h^{-1})	**Slope**	**Intercept**	**E_A (kJ/mol)**	**k_0 (h^{-1})**
0.26	-19,84	31.98	165.0	$1.88x10^{12}$
0.52	-22,12	28.26	183.9	$7.74x10^{13}$
Average	-21,11	30.33	175.5	$1.48x10^{13}$

Although values for k_0 vary greatly from different space velocities, activation energies are in the same range, and they are within typical values of thermal decomposition of large hydrocarbon molecules at moderate to low pressures, i.e. between 160 and 250kJ/mol (Le Page, 1987). The values obtained in Table 4-2 differ from those obtained in the work with supercritical water discussed previously in this section. The activation energy obtained in that case was 66kJ/mol while the pre-exponential factor was $5x10^8h^{-1}$ (Mandal et al., 2012). Differences in the results are expected since conditions used for the experiment were very different. For instance, Mandal et al. (2012) used much higher pressures (45,000kPa versus 830kPa), much higher water to oil ratios (6 versus 0.05), and higher temperatures (400-490°C versus 360-380°C). The authors claimed that water splitting into H* and OH* radicals, as shown in Equation 4-2 took place under the supercritical conditions which had the effect of catalyzing the decarboxylation reaction (Mandal et al., 2012). Thus, smaller activation energy is expected due to the catalytic effect of supercritical water.

4.1.2 Thermal Reaction Additional Results

Residue conversion is obtained from simulated distillation data and gives an idea of the amount of upgrading an oil went through. Figure 4-4 shows the cut distribution for the products at the nine different conditions tested while Table 4-3 summarizes the residue conversion.

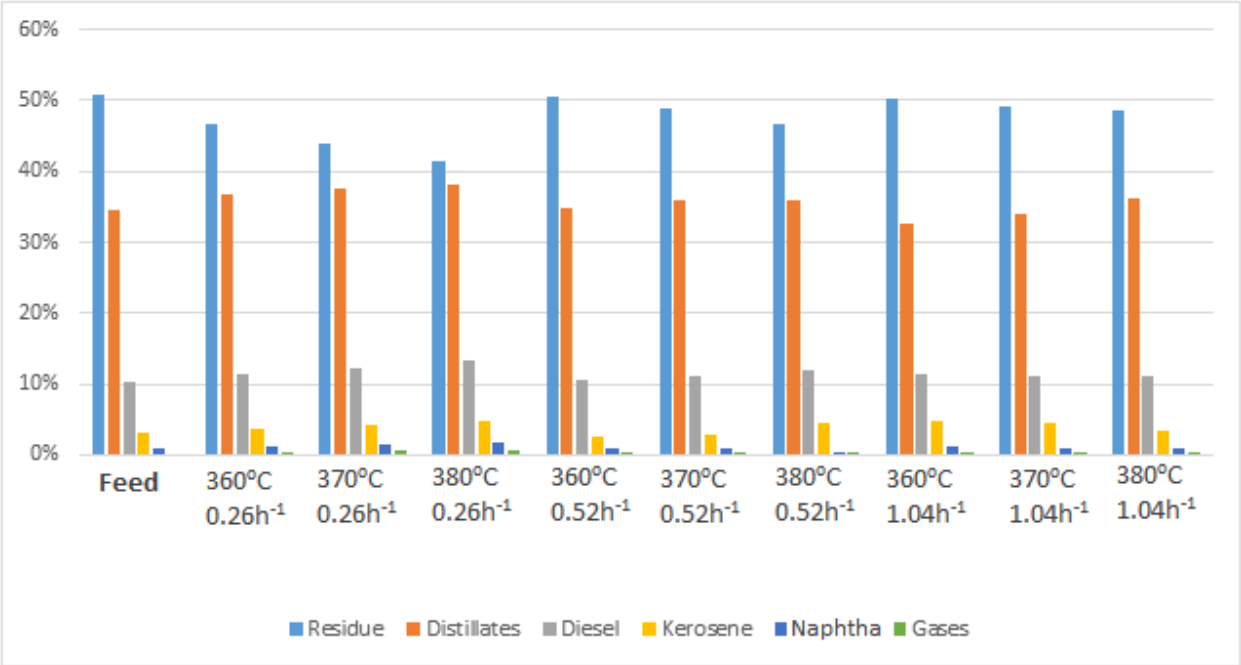

Figure 4-4: Product distribution for feed and products after thermal reaction at different space velocities and temperatures.

Table 4-3: Residue content and residue conversion for thermal reaction at different space velocities and temperatures.

	Space Velocity (h^{-1})	**Temperature (°C)**		
		360	**370**	**380**
Residue content (%wt)	0.26	46.5%	44.0%	41.4%
	0.52	50.6%	48.9%	46.7%
	1.04	50.1%	49.2%	48.5%
	Feedstock		50.9%	
Residue conv.	0.26	8.6%	13.6%	18.7%
	0.52	0.6%	3.9%	8.2%
	1.04	1.6%	3.4%	4.8%

Figure 4-4 shows that, at constant space velocity and varying temperatures, an increase in temperature decreased the amount of residue, and tended to increase the amount of distillates and diesel in the products. Mixed trends were observed for the lighter fractions, i.e. kerosene and naphtha. Table 4-3 highlights the trend of increasing residue conversion with temperature. Although space velocity $0.26h^{-1}$ showed a considerably higher conversion than other space velocities at same temperature, for space velocity 0.52 and 1.04 h^{-1}, the conversions at a given temperature were almost undistinguishable, especially at lower temperatures. This is due to analytical errors on SimDist analysis that become relatively high when conversions are below 5%.

Figure 4-5 shows the dependence of residue conversion with temperature. For the range of conditions tested, a linear relationship could be drawn from the results obtained. High values obtained for the regression coefficient showed an agreement to the proposed linear relationship.

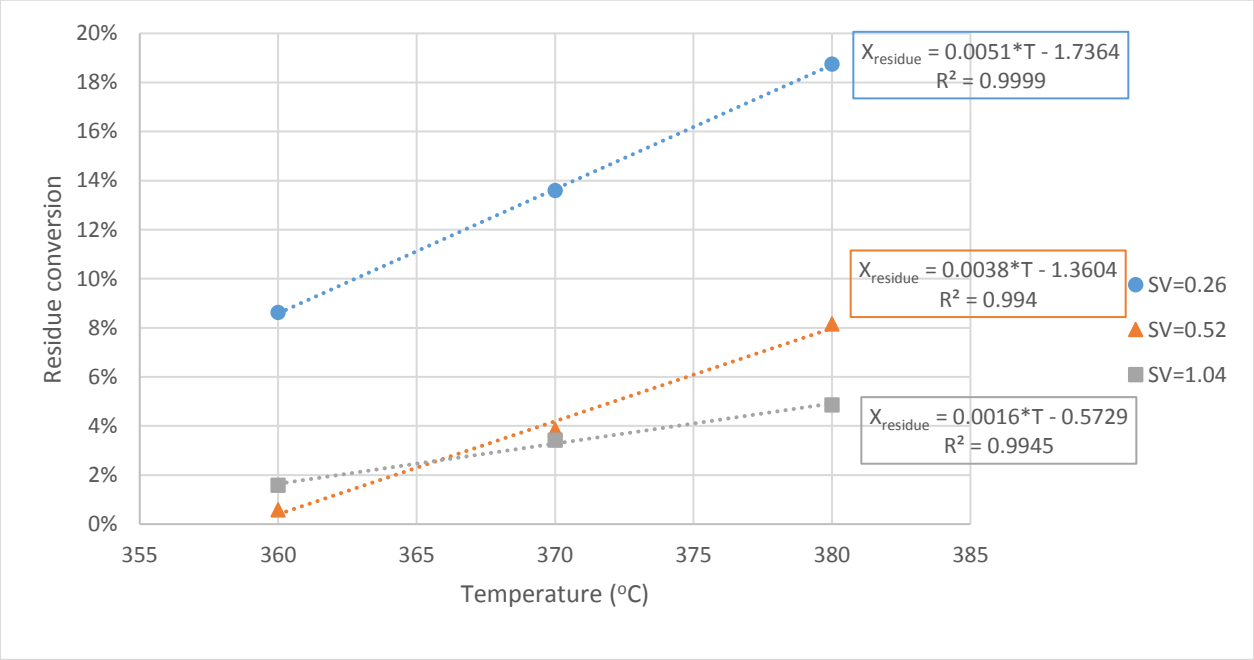

Figure 4-5: Residue conversion as a function of temperature for thermal reaction at space velocities: ● $0.26h^{-1}$, ▲ $0.54h^{-1}$, and ■ $1.02h^{-1}$.

Figure 4-6 shows the dependence of residue conversion in relation to space velocity. For this situation, the only case in which a straight line relationship could be observed was for 380°C since that was the only temperature that produced a considerable conversion at residence times as low as 1h. For the other temperatures, conversions at such low residence times were almost negligible,

most likely due to the residence time being shorter than the induction time for residue conversion, which makes the curve deviate from linearity.

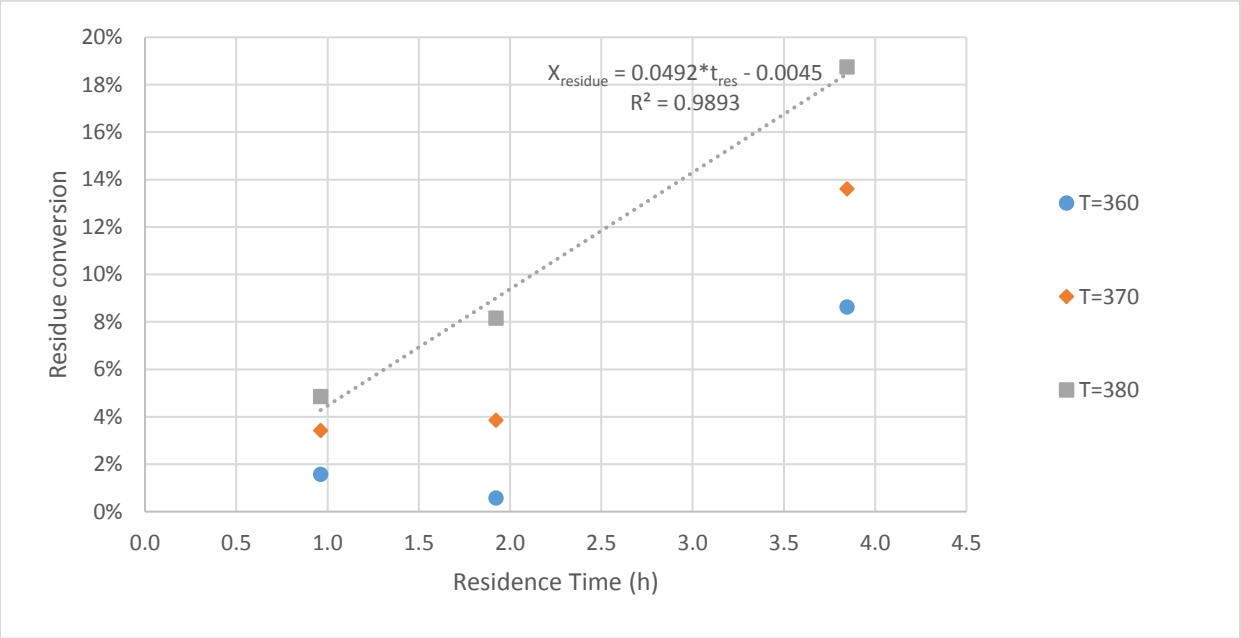

Figure 4-6: Residue conversion in function of space velocity for thermal reaction at temperatures: ● 360ºC, ▲ 370ºC, and ■ 380ºC.

Table 4-4 shows the relationship between viscosity reduction and the conditions used.

Table 4-4: Viscosity in cP at 40ºC and viscosity reduction for thermal reaction at different space velocities and temperatures.

	Space Velocity (h^{-1})	**Temperature (ºC)**		
		360	**370**	**380**
Viscosity (cP at 40ºC)	0.26	5,180	2,960	1,670
	0.52	6,850	4,440	1,850
	1.04	7,960	7,590	6,290
	Feedstock		18,500	
Viscosity decrease	0.26	72%	84%	91%
	0.52	63%	76%	90%
	1.04	57%	59%	66%

The trends observed were similar to the ones seen for residue conversion, i.e. viscosity was lower for higher temperatures and lower space velocities. That was related to the cracking of residue

components that are heavy molecules that greatly increased the viscosity of oil. Conversely, light materials produced out of cracking reaction, such as naphtha, kerosene, and diesel are much lighter and less viscous. It has been reported, for a similar steam cracking unit, an exponential relationship between viscosity and residue conversion for a deasphalted oil (DAO) feedstock (Garcia-Hubner, 2015). According to this relationship, a 62% viscosity reduction for a 10% residue conversion is expected. The reduction goes above 90% when residue conversion is around 30%. Considering differences in feedstocks, i.e. bitumen versus DAO, and experimental conditions, both studies agree on the level of viscosity reduction due to residue conversion.

Table 4-5 shows the API gravity increase for the products in relation to the feedstock for different conditions tested.

Table 4-5: API gravity and API gravity absolute change for thermal reaction at different space velocities and temperatures.

	Space Velocity (h^{-1})	**Temperature (°C)**		
		360	**370**	**380**
°API	0.26	9.6	9.9	10.1
	0.52	9.8	9.9	9.8
	1.04	9.6	9.7	9.7
	Feedstock		8.9	
°API increase	0.26	0.7	1.0	1.2
	0.52	0.9	1.0	0.9
	1.04	0.7	0.8	0.8

API gravity is consistently improved in all thermal cracking conditions and it averages around 1.0 increase. No clear relationship between °API increase and temperature or space velocity is observed since errors in °API analytics overcome differences of product quality at different conditions.

Table 4-6 shows the microcarbon increase (or decrease, when the number is negative) for the products in relation to the feedstock at different conditions. The results show that it was not observed any high increase in microcarbon except in the most severe condition, i.e. 380°C and $0.26h^{-1}$. For temperatures around 360 and 370°C and space velocities of $0.52h^{-1}$ and higher no

substantial microcarbon increase was noticed. Only when using very low space velocities or higher temperatures some microcarbon increase was observed.

Table 4-6: Products microcarbon and microcarbon increase for thermal reaction at different space velocities and temperatures.

	Space Velocity (h^{-1})	**Temperature (ºC)**		
		360	**370**	**380**
Microcarbon (%wt)	0.26	13.9%	13.9%	14.4%
	0.52	13.1%	12.8%	13.5%
	1.04	13.0%	13.1%	13.6%
	Feedstock		13.1%	
MC increase	0.26	6.2%	6.2%	10.3%
	0.52	-0.1%	-2.3%	3.1%
	1.04	-0.9%	0.0%	3.8%

The thermal reaction results show that temperatures at 370ºC and lower and space velocities at $0.52h^{-1}$ and higher are suitable for running the reaction since thermal degradation was minimal at those conditions. Furthermore, it has been seen that residue conversion and total acid number conversion were also low under those conditions which means that the thermal reaction had a minimum influence on the oil upgrading.

As discussed in section 2, industrial applications for oil processing commonly increase the temperature of reaction to compensate for losses in activity. This methodology is exemplified, for hydroprocessing, in Figure 2-3 and Figure 2-4. For this reason, it is important to develop a catalyst active enough to allow the use of temperature increases along the reaction in case of deactivation. Then, a base condition using temperature at 360ºC and space velocity at $1h^{-1}$ was set as the starting point for catalyst and condition screening. This condition is ideal in the sense that thermal effects are minimum for the starting condition and for temperature increases up to, at least, 20ºC.

The results obtained for the thermal reaction can be used for comparison with the catalytic reactions in order to understand the extent in which the catalysts are participating in the reaction. A comparison between thermal and catalytic reactions at different conditions can be found in the following section of this thesis.

4.2 Catalytic Condition Screening

Five different catalyst, as described in section 3.4, were tested on the pilot plant in order to evaluate their activity towards total acid number reduction. For catalyst TR1, a comprehensive study including several temperatures and space velocities was conducted for better understanding catalytic behavior on total acid number reduction. All other catalysts were tested for a minimum of 30 hours at 360ºC, space velocity $1h^{-1}$, water content 5%v/v, and 5mL/min of nitrogen as inert. The mass of catalyst used during each reaction was 42 grams. The following sections show the results related to the experiments performed for catalyst screening.

4.2.1 Catalyst TR1 Temperature Screening

A temperature screening reaction was performed with catalyst TR1 in order to evaluate the acidity reduction in the products at different conditions. For this experiment, a reaction condition was set at 360ºC and $1h^{-1}$. Temperatures of 370, 380, and 390ºC were tested and returned to the base condition to evaluate levels of deactivation for the catalyst. Figure 4-7 shows a schematic representation of the temperature screening experiment.

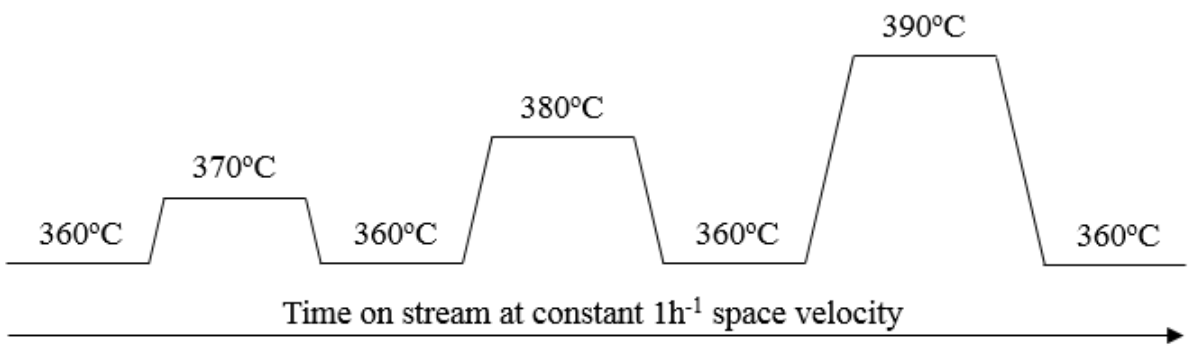

Figure 4-7: Temperature screening schematic representation for catalyst TR1 at constant space velocity.

Figure 4-8 shows the evolution of total acid number reduction over time during reaction using catalyst TR1. This figure also shows the temperature profile, as represented in Figure 4-7, and the thermal conversion. The thermal conversion for 390ºC was estimated by using the activation energy and pre-exponential factor obtained in Table 4-2 to calculate the reaction constant at 390ºC, as shown in Equation 4-10, and then solving Equation 4-22 for thermal conversion.

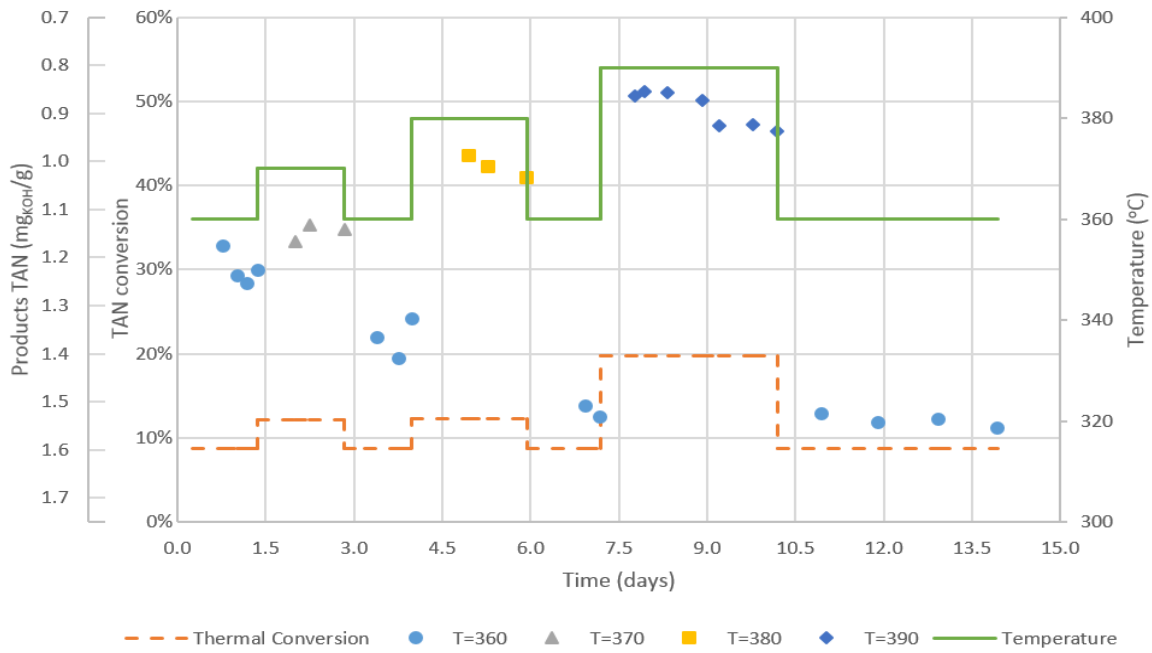

Figure 4-8: Temperature (continuous line), thermal (discontinuous line), catalytic TAN, and TAN conversion over time using catalyst TR1 at constant space velocity ($1h^{-1}$) and temperatures: ● 360ºC, ▲ 370ºC, ■ 380ºC, and ♦ 390ºC.

One important observation to be made in relation to Figure 4-8 is that throughout the entire experiment, catalytic reaction conversion was consistently above thermal reaction conversion. In fact, for most cases, the catalytic conversion was around 20-30% higher than thermal, especially for higher temperatures. Figure 4-9 schematically represents the differences in conversions.

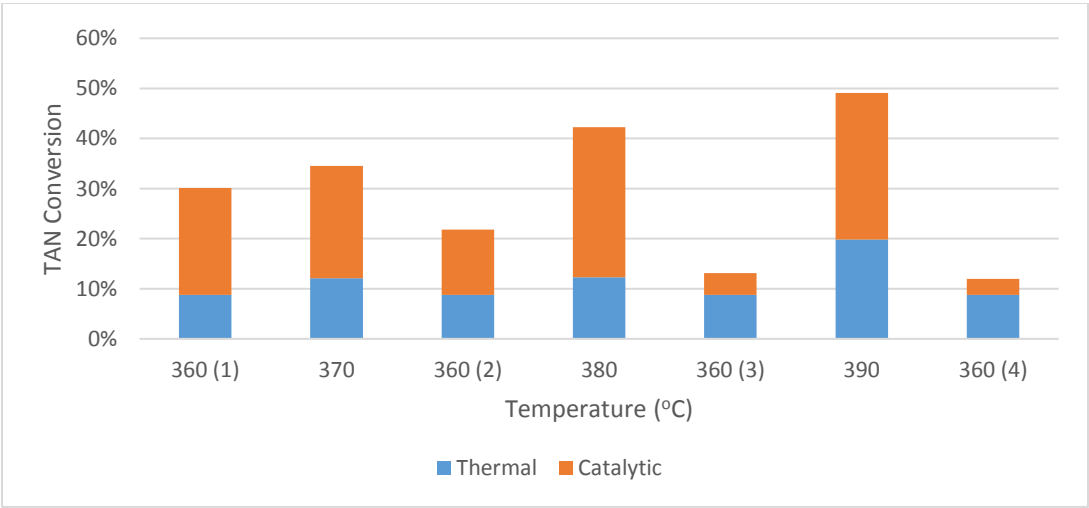

Figure 4-9: Schematic representation of catalytic and thermal conversions for catalyst TR1 at constant space velocity ($1h^{-1}$) and different temperatures.

Table 4-7 summarizes the average conversion for each condition tested.

Table 4-7: Catalytic and thermal average total acid number reduction for catalyst TR1 at different temperatures.

Temperature (ºC)	Catalytic Conversion	Thermal Conversion	Conversion Difference
360 (1)	30.1%	8.8%	21.3%
370	34.5%	12.1%	22.4%
360 (2)	21.8%	8.8%	13.0%
380	42.3%	12.3%	30.0%
360 (3)	13.1%	8.8%	4.3%
390	49.1%	19.8%	29.3%
360 (4)	12.0%	8.8%	3.2%

A clear trend observed on Figure 4-8, is a loss of activity on the catalytic reaction over time. If only the data related to temperatures at 360ºC is taken into account, Figure 4-10 can be obtained.

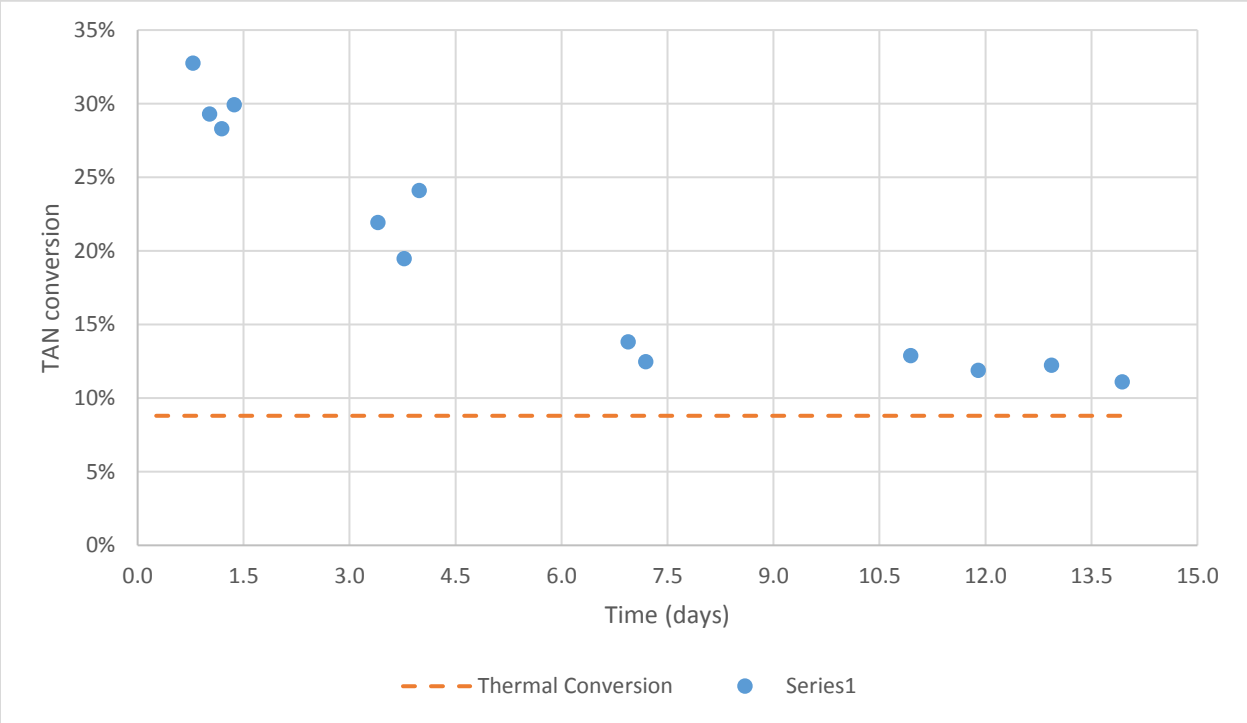

Figure 4-10: Thermal and catalytic total acid number conversion over time for 360ºC using catalyst TR1.

In Figure 4-10, the deactivation profile can be observed for catalyst TR1. A clear drop in activity was obtained in the first few hours of reaction. In fact, the TAN conversion dropped from 33% after 19 hours to 22% after 82 hours. In a slower pace, TAN conversion kept dropping until after 6 days of reaction, in which activation losses turned out to be almost negligible. From the second to fourth 360ºC condition, almost no activity was lost and the TAN conversion asymptotically approached thermal activity. Still, activity for higher temperatures were considerably above thermal reaction values as shown in Figure 4-8. For instance, taking a look at 390ºC values, catalytic conversion was still around 30% higher than thermal values and data showed a slow trend on deactivation. Conversion dropped 4.2% along the 72 hours in which samples were taken at that temperature.

The profile observed is similar to the ones reported for hydroprocessing technologies and discussed in section 2.4. The rapid loss in activity was related to the blockage of catalyst active sites and pores that took place in the first contact between oil and catalyst. That process quickly prohibited the access of oil molecules to active sites and caused the loss of activity.

4.2.2 Catalyst TR1 Kinetics Modelling

A kinetic model similar to the one developed for the thermal reaction can be used to estimate activation energy and pre-exponential factor for catalyst TR1. Again, it was considered that a first order kinetics was suitable for the system. Therefore, the kinetic model developed from Equation 4-9 to Equation 4-22 was used to treat the data presented on section 4.2.1. Table 4-8 shows the final average values for TAN conversion and kinetic rate constant for the different temperatures tested.

Table 4-8: Catalytic TAN reduction averages for different temperatures for catalyst TR1.

Temperature (ºC)	**Catalytic TAN Conversion**	**k (h^{-1})**
360	22.3%	0.25
370	34.5%	0.42
380	42.3%	0.55
390	49.1%	0.68

With the data in Table 4-8, a similar plot to Figure 4-3 can be made to evaluate the activation energy and pre-exponential factor for this catalytic reaction. This plot can be seen in Figure 4-11 while the calculation and values for activation energy and pre-exponential factor can be seen in Equation 4-23 and Equation 4-24, respectively.

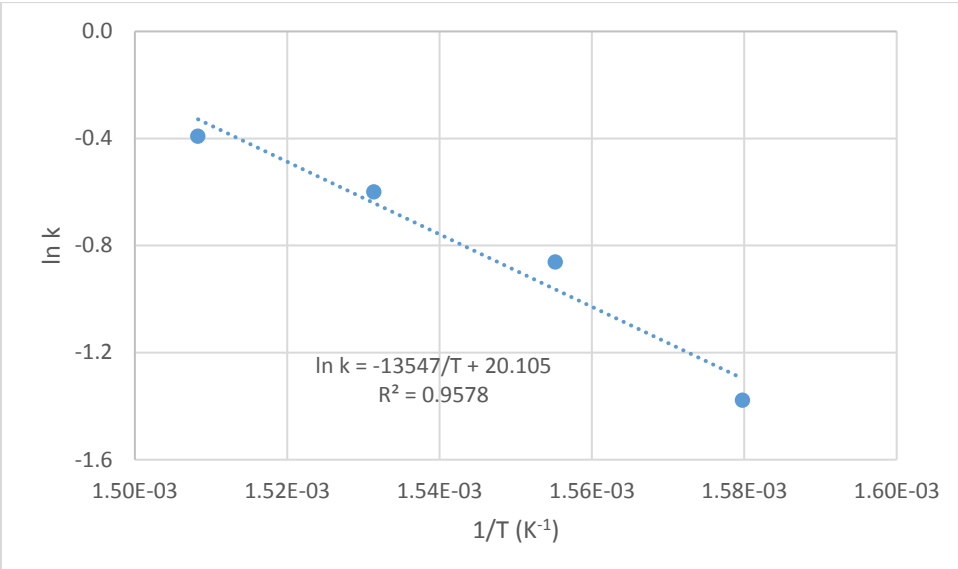

Figure 4-11: Logarithm of kinetic rate constant versus inverse of temperature for activation energy and pre-exponential factor calculations for catalyst TR1.

$$E_{A,TR1} = -R \times slope = 112.6\, kJ/mol \qquad \text{Equation 4-23}$$

$$k_{0,TR1} = exp(intercept) = 5.39 \times 10^{8} h^{-1} \qquad \text{Equation 4-24}$$

The ongoing gradual deactivation causes a few errors in the calculation of both kinetic constants. For instance, since the condition 370ºC (represented in Figure 4-11 by 1/T=1.555x10^{-3}) was performed closer to the beginning of the reaction, its kinetic rate constant value could be slightly over-estimated in relation to the higher temperature conditions that were performed later on the experiment. In the chart, that is visible since that point is the one the furthest above the line that fits all the data. Conversely, 390ºC (1/T=1.508x10^{-3}), which was the last tested condition, is slightly underestimated and it is encountered below the fitting line. The value related to 360ºC takes into consideration the data at different deactivation stages and, thus, it averages all the different reaction activity levels. Since the deactivation is only strong in the first few hours of reaction, this is not a major error in the calculations and values obtained represent an average of activation energy and pre-exponential factor for the catalyst at deactivation levels of 1-14 days.

The high value obtained for R^2, i.e. the regression coefficient, shows that errors in the values and model used are minimum.

If activation energy is compared between thermal and catalytic reactions (175.5kJ/mol versus 112.6kJ/mol respectively), it can be noticed that the catalytic is around 35% lower than the thermal value. Thus, the active sites are effectively participating and promoting the reactions that reduces acidity of the feedstock. The effects of a lower activation energy can also be seen in Table 4-7, in which the difference between thermal and catalytic conversions tends to increase at higher temperatures.

4.2.3 Catalyst TR1 First Order Kinetics Assumption

The first order assumption can be tested by a plot similar to the one in Figure 4-2, in which different space velocities are evaluated at the same temperature. For that purpose, the reaction represented so far in this chapter was continued using a temperature of 380ºC and space velocities ranging from 0.35 to $1.5h^{-1}$. The linearization of $-\ln(1-X_{TAN})$ versus residence time, as given in Equation 4-22, should give a straight line and go through the chart origin if first order kinetics is a suitable model for the reaction as discussed in section 4.1.1.

Figure 4-12 shows the linearization results while Table 4-9 shows the conversion for different residence times.

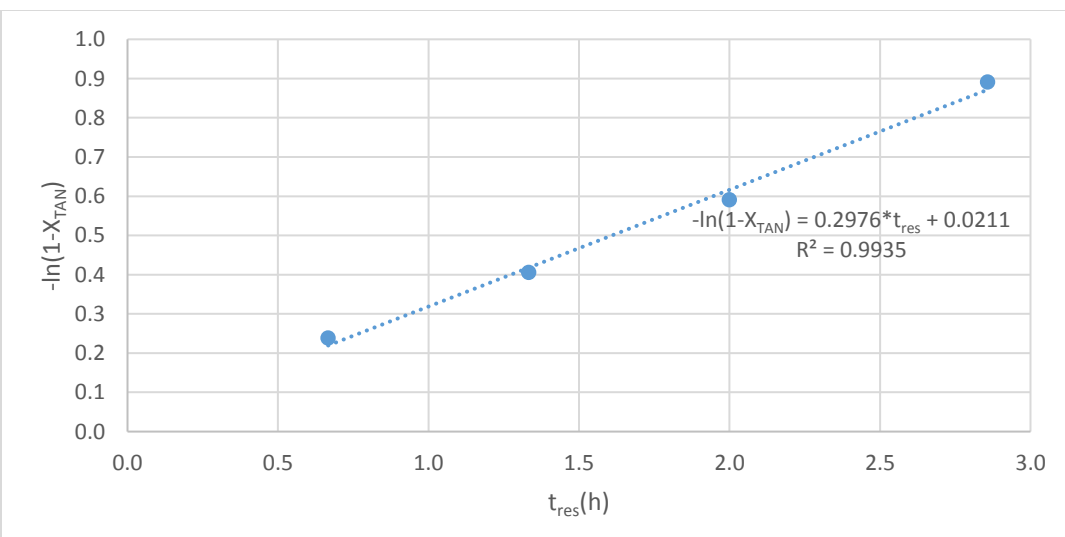

Figure 4-12: First-order reaction assumption evaluation through plot of $-\ln(1-X_{TAN})$ versus residence time for catalyst TR1.

Table 4-9: Catalytic TAN reduction averages for different space velocities for catalyst TR1.

Space Velocity (h^{-1})	**Residence Time (h)**	**Catalytic Conversion**	**Thermal Conversion**
0.35	2.9	59.0%	32.1%
0.50	2.0	44.6%	23.7%
0.75	1.3	33.4%	16.5%
1.50	0.7	21.2%	8.6%

In Table 4-9, the thermal conversion was calculated using the pre-exponential factor and activation energy for thermal reaction as obtained in section 4.1.1. From all the data at 380ºC, only space velocity $1h^{-1}$ was not used on the first order evaluation since this condition was used on the initial phase of the reaction where temperatures were varied for the activation energy and pre-exponential factor constant calculation. Therefore, that condition represents a much less deactivated catalyst and could not be used for comparison with the other space velocities that were tested at similar deactivation levels. The high value obtained for the regression coefficient showed the appropriateness of the chosen model. Also, the small intercept obtained was related to minor experimental errors, normal in pilot plant operations, characterization methodology, and chosen model. If the intercept obtained by the linearization method on Figure 4-12 is used to calculate conversion at residence time equals to zero, which should be zero, the obtained conversion is only 2%, thus, deviations from the model were minimum. The effects of deactivation are much smaller in this chart since those samples were taken in a smaller time interval (eight days versus fourteen days for temperature screening).

4.2.4 Catalyst TR1 Additional Results

A few additional properties for the products were investigated to understand the impact of temperature and space velocity on the final product quality. The simulated distillation (SimDist) allows us to understand the degree of conversion the oil went through. Figure 4-13 shows the cut distribution for the feed and products after reaction for different temperatures while Figure 4-14 shows it for different space velocities.

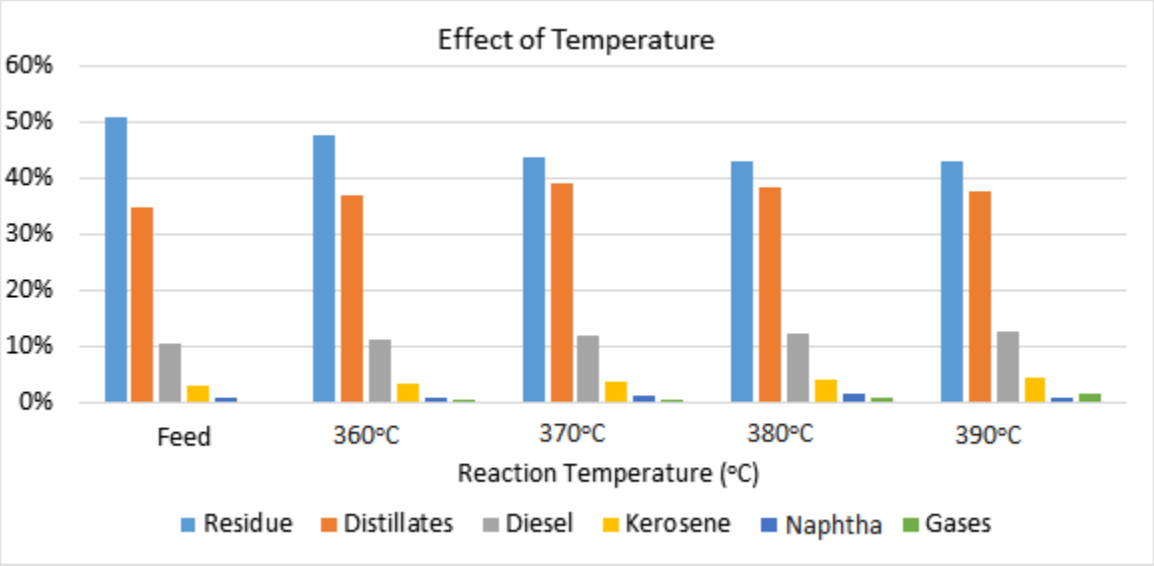

Figure 4-13: Cut distribution for TR1 catalytic reaction at different temperatures.

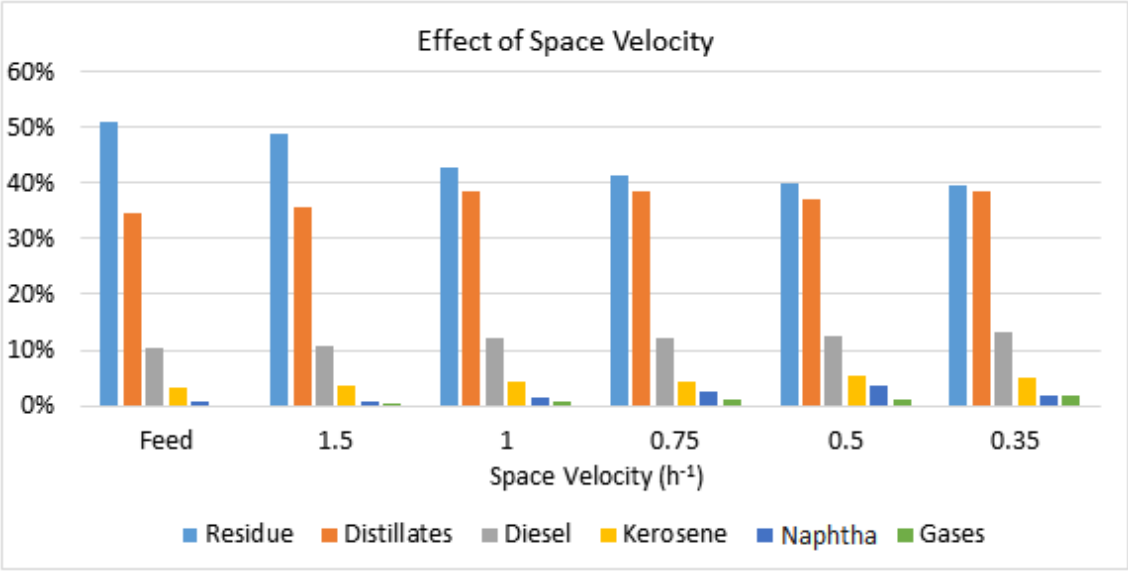

Figure 4-14: Cut distribution for feed and products after TR1 catalytic reaction for different space velocities.

Table 4-10 shows the residue conversion levels for the temperatures and space velocities tested. Table 4-3 gives the conversion levels for the thermal reaction at similar conditions.

Table 4-10: Residue conversion for TR1 catalytic reaction at different space velocities and temperatures.

Space Velocity (h^{-1})	**Temperature (ºC)**			
	360	**370**	**380**	**390**
0.35			22.3%	
0.50			21.7%	
0.75			18.8%	
1.00	6.4%	13.9%	15.8%	17.0%
1.50			3.7%	

Recalling results from Table 4-3, thermal conversions were below 10% for most of the conditions tested but for space velocities of $0.26h^{-1}$. The conversions for space velocity $1.04h^{-1}$ for 360, 370, and 380ºC were 1.6%, 3.4%, and 4.8%, respectively. Therefore, the catalytic residue conversion for the range tested was around 3-4 times higher than the one obtained in the thermal reaction. This means that catalyst TR1 was actively participating in residue cracking reactions that produces a lighter oil than the feedstock. Another important comparison between both types of reaction are the results obtained at 380ºC and $0.50h^{-1}$. For the catalytic reaction, the conversion was close to 21% while thermally it did not pass 8%. The consistency of the results, i.e. the fact that the catalytic reaction had consistently higher conversions for all comparable conditions, shows that this catalyst could be potentially used for residue upgrading. Due to the long term reaction, it showed that residue upgrading was little affected by deactivation throughout the reaction.

Figure 4-15 shows the viscosity results for the catalytic reaction while, alternatively, Figure 4-16 shows the logarithm of viscosity in function of temperature.

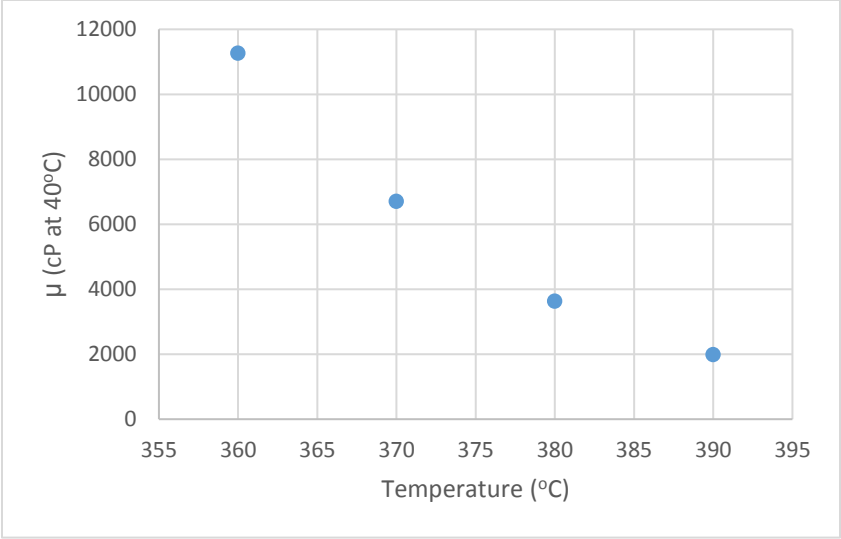

Figure 4-15: Products viscosity for TR1 catalytic reaction at different temperatures.

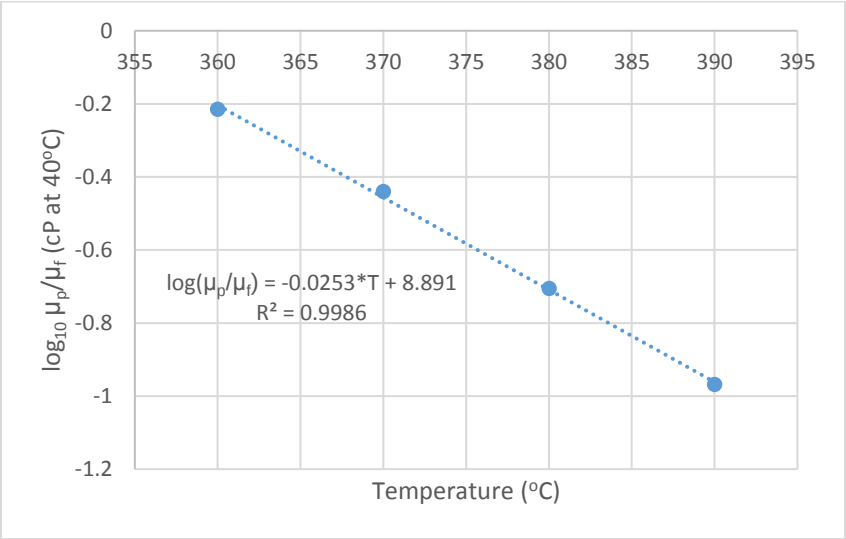

Figure 4-16: Logarithm of products-to-feedstock viscosity ratio for TR1 catalytic reaction at different temperatures.

In both figures the viscosity drops logarithmically with reaction temperature. In the Garcia-Hubner (2015) work for thermal steam cracking of Vacuum Gas Oil, a linear relationship was found between the logarithm of product viscosity and residue conversion (Garcia-Hubner, 2015). This plot for the catalytic results obtained in this project can be seen in Figure 4-17. The curve differed considerably from linearity especially at higher residue conversions. At higher residue conversions, the viscosity dropped faster which shows that catalytic residue conversion had a

different mechanism than thermal conversion. The levels of viscosity reduction were around 40-90% for the range of temperatures tested, as shown in Table 4-11.

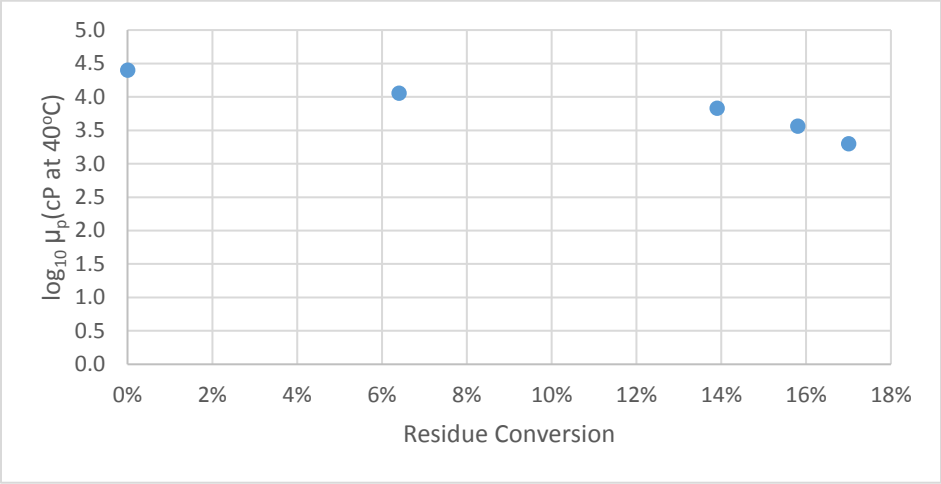

Figure 4-17: Logarithm of products viscosity for TR1 catalytic reaction at residue conversions.

Table 4-11: Products viscosity in cP at 40ºC and viscosity relative reduction for TR1 catalytic reaction at different space velocities and temperatures.

	Space Velocity (h^{-1})	**Temperature (ºC)**			
		360	**370**	**380**	**390**
Viscosity (cP at 40ºC)	0.35			1,760	
	0.50			1,890	
	0.75			2,220	
	1.00	11,270	6,700	3,640	1,980
	1.50			8,200	
	Feedstock		18,500		
Visc. Reduction	0.35			90.5%	
	0.50			89.8%	
	0.75			88.0%	
	1.00	39.1%	63.8%	80.3%	89.3%
	1.500			55.6%	

Table 4-11 results shows a trend in decreasing the product viscosity when temperature was increased or space velocity was decreased. This effect was more relevant at high space velocities or low temperatures. When compared with thermal reactions, catalytic reactions also improved

viscosity reduction, especially at higher temperatures. The thermal viscosity reduction at 380ºC and $1h^{-1}$ was 66% while the catalytic was 80%. The improvements were related to the higher residue conversion obtained in the catalytic reaction. Those improvements were also more prominent at higher temperatures. Table 4-12 shows the results for API gravity increase for TR1 catalytic reaction under different conditions.

Table 4-12: Products API gravity and API gravity absolute change for TR1 catalytic reaction at different space velocities and temperatures.

	Space Velocity (h^{-1})	**Temperature (ºC)**			
		360	**370**	**380**	**390**
ºAPI	0.35			9.6	
	0.50			10.7	
	0.75			10.1	
	1.00	9.1	8.7	9.4	10.1
	1.50			8.8	
	Feedstock		8.9		
ºAPI difference	0.35			0.7	
	0.50			1.8	
	0.75			1.2	
	1.00	0.2	-0.2	0.5	1.2
	1.500			-0.1	

The catalytic results do not show improvements in relation to API gravity. Some of the ºAPI differences, for low temperatures or high space velocities, were slightly negative numbers which suggests a small degradation of the product quality. Though this could be related to errors in the measurements of API gravity. In general, more severe conditions showed an increase of API gravity at around 1-2 points, while, comparatively, thermal reaction improved API gravity by 1.0 on average. Surprisingly, API measurements had a discontinuity at temperature 380ºC and space velocity $0.35h^{-1}$, where it fell by 1.1 when increasing severity. This could be related to the high severity and long residence time of this reaction that could be allowing polymerization reactions to take place, or modifications of the intramolecular forces of the produced molecules. Those changes offset part of the benefits of heavy molecules cracking.

Table 4-13 shows the microcarbon increase for the different conditions applied to catalyst TR1.

Table 4-13: Microcarbon relative increase for TR1 catalytic reaction at different space velocities and temperatures.

	Space Velocity (h^{-1})	**Temperature (ºC)**			
		360	**370**	**380**	**390**
Microcarbon (%wt)	0.35			14.1%	
	0.50			14.2%	
	0.75			13.8%	
	1.00	13.1%	13.9%	14.2%	14.6%
	1.50			13.3%	
	Feedstock		13.1%		
Microcarbon Relative Increase	0.35			7.6%	
	0.50			8.3%	
	0.75			5.3%	
	1.00	0.1%	6.2%	8.4%	11.6%
	1.500			1.9%	

Table 4-13 shows that microcarbon was highly related to the temperature of reaction and it seemed to increase by 0.5% for every 10ºC increase in the range of temperatures tested. At the same time microcarbon values were not affected as much by space velocity since most of the values fluctuated around the same value for a constant temperature.

Although catalyst TR1 proved to be capable of significantly reducing total acid number and residue content on the final oil, its improvements only took place at higher temperatures. The issue in starting a reaction at a high temperature is the risk of a higher degradation of the feedstock, as shown in the microcarbon analysis. This degradation will be even more severe after deactivation as there will be the need to increase reaction temperature, as it is similarly done in hydroprocessing. Starting the reaction at high temperatures will also have the parallel effect of increasing other rate of reactions, such as coke formation, that promote catalyst deactivation. Comparison between TR1 and other catalysts, i.e. TR2 to TR5, can be found in section 4.3.

4.3 Catalyst Screening

Catalyst TR1 proved to be capable of reaching TAN conversions at much higher levels than thermal reactions. Nevertheless, its conversion is still far from the minimum levels necessary to produce a non-acidic oil. For instance, considering the used feedstock, that had a TAN of 1.75mg_{KOH}/g, a conversion around 70% is required to achieve 0.5mg_{KOH}/g which is considered non-acidic (Bacon et al., 2005). Also, diluent needs to be added to the products to achieve minimum requirements of viscosity for pipeline transportability. The viscosity requirement for transportability is usually considered to be around 350cSt at the piping temperature (Banerjee, 2012). If the amount of sweet diluent mixed with the products to achieve transportability criteria is taken into account, the TAN conversion required on the bitumen pre-dilution would still be around 60% to obtain a final dilbit product below TAN of 0.5mg_{KOH}/g.

Since the targeted TAN conversion was not obtained even for the most severe conditions tested, different catalyst formulations were developed and tested to try to overcome the low initial activity issue of catalyst TR1. Short runs under the same condition were used to evaluate different catalysts. The base condition used in this project was 360ºC and $1h^{-1}$ in order to minimize side reactions that eventually will degrade oil quality. Furthermore, starting with a low severity condition allowed the use of temperature increasing to compensate for catalytic deactivation in longer reactions. All catalysts, except TR3, were tested at 830kPa. Catalyst TR3 was tested at 2,760kPa to take advantage of hydrogenating functions in its formulation. Nevertheless, the work of Garcia-Hubner (2015) showed that the change of pressure did not affect product total acid number but improved other oil properties such as viscosity and API gravity. Thus, TAN conversion for all catalysts can be compared.

4.3.1 Total Acid Number Results

Section 3.4, page 54, contains a summary of the catalyst compositions and active sites. Figure 4-18 shows the TAN conversion for all catalysts used (TR1 to TR5) at the same temperature (360ºC) and space velocity ($1h^{-1}$) after 30 hours of reaction. This figure also provides the thermal reaction conversion under the same conditions for comparison.

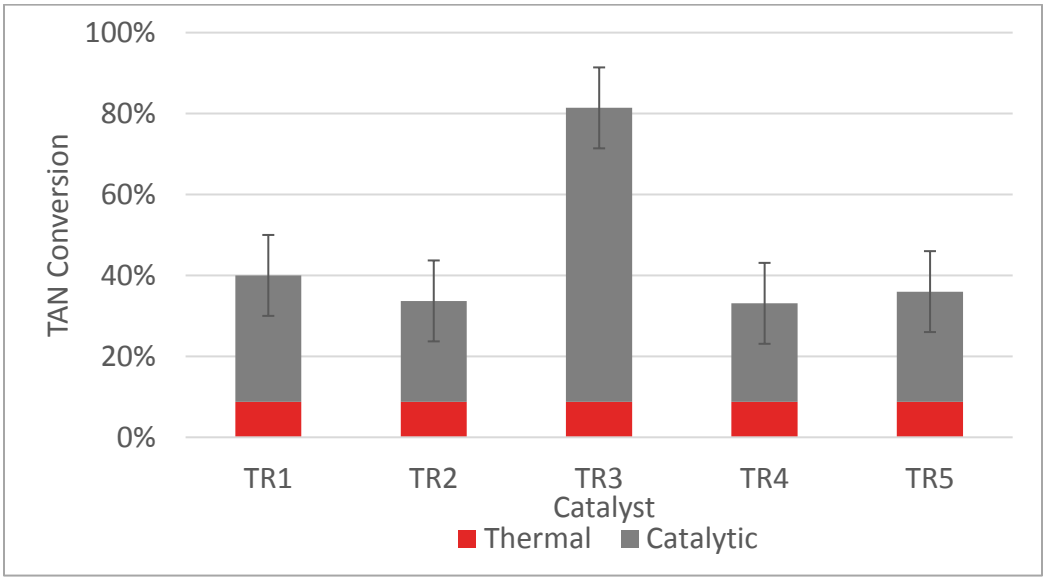

Figure 4-18: Total acid number over time for catalysts TR1, TR2, TR3, TR4, TR5, and thermal conversion for 360ºC and $1.0h^{-1}$.

When comparing catalysts with similar composition, i.e. TR1 and TR4, or TR2 and TR5, no improvement in conversion is observed. In general, TAN conversions fluctuate around the same values for the pair of catalysts. Thus, improvements from higher metal content and from exchanging sodium ions for protons during catalyst preparation are within errors produced during plant operation and TAN measurement. Further investigation of those differences were not considered since catalyst TR3 already showed a much higher activity towards TAN reduction than any other catalyst formulation. All catalysts showed a considerably higher conversion than the thermal reaction. While most of the catalysts showed TAN conversions in the range of 20-50%, catalyst TR3 had its conversion ranging from 70-90%. That was the only catalyst that considerably distinguishes itself from the others and the only one able to perform TAN reduction, at the base condition, i.e. 360ºC and $1h^{-1}$, at the levels necessary to produce a sweet product. Table 4-14 summarizes all the relevant results for the catalysts tested at the same condition.

Table 4-14: Products properties for all catalysts at 360ºC and 1h^{-1}.

	TR1	**TR2**	**TR3**	**TR4**	**TR5**	**Thermal**
Feedstock	220ºC+	220ºC+	Dilbit	Dilbit	Dilbit	220ºC+
Products TAN	1.23	1.16	0.32	1.17	1.14	1.59
Products Residue Content	47.6%	49.0%	47.6%	48.5%	47.6%	50.1%
Products Viscosity (cP at 40ºC)	11,270	6,850	1,320	1,540	1,180	7,960
Products ºAPI	9.1	9.1	12.2	12.7	12.1	9.6
Products microcarbon	13.1%	13.8%	13.1%	13.6%	12.4%	13.0%
TAN reduction	30%	34%	81%	31%	33%	9%
Residue conversion	6.4%	3.8%	7.9%	6.2%	7.9%	1.6%
Viscosity reduction	39.1%	63.0%	60.1%	53.3%	64.1%	57.0%
ºAPI difference	0.2	0.2	0.4	0.9	0.3	0.7
Microcarbon increase	0.1%	5.4%	2.3%	5.9%	-3.4%	-0.9%

Table 4-14 shows that the average TAN reduction for all catalyst, except TR3, were close to 30%. Catalyst TR3 had TAN reductions at much higher levels, averaging at 81%. Table 4-14 also shows that the average catalytic residue conversion was 6.0% and the values fluctuated around that number. That value was four times higher than the thermal conversion but it was still rather low. The viscosity reduction of all catalysts, but TR1, were around the thermal results and the differences were within the error of the used analytics. It should be noted that for the condition tested, there was no appreciable catalytic effect on viscosity reduction. Similarly to viscosity, API gravity results fluctuate close to feedstock levels. None of the products were even one point away in API gravity from the feedstock reflecting the low severity of the conditions used. Microcarbon also had a similar trend of fluctuating values close to the feedstock. All microcarbon values were less than 1.0% away from the absolute feedstock value, which reinforces the low level of degradability of the oil under the conditions used. All TAN conversions were well above thermal conversion with 360ºC and 1h^{-1} seems to show an ideal condition to reduce TAN with minimal impact on other oil properties.

Due to the outstanding activity of catalyst TR3 towards TAN reduction, this catalyst was chosen to proceed to the deactivation studies that can be found in chapter 5.

4.3.2 Gas Composition and Yields

Gas composition is an important property to be tracked since it gives an indication of the reactions that are taking place and their extents. Figure 4-19 shows the gas yield for major gas components for all tested catalysts while Figure 4-20 has the results for catalyst TR1 at different temperatures.

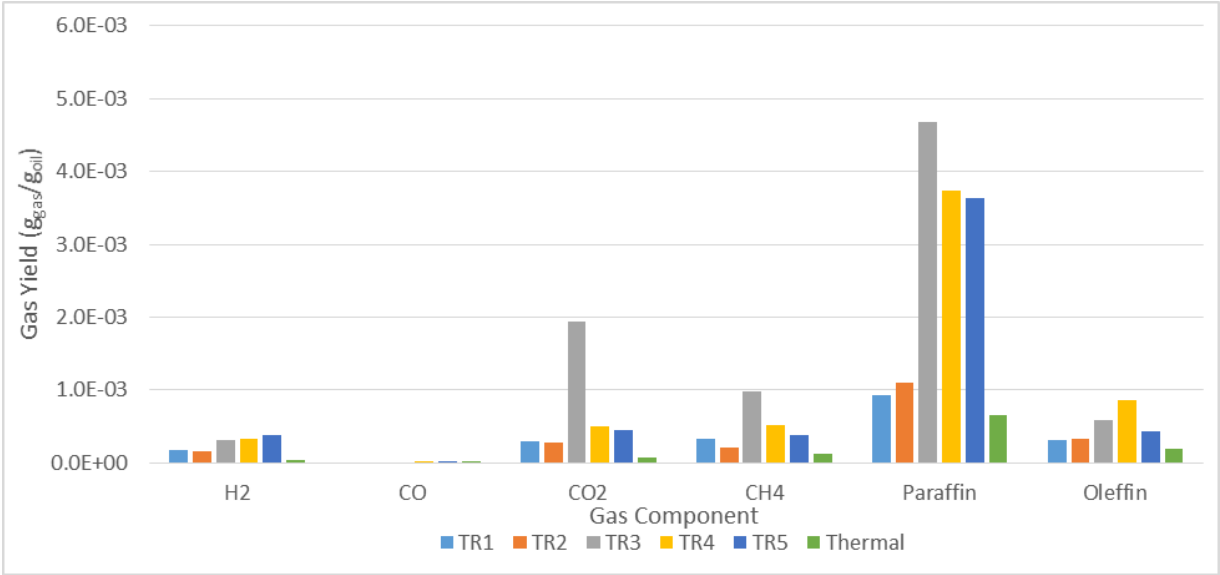

Figure 4-19: Gas yield for different gas components for all catalysts tested at 360°C and 1h^{-1}.

According to Figure 4-19, the gas yields for the thermal reaction were low and always below the levels of the catalytic reactions for any gas component. That observation agrees with the other results found in this chapter, such as in TAN and residue conversion that happened to a lower extent than in the presence of catalyst. Conclusively, the conditions used were not severe enough for thermally processing the feedstock. The only considerable yield from thermal cracking, yet below the levels of all catalysts, were the yields to paraffinic (including methane) and olefinic molecules in the gas. The origin of those molecules are most likely from thermal cracking of side branches on long, heavy molecules. The small amount of hydrogen or oxygen-containing gas molecules is an indication of the inability to perform water dissociation thermally. The small hydrogen yield at those conditions is probably related to minimal thermal dehydrogenation of organic molecules.

One important observation was the negligible yield of CO for all the tests performed. That meant that after cracking, carbon-containing molecules were being completely oxidized to CO_2. The complete and partial oxidations of side branches are represented by Equation 4-25 and Equation

4-26, respectively. Note that reaction Equation 4-25 is a combination of Equation 4-26 and the water-gas shift reaction (Equation 4-27). Furthermore, Equation 4-28 shows the Boudouard reaction, in which two CO molecules react to produce a CO_2 and carbon. Because there was no CO in the gas products, it can be concluded that all CO produced from Equation 4-26 goes through either water-gas shift or Boudouard reaction.

$$R - CH_3 + 2H_2O \rightarrow RH + CO_2 + 3H_2 \qquad \text{Equation 4-25}$$

$$R - CH_3 + H_2O \rightarrow RH + CO + 2H_2 \qquad \text{Equation 4-26}$$

$$CO + H_2O \rightarrow CO_2 + H_2 \qquad \text{Equation 4-27}$$

$$2CO \rightarrow CO_2 + C \qquad \text{Equation 4-28}$$

Catalyst TR3 was the one with the largest CO_2 yield among all reactions. That is an indication that oxygen transfer between water splitting sites and cracking sites was well performed by this catalyst. Since TR3 was the most active catalyst in TAN reduction, the high CO_2 yield can also be expected as a byproduct from naphthenic acid decarboxylation reaction.

This catalyst also showed the highest yield of paraffinic gases although its olefin yield was comparatively low, which highlights the catalyst's potential to induce both cracking and hydrogenating reactions. The lower yield for hydrogen for catalyst TR3 could be related to hydrogenating and hydrocracking reactions, which would decrease both hydrogen and olefin yield and increase paraffin yield as observed in Figure 4-19.

The high yields of hydrogen presented by all catalysts raises a concern on its origin since dehydrogenation reactions, when producing olefins, reduces the overall oil quality. Taking Equation 4-25, for example, the decarboxylation of a side branch through the water splitting mechanism yields 3 times more hydrogen, in moles, than CO_2. Transforming to mass yield, the expected ratio H_2/CO_2 is 0.14. Considering that R is a hydrogen, i.e. R-CH_3 is a methane molecule, the mass ratio goes to 0.18, and it is the maximum that reaction can yield. TR3 was the only catalyst that has hydrogen to CO_2 levels in a similar interval of values, ranging from 0.15-0.21. All the other catalyst had H_2/CO_2 at higher levels. The rest of the hydrogen produced came probably from dehydrogenation reactions, as shown in Equation 4-29 that can be accessed by the bromine number in a sample of oil. This analysis was performed in some selected samples and the results are shown in Table 4-15. Bromine number was used to evaluate the general trend in increasing or decreasing the level of saturation on the oil molecules. It is important to mention that resins in heavy oils

brings inaccuracies to bromine number analysis and, thus, it is only accurate for light fractions (Banerjee, 2012).

$$R_1 - CH_2 - CH_2 - R_2 \rightarrow R_1 - CH = CH - R_2 + H_2 \qquad \text{Equation 4-29}$$

Table 4-15: Bromine number increase for different catalysts and thermal reaction.

	TR1	**TR2**	**TR3**	**TR4**	**TR5**	**Thermal**
Bromine Number (g_{Br2}/100g)	17.9	19.2	18.4	18.0	20.3	19.4
Bromine Number Increase (g_{Br2}/100g)	0.8	2.1	5.0	4.6	6.9	2.3
Bromine Number Relative Increase	5%	12%	37%	34%	51%	13%
Dehydrogenation Calculated H_2 Yield (x10^{-4} g_{H2}/g_{feed})	1.0	2.6	6.2	5.8	8.6	2.9
Hydrogen Yield (x10^{-}4 g_{H2}/g_{feed})	1.8	1.6	3.1	3.3	4.6	3.8

Bromine number increase was used to calculate the yield of hydrogen produced per gram of feedstock through dehydrogenation mechanisms as shown in Equation 4-30. The calculations took into consideration that all incremental bromine number represented an increase of hydrogen deficiency of the molecules. Further, bromine number was converted to hydrogen equivalent considering a stoichiometric relationship of 1:1.

$$(H_2\ Yield)_{dehydrogenation} = \frac{Br.Number\ Increase}{MW_{Bromine}} MW_{H_2} \qquad \text{Equation 4-30}$$

For all the catalysts, but TR1, the calculated hydrogen yield through dehydrogenation surpassed the total hydrogen produced at the reactor as it can be seen in Table 4-15. This discrepancy can be understood through the hydrocracking reaction shown in Equation 4-31.

$$R_1 - CH_2 - CH_2 - R_2 + H_2 \rightarrow R_1 - CH_3 + R_2 - CH_3 \qquad \text{Equation 4-31}$$

In Equation 4-31, the bromine number for reactants and products of that reaction is exactly the same though there is a consumption of a hydrogen molecule. Therefore, excess hydrogen from dehydrogenation and water splitting was consumed through hydrocracking reactions and, thus, not all produced hydrogen left the reactor unconverted. Another evidence of hydrocracking reactions

are in the relatively high yields of paraffinic gases that could be produced from hydrocracking of side branches.

In any case, H_2/CO_2 ratios could be higher than expected since CO_2 levels could be under estimated in the gas analysis since part of this component yield could have been lost due to its solubility in and interaction with water. For instance, Henry's law can be used to estimate the carbon dioxide and hydrogen solubility in water. Henry's law constant at 25ºC for carbon dioxide is 0.034mol/kg.bar (National Institute of Standards and Technology, 2016a) while for hydrogen is 0.00078mol/kg.bar (National Institute of Standards and Technology, 2016b). Those constants can be used to calculate concentrations of hydrogen and carbon dioxide in water at different pressures. In the cases of both 830kPa and 2,760kPa, the carbon dioxide solubility was almost 1000 times higher than that of hydrogen. Considering the water-to-oil ratio, if water was saturated with CO_2, a total of $6x10^{-4}$ g_{CO2}/g_{oil} could be missing from the gas stream for reactions at 830kPa while $21x10^{-4}$ g_{CO2}/g_{oil} would be missing from reactions at 2,760kPa. Alternatively, if the water were saturated with hydrogen, the missing yield would be $6x10^{-7}g_{H2O}/g_{oil}$ for 830kPa and $22x10^{-7}g_{H2O}/g_{oil}$, both negligible to the amount of hydrogen on the gas stream. If the missing CO_2 and H_2 is added to the overall yields, the H_2/CO_2 ratios for all catalyst goes to the range of 0.09-0.40, much closer to the expected range due to steam dealkylation reactions. A summary of Henry's law constants and gases concentration can be found in Table 4-16.

Table 4-16: Henry's law constant for hydrogen and carbon dioxide and calculated concentration on water for 830kPa and 2,760kPa at 25ºC (National Institute of Standards and Technology, 2016a) (National Institute of Standards and Technology, 2016b).

	Henry's Law Constant (mol_{gas}/kg_{wat}.bar)	**Concentration on water (mol_{gas}/g_{wat})**	**Concentration on water (g_{gas}/g_{wat})**
H_2 at 830kPa and 25ºC	0.00078	$6.5x10^{-6}$	$1.3x10^{-5}$
H_2 at 2,760kPa and 25ºC	0.00078	$2.2x10^{-5}$	$4.3x10^{-5}$
CO_2 at 830kPa and 25ºC	0.034	$2.8x10^{-4}$	$1.2x10^{-2}$
CO_2 at 2,760kPa and 25ºC	0.034	$9.4x10^{-4}$	$4.1x10^{-2}$

Another possible explanation for the high values of H_2/CO_2 ratios was the oxygen addition to hydrocarbon molecules in other forms than CO_2, such as alcohols and aldehydes.

Figure 4-20 shows the effects of temperature in the gas yields for catalyst TR1.

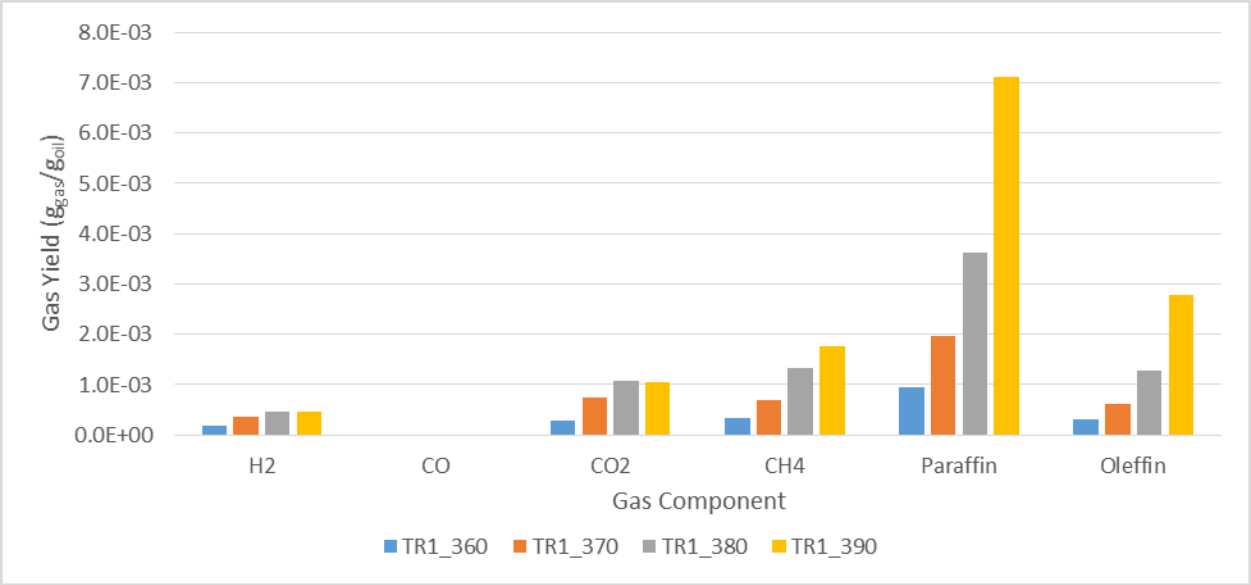

Figure 4-20: Gas yield for catalyst TR1 tested at different temperatures.

According to Figure 4-20, an increase in temperature led to an increase in the production of paraffinic and olefinic molecules, which are related to the ability of cracking side branches on heavy molecules. An increase in hydrogen and CO_2 production was not necessarily observed when temperatures were increased. Also, the yield ratio olefin/paraffin yields varied very little between different temperatures. Thus, low hydrogen yield at higher temperatures were most likely related to a considerable increase in hydrocracking reactions, that increased both paraffin and olefin yields, but it was not followed by a considerable increase on hydrogenating reactions that would shift the olefin-to-paraffin ratio to lower levels. Low hydrogen levels could be related to a decrease, or stabilization, in the catalyst ability on water splitting to produce hydrogen, which would be achieving its maximum at 380ºC. Higher temperatures could be facilitating the oxygen addition reaction towards other molecules than CO_2, which would also explain the lower yields of this gas component. Furthermore, the 390ºC condition was performed last throughout the reaction and low H_2 and CO_2 contents could be a reflex of deactivation of active sites that perform water splitting. Since the ratio olefin/paraffin showed little changes, it is expected that dehydrogenation reactions were slightly impacted by an increase in temperature in the range tested. The methanation reaction, shown in Equation 4-32, could also be used to understand the smaller yields of hydrogen and carbon dioxide in the 390ºC test. In that reaction, hydrogen and carbon dioxide are consumed to produce methane, which yield was also increased in that test.

$$CO_2 + 4H_2 \rightarrow CH_4 + 2H_2O \qquad \text{Equation 4-32}$$

The results on chapter 4 show that catalytic steam cracking is a powerful technology to reduce acidity in heavy oils. All catalysts tested had a considerably higher TAN conversion than the thermal reaction. Between all catalysts, TR3 proved the most suitable to perform TAN reduction due to its high activity. For this reason, this catalyst was submitted to long time-on-stream test to evaluate its aging. Chapter 5 have the results related to those experiments.

5 Deactivation Study on Total Acid Number Reduction for Catalyst TR3

Catalyst screening results in chapter 4 indicated that catalyst TR3 was the most suitable catalyst to perform TAN reduction under low severity conditions. Thus, a comprehensive study on TR3 deactivation was done and its results are shown in this chapter. The experiments in this section consisted mostly of 6-7 days reactions at constant reaction conditions in which the TAN reduction profile was observed and modeled. The goal was to understand the rate at which deactivation took place and the conditions that favored a long catalyst life. Catalyst regeneration was also tested in order to understand the possibilities of different reactor configurations for TAN reduction. Finally, an economic analysis was performed to evaluate the feasibility of implementing this process in an oil producing facility.

5.1 Deactivation Kinetics Model

The first order kinetics equations shown in section 4.1.1 are recalled by Equations 5-1 and 5-2.

$$r = k(T) \times TAN \qquad \text{Equation 5-1}$$

$$k(T) = k_0 \times exp\left(\frac{-E_A}{RT}\right) \qquad \text{Equation 5-2}$$

The kinetic constant in those equations is a function of temperature, but not of time, though, a deactivation due to coke deposition is expected to take place, at the beginning of the reaction. This deactivation can be modeled by Equation 5-3, in which C is coke build-up, C_{max} is the maximum monolayer coke formation, K is an adsorption constant, and w is the cumulative feed-to-catalyst ratio (Kam et al., 2005).

$$C = C_{max}[1 - \exp(-Kw)] \qquad \text{Equation 5-3}$$

In the equation, w can also be taken as the time-on-stream if flow rates are constant throughout the reaction, which is the case for the experiments carried out in this section. When a complete monolayer is formed, all active sites are covered and the catalyst loses all activity. Equation 5-3 can be mathematically manipulated and rewritten to produce Equation 5-4.

$$1 - \frac{C}{C_{max}} = exp(-k_d t) \qquad \text{Equation 5-4}$$

Considering that coke deposition is directly related to the loss of available active sites, the relationship between activity and carbon deposited is given by Equation 5-5.

$$1 - \frac{C}{C_{max}} = \frac{k}{k_i} \qquad \text{Equation 5-5}$$

Note that in Equation 5-5, k_i represents the activity of a catalyst at a given condition before any deactivation takes place. Substituting Equation 5-5 in Equation 5-4, Equation 5-6 and Equation 5-7 are obtained.

$$\frac{k}{k_i} = exp(-k_d t) \qquad \text{Equation 5-6}$$

$$k = k_i exp(-k_d t) \qquad \text{Equation 5-7}$$

The shape of deactivation profile observed on Figure 4-10 is also the same as that expected by the derived Equation 5-7. Equation 5-6 is similar to the Voorhies relationship for fluid catalytic cracking deactivation due to coke deposition that is given in Equation 5-8. In that equation, α is an empirical coking factor while t represents the time for which the catalyst has been exposed to the feedstock (Degnan et al., 2000).

$$Fraction\ of\ initial\ activity = \frac{k}{k_i} = exp(-\propto t) \qquad \text{Equation 5-8}$$

Equation 5-7 can be linearized by taking the logarithm of both sides, resulting in Equation 5-9.

$$\ln k = \ln k_i - k_d t \qquad \text{Equation 5-9}$$

Recalling from section 4.1.1, the reaction constant rate (k), at any condition and time on stream, can be calculated as a function of the TAN conversion as shown in Equation 5-10.

$$k = \frac{-\ln(1 - X_{TAN})}{t_{res}} \qquad \text{Equation 5-10}$$

Finally, the constants k_i and k_d can be calculated in a plot between ln (k) over time. The final constants can be calculated by Equations 5-11 and 5-12.

$$k_i = exp(intercept) \qquad \text{Equation 5-11}$$

$$k_d = -slope \qquad \text{Equation 5-12}$$

In the plots of ln k versus time, it is important to highlight the role of errors in the estimation of kinetic constants. Figure 5-1 shows the value obtained for ln k for different total acid number conversions at the same residence time (1 hour). Since the error in the TAN analysis is around 10%, when TAN conversion is below 20% or above 80%, the error in TAN measurement can greatly impact the value of ln k obtained and, consequently, the value of the constants k_i and k_d.

For that reason, in the following sections, only TAN conversions between 20% and 80% were used for the determination of k_i and k_d. However, when simply plotting the total acid number conversion over time, all values were shown.

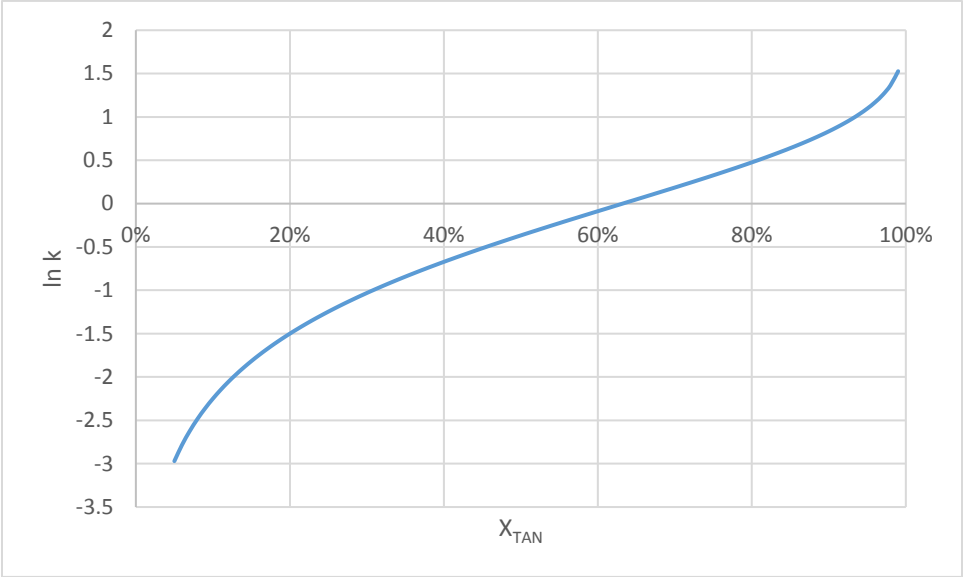

Figure 5-1: Logarithm of kinetic rate constant as function of total acid number conversion for residence time equals to 1 hour.

The deactivation model proposed in this section was used in the following sections to evaluate k_i and k_d for different conditions. Section 5.2 uses the model as a tool to evaluate the reproducibility of the experiments. Section 5.3 compares the effects of different water-to-oil ratios in the reaction, while section 5.4 evaluate the differences between reactions at different temperatures. Finally, section 5.5 compares the deactivation patterns at different reaction pressures.

5.2 Base Condition and Duplicate Reactions

The base condition reaction, i.e. a reaction with fresh catalyst at 360°C, space velocity of $1h^{-1}$, water-to-oil ratio of 5%, and pressure of 2,760kPa, was ran in order to evaluate its deactivation profile. Note that this same reaction was used to compare the results with other catalysts in section 4.3. The experiment was conducted in replicate to assess the repeatability of the reaction and the results obtained from it. The total acid number conversion over time for both reactions can be found in Figure 5-2.

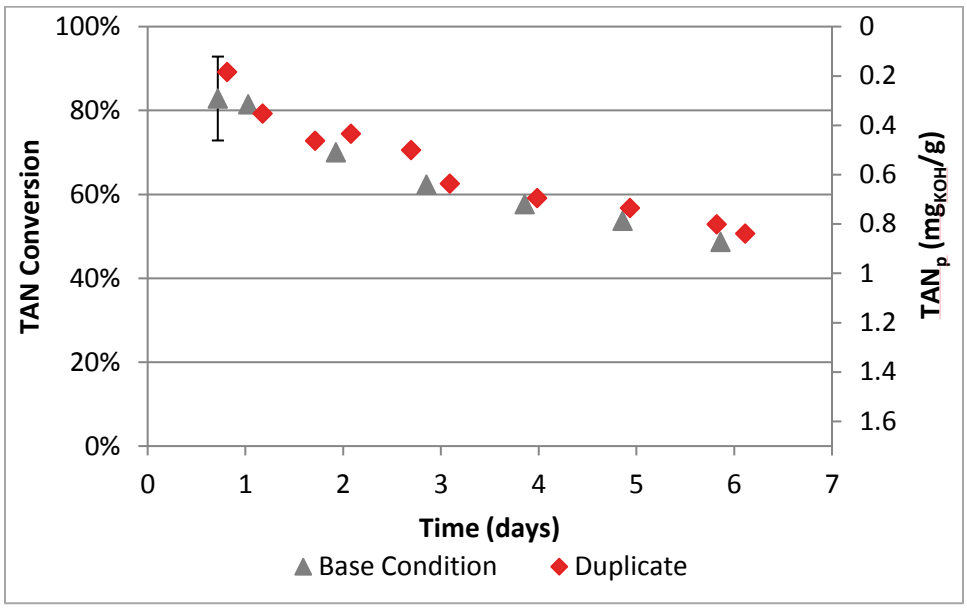

Figure 5-2: Total acid number conversion for reaction with catalyst TR3 at 360°C, 2,760kPa, 5% WOR and space velocity $1h^{-1}$ (base condition reaction); and its duplicate.

Figure 5-2 shows that TAN conversion values for both runs were very close and they varied within 10% of each other at almost any given time. The plot of the logarithm of k over time can be seen in Figure 5-3 for both reactions. The results for k_i and k_d can be found in Table 5-1.

Table 5-1: Initial reaction constant rate and deactivation constant for base case and duplicate.

	k_i (h^{-1})	k_d ($days^{-1}$)
Base Case	1.53	0.144
Base Case Duplicate	1.78	0.154

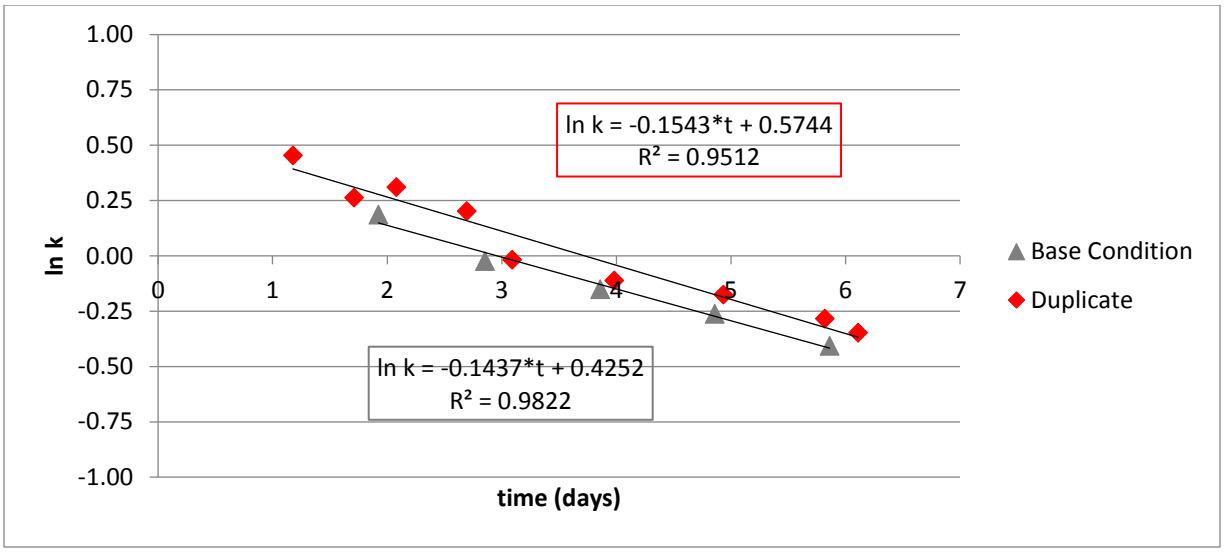

Figure 5-3: Logarithm of rate constant over time for reaction with catalyst TR3 at 360°C and 1h^{-1} (base condition -▲) and its duplicate (♦).

Both k_i and k_d values in Table 5-1 were very close, as expected, since the TAN conversion curves, as seen in Figure 5-2, were very similar. The small differences in the two curves can be associated with errors in the TAN measurements, or experimental errors. For instance, the TAN measurement errors are close to 10% for the range of values tested. Moreover, fluctuations in reaction conditions, such as temperatures and pressures, are another source of experimental errors. Figure 5-4 shows the cut distribution, and residue conversion throughout the reaction.

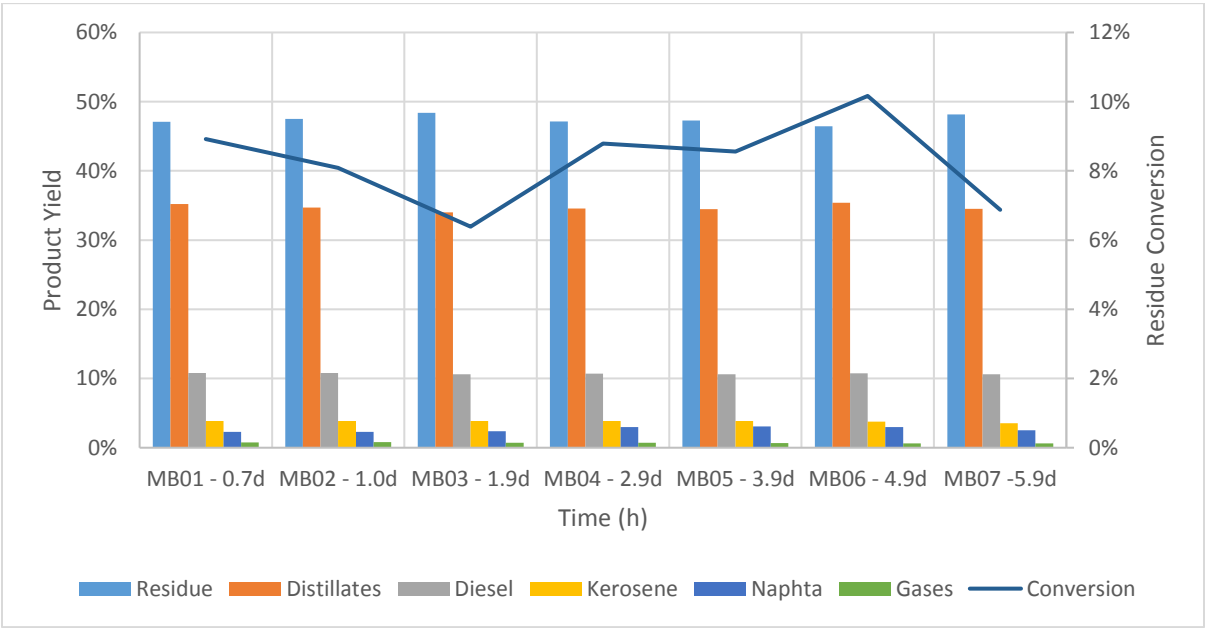

Figure 5-4: Cut distribution and residue conversion for base condition using catalyst TR3.

According to Figure 5-4, very little deactivation was observed along the six days of reaction in relation to residue conversion. The residue conversions fluctuated around the average value of 8.3% with no clear trend of increasing or decreasing its value over time. A possible reason why deactivation was not observed is the very low conversion obtained that would make small changes hard to detect and within the error range of the Simulated Distillation analytical technique. The duplicate reaction had an average residue conversion around 7.0%, which was also within error from the results of the previous run. Other products properties related to these two and other reactions in this chapter can be found in section 5.8.2, page 118.

5.3 Water-to-Oil Ratio Screening

The water-to-oil ratio (WOR) is an important factor in the system kinetics and dynamics. According to previous results on preliminary developments of the process in the research group, a 5% v/v of water in relation to oil was considered ideal for maximizing reaction on steam catalytic cracking. Though, none of the preliminary studies took into consideration deactivation issues and, then, 2.5% and 7.5% ratios were tested in this project. The software VMGSim® was used to simulate the gas and liquid fractions in a reactor for the different water-to-oil ratios. It is important to highlight that the pumped water went through a phase change to the vapor state in the studied reaction conditions. Table 5-2 has the results regarding gas and liquid fractions obtained in the simulation.

Table 5-2: Gas and liquid fraction for reactions at 360ºC and 2,760kPa and different WOR.

WOR	**2.5%**	**5.0%**	**7.5%**
Total Gas fraction	73.3%	83.4%	87.9%
Nitrogen fraction	12.7%	7.9%	5.7%
Steam fraction	60.6%	75.5%	82.2%
Liquid fraction (100% oil)	26.7%	16.6%	12.1%

A decrease in water-to-oil ratio had the effect of increasing the oil fraction in the reactor that translates into a longer actual residence time for the oil fraction. On the other hand, water was one of the reactants in the reaction mechanisms for this system as exemplified by the proposed naphthenic acid decarboxylation reaction reviewed by Equation 5-13. Thus, a decrease in its content is expected to decrease the overall reaction rate.

$$R - CH_2 - COOH + 2H_2O \rightarrow R - H + 2CO_2 + 3H_2 \qquad \text{Equation 5-13}$$

In the decarboxylation reaction, two molecules of water are necessary to react with one molecule of naphthenic acid. Knowing that the feedstock total acid number is 1.7mg_{KOH}/g, and assuming all acidity comes from naphthenic acids, this number can be converted into a number of acid groups, i.e. carboxyl acid groups, represented by –COOH, as shown in Equation 5-14.

$$COOH_{total} = \frac{TAN}{56.11 \times 10^3 \frac{mg_{KOH}}{mol_{KOH}}} = 3.03 \times 10^{-5}\, acid\ groups/g_{feed} \qquad \text{Equation 5-14}$$

The API gravity of the feedstock is 11.8 and, hence, its density is 0.9874g/cm^3. The volumetric concentration of acid can be obtained according to Equation 5-15.

$$C_{COOH} = COOH_{total} \times 0.9874 \frac{g_{feed}}{cm^3_{feed}} = 2.99 \times 10^{-5} \frac{acid\ groups}{cm^3_{feed}} \qquad \text{Equation 5-15}$$

A 5% water-to-oil ratio would mean that, for the total amount of acid sites shown in Equation 5-15, the molar quantity of water available for reaction is the one calculated by Equation 5-16.

$$water = \frac{0.05 cm^3_{H_2O} \times 0.9982 \frac{g_{H_2O}}{cm^3_{H_2O}}}{18.015 \frac{g_{H_2O}}{mol_{H_2O}}} = 2.75 \times 10^{-3} mol_{H_2O} \qquad \text{Equation 5-16}$$

Hence, there is 92 times more water molecules than acid groups which represents 46 times more than the stoichiometry ratio from Equation 5-13. Similarly for 2.5% and 7.5%, the ratio water to acid groups is 46 and 138, respectively, which represents 23 and 69 times more water than the reaction stoichiometry. Although it seemed the water excess was such that the differences in its quantity should not affect reaction rates, it is unclear which reaction step is the rate-determining one of the process kinetics. If, for instance, water splitting was the rate determining step, the water partial pressure on the reactor could affect the reaction rate. Figure 5-5 shows the TAN conversion for the different water-to-oil ratio reactions.

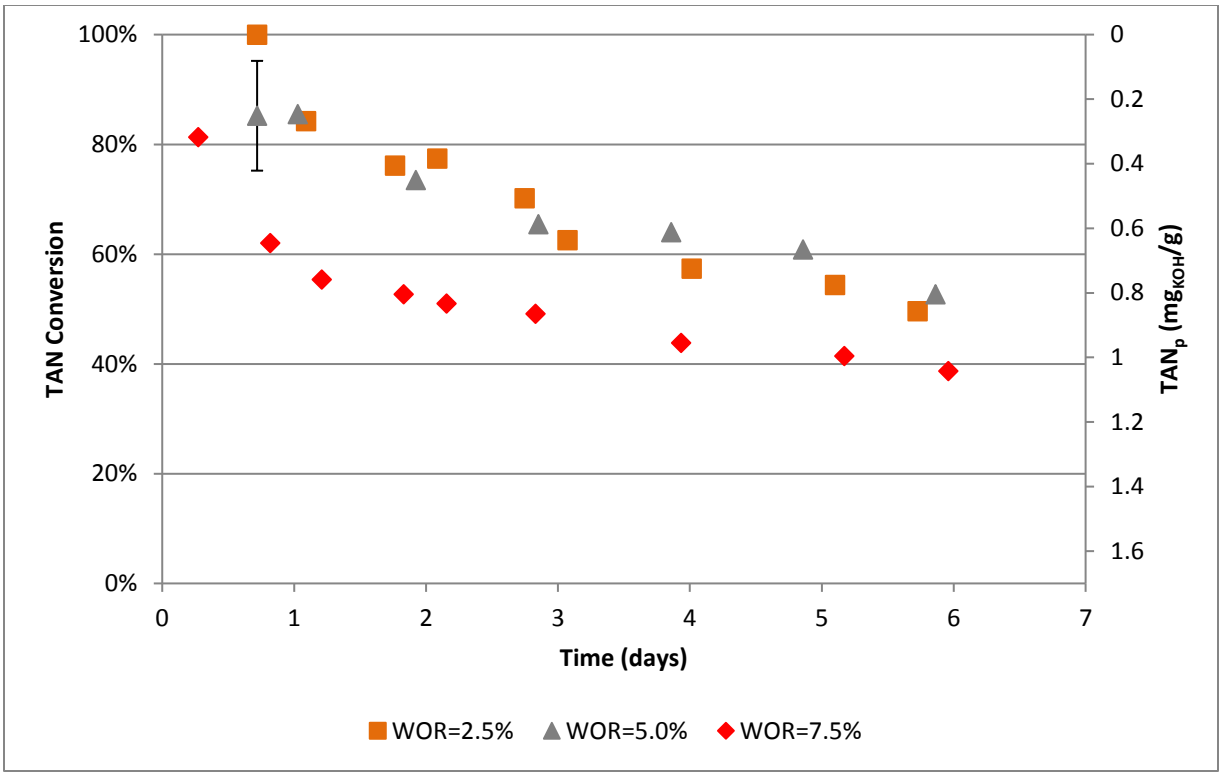

Figure 5-5: Total acid number conversion for catalyst TR3 at 360ºC, 2,760kPa, space velocity $1h^{-1}$, and varying water-to-oil ratios.

From Figure 5-5, it is clear that water-to-oil ratio around 7.5% had a much lower activity than the other two values tested. That could be related to the already high excess of water in the reactor that did not improve the rate of reaction but decreased the effective residence time for oil molecules. Nevertheless, especially after 1 day of reaction, WOR=7.5% was the reaction condition that seemed more stable and suffered less deactivation, indicating that water had a role in inhibiting deactivation. It was expected that most deactivation came from coke formation and deposit into the pores and active sites of the catalyst. The excessive amount of water had the effect of inhibiting and retarding those processes by limiting the contact between oil and catalyst and by providing oxygen and hydrogen necessary to process the heavy oil molecules before acting as coke precursors. Comparing WOR 2.5% and 5.0%, TAN conversion for WOR 2.5% was higher for the beginning of reaction but became lower after around three days. In this case, the smaller gas fraction on the reactor made the initial activity to be high which was shown by the high conversions in the initial days. However, the lack of water, essential for coke inhibition mechanisms, made deactivation for this reaction faster than for the high WOR level ones. Figure 5-6 shows the plot

of the logarithm of k versus time for the three reactions while Table 5-3 summarizes the values of k_i and k_d obtained.

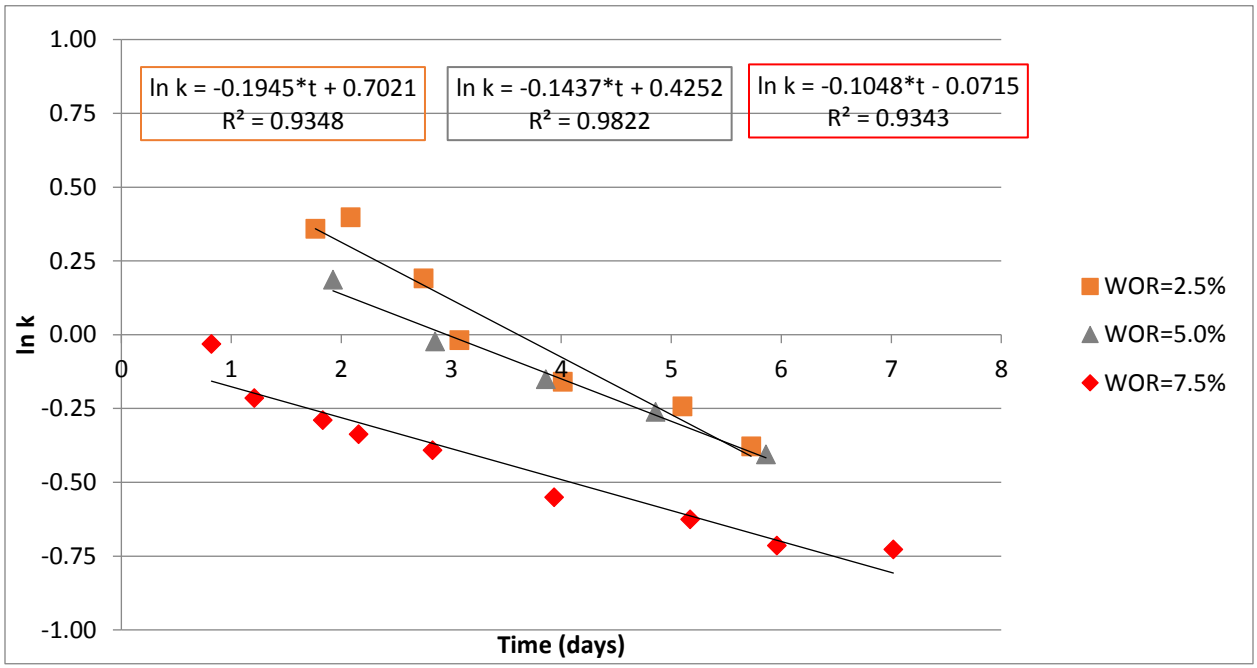

Figure 5-6: Logarithm of kinetic rate constant over time for catalyst TR3 with WOR of 2.5% (♦), 5.0%(▲), and 7.5% (■).

Table 5-3: Initial reaction constant rate and deactivation constant for catalyst TR3 with WOR varying from 2.5% to 7.5%.

WOR	**k_i (h^{-1})**	**k_d ($days^{-1}$)**
2.5%	2.02	0.195
5.0%	1.53	0.144
7.5%	0.93	0.105

Table 5-3 and Figure 5-6 reinforces the remarks about Figure 5-5. The error regression coefficient for all curves were close to 0.95 showing good fitting between data and proposed model.

5.4 Temperature Screening

Reaction temperature was found to be a fundamental variable in the balance between reaction and deactivation kinetics. An increase in temperature was expected to increase, exponentially, the reaction rate as seen in Equation 5-2. Coke formation is a reaction that also follows Arrhenius equation and, then, was also expected to increase its rate with an increase in temperature. To get a more comprehensive look into the effects of a temperature increase, a reaction at 380ºC was carried out and the total acid number results are shown in Figure 5-7.

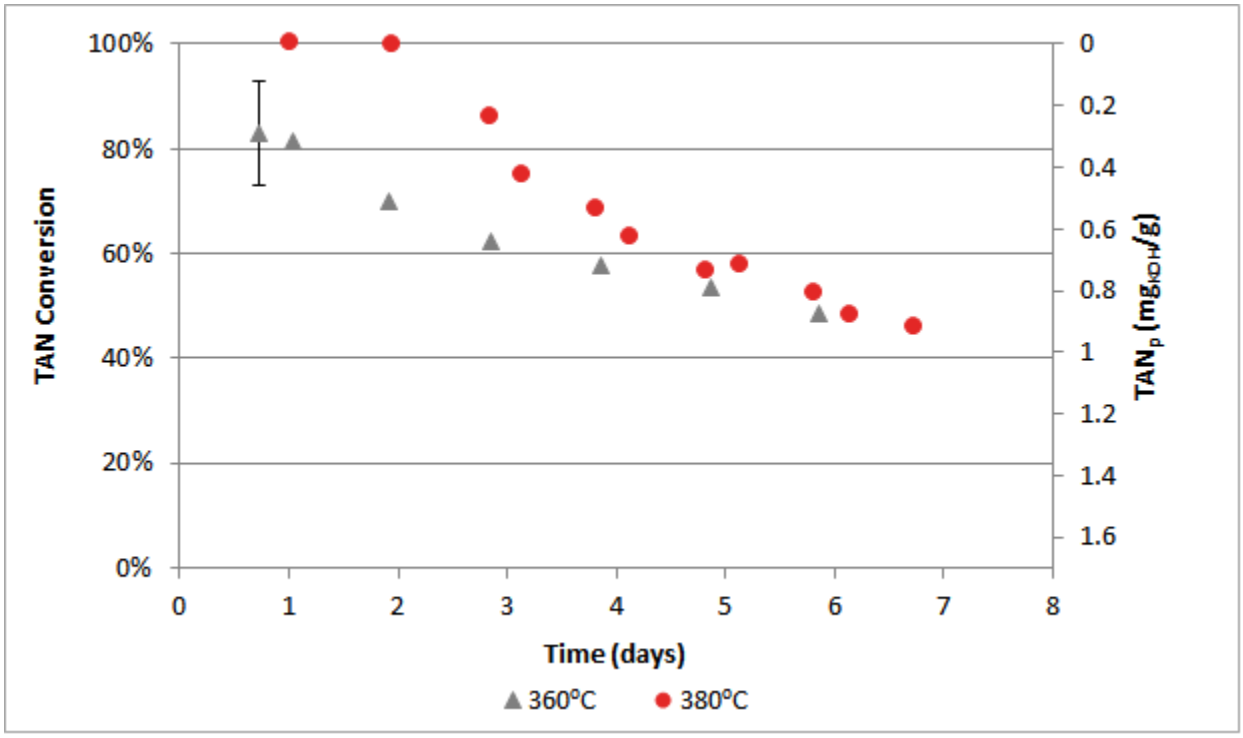

Figure 5-7: Total acid number conversion for catalyst TR3 at 2760kPa, 5% WOR, space velocity 1h^{-1} and temperatures of 360ºC and 380ºC.

Figure 5-7 very clearly shows that, as expected, the initial activity for the reaction at 380ºC was much higher than at 360ºC. In fact, when reacting at 380ºC the TAN conversion was 100% for over 48 hours while at 360ºC such a level of conversion was never achieved. At the same time, the rate of deactivation for that reaction was such that after only four days its activity was almost the same of the reaction at 360ºC. As a result, extrapolation in the trends of conversion levels would lead to a crossover between the two curves. That means that the rate of coke deposition and pore blockage rates at 380ºC are much higher than the ones at 360ºC. Therefore, for catalyst TR3, starting the reaction at high temperatures was counter-productive in the sense of extending the

catalyst life. Figure 5-8 shows the plot of the logarithm of kinetic rate constant over time while Table 5-4 shows the initial kinetic rate constant and the deactivation constant for both reactions.

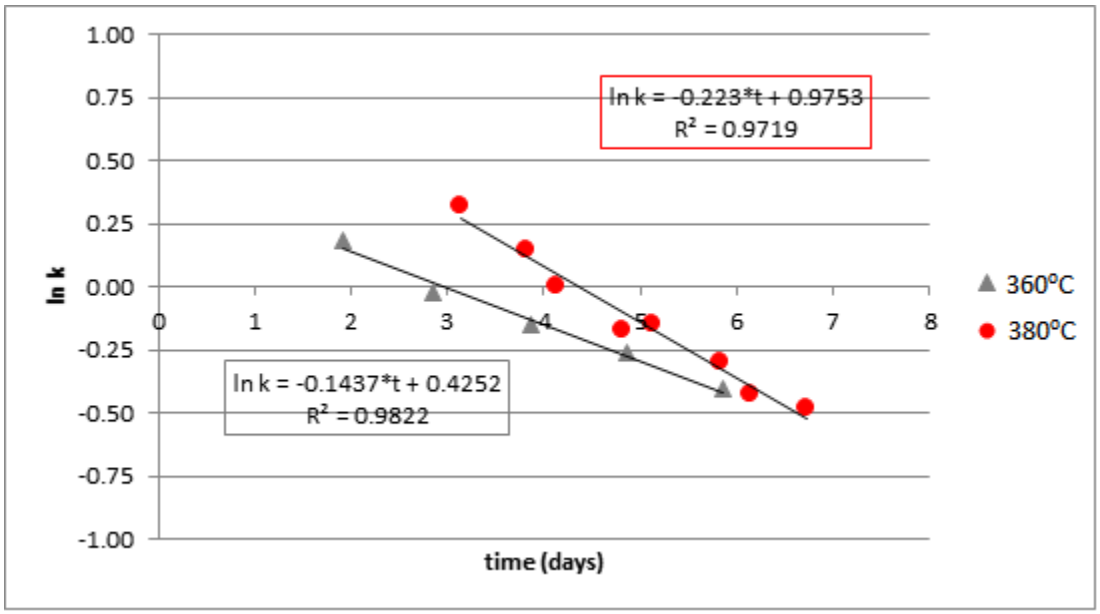

Figure 5-8: Logarithm of kinetic rate constant over time for reaction temperatures of 360°C (▲) and 380°C (●).

Table 5-4: Initial reaction constant rate and deactivation constant for reaction temperatures of 360°C and 380°C.

Temperature	**k_i (h^{-1})**	**k_d ($days^{-1}$)**
360°C	1.53	0.144
380°C	2.65	0.223

Figure 5-8 shows a high correlation between proposed model and correlated data with both regression coefficients above 0.97. Figure 5-8 trends also point towards a crossover between the TAN conversions after 7 days since the reaction at 380°C had both kinetic and deactivation rate constants higher than the reaction at 360°C by, respectively, 73% and 55%. In fact, if data from Figure 5-8 and Table 5-4 were used to extrapolate to 10 days of time on stream, the calculated conversion for the 360°C reaction would be 21% while the 380°C reaction would be only 10%. Because the deactivation constant reduces the catalyst activity in an exponential rate, the crossover is possible between the two reactions. Figure 5-9 shows the effects of temperature in coke deposition for hydroprocessing catalysts (Furimsky, 1999).

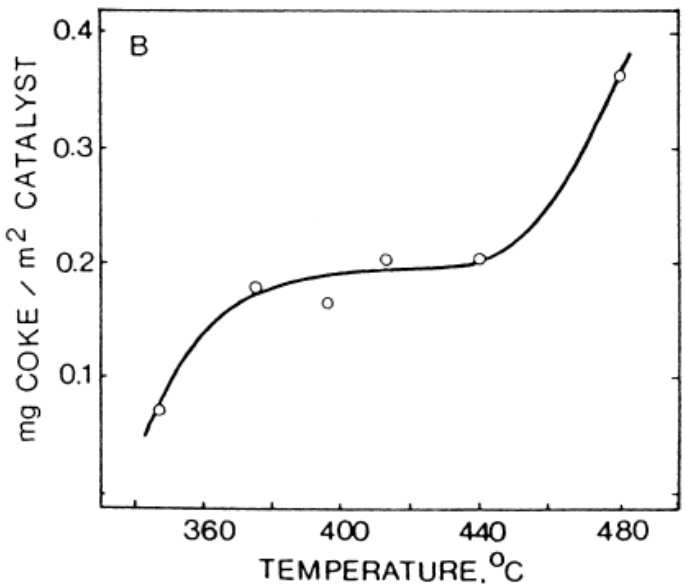

Figure 5-9: Temperature effects in coke deposition for hydroprocessing catalyst (Furimsky, 1999).

Figure 5-9 shows that an increase in temperature leads to an increase in coke deposition for most of the range of temperatures tested. The flat part of the curve, at temperatures around 400-440ºC, is related to an increase in hydrogenating and cracking of heavy molecules that compensates for the increase in polymerization of those molecules. Above 440ºC the increase in polymerization rate is much larger than the ones in hydrogenating and cracking which increases the rate of coking.

The data in Table 5-4 can be used to estimate the activation energy of catalyst TR3 and its results are summarized in Table 5-5. Note that activation energy and pre-exponential factor were calculated through equations Equation 4-23 and Equation 4-24 that used the slope and intercept of a plot between ln k versus the inverse of temperature. Also, note that this plot was not represented in this chapter for catalyst TR3 since only two points were being used and the analysis of the data fitting and the error regression coefficient become pointless.

Table 5-5: Pre-exponential factor and activation energy for thermal and catalysts TR1 and TR3.

	TR1	**TR3**	**Thermal**
k_0 (h^{-1})	5.39×10^{8}	9.66×10^{7}	1.48×10^{13}
E_A (kJ/mol)	112.6	94.5	175.5

According to Table 5-5, catalyst TR3 had a lower activation energy than catalyst TR1 and both were considerably lower than the activation energy for thermal reactions.

5.5 Pressure Screening

Hydrogenating catalysts usually require high pressures to perform hydrogenation reactions as discussed in section 2.5. Since catalyst TR3 had a hydrogenating function, a higher pressure, i.e. 4,140kPa, was tested to evaluate if improvements on oil quality were observable. Because the target for this process is to be implemented in a field facility, simplicity of operation and conditions are of major importance in its design. Therefore, although common hydrotreating processes run at pressures around 5,500-17,000kPa (Speight, 2013a), the operating pressures for this process were chosen to be at lower levels. Figure 5-10 shows the total acid number conversion for the reactions at low and high pressures while Figure 5-11 shows the plot regarding the calculation of initial kinetic rate constant and deactivation constant.

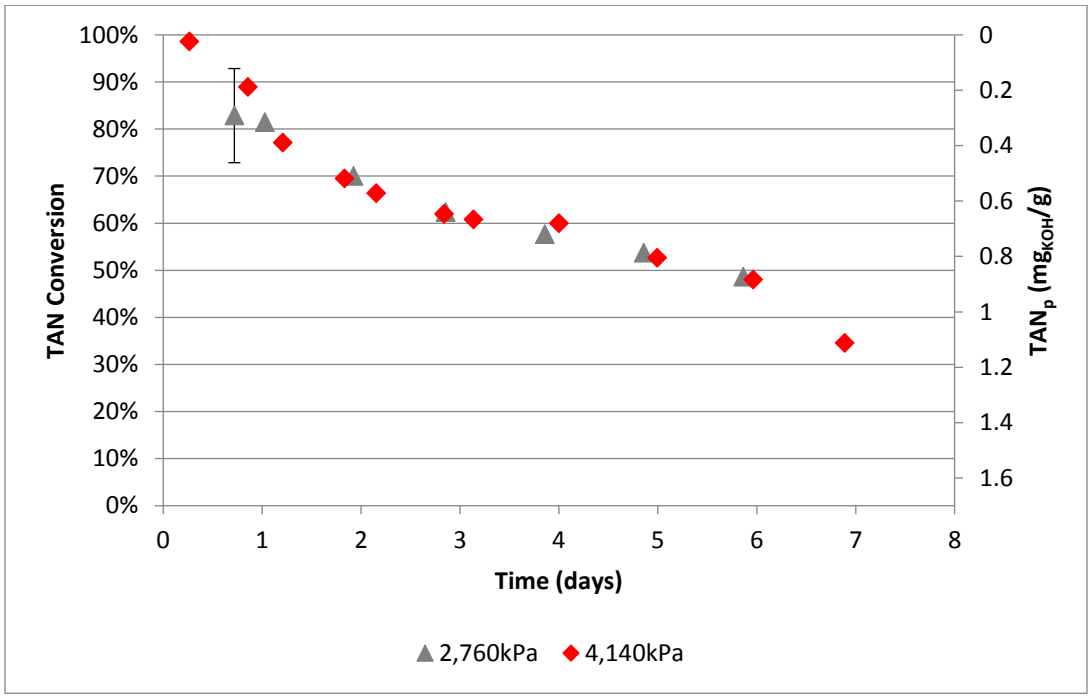

Figure 5-10: Total acid number conversion for catalyst TR3 at 360ºC, space velocity of 1h^{-1}, 5% WOR and pressures at 2,760kPa and 4,140kPa.

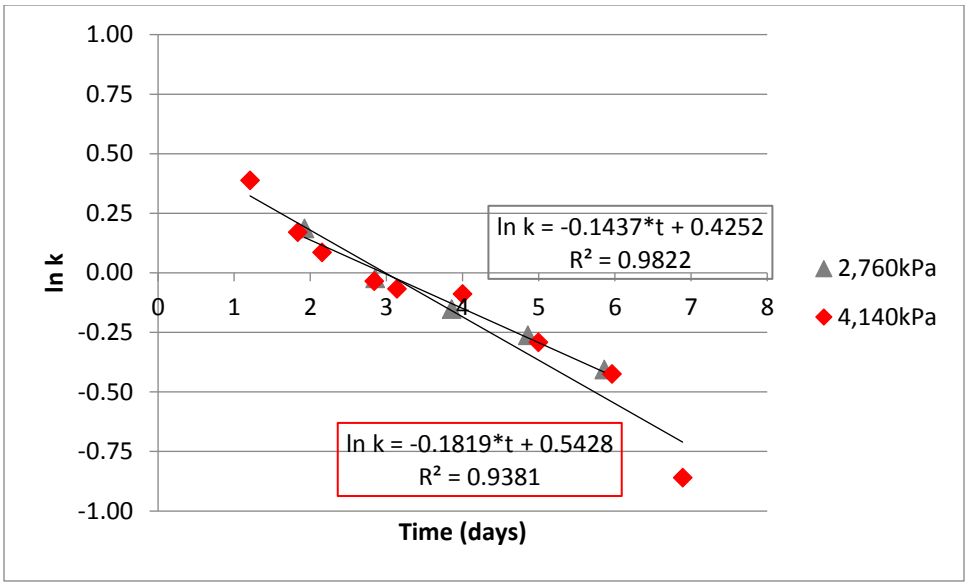

Figure 5-11: Logarithm of kinetic rate constant over time for catalyst TR3 at 2,760kPa (▲) and 4,140kPa (♦).

Analyzing both Figure 5-10 and Figure 5-11, it is possible to note that total pressure had little effect in the total acid number reduction. The high pressure reaction started at higher conversion than the low pressure reaction but quickly moved to values within TAN analysis error. Considering the proposed reaction given by Equation 5-13, an increase in pressure should have the effect of decreasing the reaction rate since there are more molecules of gas being produced than consumed (5:2). However, the CO_2 and H_2 desorption from active sites might not be a rate determining step and, therefore, its concentration in the media might not strongly impact the overall TAN conversion as observed in Figure 5-10. On the other hand, the increase in pressure compressed the gases in the reactor, changing the hydrodynamics of the system, as shown in Table 5-6. The total volumetric flow at reactor conditions dropped by 30% which meant a higher actual residence time for the reactants which has the effect of increasing reactant conversion. Since both reactions had similar activity, the opposite effects of slowing the rate of reaction and increasing the residence time cancelled each other.

Table 5-7 has the final values for initial rate of reaction constant and deactivation constant.

Table 5-6: Gas and liquid fraction for reactions for reaction pressures of 2,760kPa and 4,140kPa.

Condition	**2,760kPa**	**4,140kPa**
Gas fraction	83.4%	76.6%
Nitrogen fraction	7.9%	7.5%
Steam fraction	75.5%	69.1%
Liquid fraction (100% oil)	16.6%	23.4%
Total flow at reaction conditions (mL/min)	5.0	3.6

Table 5-7: Initial reaction constant rate and deactivation constant for reaction pressures of 2,760kPa and 4,140kPa.

Pressure (kPa)	**k_i (h^{-1})**	**k_d ($days^{-1}$)**
2,760	1.53	0.144
4,140	1.72	0.182

The values in Table 5-7 confirm the interpretations made for Figure 5-10 and Figure 5-11. Higher pressure reactions had a slightly higher initial activity that could be related to a longer actual residence time. High pressures could also be improving diffusion limitations of reactants towards catalyst pores, which would improve reaction rates due to high accessibility of active sites. At the same time, high pressure reaction also had a higher deactivation constant since it could be helping the diffusion of high molecular weight molecules into catalyst pores where they could act as coke precursors and deposit on active sites and other pore mouths, further decreasing the overall catalyst activity. As the initial kinetic constant, this difference could be related to the errors in the total acid number measurements.

The deactivation that the catalyst goes through in all conditions tested raises a concern in the nature of the deactivation. Section 5.6 reviews results related to the metal content on the feedstock, a potential cause for irreversible deactivation. Section 5.7 studies the possibility of regenerating the catalyst activity with an oxidative process.

5.6 Metal Deposition Deactivation

The metal content when processing oil is a concern regarding catalyst deactivation since they can poison the active sites by irreversibly adsorbing on the catalyst. As shown in Table 2-5, vanadium and nickel are some of the poisons commonly present in Alberta bitumen. A metal analysis for the diluted bitumen used on the deactivation reactions is given in Table 5-8 and, similarly to Table 2-5, the only considerable amounts of metal presents are nickel and vanadium.

Table 5-8: Metal analysis for Alberta bitumen used on deactivation study.

Metal	Metal Composition (ppm)
Mo	8
Ni	67
V	170
Fe	8

The bitumen demetallization after reaction is the key to understanding the level of deactivation due to metal deposition in active sites. Table 5-9 shows the level of demetallization for different reaction conditions. This table only shows results for nickel and vanadium since the values for iron and molybdenum were negligible.

Table 5-9: Demetallization levels after reaction for TR3 catalyst at different temperatures, pressures, and water-to-oil ratios.

Reaction	1	2	3	4	5	Average
Temperature (^{o}C)	360	360	360	360	380	-
Pressure (kPa)	2,760	2,760	2,760	4,140	2,760	-
Water-to-oil ratio	5.0%	2.5%	7.5%	5.0%	5.0%	-
Ni relative change	-7.0%	+1.6%	-10.4%	+6.7%	-7.9%	-3.4%
V relative change	-6.4%	-1.8%	-10.6%	+7.2%	-7.9%	-3.9%

The results in Table 5-9 are very disperse and, for a few cases, the amount of metals are slightly higher than in the initial bitumen. That is a fact even for vanadium that has no other source on the system other than the bitumen itself. Though, the reason for such a discrepancy was related to the error on the analysis that was around 10% relative change for the values measured. If the average of all samples were taken as a more reliable source of demetallization values, the results gave a

reduction in nickel and vanadium of 3.4% and 3.9% respectively. That meant a reduction in 2.5 ppm for nickel and 7.2 ppm for vanadium. Considering the course of six days of reaction at the approximate flowrate of 1kg/day used on the reactions, the total amount of nickel and vanadium retained by the catalyst is, respectively, 2.6×10^{-4} and 8.5×10^{-4} moles. Considering an average 42 grams of loaded catalyst per reaction and the metal concentration given by Table 3-2, the total amount of metals in a reactor was around 1.35×10^{-1} moles. Thus, even if the guard catalyst was not responsible for any of the metal retention, the maximum amount of active sites poisoned by metals in the feedstock was 0.8% over six days of reaction, which would be undetectable in the results so far. These results indicate that the deactivation observed so far is mostly due to coke deposition. Metal deposition will only have a considerable effect over much longer times on stream.

5.7 Regeneration Study

Due to the deactivation rate that the catalyst went through, an understanding of its regenerability became of fundamental importance for the process economics. The extremely low level of demetallation of the feedstock indicated that most of the loss of activity was due to coke deposition, which can be recovered. The regeneration study was performed on the base condition and its activity was compared to the one prior to regeneration. During a regeneration cycle, the carbon deposited on the surface of the catalyst can be burnt in the presence of oxygen to produce CO or CO_2. The full and partial combustions can be seen in Equation 5-17 and Equation 5-18.

$$C_{(coke)} + O_2 \rightarrow CO_2 \qquad \text{Equation 5-17}$$

$$C_{(coke)} + {}^{1}/_{2}\, O_2 \rightarrow CO \qquad \text{Equation 5-18}$$

Since coke is a very hydrogen-deficient species, its formula was simplified to pure carbon for calculation simplicity. To avoid physical and/or chemical transformations on the catalyst matrix and active sites, the combustion temperature was set to 430ºC.

As mentioned in section 3.2.5, the combustion reaction progress was followed via two different paths. The first one was through gas chromatography in which the levels of O_2, CO, and CO_2 were constantly measured. During combustion, no oxygen could be detected in the reactor exit while after the end of combustion CO_2 levels dropped to zero. No CO was detected at any time during regeneration, which indicated that partial combustion did not take place. The second path in which

regeneration was monitored was through reactor internal temperature. Due to its exothermicity, the internal temperature would increase while combustion was taking place in the particular area in which the thermocouple was placed and it would drop back to the original value after combustion was complete. The temperature profiles for all internal temperature indicators were shown in Figure 3-6, page 50.

The total volume of oxygen used during regeneration can be estimated by Equation 5-19 while the final coke amount can be calculated using the stoichiometry of full combustion in Equation 5-17 and is represented by Equation 5-20. It is important to highlight that the amount of coke calculated was over-estimated since it considered a totally hydrogen-deficient coke. For instance, if the hydrogen to carbon ratio in coke was 1:1, the total amount of coke estimated would drop by 13%. Also, not all material inside the reactor was coke since the cleaning procedure did not necessarily removed all feedstock from the reactor.

$$V_{O_2} = Q_{air} x_{O_2} t_r \qquad \text{Equation 5-19}$$

$$w_{coke} = MW_{coke} \frac{PV_{O_2}}{RT} \qquad \text{Equation 5-20}$$

The calculations lead to a total maximum mass of coke, or hydrocarbon material, burnt around 23.5g, which represents roughly 56% of the mass of catalyst loaded to the reactor. The total acid number conversion for the catalyst before and after regeneration can be seen in Figure 5-12 while the plot of ln k over time for k_i and k_d estimations can be found in Figure 5-13

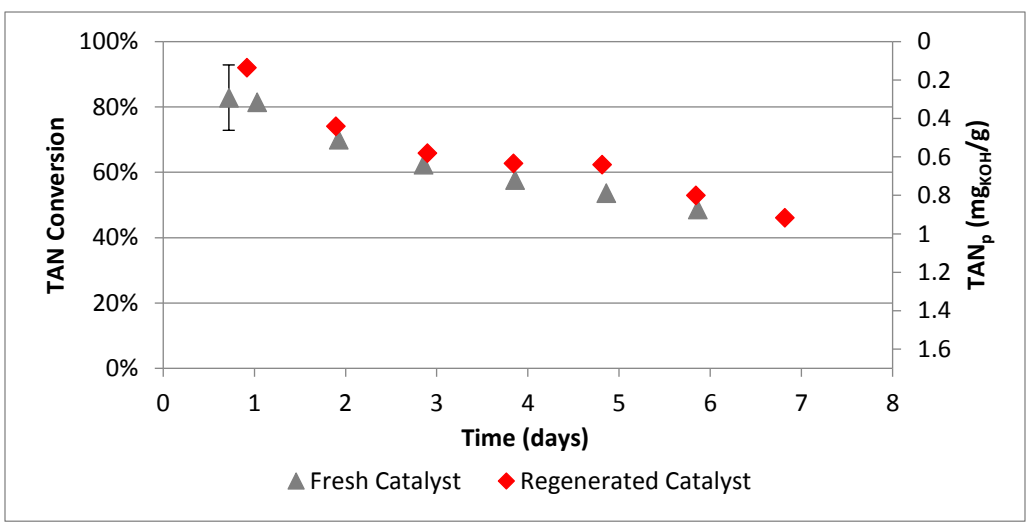

Figure 5-12: Total acid number conversion over time with fresh and regenerated TR3 catalyst at 360°C, space velocity 1h^{-1}, 2,760kPa, and 5% WOR.

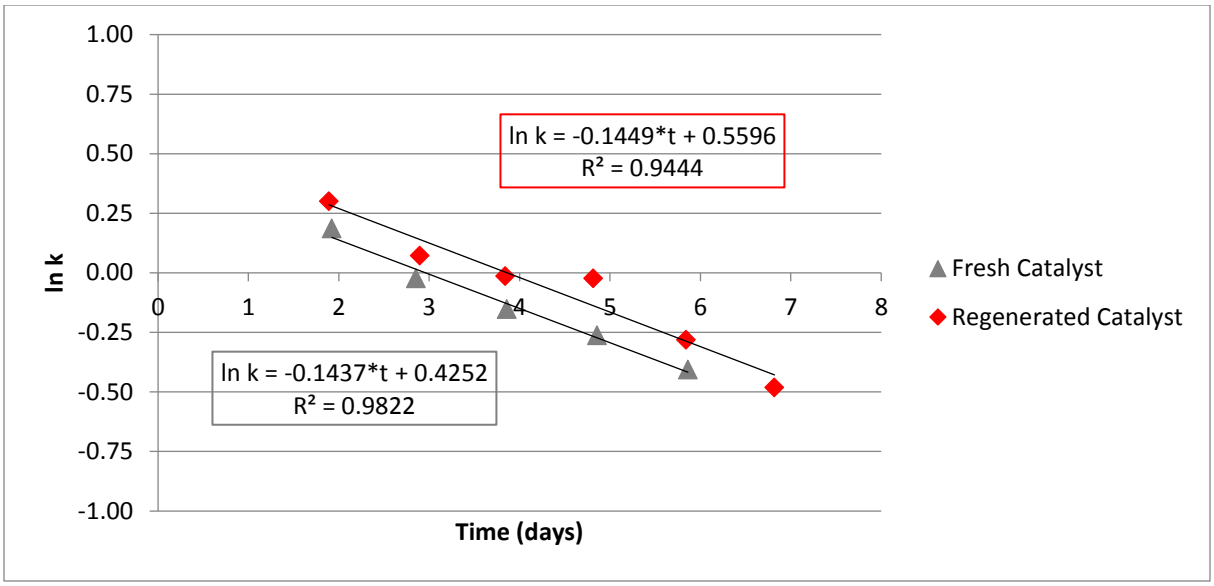

Figure 5-13: Logarithm of kinetic rate constant over time with fresh (▲) and regenerated (♦) catalyst TR3.

With the plot in Figure 5-13 the constants k_i and k_d can be calculated and are given in Table 5-10.

Table 5-10: Initial reaction constant rate and deactivation constant for reaction at 360ºC, 2,760kPa, 5.0% water and its regenerated version.

Catalyst	**k_i (h^{-1})**	**k_d ($days^{-1}$)**
Fresh	1.53	0.144
Regenerated	1.75	0.145
Duplicate	1.78	0.154

The results in this section show a strong agreement between the values of deactivation rate constants, which indicate that the mechanisms of deactivation remained similar for both cases. One interesting point to highlight in the obtained results is that the regenerated catalyst had a higher activity than the fresh catalyst. Explanations for the difference are fluctuations on the oil quality, small variations on conditions during the experimental method, and errors on analytical procedures. Interestingly, regenerated values are even more similar to duplicate reaction, which reinforces the hypothesis of small experimental errors during first reaction.

Finally, it may also be possible that some transformations occurred in the catalyst or active site phases during the regeneration leading to a slightly more active catalyst towards total acid number reduction. An example of the transformation that could have happened in this situation is the

oxidation of molybdenum carbide into different molybdenum oxide forms as proposed by Equation 5-21 and Equation 5-22.

$$Mo_2C + 3O_2 \rightarrow 2MoO_2 + CO_2 \qquad \text{Equation 5-21}$$

$$Mo_2C + 4O_2 \rightarrow 2MoO_3 + CO_2 \qquad \text{Equation 5-22}$$

Studies with molybdenum carbide during dry methane reforming at low pressure and high temperatures have already reported the transformation of molybdenum carbide into dioxide during reaction. Yet, the transformation was responsible for a considerable loss of activity for the targeted reaction (Claridge et al., 1998). Also, molybdenum oxides have been used for heterogeneous catalysis in hydrogenation of low molecular weight alkenes (Mohamed et al., 2015), thus, it may also present activity towards total acid reduction.

Deactivation rates and patterns correlated extremely well between the two reactions which highlights that deactivation mechanisms are probably exactly the same. Since other active sites, as the molybdenum oxides, are expected to change the mechanisms and rates of deactivation, it is very unlikely that the reactions exemplified by Equation 5-21 and Equation 5-22 took place to a significant extent during regeneration.

5.8 Additional Results

5.8.1 Gas Analysis

Figure 5-14 shows the relevant gas products yields for the reactions. All the yields were taken after one day of reaction since at this stage the reaction had already passed the stabilization period and only had small deactivation effects.

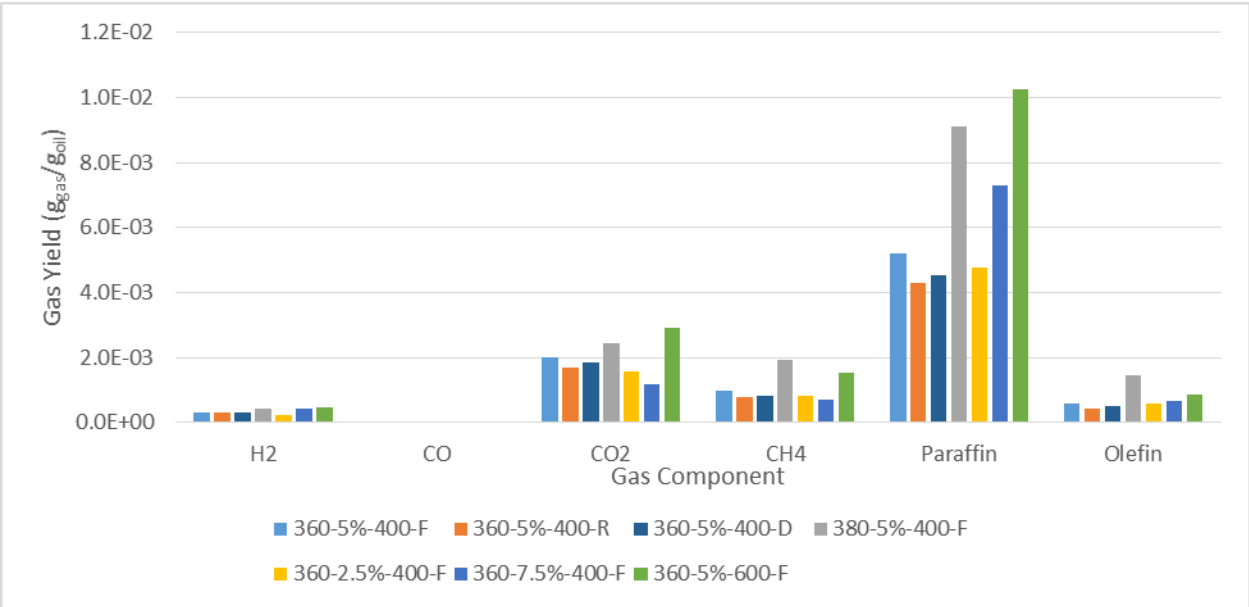

Figure 5-14: Gas yield for different gas products after1 day for fresh (F), regenerated (R), or duplicate (D) TR3 catalyst reaction at different temperatures (360°C, and 380°C), water-to-oil ratios (2.5%, 5.0%, and 7.5%), and pressures (2,760kPa, and 4,140kPa).

A comparison of reactions performed with fresh and regenerated catalysts showed a high level of correlation between the two values and it indicated a possible small loss of activity after catalyst regeneration. All gas components had its yield reduced up to 18% after regeneration was carried out. However, that difference was similar to the one obtained in the duplicate reaction which highlights that the difference is within experimental and analytical errors. In most cases, the total gas yield was around 1%, thus a very low flow rate was obtained. Flow rate is easily affected by fluctuation of conditions, such as pressure, which in turn is affected by sampling. Thus, the small differences observed were irrelevant. Yield ratios were less susceptible to fluctuations in conditions. From fresh to regenerated catalyst reaction, H_2/CO_2 ratios went from 0.15 to 0.18 while the olefin to paraffin ratio stayed almost flat, varying from 0.11 to 0.10. Duplicate values were in

the same range as the base condition, 0.16 and 0.12 respectively. The very similar product proportions showed that the three experiments had very similar reactions taking place.

Figure 5-14 shows that higher temperature, pressure, and water-to-oil ratios tended to increase the yield of hydrogen in the reaction. Higher temperature can be understood as an increase in the rate of reactions that produced hydrogen, such as water splitting, and hydrocarbon dehydrogenation. Higher pressure had the effect of favoring the diffusion of molecules into the catalyst pores that increased the access to active sites and, consequently, increased the rates of reactions. Water-to-oil ratios translated into a higher amount of water available for splitting, thus the higher production of hydrogen.

Carbon dioxide yields parallel hydrogen yields except for the tests performed at different water to oil ratios. In fact, WOR of 7.5% had the lowest CO_2 yield of all reactions. Despite that, these results corroborate the idea that CO_2 was not being totally recovered in the gas stream since part of it was lost dissolved in water. Because 7.5% WOR had a higher water proportion in the products, the amount of carbon dioxide dissolved was also higher, which explains the low yield observed in the gas stream. However it could also happen that the liquid hold-up inside the reactor is extremely poor to wet all the catalyst particles, forming preferential channels for the liquid, effectively increasing the space velocity for the 7.5% WOR.

Paraffins (including methane) and olefins were strongly affected by the increase of temperature or pressure as seen in Figure 5-14. The reaction carried out at 380ºC had the highest methane and olefin yield while the reaction at 4,140kPa had the highest paraffin yield. As discussed for hydrogen yield, temperature had the effect of providing energy that increased the rate of reactions while pressure increased active sites accessibility. Nevertheless, from all reactions, the one at 380ºC had the largest olefin-to-paraffin ratio. That shows that an increase in temperature was effectively increasing dehydrogenation reactions. In addition, the reaction at 4,140kPa had the lowest olefin-to-paraffin ratios, which showed that an increase in pressure improved hydrogenation reactions while also improved cracking reactions. Although on a smaller scale, increasing water-to-oil ratios had a similar effect to increasing pressures.

Table 5-11 displays the bromine number increase for each one of the conditions tested. Almost all conditions had similar bromine number increases and due to this technique's inaccuracy for heavy oil measurements, as discussed in section 3.5.8, few conclusions can be drawn from the trends

observed. Still, the reaction at 380ºC showed a distinctively higher value for bromine number which, again, indicates the high rate of dehydrogenation reactions for this condition.

Table 5-11: Bromine number for reactions using fresh (F) or regenerated (R) TR3 catalyst at different temperatures (360ºC, and 380ºC), water-to-oil ratios (2.5%, 5.0%, and 7.5%), and pressures (2,760kPa, and 4,140kPa).

Reaction	**1**	**2**	**3**	**4**	**5**	**6**
Catalyst	F	R	F	F	F	F
Temperature (ºC)	360	360	380	360	360	360
Water-to-Oil Ratio (v/v)	5.0%	5.0%	5.0%	2.5%	7.5%	5%
Pressure (kPa)	2,760	2,760	2,760	2,760	2,760	4,140
Bromine Number (g_{Br2}/100g)	18.4	18.5	19.9	19.0	18.8	18.9
Bromine Number Increase (g_{Br2}/100g)	5.0	4.9	6.5	5.6	5.4	5.5
Bromine Number Relative Increase	37%	36%	48%	42%	40%	41%

5.8.2 Additional Oil Properties

The objective of this project was to develop a process selective to total acid number conversion. Table 5-12 shows residue conversion, viscosity reduction, API gravity difference, and microcarbon increase for the base condition, its regeneration, and duplicate reactions. The values in all cases were similar, although regenerated catalyst seemed to be slightly less active towards upgrading reactions. As discussed in section 3.5.4, the error in the determination of heavy fractions through simulated distillation is 4%. Thus, all three catalytic reactions had the same residue conversion and, at the same time, they were all higher than the thermal reaction. Viscosity measurement errors were around 5%, thus viscosity values were also within margin of errors, even though regenerated catalyst seemed to be slightly higher. All reactions did not show any major difference in relation to API gravity and microcarbon. Since TAN reactions were little affected by regeneration, it is safe to state that the catalyst successfully remained very selective towards TAN reduction after regeneration for the condition tested.

Table 5-12: Products properties for reactions with fresh and regenerated catalyst TR3 at 360ºC and 1h^{-1} and its duplicate.

Condition	Base Condition	Regenerated	Duplicate	Thermal
Residue content (%wt)	47.3	48.7	48.1	50.1
Viscosity (cP at 40ºC)	1,320	1,630	1,460	7,960
API gravity	12.2	12.3	12.6	9.6
Microcarbon (%wt)	13.1	13.1	12.8	13.0
Residue conversion	8.6%	5.8%	7.0%	1.6%
Viscosity reduction	60.4%	50.5%	55.9%	57.0%
API gravity difference	0.32	0.5	0.85	0.7
Microcarbon increase	2.3%	1.3%	0.0%	-0.9%

Table 5-13 shows the results related to different pressures and water-to-oil ratios. Most of the values were within analytical error and the catalyst was still very selective towards TAN reduction. The only distinct value was WOR=7.5% viscosity reduction that was below the other two reactions, as it was its TAN values. The results for different pressures were also within analytical error. However, high pressure reactions seemed to slightly improve ºAPI and microcarbon values in relation to low pressure, which could be related to a higher hydrogenating reaction rate.

Table 5-13: Products properties for reactions with catalyst TR3 at different WOR and pressures.

	2.5% 2,760kPa	**5.0% 2,760kPa**	**7.5% 2,760kPa**	**Thermal**	**5.0% 4,140kPa**
Residue content (%wt)	48.6	47.6	48.1	50.1	48.1
Viscosity (cP at 40ºC)	1,320	1,320	1,610	7,960	1,290
API gravity	11.9	12.2	11.7	9.6	12.8
Microcarbon (%wt)	13.3	13.1	13.3	13.0	12.7
Residue conversion	5.9%	7.9%	7.0%	1.6%	6.9%
Viscosity reduction	59.9%	60.1%	51.1%	57.0%	61.0%
API gravity difference	0.1	0.1	-0.1	0.7	1.0
Microcarbon increase	3.6%	2.3%	4.2%	-0.9%	-0.6%

Table 5-14 shows the other relevant product properties at 380ºC and its comparison with 360ºC and the thermal values for both temperatures.

Table 5-14: Averaged products properties for catalytic reactions at 360ºC and 380ºC and its respective thermal reaction values.

	Cat TR3 360ºC	**Thermal 360ºC**	**Cat TR3 380ºC**	**Thermal 380ºC**
Residue content (%wt)	47.6	50.1	44.6	48.5
Viscosity (cP at 40ºC)	1,320	7,960	850	6,290
API gravity	12.2	9.6	12.8	9.7
Microcarbon (%wt)	13.1	13.0	14.4	13.6
Residue conversion	7.9%	1.6%	13.8%	4.8%
Viscosity reduction	60.1%	57.0%	74.2%	66.0%
API gravity difference	0.4	0.7	1.0	0.8
Microcarbon increase	2.3%	-0.9%	12.5%	3.8%

Table 5-14 shows that residue conversion, viscosity reduction, and API increase had higher values for 380ºC than for 360ºC. The cracking of heavy oil molecules that are present in residue and other heavy cuts benefited from an increase of temperature and that was the reason for the better performance at 380ºC. However, microcarbon also considerably increased at higher temperature since undesirable side-reactions tended to form coke precursors in the oil. These reactions are polymerization and condensation reactions. The high microcarbon levels on reactions at higher temperature showed the higher level of oil degradation that, with the higher deactivation rate calculated in section 5.4, are the reasons for which starting the reaction at 380ºC is not recommended.

Catalyst TR3 at 380ºC also showed higher residue conversion, viscosity reduction, API difference, and microcarbon increase than thermal reaction. That differs from 360ºC that had similar values than the ones obtained in thermal reaction. This indicates that reactions related to oil upgrading also have lower activation energy for the catalytic reaction and, thus, tend to deviate from thermal levels at higher temperatures.

5.9 Process Economics

5.9.1 Catalyst Life Reaction

An accelerated catalyst aging test was performed with catalyst TR3 in order to get insights into the extent of its catalyst life. The accelerated aging test is an experiment performed at space velocities higher than the ones expected to be used in the industrial size facility. Thus, it evaluates the aging of a catalyst in a relatively short reaction. This reaction was performed starting at 360ºC, $1h^{-1}$, 5.0% water, and 2,760kPa. The industrial size facility is expected to use space velocities around $0.25h^{-1}$. The reaction was a continuation of the base condition reaction and used the methodology of increasing its temperature to compensate for the deactivation pattern. The space velocity, pressure and WOR were kept constant throughout the experiment. Temperatures were increased after total acid number reduction went below the target level, i.e. $0.7mg_{KOH}/g$, which represents a minimum of 59% reduction. The TAN reduction and temperature profiles can be seen in Figure 5-15. The delay imposed between obtaining a sample and performing the necessary analysis made the TAN conversion curve to be below the target at some times, even after the start of the temperature ramping procedure. Still, the cumulative TAN conversion, i.e. the weighted average TAN conversion for all products obtained on this reaction was 54%, which is close to the stipulated target.

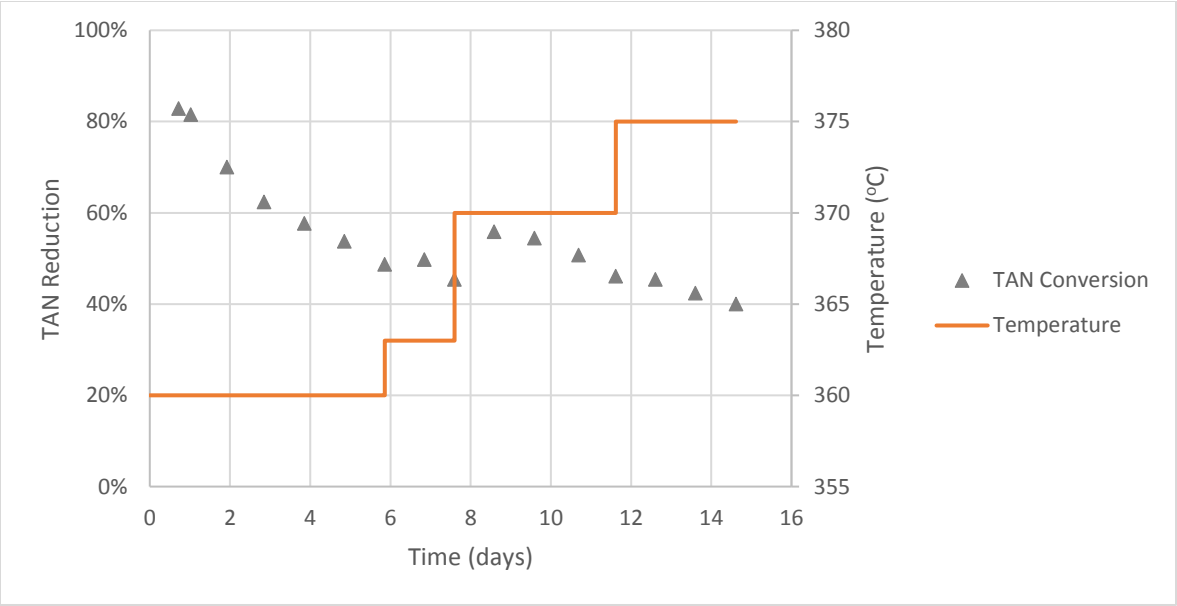

Figure 5-15: Total acid number reduction and temperature profile for catalyst TR3 during temperature compensating aging test at space velocity $1h^{-1}$, pressure of 2,760kPa, and 5% WOR.

Other related product properties were also affected by the temperature increasing and Table 5-15 shows the properties at the beginning, i.e. 360ºC, and end of reaction, i.e. 375ºC.

Table 5-15: Products properties differences at beginning and end of aging reaction for catalyst TR3.

	360ºC	**375ºC**
Residue content (%wt)	47.6	47.3
Viscosity (cP at 40ºC)	1,320	810
API gravity	12.2	12.6
Microcarbon (%wt)	13.1	13.5
Residue conversion	7.9%	8.6%
Viscosity reduction	60.1%	75.6%
API gravity difference	0.44	0.81
Microcarbon increase	2.3%	5.2%

Table 5-15 shows that residue conversion levels were similar from the beginning to the end of the reaction. Section 5.4 results for shorter runs showed that residue conversion for 380ºC is almost double of those obtained at 360ºC. This indicates that, although deactivation in residue conversion was slow and hard to detect due to analytical errors, it existed and it can be observed in longer time-on-streams runs. The gradual increase in temperature also had the effect of increasing the viscosity reduction for this system as shown in Table 5-15. Moreover, microcarbon increased but did not pass, or even got close, to levels obtained at 380ºC which indicates that reactions that were responsible for degrading the oil were at least partially contained.

Hence, the catalyst seemed to be able to successfully perform TAN reduction close to the stipulated target for a minimum of 15 days with a temperature profile ending at 375ºC. This process produced during that period a mostly non-acidic oil, with low level of degradation, and some partial upgrading, as seen in the higher API gravity and lower viscosity. This test run was the one that went through a successful regeneration as shown in section 5.7, which showed that this catalyst is still re-generable after 15 days on stream without loss of initial activity.

5.9.2 Proposed Reaction Set-up Scheme

Previous results in this chapter showed that catalyst TR3 went through some deactivation in the first days of total acid number reduction reactions but it also successfully allowed its regeneration. Thus, the proposed reaction set-up is a swing-type of packed-bed plug-flow reactors in which one or more reactors are regenerating while the rest of them perform the reaction.

To minimize the frequencies in which regeneration and reducing steps are required, the proposed reaction operation was designed to run at a space velocity of $0.25h^{-1}$. Thus, a total of 60 days of operation are expected before regeneration is needed.

The regeneration results and reduction methodology showed that a total of 5 days were necessary to clean, regenerate, reduce, and start-up the catalyst. Due to the larger size of the reactors, it was conservatively considered that those steps will also take four times longer than the pilot plant scale, in a total of 20 days. Thus, a cycle in which ¾ of the reaction units are running while ¼ of them are reducing, optimizes the operational efforts of the reaction unit.

Also, a furnace is necessary to heat up the reactants, i.e. water and bitumen, to reaction conditions. Energy integration was possible in the system since hot products can be used to partially heat up cold reactants. A three-way separator is used at the exit of the system to separate oil, water, and produced gases. Storage tanks and pumps were considered available in the production site and not considered in this preliminary economic analysis. Figure 5-16 shows the block flow diagram (BFD) for the proposed units and the expected existing units in an oil producing facility. Note that the dilution system is another unit that was considered available on the field since it is a required unit regardless of the use of this process.

The proposed industrial size unit was designed for processing capability of 38,000 barrels per day (bpd) of the feedstock used in the deactivation studies in this chapter. Note that this feedstock went through a small pre-addition of diluent. The on-stream factor, i.e. the percentage of time that the plant is running over a year, for this plant was considered 92%.

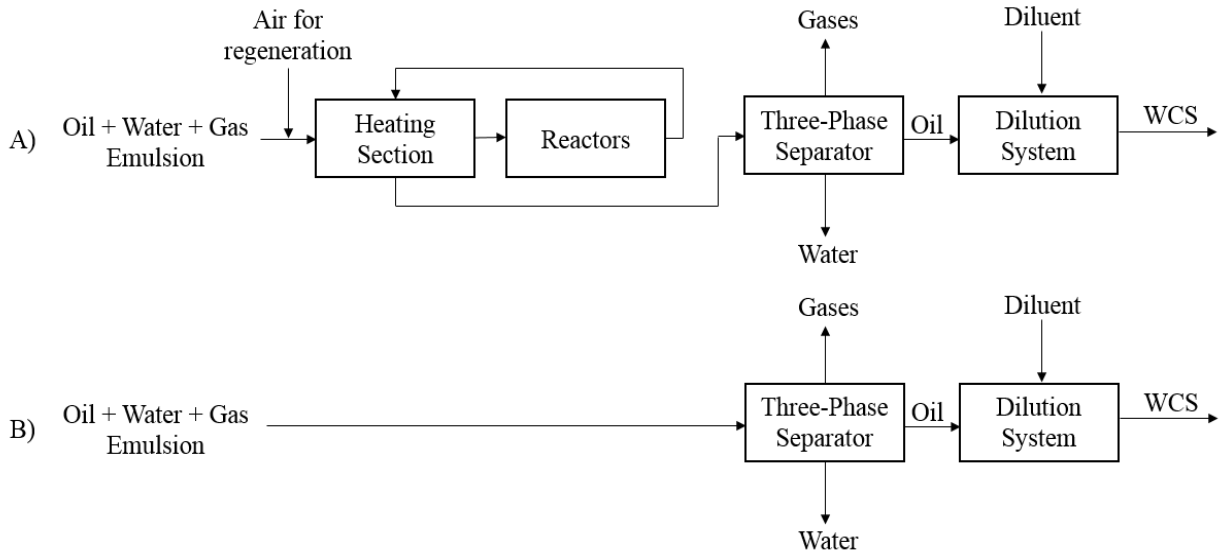

Figure 5-16: Block diagram for A) Proposed reaction, separation and dilution facilities; and B) Current units in heavy-oil production facilities.

5.9.3 Total Fixed Capital Cost

Appendix I shows the calculations for the dimensions and costs of the equipment considered in the economic analysis. Table 5-16 has a summary of the equipment costs for reaction, heating, and separation units. Table 5-17 has the estimation of the total project fixed capital cost using estimated factors for fluid processing (Towler et al., 2013). Other major results from Appendix I are an estimated cost of M$19.9 per catalyst batch that needs replacement after 10 regenerations, i.e. every 2.6 years.

Table 5-16: Equipment purchasing costs.

Unit	**Investment (M$)**
Reaction	6.75
Heating	2.64
Separation	0.28
Total	9.67

Table 5-17: Total fixed capital cost breakdown.

Item	**Cost Equation**	**Cost (M$)**
Equipment Cost ($C_{e,CS}$)	$C_{reac,CS}$+ $C_{sep,CS}$+ $C_{furn,CS}$	8.0
Material Upgrade Cost (C_m)	0.30 ($C_{reac,CS}$+ $C_{exc,CS}$ +$C_{sep,CS}$)	1.8
Equipment delivery (f_d)	0.10 $C_{e,CS}$	0.8
Equipment Erection (f_e)	0.30 $C_{e,CS}$	2.4
Piping (f_p)	0.80 ($C_{e,CS}$ + C_m)	7.8
Instrumentation and control (f_i)	0.30 $C_{e,CS}$	2.4
Electrical Systems (f_{es})	0.20 $C_{e,CS}$	1.6
Service Facilities (f_s)	0.30 $C_{e,CS}$	2.4
Structures and buildings (f_{sb})	0.20 $C_{e,CS}$	1.6
Yard Improvements (f_y)	0.10 $C_{e,CS}$	0.8
Catalyst	-	19.9
ISBL Cost		49.5
Offsites (OS)	0.30 ISBL	14.9
Design & Engineering	0.30 (ISBL+OS)	19.3
Contingency	0.10 (ISBL+OS)	6.4
Total Fixed Capital Cost		**90.1**

In Table 5-7 the total inside the battery limits cost (ISBL) is close to M$50. This cost is related to procurement, shipping and installation of equipment. Nevertheless, ISBL does not include cost related to offsite work, engineering, and contingency.

5.9.4 Operating Costs

Appendix II shows the considerations and calculations regarding operating costs. Table 5-18 summarizes all operating costs being considered

Table 5-18: Total operating costs breakdown.

Unit	Cost (M$/yr)
Labor	1.13
Natural Gas	1.82
Maintenance	1.98
Land and Taxes	1.80
Insurance	0.90
Others	1.70
Total	9.33

5.9.5 Gross Profit

Appendix III contains the calculations and assumptions in the estimation of the gross profit. The revenues from operating this process come from a reduction in the oil acidity and a decrease on diluent requirements due to lower product viscosity. Table 5-19 summarizes the discount due to TAN and costs with diluent for both cases.

Table 5-19: Acidity discount and diluent costs for feedstock and products.

Property	Diluted Feedstock	Diluted Products
TAN	1.3	0.63
TAN discount (CAD$/bbl)	1.85	0.38
Total WCS production (bbl/day)	53,700	50,500
Daily revenue from sales (MCAD$/day)	2.33	2.26
Yearly revenue from sales (MCAD$/year)	782	760
Diluent requirements per barrel (bbl/day)	15,700	12,600
Daily diluent costs (CAD$/day)	929,000	746,000
Yearly diluent costs (MCAD$/year)	312	250

5.9.6 Cash-Flow

The following assumptions were made in order to generate a cash-flow for the industrial plant, which is shown in Figure 5-17.

- Total project life is 30 years.
- Depreciation follows a straight line curve over the first 20 years of operation.
- Total taxes are 27% (15% federal and 12% provincial).
- Inflation rate is 2% over the 30 years period.
- Investments were made in year 0 and operations started in year 1.
- Working capital was considered as 15% of ISBL+OSBL. Total working capital is M$13.52 and it is recoverable after the end of operation. Working capital investment happens at the beginning of year 1.
- Catalyst replacement costs were normalized per year, i.e. although the replacement was only set to happen every 2.6 years, the payments for the replacement were done every year. The total number of replacements was given by the number of years divided by the rate of replacement, and rounded up to an integer number.
- Cash-flow did not consider an interest rate in its calculations.

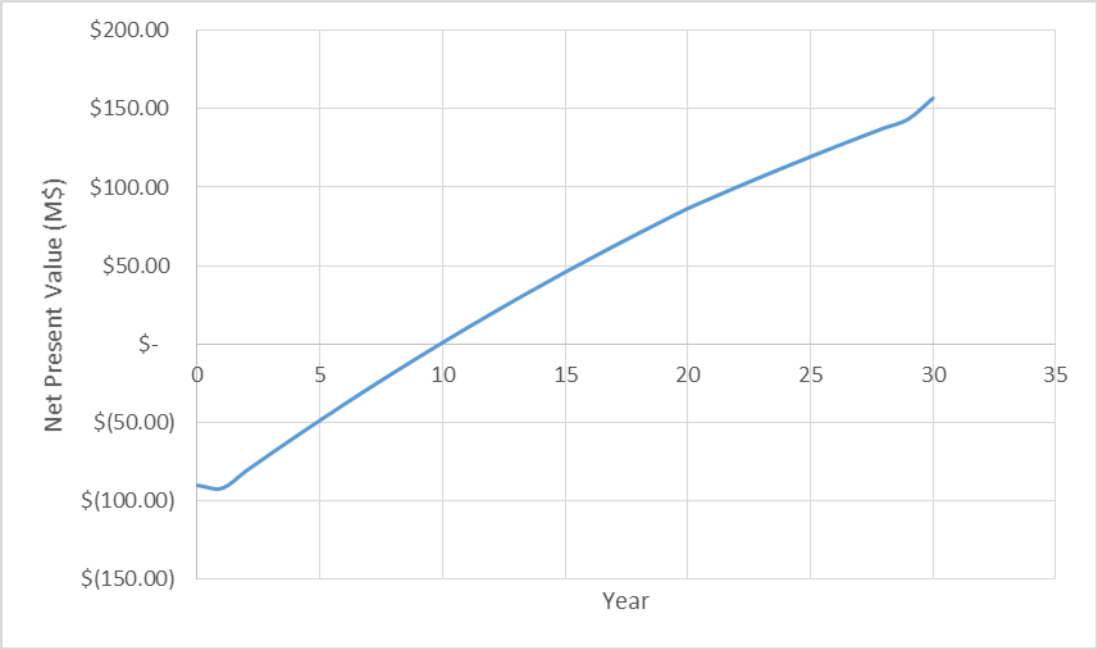

Figure 5-17: Cash-flow diagram in present value units for total acid number reduction industrial facility over a period of 30 years of operation

The economics of the project were evaluated in relation to net present value (NPV), payback period (PBP), and internal rate of return (IRR). NPV is the value of the investment, in present money, after the end of its life. It includes all investments and cash-flows generated by it. PBP is the time in which the net present value is zero, i.e., the cash flow generated by the plant just recovered its initial investment. Finally, IRR is the interest rate that brings the net present value, after the end of the project, to zero. According to the developed economics and the cash-flow shown in Figure 5-17, the investment has a payback time under 10 years with an internal rate of return of 8.6% for the 30 years investment. Also, the net present value over the project life is around M$157.

Some sensitivity analyses were performed in the assumptions done throughout this thesis and also on the variables that are more likely to vary over the next years. All the sensitivity analysis can be seen in Appendix IV. In this section, the four variables with largest impact on the economics are reviewed.

Figure 5-18 shows the effects of a different price on the crude oil (WCS) and on the diluent (EC). Note that the abscissa shows the percentage difference between the tested price and the price considered in the economic evaluation. WCS and EC are important economic factors because they were both related to the savings that decreased acidity and diluent requirements can provide.

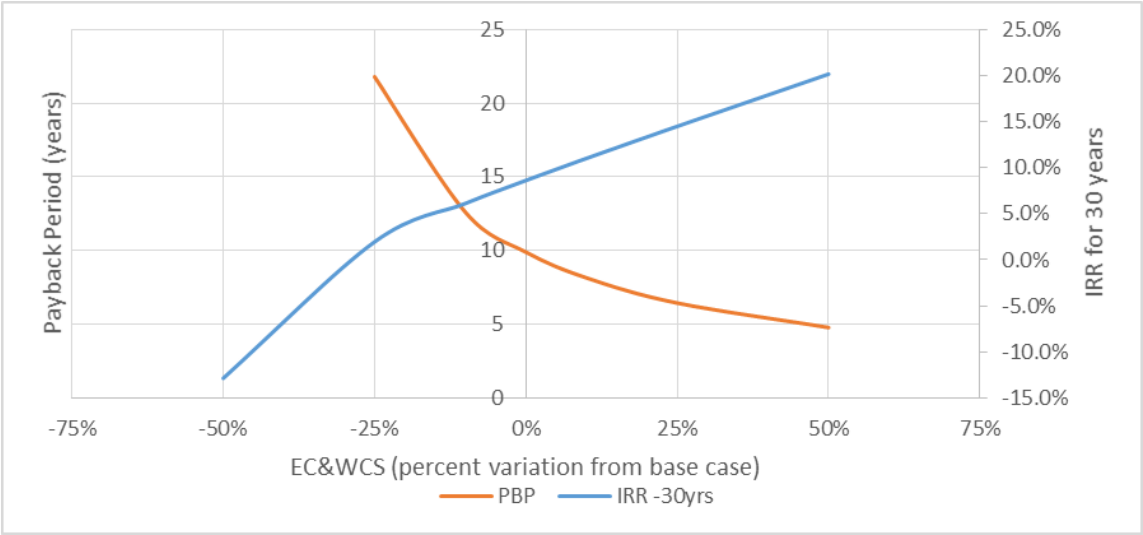

Figure 5-18: Sensitivity analysis on Western Canadian Select and Edmonton Condensate prices with both WCS and EC varying at the same rate.

In Figure 5-18, it can be noted that payback period is as low as five years when increments in WCS and EC are 50%, i.e. WCS is 67.80 CAD$/bbl and EC is 88.89 CAD$/bbl. Although such

increment seems high, current oil prices are considerably lower than average in the past years due to an oversupply crisis that could solve itself in the near future. In fact, WCS above 67.80 CAD$/bbl was a reality in five of the past ten years as shown in Table 5-20 that contains historical WCS prices. Also, all but 2015 heavy oil price was above the WCS price considered in the economics (Baytex Energy, 2016). Nevertheless, if the oversupply crisis tends to deepen itself in the future, as shown in the negative part of the abscissa, that could potentially bring internal rate of returns to negative values.

Table 5-20: Historical average per year prices of WCS and WTI benchmarks in Canadian dollars (Baytex Energy, 2016).

Year	**WCS (CAD$/bbl)**	**WTI (CAD$/bbl)**
2006	51.08	75.10
2007	53.11	77.39
2008	84.42	105.70
2009	59.26	70.24
2010	67.25	81.91
2011	77.09	94.05
2012	73.11	94.12
2013	74.94	100.90
2014	81.28	102.71
2015	45.05	62.32
Average	66.66	86.44

Figure 5-19 shows the sensitivity analysis for product viscosity

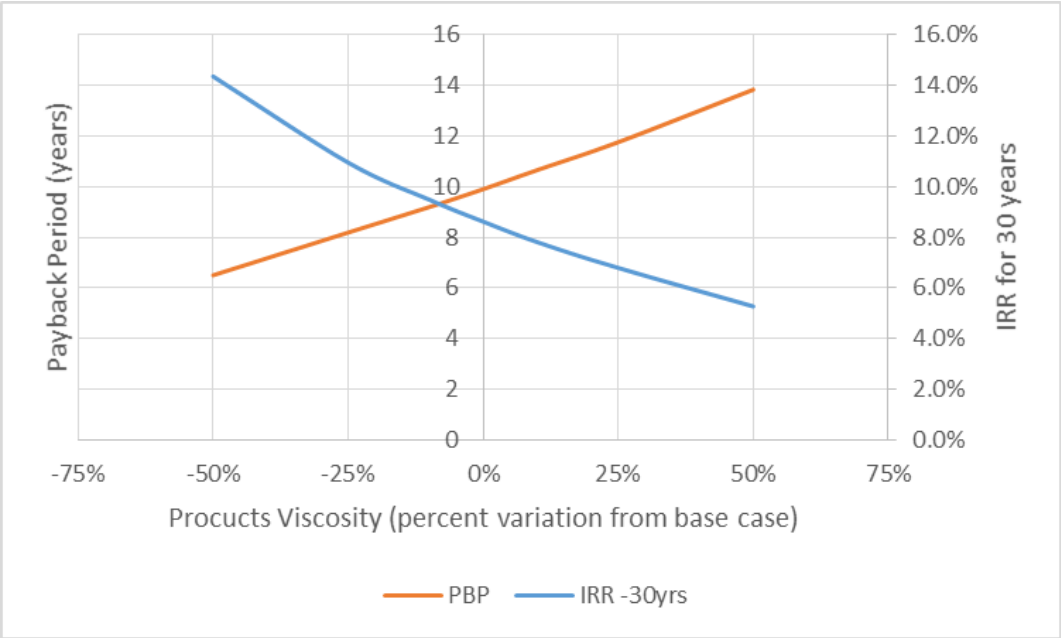

Figure 5-19: Sensitivity analysis for variations in products viscosity.

Figure 5-19 shows the importance of viscosity levels for the process economics. The current viscosity value used, i.e. 1185cP at 40°C and variations in ±50% in its value makes payback period vary over a range of 7.3 years while it makes internal rate of returns vary over a 9.1% range. Viscosity is probably the oil property most susceptible to manipulation and changes. For instance, in section 5.4, an increase in 20°C in reaction temperature made the viscosity of products drop by 35%. A further reduction on viscosity to below 600cP can easily lead to payback periods of 6.5 years. In the extreme case that no diluent is necessary, the payback period becomes 1.6 years with IRR over 60%. However, it is important to remember that decreasing viscosity requires high severity reaction conditions that can further degrade oil by increasing its microcarbon content, olefin content, coke yield, and gas yield. The sensitivity analysis was performed without considering those side effects and reactions carried at such severity need to be further studied to better understand the economics of the process at those levels of viscosity reduction. Figure 5-20 shows the effects of variations in the total acid number in the products.

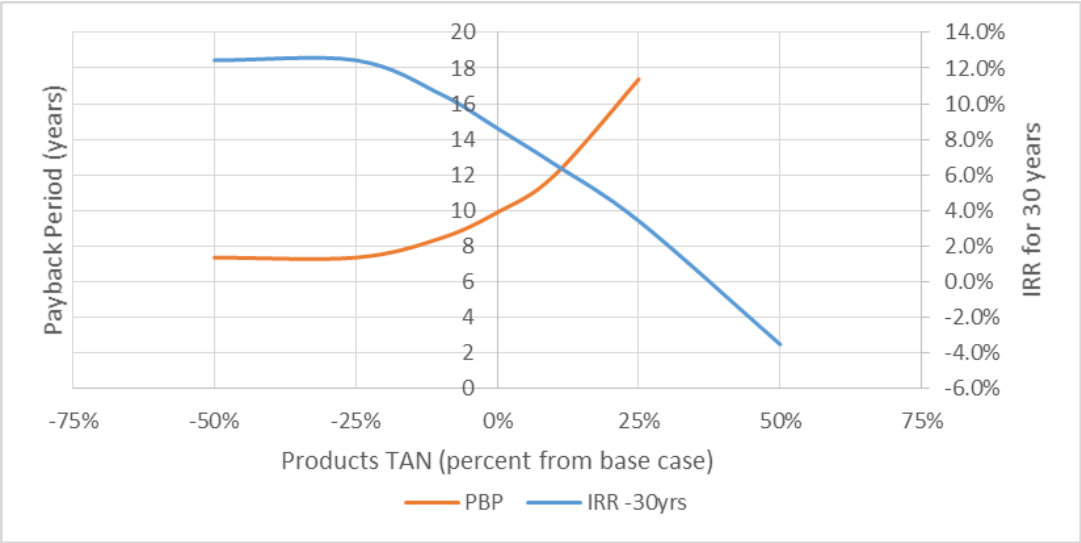

Figure 5-20: Sensitivity analysis for variations in products total acid number.

Products total acid number has a large effect on the economics. That is because of the direct relationship between the price of the product and its acidity. When TAN is further decreased, payback time and IRR tend to reach a flat region in the chart since acidity discounts are only valid for oil above 0.5 mg_{KOH}/g. Conversely, increasing products total acid number can quickly increase payback period and decrease IRR. Controlling conditions and properly regenerating the catalyst are important to keep process profitability.

Figure 5-21 shows the sensitivity analysis for the total investment in the industrial plant.

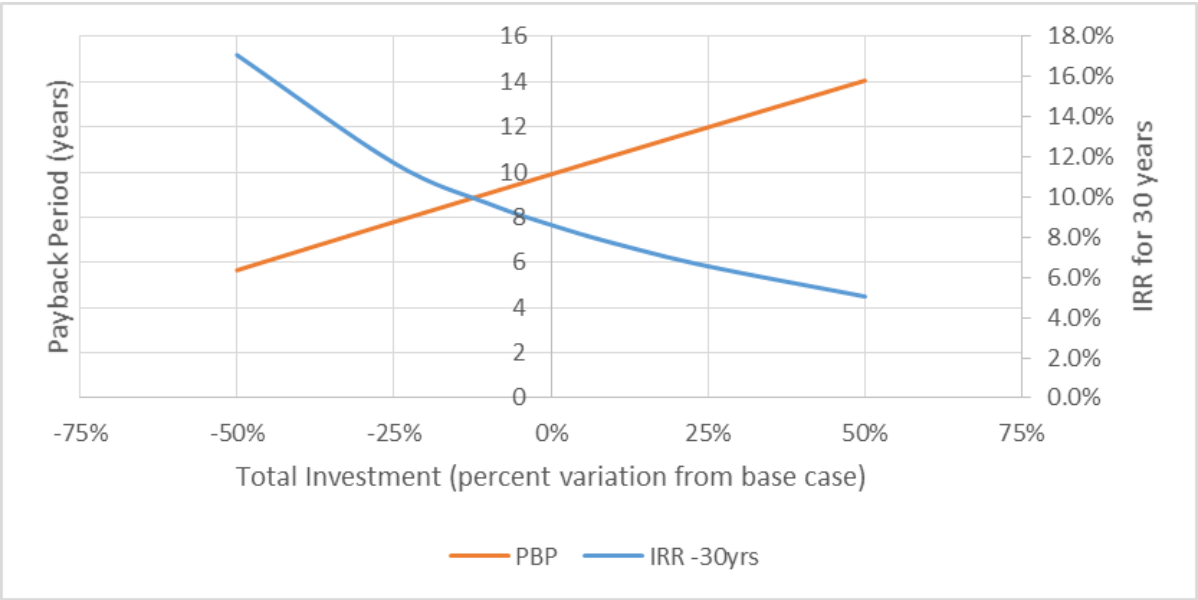

Figure 5-21: Sensitivity analysis for variations in total investment.

Considering this economic analysis as a Class V, the expected error in its value is around ±50% which means that the expected total investment is somewhere between M$45 and M$135. Through all this considered range of values, the process is profitable and it pays itself before the end of the investment. For the best case scenario, i.e. M$45 investment, payback period is 6 years while IRR is around 15%. For the case that investments add up to be M$135, payback period goes to 14 years and IRR is around 5%. Although important to the process economics, the impacts of variations on total investment are not as relevant as oil prices, and total acid number.

Tornado charts are powerful tools to help understand the impacts of different variables on the project economics. They show the impacts on the economic variable of interest when the different process variables vary. For the tornado charts in Figure 5-22, Figure 5-23, and Figure 5-24; the variables were varied by 25%. The variables are ranked from the highest to the lowest spread of values.

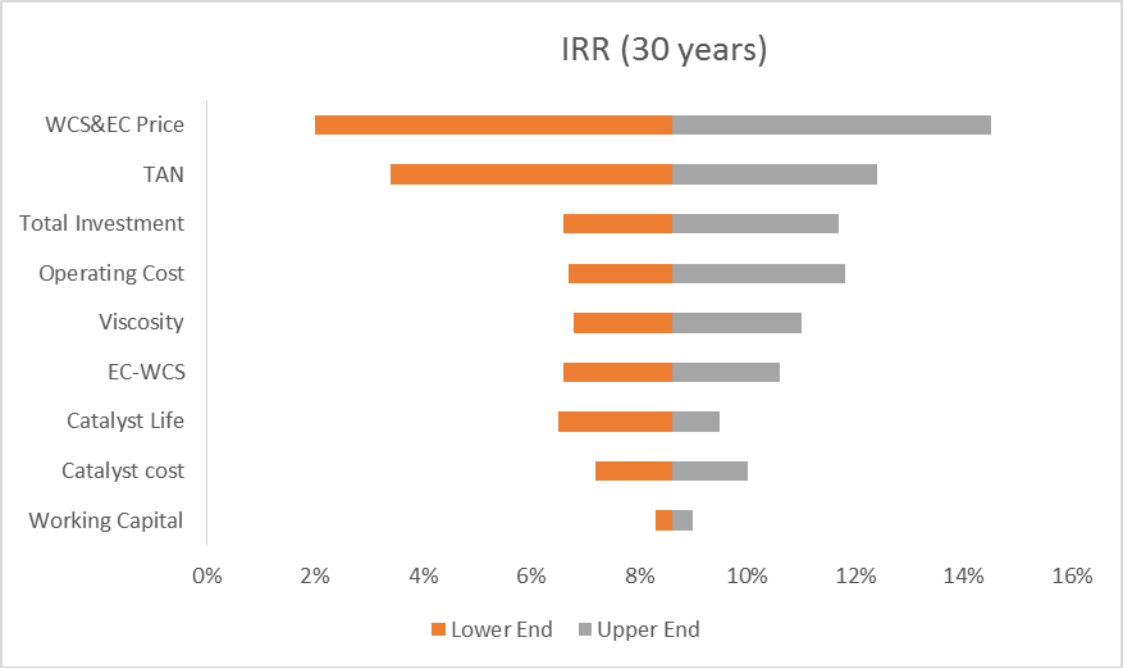

Figure 5-22: Tornado chart for internal rate of return for a 30 years investment.

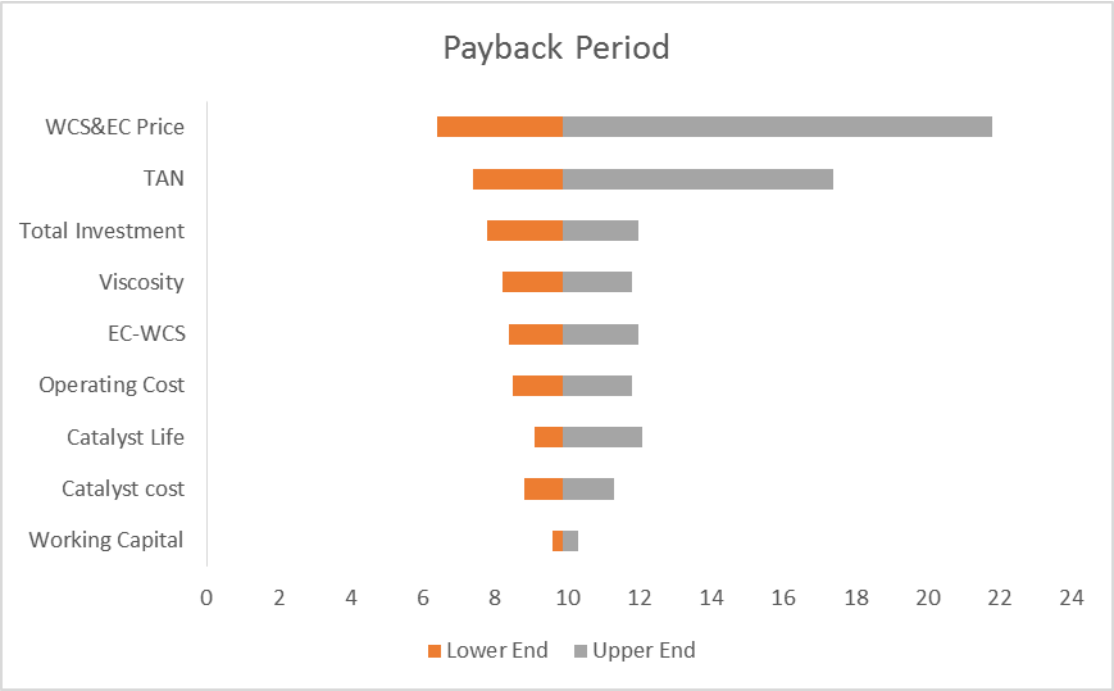

Figure 5-23: Tornado chart for payback period.

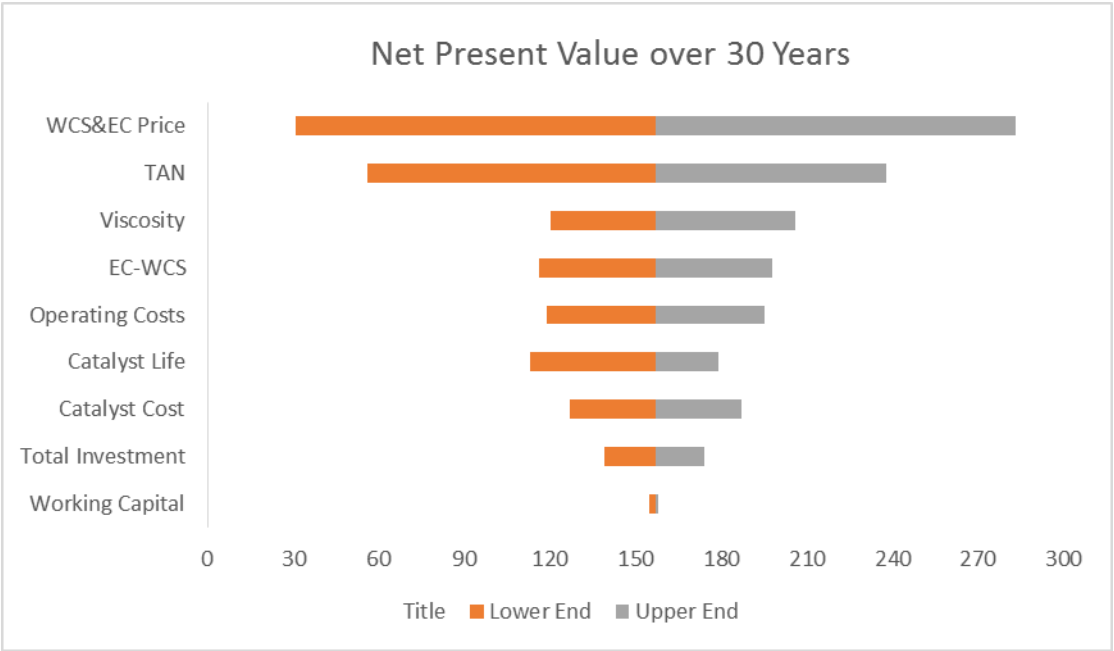

Figure 5-24: Tornado chart for net present value after 30 years of operation.

Figure 5-22 to Figure 5-24 show that the price of WCS and EC, which is the top variable for all cases, total acid number, products viscosity, and total investments are consistently high placed in

order of impact on the project economics. On the intermediate level are ranked operating costs and the price differential between WCS and EC.

Catalyst life, catalyst cost and working capital are variables that vary little the project economics. For that reason, those variables should not be the main target of the research going forward. Nonetheless, sensitivity analysis done on catalyst life and shown in Appendix IV indicates that a minimum of 2 years of catalyst life is important to secure process profitability. Further improvements in catalyst life have only a relatively small impact on the economics.

Taking into consideration the tornado charts available, the outlook for this process economics is positive in the long term since the high ranked variables have positive outlooks in the future. As discussed before, WCS and EC prices are currently below multi-year averages and, thus, expectations are for an increase of those prices, even if a modest one. Total acid number reduction can be manipulated by the severity of reaction and, consequently, ensuring that its level will, at least, remain on the target. Viscosity reduction is a variable that was never targeted on this process and, for this reason, some research can probably tune operating conditions towards viscosity reduction.

Finally, a combination of conditions improvements and global oil economic situation can lead to very profitable project economics. For instance, an increase in 10% in WCS and EC prices, a decrease in 25% in products viscosity, and a products TAN of 0.6 (instead of 0.78) leads to an IRR of 17.8%, payback period of 5.4 years, and net present value close to M$360.

6 Final Remarks and Future Work

Section 1.3 listed the major objective of this project that are reviewed and summarized in this chapter. First, it was listed the design and construction of a reliable experimental set-up, that was accomplished as shown throughout the project. Reliability was achieved by the development of Bang-Bang sampling system and with big efforts on increasing system controllability through the implementation of LabView software. Mass balances throughout the project were usually within the 97-103% range, which showed a high reliability on oil processing. Also, the duplicate reaction showed that only minor differences in the results were obtained when running the same reaction for a second time.

The second goal of this project was to test different thermal reactions as it was shown in section 4.1. The thermal reaction showed very poor results in relation to total acid number reduction for the temperature range tested. In fact, thermal reaction only achieved 35.7% of acidity reduction at very severe conditions. Some partial upgrading of oil, as seen in viscosity reduction, residue conversion, and API gravity increase, take place during thermal reaction.

The evaluation of different catalyst and conditions was shown throughout chapters 4 and 5, first, by changing conditions with catalyst TR1, and later by evaluating deactivation with catalyst TR3. It was found that catalyst TR3 was the one that most significantly improved the total acid number reduction. Gas yields for different catalytic reactions also showed that catalyst TR3 was the one that promotes hydrogen production mainly through water dissociation mechanisms instead of through undesirable dehydrogenation reactions. All catalysts showed considerably higher TAN conversion than the thermal reaction presented. Screening of conditions and catalysts showed that temperatures around 360ºC and space velocities of $1h^{-1}$ were suitable for performing TAN conversion with catalyst TR3. Although catalytic TAN conversion showed improvements in relation to thermal results, other partial upgrading properties, such as viscosity, API gravity, and residue conversion are only slightly improved when using mild conditions.

The kinetic model for both thermal and catalytic reactions was developed. It was found that a first order reaction in relation to acid groups in the organic phase was suitable for the experimental data. The activation energy for catalytic total acid number reactions was estimated to be 112.6kJ/mon for catalyst TR1 and 94.5kJ/mol for catalyst TR3. Both numbers were considerably

lower than thermal reaction value of 175.5kJ/mol which highlighted the role of the catalyst on the total acid number reduction.

A deactivation model was also developed from theoretical equations based on coke deposition. The experimental data fitted the linearized model successfully and deactivation constants were calculated and compared for different conditions. Conditions, such as temperature and water-to-oil ratio, were found to play a fundamental role on both deactivation and initial activity. For instance, it was found that starting the reaction at 380ºC instead of 360ºC increases considerably the deactivation rate in a way that quickly compensates for the higher initial activity obtained at that temperature. Therefore, even if the activity in the first days of reaction is higher for 380ºC, the rapid loss of active sites due to coke deposition reduced the rate of reaction to levels below the reaction at 360ºC. Similar to the effect of increasing temperature, the decrease of water-to-oil ratio tended to increase deactivation while simultaneously increasing activity. This was found to be related to water being active in the deactivation inhibition process and to the large volume taken by steam at reaction conditions that affected the real residence time for reactants.

Although deactivation seemed to happen at high rates in the reactor, the regeneration test performed on catalyst TR3 showed that the activity can be recovered by a simple regeneration step. Metal content analysis performed in both feedstock and products highlighted that there was only a minimum retention of those compounds on the catalyst. As those compounds tend to adsorb irreversibly in active sites, the low retention of those metals indicated that the catalyst can continually have its activity restored, and thus its life prolonged, by consecutive regenerations. Moreover, the complete recovery of catalyst activity indicated that regeneration had little effect on catalyst structure and active sites.

Based on the deactivation patterns observed for this process, a single-bed reaction unit would be unfeasible from the processing point of view since it would require constant production shut-downs for catalyst regeneration. Since the catalyst showed a high potential for being regenerated, a swing-type reactor was proposed and economically evaluated. In this reaction system, three catalytic beds process bitumen in parallel while one catalytic bed is regenerated. After the end of regeneration, the catalyst bed is put back to process bitumen while another bed starts the regeneration process. In this way, production is continuous throughout operation until the catalyst beds need to be replaced.

The economic evaluation of this process showed a required initial investment of 90.1M$ and operating costs close to 9.3M$/year. The revenues coming from total acid number reduction and diluent requirements reduction overcame the operating costs and generated a total revenue around 31M$/year. Over the course of a 30 year investment, the project is expected to have a payback period close to 10 years, generate a net present value of 157M$, and have an internal rate of return of 8.6%. Still, the future prospects can be considered even more positive if further research is developed in order to maximize gains in total acid number reduction, and diluent reduction.

According to sensitivity analysis performed on this project, studies should be conducted in order to understand the extent to which diluent reduction can be optimize. It is expected that this can happen by increasing reaction severity and understanding the other effects of this action, such as further decrease in TAN, increase in API gravity, increase in deactivation and products deterioration, is of major importance on the project economics. Although this project initial focus was on total acid number reduction, it is clear now that diluent requirement reduction has a potential in increasing the products value.

However, some work remains to be done in the future to better understand the process and its economics. For instance, the number of regenerations a catalyst can stand, which is related to its life duration before replacement, still needs to be addressed. Then, it is necessary to perform an experiment that runs the catalyst at constant conditions with multiple regenerations and tracks the rate of decay on the results. Although this is a costly and time-consuming experiment, this effort must be made in the future in order to really understand the potential of this application. For instance, the economics were designed based on successfully regenerating the catalyst for ten times and the reliability of this assumption is key to the economics of the process.

The development of a guard reactor is another area that requires future work and that can greatly impact the process performance. Although a guard reactor was used for most of the experiments in this project, it showed little potential in retaining metals and/or coke precursors that promote deactivation of the catalyst. A better selection of guard catalyst material and better understanding of its condition could be fundamental in prolonging catalyst life. Furthermore, the capability of retaining metal compounds and coke promoters would ultimately increase the product value since both components are prone to deactivate common refinery operating units and decrease overall oil price in the market.

Some modifications on the reaction design is another possibility for process and economics improvement. For instance, the process is expected to generate over 600 metric tons of hydrogen per year that could be recycled to the reactor to improve performance of catalytic hydrogenating functions. Otherwise, a process could be studied to separate hydrogen from remaining gas products in order to enable the commercialization of that by-product. Another possibility for recycling in the system is the unreacted water. Again, studies could be conducted to understand if water could either be recycled to the reactor or used in other facilities such as in SAGD operations.

Bibliography

Alberta Learning Information Services. (2015). Wage Profile: Petroleum, Gas and Chemical Process Operators. Retrieved December 7, 2016, from http://occinfo.alis.alberta.ca/occinfopreview/info/browse-wages/wage-profile.html?id=9232

Ancheyta, J. (2013). *Modeling of Processes and Reactors for Upgrading of Heavy Petroleum*. Boca Raton: CRC Press.

Ancheyta, J., Trejo, F., & Singh Rana, M. (2009). *Asphaltenes: Chemical Transformation during Hydroprocessing of Heavy Oils*. Boca Raton: CRC Press.

ASTM International. (1995). Standard ASTM D-4175. Standard Terminology Relating to Petroleum, Petroleum Products, and Lubricants, 1–65.

ASTM-International. (2011). ASTM D664 -Standard Test Method for Acid Number of Petroleum Products by Potentiometric, 1–10. http://doi.org/10.1520/D0664-11A.This

Bacon, R., & Tordo, S. (2005). Crude Oil Price Differentials and Differences in Oil Qualities: a Statistical Analysis. *ESMAP Technical Paper*, (81), 1–40.

Banerjee, D. K. (2012). *Oil Sands, Heavy Oil & Bitumen*. Tulsa: PennWell Corporation.

Baytex Energy, C. (2016). Benchmark Heavy Oil Prices. Retrieved June 7, 2016, from http://www.baytexenergy.com/operations/marketing/benchmark-heavy-oil-prices.cfm

British Petroleum Global. (2015). BP Statistical Review of World Energy. Retrieved April 11, 2016, from bp.com/statisticalreview

Cantrell, D. G., Gillie, L. J., Lee, A. F., & Wilson, K. (2005). Structure-reactivity correlations in MgAl hydrotalcite catalysts for biodiesel synthesis. *Applied Catalysis A: General*, *287*(2), 183–190.

Cejka, J., Vondrova, A., Wichterlova, B., Vorbeck, G., & Fricke, R. (1994). The effect of AI, Fe, and in substitution in the MFI silicate structure on the aromatic hydrocarbon transformation: SiOHM site strength. *Zeolites*, *14*(2), 147–153.

Claridge, J. B., York, A. P. E., Brungs, A. J., Marquez-Alvarez, C., Sloan, J., Tsang, S. C., & Green, M. L. H. (1998). New Catalysts for the Conversion of Methane to Synthesis Gas: Molybdenum and Tungsten Carbide. *Journal of Catalysis*, *180*(1), 85–100.

Clemente, J. S., & Fedorak, P. M. (2005). A review of the occurrence, analyses, toxicity, and biodegradation of naphthenic acids. *Chemosphere*, *60*(5), 585–600.

Crude Monitor Inc. (2016). Condensate Blend (CRW). Retrieved June 1, 2016, from http://www.crudemonitor.ca/condensate.php?acr=CRW

Degnan, T. F., Chitnis, G. K., & Schipper, P. H. (2000). History of ZSM-5 fluid catalytic cracking additive development at Mobil. *Microporous and Mesoporous Materials*, *35-36*, 245–252.

Dettman, H. D., Li, N., & Luo, J. (2009). NACE International Corrosion Conference & Expo. In *Refinery Corrosion, Organic Acid Structure, and Athabasca Bitumen* (pp. 1–13). Atlanta,

GA.

Diaz, I., Kokkoli, E., Terasaki, O., & Tsapatsis, M. (2004). Surface structure of zeolite (MFI) crystals. *Chemistry of Materials*, *16*(25), 5226–5232.

Duan, Y., Yu, F., & Cui, Z. (2012). Naphthenic Acid Corrosion Control Strategies in Refineries: A Review of Recent Patents. *Recent Patents on Corrosion Science*, (6), 142–147.

Dumitriu, E., Hulea, V., Fechete, I., Catrinescu, C., Auroux, A., Lacaze, J.-F., & Guimon, C. (1999). Prins condensation of isobutylene and formaldehyde over Fe-silicates of MFI structure. *Applied Catalysis A: General*, *181*(1), 15–28.

Duncan, J. A. (2010). *Asphaltenes Characterization, Properties and Applications*. New York: Nova Science Publishers, Inc.

Duprez, D. (1992). Selective steam reforming of aromatic compounds on metal catalysts. *Applied Catalyst A: General*, *82*, 111–157.

Energy Information Administration, U. S. (2014). Today in Energy. Retrieved June 3, 2016, from http://www.eia.gov/todayinenergy/detail.cfm?id=18571

Energy Information Administration, U. S. (2016). Today in Energy. Retrieved June 3, 2016, from http://www.eia.gov/todayinenergy/detail.cfm?id=25112

Fathi, M. M., & Pereira-Almao, P. (2011). Catalytic aquaprocessing of arab light vacuum residue via short space times. *Energy and Fuels*, *25*(11), 4867–4877.

Ferretti, A. M., Forni, L., Oliva, C., & Ponti, A. (2002). EPR study of iron-doped MFI zeolite and silicalite catalysts: effect of treatments after synthesis. *Research on Chemical Intermediates*, *28*(2-3), 101–116.

Fogler, H. S. (2006). *Elements of Chemical Reaction Engineering* (4th ed.). Westford, MA: Pearson Education Inc.

Frauwallner, M. L., López-Linares, F., Lara-Romero, J., Scott, C. E., Ali, V., Hernández, E., & Pereira-Almao, P. (2011). Toluene hydrogenation at low temperature using a molybdenum carbide catalyst. *Applied Catalysis A: General*, *394*(1-2), 62–70.

Furimsky, E. (1999). Deactivation of hydroprocessing catalysts. *Catalysis Today*, *52*(4), 381–495.

Gaikar, V. G., & Maiti, D. (1996). Adsorptive recovery of naphthenic acids using ion-exchange resins. *Reactive and Functional Polymers*, *31*(2), 155–164.

Gao, W., & Li, Z. (Eds.). (2008). *Developments in High-Temperature Corrosion and Protection of Materials*. Cambridge: Woodhead publishing limited.

Garcia-Hubner, E. A. (2015). *Catalytst Evaluation for Catalytic Steam Cracking of De-asphalted Oil in a Fixed Bed Reactor*. University of Calgary.

Gas Alberta. (2016). Pricing Market. Retrieved June 1, 2016, from http://www.gasalberta.com/pricing-market.htm

Ghorpadkar, S. (1993). *A Study of Coke Deposition in Hydrotreating Catalysts*. University of

Alberta.

Gu, J., Wu, Y., Jin, Y., & Wang, J. (2013). Hydrothermal incorporation of Ce(La) ions into the framework of ZSM-5 by a multiple pH-adjusting co-hydrolysis. *Journal of Porous Materials*, *20*(1), 7–13.

Guichard, B., Roy-Auberger, M., Devers, E., Pichon, C., & Legens, C. (2009). Characterization of aged hydrotreating catalysts. Part II: The evolution of the mixed phase. Effects of deactivation, activation and/or regeneration. *Applied Catalysis A: General*, *367*(1-2), 9–22.

Guichard, B., Roy-Auberger, M., Devers, E., Rebours, B., Quoineaud, A. A., & Digne, M. (2009). Characterization of aged hydrotreating catalysts. Part I: Coke depositions, study on the chemical nature and environment. *Applied Catalysis A: General*, *367*(1-2), 1–8.

Guisnet, M., & Magnoux, P. (1989). Coking and deactivation of zeolites. Influence of the Pore Structure. *Applied Catalysis*, *54*(1), 1–27.

Guisnet, M., & Magnoux, P. (2001). Organic chemistry of coke formation. *Applied Catalysis A: General*, *212*(1-2), 83–96.

Hilyard, J. F. (2012). *The Oil & Gas Industry: A Nontechnical Guide*. Tulsa: Penn Well Corporation.

Hsu, C. S., & Robinson, P. R. (2006). *Practical Advances in Petroleum Processing - Volume 2*. New york: Springer Science+Business Media.

Huc, A.-Y. (2011). *Heavy Crude Oils: From Geology to Upgrading. An Overview.* (Editions T). Paris.

International Energy Agency. (2015a). *Key World Energy Statistics 2015*.

International Energy Agency. (2015b). *Oil Medium-Term Market Report*. Paris.

Javaherdashti, R., Nwaoha, C., & Tan, H. (Eds.). (2013). *Corrosion and Material in the Oil and Gas Industries*. Boca Raton: CRC Press.

Jones, D., & Pujado, P. (2006). *Handbook of Petroleum Processing*. Dordrecht, Netherlands: Springer Science+Business Media.

Kam, E. K. T., Al-Shamali, M., Juraidan, M., & Qabazard, H. (2005). A hydroprocessing multicatalyst deactivation and reactor performance model-pilot-plant life test applications. *Energy and Fuels*, *19*(3), 753–764.

Kondoh, H., Nakasaka, Y., Kitaguchi, T., Yoshikawa, T., Tago, T., & Masuda, T. (2016). Upgrading of oil sand bitumen over an iron oxide catalyst using sub- and super-critical water. *Fuel Processing Technology*, *145*, 96–101.

Kondoh, H., Tanaka, K., Nakasaka, Y., Tago, T., & Masuda, T. (2016). Catalytic cracking of heavy oil over TiO2–ZrO2 catalysts under superheated steam conditions. *Fuel*, *167*, 288–294.

Le Page, J. F. (1987). *Applied heterogenous catalysis: design, manufacture, use of solid catalysts*. (Technip, Ed.).

Le Page, J. F., Chatila, S. G., & Davidson, M. (1992). *Resid and Heavy Oil Processing*. (E. Technip, Ed.). Paris: Imprimerie Louis-Jean.

Leach, B. E. (1983). *Applied Industrial Catalysis - Volume 1*. New York: Academic Pressi, Inc.

Lee, J. S., Oyama, S. T., & Boudart, M. (1987). Molybdenum Carbide Catalysts. *Journal of Catalysis*, *106*, 125–133.

Lee, J. S., Yeom, M. H., Park, K. Y., Nam, I. S., Chung, J. S., Kim, Y. G., & Moon, S. H. (1991). Preparation and benzene hydrogenation activity of supported molybdenum carbide catalysts. *Journal of Catalysis*, *128*(1), 126–136.

Lieberman, N. P. (1991). *Troubleshooting Process Operations* (3rd ed.). Tulsa: PennWell Publishing Company.

Liu, X. (2015). *In-situ Heavy Oil Upgrading with Molybdenum Carbide Nanoparticles: a Multiscale Modelling Approach*. University of Calgary.

Mandal, P. C., Wahyudiono, Sasaki, M., & Goto, M. (2012). Reduction of total acid number (TAN) of naphthenic acid (NA) using supercritical water for reducing corrosion problems of oil refineries. *Fuel*, *94*, 620–623.

Martínez, M. T., Benito, A. M., & Callejas, M. a. (1997). Thermal cracking of coal residues: Kinetics of asphaltene decomposition. *Fuel*, *76*(9), 871–877.

McHugh, M., & Krukonis, V. (1994). *Supercritical Fluid Extraction* (2nd ed.). Stoneham: Butterworth-Heinemann.

McKetta, J. J. (1990). *Encyclopedia of Chemical Processing and Design - Vol. 35*. New York: Marcel Dekker, Inc.

Mohamed, A. M., & Katrib, A. (2015). Catalytic Hydrogenation Reactions on Molybdenum Oxide, *4*, 36–42.

Nadkarni, R. A. K. (2007). *Guide to ASTM Test Methods for the Analysis of Petroleum Products and Lubricants* (2nd ed.). West Conshohocken: ASTM International.

National Institute of Standards and Technology. (2016a). Carbon Dioxide. Retrieved June 27, 2016, from http://webbook.nist.gov/cgi/inchi?ID=C124389&Mask=10#Solubility

National Institute of Standards and Technology. (2016b). Hydrogen. Retrieved June 27, 2016, from http://webbook.nist.gov/cgi/cbook.cgi?ID=C1333740&Mask=10#Solubility

Neumann, G. T., & Hicks, J. C. (2012). Novel Hierarchical Cerium Incorporated MFI Zeolite Catalysts for the Catalytic Fast Pyrolysis of Lignocellulosic Biomass. *ACS Catalysis*, *2*, 642–646.

Papavinasam, S. (2014). *Corrosion Control in the Oil and Gas Industry*. Walthman, MA: Golf Professional Publishing.

Pereira-Almao, P., Trujillo, G., Peluso, E., Galarraga, C., Sosa, C., Scott algara, C., Zerpa, N. G. (2013). US 20130015100 A1 - Systems and Methods for Catalytic Steam Cracking of Non-Asphaltenes Containing Heavy Hydrocarbons.

PSAC. (2016). Market News. Retrieved April 7, 2016, from http://www.psac.ca/business/firstenergy/

Raia, J. C., Villalanti, D. C., Subramanian, M., & Williams, B. (2000). Application of High-Temperature Simulated Distillation to the Residuum Oil Supercritical Extraction Process in Petroleum Refining. *Journal of Chromatographic Science*, *38*(1), 1–5.

Rakshe, B., Ramaswamy, V., Hegde, S. G., Vetrivel, R., & Ramaswamy, A. V. Ã. (1997). Crystalline, microporous zirconium silicates with MFI structure. *Catalysis Letters*, *45*, 41–50.

Resini, C., Montanari, T., Barattini, L., Ramis, G., Busca, G., Presto, S., Costantino, U. (2009). Hydrogen production by ethanol steam reforming over Ni catalysts derived from hydrotalcite-like precursors: Catalyst characterization, catalytic activity and reaction path. *Applied Catalysis A: General*, *355*(1-2), 83–93.

Rodriguez-DeVecchis, V. M., Carbognani Ortega, L., Scott, C. E., & Pereira-Almao, P. (2015). Use of Nanoparticle Tracking Analysis for Particle Size Determination of Dispersed Catalyst in Bitumen and Heavy Oil Fractions. *Industrial & Engineering Chemistry Research*, *54*(40), 9877–9886.

Sartori, G., W. Savage, D., C. Dalrymple, D., H. Ballinger, B., C. Blum, S., & E. Wales, W. (2001). US6251305 Esterification of Acidic crudes. USA.

Speight, J. G. (1999). *The Chemistry and Technology of Petroleum* (3rd ed.). New York: Marcel Dekker, Inc.

Speight, J. G. (2013a). *Heavy and Extra-Heavy Oil Upgrading Technologies*. Oxford: Elsevier Inc.

Speight, J. G. (2013b). *Heavy Oil Production Processes*. Walthman, MA: Gulf Publishing Company.

Speight, J. G. (2014a). *High Acid Crudes*. Oxford, UK: Elsevier Inc.

Speight, J. G. (2014b). *Oil and Gas Corrosion Prevention*. Oxford, UK: Elsevier Inc.

SRI-Instruments. (2005). Operation Manual and Reference Guide. Torrance. Retrieved from http://www.srigc.com/pages/document_downloads/

Tissot, B. P., & Welte, D. H. (1984). *Petroleum Formation and Occurrence* (2nd ed.). Berlin: Springer-Verlag.

Towler, G., & Sinnott, R. (2013). *Chemical Engineering Design: Principles, Practice and Economics of Plant and Process Design* (2nd ed.). Walthman, MA: Elsevier Ltd.

Trujillo, G. L. F. (2008). *Thermal and Catalytic Steam Reactivity Evaluation of Athabasca Vacuum Gasoil*. University of Calgary.

Vitale, G., Frauwallner, M. L., Scott, C. E., & Pereira-Almao, P. (2011). Preparation and characterization of low-temperature nano-crystalline cubic molybdenum carbides and insights on their structures. *Applied Catalysis A: General*, *408*(1-2), 178–186.

Vitale, G., Molero, H., Hernandez, E., Aquino, S., Birss, V., & Pereira-Almao, P. (2013). One-pot preparation and characterization of bifunctional Ni-containing ZSM-5 catalysts. *Applied Catalysis A: General*, *452*, 75–87.

Wang, X., & Michael, E. (2009). *Advanced Natural Gas Engineering*. Houston, TX: Gulf Publishing Company.

Wang, Y. Z., Sun, X. Y., Liu, Y. P., & Liu, C. G. (2007). Removal of Naphthenic Acids from a Diesel Fuel by Esterification. *Energy & Fuels*, (21), 941–943.

Wrisberg, G. H. J., Kjeld, T. J. A., & Mogensen, R. E. (1973). Catalytic Steam Cracking of Hydrocarbons and Catalysts Therefor. Denmark.

Yu, J., Gan, F., Hao, L., & Chen, Z. (2009). Temperature naphthenic acid corrosion of steel in high TAN refining media. *Journal of the Chinese Society of Corrosion and Protection*, *29*(6), 481–486.

Zhang, A., Ma, Q., Wang, K., Liu, X., Shuler, P., & Tang, Y. (2006). Naphthenic acid removal from crude oil through catalytic decarboxylation on magnesium oxide. *Applied Catalyst A: General*, *303*, 103–109.

Zurita, J. P., Bartolini, M., Righi, T., Vitale, G., & Pereira Almao, P. (2015). Hydrotalcite type materials as catalyst precursors for the Catalytic Steam Cracking of toluene. *Fuel*, *154*, 71–79.

Appendix I: Total Capital Investments

Appendix I shows the calculations and assumptions in the industrial plant sizing and cost estimation. Section I.1, 0, and I.3 present the information related to the reaction, heating, and separation units, repectively.

I.1 Reaction Unit

Table I-1 shows the major assumptions taken on the design of the reaction unit.

Table I-1: Major assumptions on reactor design for total acid number reduction unit.

Variable	Value
Residence time (h)	4.0
Water-to-Oil Ratio	5% v/v
Weight hourly space velocity (h^{-1})	0.25
On-stream factor	0.92
Average oil production rate (bpd)	38,000
Catalyst bed density (kg/m^3)	900
Catalyst running to regenerating ratio	0.75
Reactor material	SS 316

The total amount of bitumen and water to be processed can be estimated using Equation I-1 and Equation I-2 that uses the oil production rate, feedstock density, and water-to-oil ratio.

$$\dot{w}_o = 38{,}000 bpd \times 0.159\, m^3/bbl \times 987.4\, kg/m^3 = 5.97 \times 10^6\, kg/day = 249 \times 10^3\, kg/h \qquad \text{Equation I-1}$$

$$\dot{w}_w = 0.05 \times 38{,}000 bpd \times 0.159\, m^3/bbl \times 998.2\, kg/m^3 = 3.02 \times 10^5\, kg/day = 12.6 \times 10^3\, kg/h \qquad \text{Equation I-2}$$

The amount of catalyst reacting, at a given time, can be calculated using the weight hourly space velocity as shown in Equation I-3. The total amount of catalyst, which also accounts for the catalyst being regenerated, is shown in Equation I-4. Finally, the total volume for the catalyst bed is given by Equation I-5.

$$W_{cat,reacting} = \frac{\dot{w}_o}{WHSV} = \frac{249 \times 10^3\, kg/h}{0.25 h^{-1}} = 9.95 \times 10^5 kg_{cat} \qquad \text{Equation I-3}$$

$$W_{cat,total} = \frac{W_{cat,reacting}}{0.75} = \frac{9.95 \times 10^5 kg_{cat}}{0.75} = 1.33 \times 10^6 kg_{cat} \qquad \text{Equation I-4}$$

$$V_{cat,total} = \frac{W_{cat,total}}{\rho_{cat}} = \frac{1.33 \times 10^6 kg_{cat}}{900\, kg_{cat}/m^3} = 1475 m^3 \qquad \text{Equation I-5}$$

The total acid number reduction system of reactions is complex since a very large amount of distinct naphthenic acids contribute for the overall oil acidity. Therefore, to estimate the heat of reaction, two model molecules were used: phenylethanoic acid, and n-eicosanoic acid. The proposed acid reduction reactions are shown in Equation I-6 and Equation I-7. The first model molecule represents the predominantly aromatic molecules and the second one represents the predominantly saturated chain molecules.

$$C_6H_5 - CH_2 - COOH + 2H_2O \rightarrow C_6H_6 + 2CO_2 + 3H_2 \qquad \text{Equation I-6}$$

$$C_{19}H_{39} - COOH + 2H_2O \rightarrow C_{18}H_{38} + 2CO_2 + 3H_2 \qquad \text{Equation I-7}$$

Using the simulation software VMGSim, the enthalpy of each one of the molecules in both Equation I-6 and Equation I-7 could be obtained, and, then, the enthalpy of reaction could be calculated. Even with the considerable differences between model molecules, the calculated enthalpy of reaction were very similar and they are displayed in Table I-2.

Table I-2: Enthalpy for molecules and model reactions.

Molecule	**Enthalpy (kJ/mol)**
Phenylethanoic acid	42.80
n-eicosanoic acid	223.31
H_2O	20.76
CO_2	23.22
H_2	17.99
Benzene	49.48
Octadecane	229.14
$\Delta H_{r,phenylethanoic\ acid}$	65.57
$\Delta H_{r,n\text{-}eicosanoic\ acid}$	64.72

Using the same simulation package, and applying the endothermic enthalpy of reaction to the real feedstock (dilbit) on a reaction with steam, the absorbed heat from the system is only enough to decrease the system temperature in 0.6°C for a 100% TAN conversion. The main reason for the

low temperature decrease is the low concentration of acid groups in the original bitumen. In fact, 1.7mg_{KOH}/g represents a total of 3.03x10^{-5} mol of acid molecules per gram of bitumen. Thus, the reaction unit is not expected to require intermediate heating or cooling sections along the length of the catalyst bed, as it is common to hydroprocessing units. Although other side reactions, such as catalytic cracking, are also expected to play a role in the system thermodynamics, the low extent of those reactions, as expressed by the low residue conversion, shows that the impact of those reactions on system temperature should be minimal. Thus, for this stage of process design, those side reactions were taken as negligible. Finally, the inlet temperature into the adiabatic reactor should be set at a slightly higher temperature than targeted to account for endothermic reactions and system losses.

Since hydrocracking units commonly have internal diameters going up to 16 feet, i.e. 4.9 meters (Jones et al., 2006), that maximum value was used in order to minimize the number of parallel reactors needed. To achieve the minimum of 1,475 m^3 necessary for reaction, a total of 4 reactors with 65.6ft (20.0m) of length were needed, which totals 1,494 m^3. The length to diameter ratio equals, then, to 4.1 which was just above the recommended range of 1-4 (Towler et al., 2013). An extra 5m^3 was considered for the reactor heads, which added up to of 1,514L divided into 4 different reactors.

The reactor wall thickness can be calculated using Equation I-8 in which S is the maximum allowable stress and is set as 80,670, which is the value for stainless steel 316 at reaction temperature. P is the internal pressure, i.e. 2,760kPa; C_C is the corrosion allowance assumed to be 0.004m, which is the severe condition recommendation value; and E_j is the joint efficiency assumed to be 0.9 (Towler et al., 2013). The final reactor thickness is 0.095m (around 3.7 inches) and it is below the maximum thickness of 1 feet for hydrocracking units (Jones et al., 2006).

$$t_r = \frac{D_i \times P}{2S \times E_j + 1.2P} + C_C = 0.095m \qquad \text{Equation I-8}$$

The final reactor dimensions are summarized in Table I-3.

Table I-3: Final reactor dimensions.

Variable	Value
Diameter (m)	4.88
Length (m)	19.99
Wall thickness (m)	0.095
Number of reactors	4
Volume per reactor (m^3)	379
Catalyst load per reactor (tons)	336
Total reactor volume (m^3)	1,514

To calculate the total reactor cost, equations for vertical pressure vessels costs were used following correlation curves as shown in Equation I-9 (Towler et al., 2013).

$$C_{r,unit,CS} = a + bS_r^n = 11{,}600 + 34S_{reactor}^{0.85} \qquad \text{Equation I-9}$$

In which S_r is the shell mass of an individual carbon steel reactor in kg that can be calculated using Equation I-10.

$$S_r = \rho_{CS}\pi DLt = 7850\pi \times 4.88 \times 19.99 \times 0.095 = 227{,}900kg \qquad \text{Equation I-10}$$

Therefore, a carbon steel reactor unit in 2010 dollars can be calculated as shown in Equation I-11. Equation I-12 makes the final conversions into 2015 dollars, by using CEPCI indexes, into stainless steel, by stainless steel to carbon steel factors, and multiplying by the total amount of reactors (Towler et al., 2013).

$$C_{r,unit,CS} = 11{,}600 + 34(227{,}900)^{0.85} = M\$\ 1.23 \qquad \text{Equation I-11}$$

$$C_{r,total} = nf_{SS/CS}C_{r,unit,CS}\frac{CEPCI_{2015}}{CEPCI_{2010}} = 4 \times 1.3 \times \$1{,}230{,}000.00 \times \frac{562.9}{532.9} \qquad \text{Equation I-12}$$

$$= M\$\ 6.75$$

On top of the reactor cost, there is also the catalytic bed costs that can be estimated as shown in Equation I-13. In that equation, it was assumed a cost of $15/kg of catalyst.

$$C_{cat} = W_{cat,total}C_{cat/kg} = 1.33 \times 10^6 kg_{cat} \times 15\frac{\$}{kg_{cat}} = M\$\ 19.91 \qquad \text{Equation I-13}$$

Although the catalyst can be regenerated successfully as seen in section 5.7, the continuous poisoning by metallic compounds and even a possible phase structure change, will eventually

require the catalyst to be exchanged for a fresh batch of catalyst. The investment shown in Equation I-13 will need to be done in a certain frequency in the future. Since it was shown in section 5.6 that metal deposition happens at a very slow rate in the catalyst, and because regeneration did not present a lower activity towards TAN reduction, which would be an indication of an inactive phase formation, it is believed that this catalyst can have its life prolonged over several regenerations. It was considered a total of 10 regenerations, i.e. 10 runs with the same batch of catalyst, as the limit the catalyst can sustain reaction before needing a batch exchange. Therefore, the total catalyst life can be estimated as seen in Equation I-14. Note that this equation already takes into consideration the on-stream factor, i.e. the days the catalyst will not be working due to planned maintenance.

$$t_{life\ cat} = \frac{10 \times 80 + 60}{365 \times 0.92} = 2.6\ years \qquad \text{Equation I-14}$$

I.2 Heating Unit

Using the software VMGSim®, it is possible to calculate the required energy necessary to heat the quantities given in Equation I-1 and Equation I-2 to reaction temperatures. The results from the simulation are given in Table I-4. The furnace is also to be used on air heating for regeneration reactions. Considering the amount of coke formed reported in section 5.7, the maximum expected amount of coke in a spent reactor is such as shown in Equation I-15.

$$w_{coke} = 0.56\frac{g_{coke}}{g_{cat}} \times 336 tons_{cat} = 188 tons_{coke} \qquad \text{Equation I-15}$$

Considering coke as molecular carbon and the oxidation reaction given by Equation 5-17, the total amount of air at standard conditions can be obtained as in Equation I-16.

$$V_{air} = \frac{w_{coke}}{MW_{coke}}\left(\frac{P}{RT}\right)_{std.\ cond.}\frac{1}{0.21} = 3.29 \times 10^9 m^3\ @\ standard\ cond. \qquad \text{Equation I-16}$$

Over the course of the 16 days allowed for the regeneration process, the air flow rate during this step is given in Equation I-17 and it is a function of the total volume of air (V_{air}) and the regeneration time (t_r). Finally, the energy requirement for that amount is given in Table I-4.

$$\dot{V}_{air} = \frac{V_{air}}{t_r} = 1.43 \times 10^5\ m^3/min\ @\ standard\ cond. \qquad \text{Equation I-17}$$

Table I-4: Energy requirements for heating water and oil to reaction set-points.

	Oil	**Water**	**Air**
Mass flow (kg/h)	249×10^3	12.6×10^3	12.2×10^3
Energy Consumption (MW)	56.1	11.0	1.4

Two heating exchangers were used to transfer energy from products stream to reactants stream. The temperatures in and out of heat exchangers were obtained by VMGSim® for a total heat exchanged of 22MW per heat exchanger unit as represented by Figure I-1. The typical range for overall heat transfer coefficient (U) when heavy oils are used in both hot and cold fluids is 50-300 $W/m^2.^oC$ (Towler et al., 2013). For the calculations, it was assumed a value of 200 $W/m^2.^oC$. Equation I-18 is the heat exchange equation that takes into account the overall heat transfer coefficient, the area available for heat exchange (A), the temperature correction factor (F_T), and the logarithm mean different of temperature (ΔT_{ml}). ΔT_{ml} can be estimated using Equation I-19 while F_T can be estimated using charts that involve the calculation of factor R and S, as shown in

Equation I-20 and Equation I-21. The results of the calculation of R and S are given in Table I-5. The calculations are exemplified for the first heat exchanger. The charts used in this project are the ones published by Towler et al. (2013).

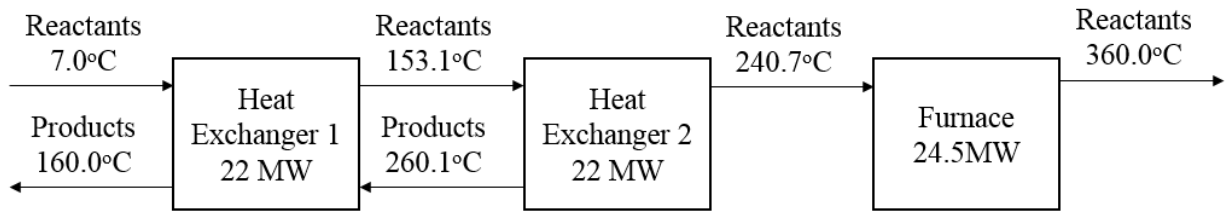

Figure I-1: Heating unit schematic representation composed of two integrated heat exchanger and a furnace.

$$Q = UAF_T \Delta T_{ml}$$ Equation I-18

$$\Delta T_{ml} = \frac{\left(T_{hot,in} - T_{cold,out}\right) - \left(T_{hot,out} - T_{cold,in}\right)}{\ln\left(\frac{T_{hot,in} - T_{cold,out}}{T_{hot,out} - T_{cold,in}}\right)}$$ Equation I-19

$$= \frac{(260.1 - 153.1) - (160.0 - 7.0)}{\ln\left(\frac{260.1 - 153.1}{160.0 - 7.0}\right)} = 129\ ^{o}C$$

$$R = \frac{T_{hot,in} - T_{hot,out}}{T_{cold,out} - T_{cold,in}} = \frac{260.1 - 160}{153.1 - 7.0} = 0.69$$ Equation I-20

$$S = \frac{T_{cold,out} - T_{cold,in}}{T_{hot,in} - T_{cold,in}} = \frac{153.1 - 7.0}{260.1 - 7.0} = 0.58$$ Equation I-21

Using a heat exchanger of two passes on the shell and four passes on the tubes, efficiencies higher than 95% can be obtained for both heat exchanger. Thus, the value of 95% was used as a conservative estimation for the efficiency. That heat exchanger configuration is preferred since it provides better efficiency than one pass in the shell and two in the tubes. The area of each heat exchanger can be then calculated with Equation I-18 and the final values are given in Table I-5.

Table I-5: Summary of heat exchangers capacity, surface area, and cost calculation.

Heat Exchanger	**1**	**2**
R	0.69	1.14
S	0.58	0.42
F_T	0.95	0.95
ΔT_{ml} (ºC)	129	113
U (W/m^2.ºC)	200	200
Q (MW)	22	22
A (m^2)	818	931
Cost (M$ in 2015)	0.27	0.31

The estimation of the cost of a heat exchanger can be done using the curve cost correlation methodology as shown in Equation I-22. This equation was corrected in function of material of construction and inflation as shown in Equation I-23. Note that both equations were solved for the first heat exchanger and both values were given in Table I-5.

$$C_{CS,he,2002} = a + bS_{he}^{n} = 28{,}000 + 54S_{he}^{1.2} = 28{,}000 + 54 \times (818)^{1.2} = M\$\ 0.20 \qquad \text{Equation I-22}$$

$$C_{SS,he,2015} = f_{\frac{SS}{CS}} C_{CS,he,2002} \frac{CEPCI_{2015}}{CEPCI_{2010}} = 1.3 \times 0.2 \times \frac{562.9}{532.9} = M\$\ 0.27 \qquad \text{Equation I-23}$$

The furnace, then, provides the remaining 24.5MW of energy necessary to heat the reactants to reaction condition. An efficiency factor of 70% was considered in the design of the furnace leading to a total energy consumption of 35.0MW as shown in Equation I-24. Using the same curve cost correlation methodology as in section I.1, the cost of a furnace can be estimated by Equation I-25 and Equation I-26 (Towler et al., 2013).

$$Q_{req} = \frac{Q}{0.7} = 35.0MW \qquad \text{Equation I-24}$$

$$C_{f,2002} = a + bS_{f}^{n} = 43{,}000 + 111{,}000S_{f}^{0.80} = 43{,}000 + 111{,}000 \times (35.0)^{0.8} = M\$\ 1.95 \qquad \text{Equation I-25}$$

$$C_{f,2015} = M\$4.55 \times \frac{562.9}{532.9} = M\$\ 2.06 \qquad \text{Equation I-26}$$

I.3 Separation Unit

For the three phase separator design, a methodology that takes into consideration holdup and surge times was used for the preliminary design (Wang et al., 2009). Due to the larger weight amount of light and heavy liquids (around 99.2% of all products) the horizontal separator is preferred. The following considerations are also taken:

- Holdup time is 10 minutes, which is the upper end of the recommended range (2-10 minutes).
- Surge time is half of the holdup time thus 5 minutes.
- Pressure of three phase separator is in the range of 1,720kPa.
- Initial L/D value set as 3.0. Recommended range is 1.5-3.0 for 0<P≤1,720kPa.

The vertical terminal velocity (v_T) is an important property on determining separator dimensions and can be estimated by Equation I-27 using a constant K that depends on the pressure of the system as shown in Equation I-28. Note that liquid density was calculated using a VMGSim® simulation while gas density comes from ideal gases law. Their values are 975.1kg/m^3 for oil, 977.5kg/m^3 for water, and 11.1kg/m^3 for gases. Consequently, oil will be treated as light liquid (ll) and water as heavy liquid (hl).

$$v_T = K\sqrt{\frac{\rho_l - \rho_g}{\rho_g}} = 0.43\, m/s \qquad \text{Equation I-27}$$

$$K = \frac{0.131 - 0.007\, ln\, P}{2} = 0.046\, m/s \qquad \text{Equation I-28}$$

The hold-up volume (V_h) and surge volume (V_s) can be estimated according to Equation I-29 and Equation I-30 that uses the assumed hold up (t_h) and surge times (t_s).

$$V_h = t_h Q_l = 44.2 m^3 \qquad \text{Equation I-29}$$

$$V_s = t_s Q_l = 22.1 m^3 \qquad \text{Equation I-30}$$

The diameter can be estimated as a function of the hold-up and surge volumes, and the L/D ratio assumed to be 3.0. That relationship can be seen in Equation I-31.

$$D = \left(\frac{4(V_h + V_s)}{0.5\pi(L/D)}\right)^{1/3} = 3.83m\ or\ 3.96m\ for\ 12ft\ wide \qquad \text{Equation I-31}$$

The cross-sectional area (A_t) can be calculated as in Equation I-32. The vapor space height (h_v) is recommended to be the minimum between 20% of the diameter or 1ft as in Equation I-33.

$$A_t = \frac{\pi D^2}{4} = 11.53m^2 \qquad \text{Equation I-32}$$

$$h_v = min(0.2D, 0.305) = 0.305m \qquad \text{Equation I-33}$$

The cross sectional area available for vapor flow (A_v) can be estimated by the Equation I-34 and Equation I-35. In Equation I-34, a_1 is -4.76x10-3, a_2 is 0.175, a_3 is 5.69, a_4 is -4.92, a_5 is -0.145, a_6 is 3.92, a_7 is -6.36, a_8 is 4.02, and a_9 is -1.80.

$$\frac{A_v}{A} = \frac{a_1 + a_2\frac{h_v}{D} + a_3\left(\frac{h_v}{D}\right)^2 + a_4\left(\frac{h_v}{D}\right)^3 + a_5\left(\frac{h_v}{D}\right)^4}{1.0 + a_6\left(\frac{h_v}{D}\right) + a_7\left(\frac{h_v}{D}\right)^2 + a_8\left(\frac{h_v}{D}\right)^3 + a_9\left(\frac{h_v}{D}\right)^4} = 0.033 \qquad \text{Equation I-34}$$

$$A_v = 0.39m^2 \qquad \text{Equation I-35}$$

The height of the two liquid levels can be set proportionally to their volumetric flows, as shown in Equation I-36 and Equation I-37.

$$h_{hl} = \frac{Q_{hl}}{(Q_{hl} + Q_{ll})}(D - h_v) = 0.17m \qquad \text{Equation I-36}$$

$$h_{ll} = D - h_{hl} - h_v = 3.35m \qquad \text{Equation I-37}$$

The cross sectional area for the heavy liquids, that are in the bottom of the separator, follow the same rule as shown in Equation I-34 when the subscript “v” are exchanged for “hl” as shown and calculated in Equation I-38 and Equation I-39. The light liquids cross sectional area is, then, given by the remaining available area as shown in Equation I-40.

$$\frac{A_{hl}}{A} = \frac{a_1 + a_2\frac{h_{hl}}{D} + a_3\left(\frac{h_{hl}}{D}\right)^2 + a_4\left(\frac{h_{hl}}{D}\right)^3 + a_5\left(\frac{h_{hl}}{D}\right)^4}{1.0 + a_6\left(\frac{h_{hl}}{D}\right) + a_7\left(\frac{h_{hl}}{D}\right)^2 + a_8\left(\frac{h_{hl}}{D}\right)^3 + a_9\left(\frac{h_{hl}}{D}\right)^4} = 0.012 \qquad \text{Equation I-38}$$

$$A_{hl} = 0.14m^2 \qquad \text{Equation I-39}$$

$$A_{ll} = A_T - A_{hl} - A_v = 11.0m^2 \qquad \text{Equation I-40}$$

The minimum length to obtain the liquid hold-up and surge volumes with the calculated cross sectional areas are estimated in Equation I-41.

$$L = \frac{V_h + V_s}{A_T - A_v} = 6.00m\ or\ 6.10m\ for\ 20ft\ long \qquad \text{Equation I-41}$$

Note that the final L/D value is 1.54 and it is different than the one used in Equation I-31. That is because L/D in that case was a first estimative to start the calculations for the different dimensions. Finally, the three phase separator wall thickness can be estimated with Equation I-42. The final separator dimensions are given in Table I-6.

$$t_s = \frac{r_i P}{SE_j + 0.6P} + C_C = 0.048m \qquad \text{Equation I-42}$$

Table I-6: Final three phase separator dimensions.

Variable	**Value**
Diameter (m)	3.96
Length (m)	6.10
Wall thickness (m)	0.048

Equation I-43 uses the curve cost correlation methodology for estimating the three-phase separator cost (Towler et al., 2013). In this equation S_{sep} is the shell mass in kg as calculated in Equation I-44. The corrected cost for the stainless steel three phase separator in 2015 dollars is given in Equation I-45.

$$C_{s,CS} = a + bS_s^n = 10{,}200 + 31S_s^{0.85} \qquad \text{Equation I-43}$$

$$S_s = \rho_{CS}\pi DLt = 7850\pi \times 3.96 \times 6.10 \times 0.048 = 28{,}600kg \qquad \text{Equation I-44}$$

$$C_{s,SS} = \$275{,}000.00 \qquad \text{Equation I-45}$$

Appendix II: Operating Costs

The major operating costs in this facility were considered to be labor, maintenance, land, insurance and natural gas. An operator salary is considered to be the same as the average for petroleum, gas and chemical process operator according Alberta Goverment, i.e. CAD$93,360/year (Alberta Learning Information Services, 2015). Two extra operators were considered to be required at all times to operate the facility. Supervision cost was taken as 25% of overall operating labor costs. In order to take into consideration holidays, long-weekends, sick days, and others, a factor between 4.2-4.8 is commonly used for the number of operators (Towler et al., 2013). Thus, a factor of 4.5 was used giving a total of 9 operators. Considering 40% cap for benefits, and insurances, the total cost per year with operators was estimated as in Equation II-1.

$$C_{labor} = 1.25 \times 1.4 \times \frac{CAD\$93{,}360}{year \times operator} \times 9operators = M\$1.47/year \qquad \text{Equation II-1}$$

The total energy requirement in the furnace was calculated in Appendix I and equals to 35.0 MW, which over a year, considering on-stream factor, corresponds to a total yearly consumption of 1.02×10^6GJ/year. Considering the average forecasted price for natural gas as CAD$2.32/GJ for the years 2016-18 (Gas Alberta, 2016), natural gas corresponded to a total investment cost of MCAD$2.36/year.

Maintenance was considered to cost around 4% ISBL investment (Towler et al., 2013). Since that investment was M$49.5, total maintenance cost per year is estimated as M$1.98/year. The cost of land and property taxes are commonly estimated as 1% of the total fixed capital cost each v. Both of them added up to M$1.80/year. Insurance was another common operating cost and is usually around 1% of total fixed capital cost investment (Towler et al., 2013), in a total of M$0.90/year.

Other operating costs were considered as 20% of all the accounted operating costs. Table II.1 summarizes all operating costs being considered. Note that a conversion of 1 USD = 1.298 CAD was used when necessary for Table II.1. Another operating costs such as: R&D, administration, and marketing were not taken into account since they would fall in the existing department of the oil and gas company that decided to develop this project.

Table II-1: Total operating costs breakdown.

Unit	**Cost (M$/yr)**
Labor	1.13
Natural Gas	1.82
Maintenance	1.98
Land and Taxes	1.80
Insurance	0.90
Others	1.70
Total	9.33

Appendix III: Gross Profits

An economic analysis can be made in relation to the proposed process to decrease the total acidity on a bitumen. There are two streams of profits that come from this partial upgrading process: lower acidity and lower viscosity which leads to smaller diluent requirements. The lower acidity is related to the premium that clients are willing to pay for a non-acidic oil, i.e. with total acid number below 0.5 mg_{KOH}/g. In 2005, Energy Sector Management Assistance Program (ESMAP), a World Bank and UNDP supported program, published a study in which a statistical analysis was performed on crude oil prices in relation to their quality in order to establish a relationship between prices and different aspects on oil properties (Bacon et al., 2005). The relationship between prices and total acid number can be seen in Equation III-1. Note that the discount for acidity is directly related to the total acid number and the current oil price. If total acid number is below 0.5 mg_{KOH}/g, the oil is not considered acid and, therefore, discount should be taken as zero. For this economic analysis, the benchmark used for the oil produced was the Western Canadian Select (WCS), priced as of 7/4/2016 at CAD$45.20/bbl (PSAC, 2016).

$$Discount_{TAN}\left(\frac{\$}{bbl}\right) = (TAN - 0.5) \times 0.051 \times WCS \qquad \text{Equation III-1}$$

Furthermore, heavy and extra-heavy oils usually have densities and viscosities that do not allow them to be pumped through pipelines and, as a result, need diluent addition to meet transportability criteria. The transportability criteria is considered to be viscosities under 350cSt and API gravity above 19 at pumping temperature (Banerjee, 2012), which was taken as 7°C in this study. The amount of diluent required to reach transportability criteria was estimated using viscosity index equations. Equation III-2 estimates a viscosity index (δ) for a certain component (i) of a blend at a given temperature (T). Equation III-3 calculates the blend viscosity index by a weighted sum of all the indexes of the different blend components. Finally, Equation III-2 can be solved for viscosity by using the blend viscosity index.

$$\delta_i = a + b \times \log\log\frac{\mu_i}{\rho_i} + c \times \log\frac{T(K)}{323} \qquad \text{Equation III-2}$$

$$\delta_{blend} = \sum_{i=1}^{n} w_i \delta_i \qquad \text{Equation III-3}$$

A partially upgraded oil will require a smaller weight content of diluent in the mix. Since diluent are costly commodities, a smaller requirement will represent savings to the oil producing company.

Because the base for the calculations is a fixed amount of heavy oil to be processed, a smaller requirement in diluent will also represent a smaller amount of final diluted products. Table III-1 shows the properties of five different oils: diluent, feedstock, diluted feedstock, products, and diluted products. Feedstock and products properties comes from analysis performed on samples before and after reaction on experimental plant. Diluent follows the properties of the Condensate Blend CRW, which is a light sweet condensate available in Edmonton, Alberta (Crude Monitor Inc., 2016). The price used for the condensate was the Edmonton Condensate benchmark (EC), priced as of 7/4/2016 at CAD$59.26/bbl (PSAC, 2016). The diluted feedstock and products are the oil properties after dilution at the concentration shown in the last column in the table. That dilution was the one calculated through the viscosity index method to achieve 350cSt at 7°C.

Table III-1: Feedstock, products, diluent, diluted feedstock, and diluted products properties.

Property	**TAN (mg_{KOH}/g)**	**Viscosity (cP)**	**API gravity**	**Diluent concentration ($kg_{diluelnt}/kg_{diluted\ product}$)**
Diluent	0.0	0.663 (at 7.5^{o}C)	62.8	1.0
Feedstock	1.7	3,323 (at 40°C)	11.8	0.0
Diluted Feedstock	1.3	319 (at 7.0^{o}C)	23.7	0.2330
Products	0.78	1,185 (at 40°C)	12.6	0.0
Diluted Products	0.63	322 (at 7.0^{o}C)	22.5	0.1974

The revenues for the plant were estimated by calculating the revenue differential between simply diluting and selling the feedstock or by processing, diluting, and selling the products. The total amount of WCS produced (WCS_p) can be estimated based using the amount of feedstock (or products) and the required dilution quantities as seen in Equation III-4. In this equation, w_d is the weight proportion of diluent in the blend as calculated by Equation III-2, SG_i is the specific gravity of the oil (either non-processed feedstock or product) before dilution while SG_f is after dilution. Equation III-4 was solved for the non-processed feed case. The revenue from the sales of WCS produced can be calculated using Equation III-5. Finally, the revenues due to WCS sales and TAN reduction can be calculated by Equation III-6. Note that this value was negative because the production of WCS was smaller for the products since it requires less amount of diluent. Nevertheless, because the diluent is more expensive than WCS, this loss in revenue is compensated by a much lower cost with diluent.

$$WCS_p = \frac{38{,}000}{(1 - w_d)} \times \frac{SG_i}{SG_f} = \frac{38{,}000}{(1 - 0.233)} \times \frac{0.9874}{0.9118} = 53{,}713\, bbl/day \qquad \text{Equation III-4}$$

$$Sales_{WCS} = WCS_p \times (WCS - Discount_{TAN}) = 53{,}713 \times (45.20 - 1.85) \qquad \text{Equation III-5}$$

$$= MCAD\$2.33/day$$

$$Revenue_{sales} = Sales_{WCS,products} - Sales_{WCS,non\ processed} \qquad \text{Equation III-6}$$

$$= -CAD\$63{,}500/day$$

The daily volume of diluent necessary for dilution (D_d) can be calculated according to Equation III-7, which was solved for the non-processed feedstock case. The cost with diluent per day (C_d) can be calculated by multiplying the total amount of diluent required by the cost per barrel of it (EC) as shown in Equation III-8. The revenue due to decreased diluent requirements (R_d) can be calculated by Equation III-9.

$$D_d = \frac{38{,}000}{(1 - w_{diluent})} \times \frac{SG_i}{SG_d} w_d = \frac{38{,}000}{(1 - 0.233)} \times \frac{0.9874}{0.7283} \times 0.233 \qquad \text{Equation III-7}$$

$$= 15{,}668\, bbl/day$$

$$C_d = D_d \times EC = 15{,}668 \times 59.26 = CAD929{,}000/day \qquad \text{Equation III-8}$$

$$R_d = D_{d,non\ processed} - D_{d,products} = 929{,}000 - 746{,}000 \qquad \text{Equation III-9}$$

$$= CAD183{,}000/day$$

Finally, the total daily revenue can be estimated using Equation III-10.

$$R_{daily} = Revenue_d + Revenue_{sales} = CAD119{,}000/day \qquad \text{Equation III-10}$$

Taking the CAD to USD conversion, and the on-stream factor of 92%, this revenue adds up to be close to M$31/year. Table III-2 summarizes the discount due to TAN and costs with diluent for both cases.

Table III-2: Acidity discount and diluent costs for feedstock and products.

Property	**Diluted Feedstock**	**Diluted Products**
TAN	1.3	0.63
TAN Discount (CAD$/bbl)	1.85	0.38
Total WCS production (bbl/day)	53,700	50,500
Diluent requirements per barrel (bbl/day)	15,700	12,600
Daily diluent costs (CAD$/day)	929,000	746,000
Yearly diluent costs (MCAD$/year)	312	250

Appendix IV: Sensitivity Analysis

Sensitivity analyses were performed in major variables in the process economics. Those analyses were done by changing the variable in a range of ±50% in relation to the assumed value in the base case. All the other variables were kept constant. The results are shown in Figure IV-1 to Figure IV-9.

Figure IV-1 shows the effects of a different price on the crude oil (WCS) and on the diluent (EC).

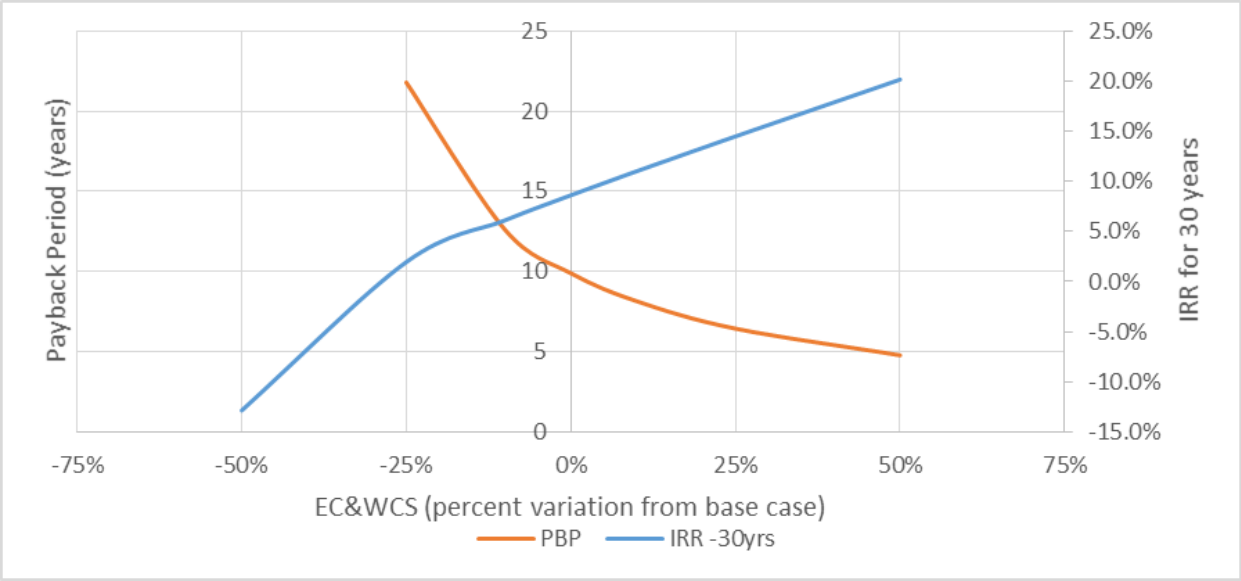

Figure IV-1: Sensitivity analysis on Western Canadian Select and Edmonton Condensate prices with both WCS and EC varying at the same rate.

Figure IV-2 shows the sensitivity analysis when the price differential between EC and WCS is varying for a constant value of WCS.

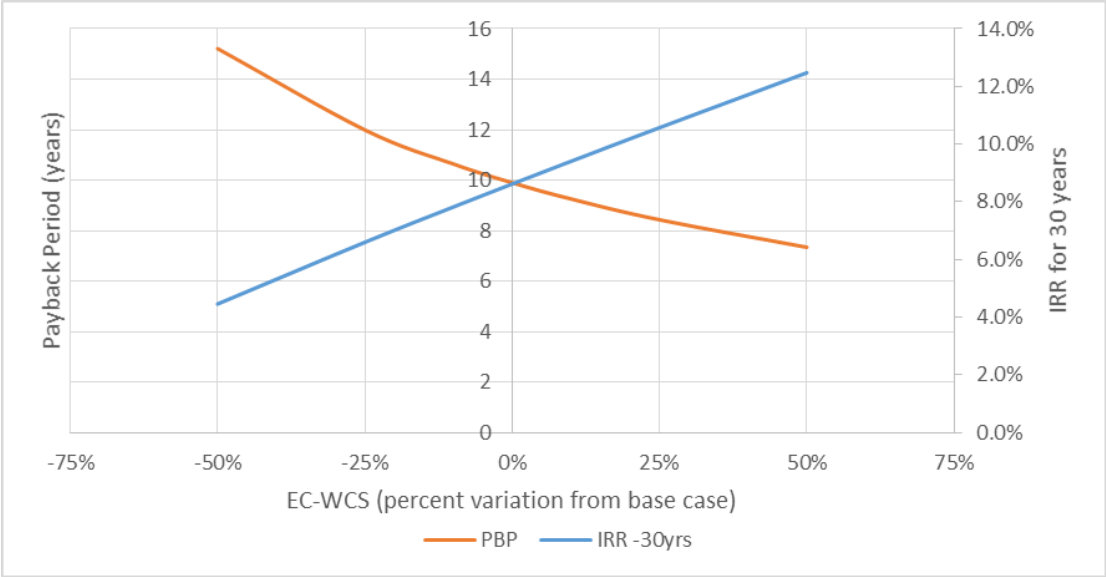

Figure IV-2: Sensitivity analysis for variations in price differential between Edmonton Condensate and Western Canadian Select.

Figure IV-3 shows the sensitivity analysis for product viscosity.

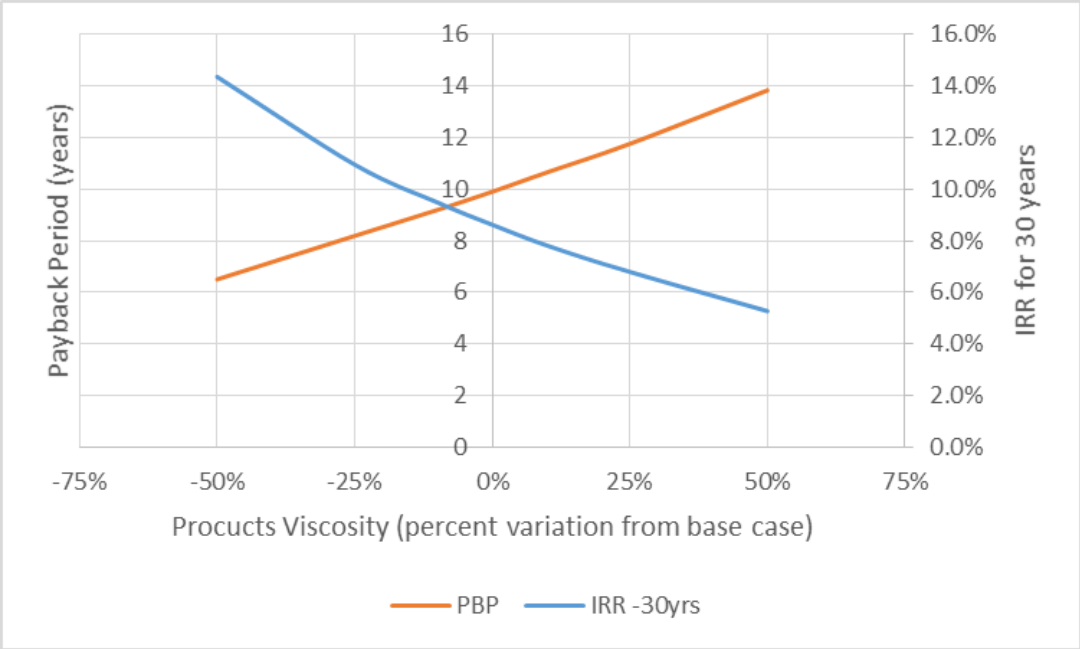

Figure IV-3: Sensitivity analysis for variations in products viscosity.

Figure IV-4 shows the effects of variations in the total acid number in the products.

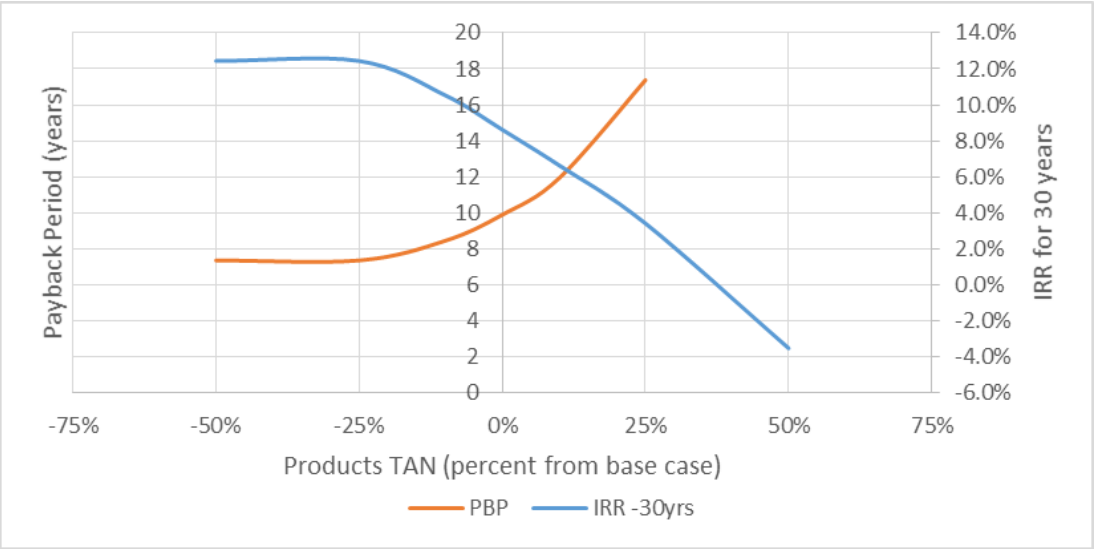

Figure IV-4: Sensitivity analysis for variations in products total acid number.

Catalyst cost was a major assumption done on the project economics and the effects of different values can be seen in Figure IV-5.

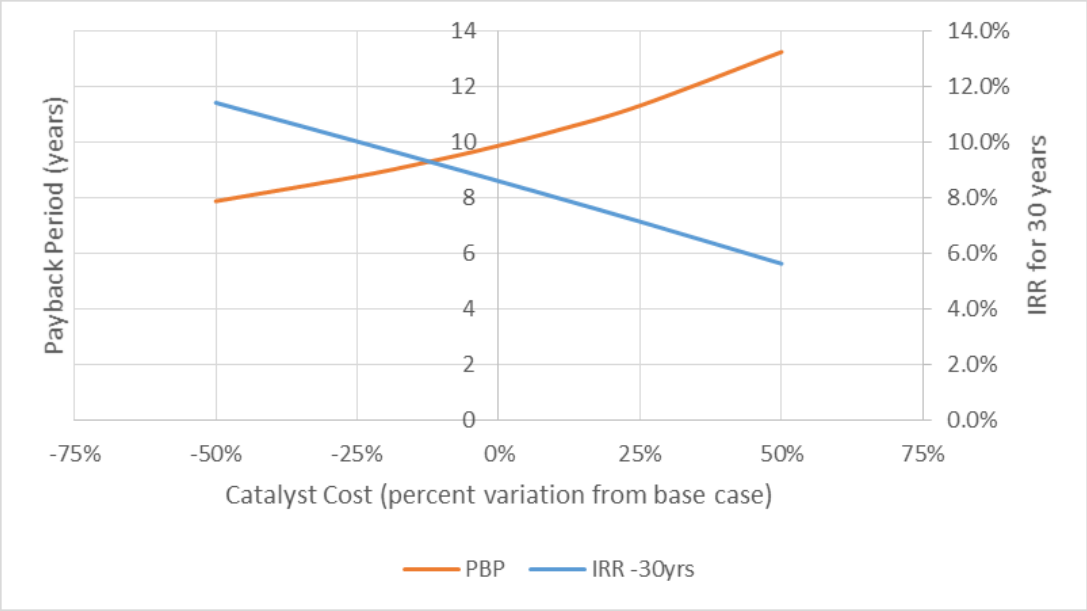

Figure IV-5: Sensitivity analysis for variations in catalyst cost.

Figure IV-6 shows the effects of catalyst life in the process economics.

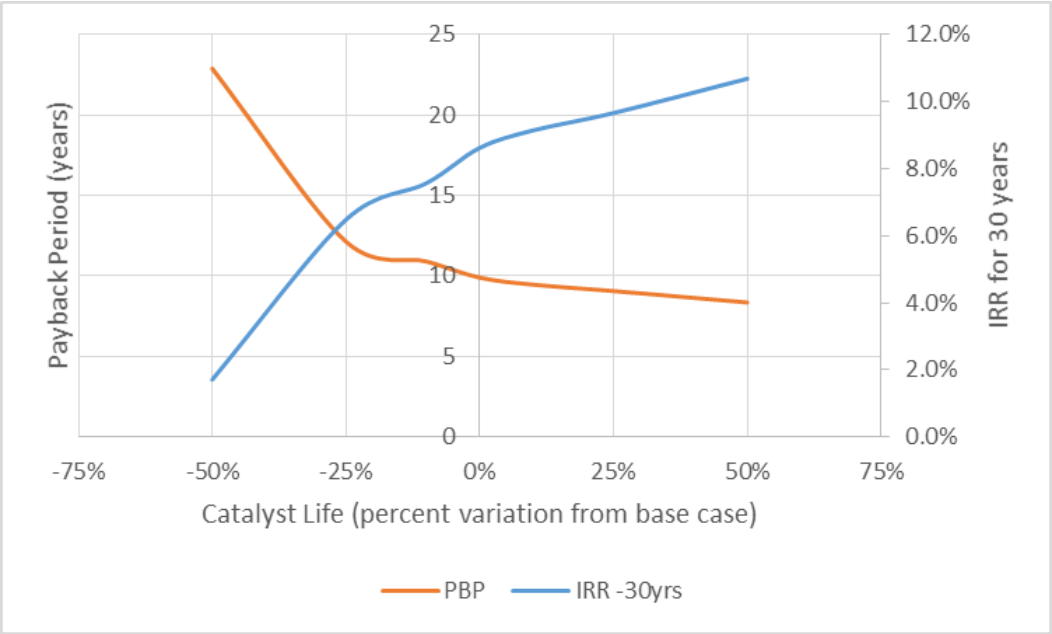

Figure IV-6: Sensitivity analysis for variations in total catalyst life.

Figure IV-7 shows the effects of operating costs in process economics.

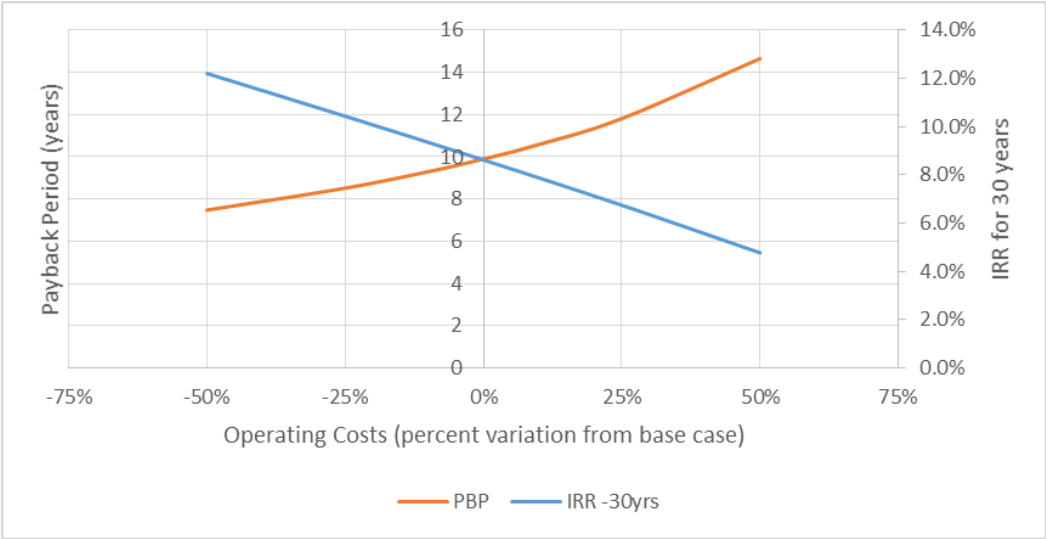

Figure IV-7: Sensitivity analysis for variations in yearly operating costs.

Figure IV-8 shows the sensitivity analysis for the total investment in the industrial plant.

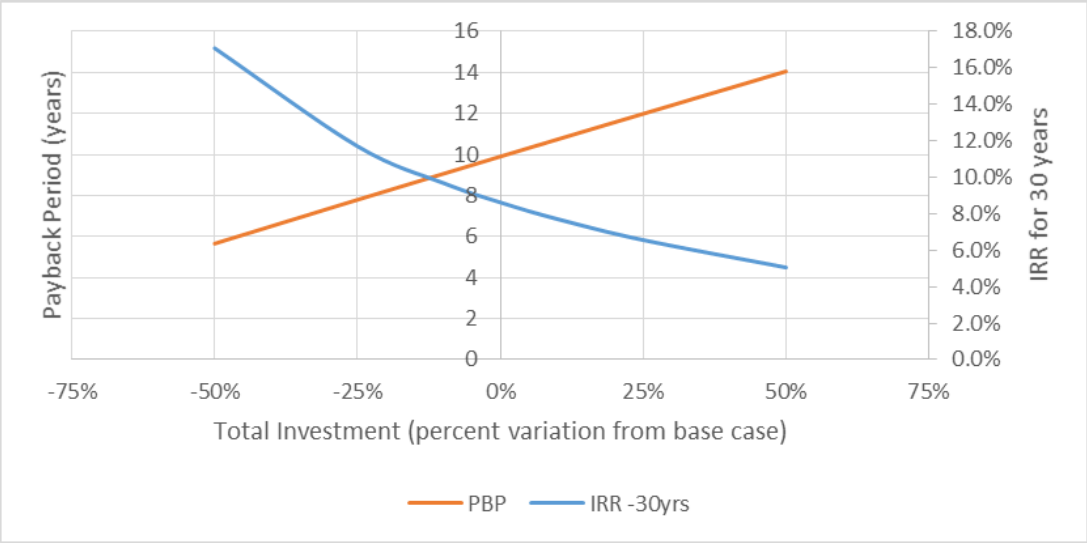

Figure IV-8: Sensitivity analysis for variations in total investment.

Figure IV-9 shows a sensitivity analysis for the total working capital.

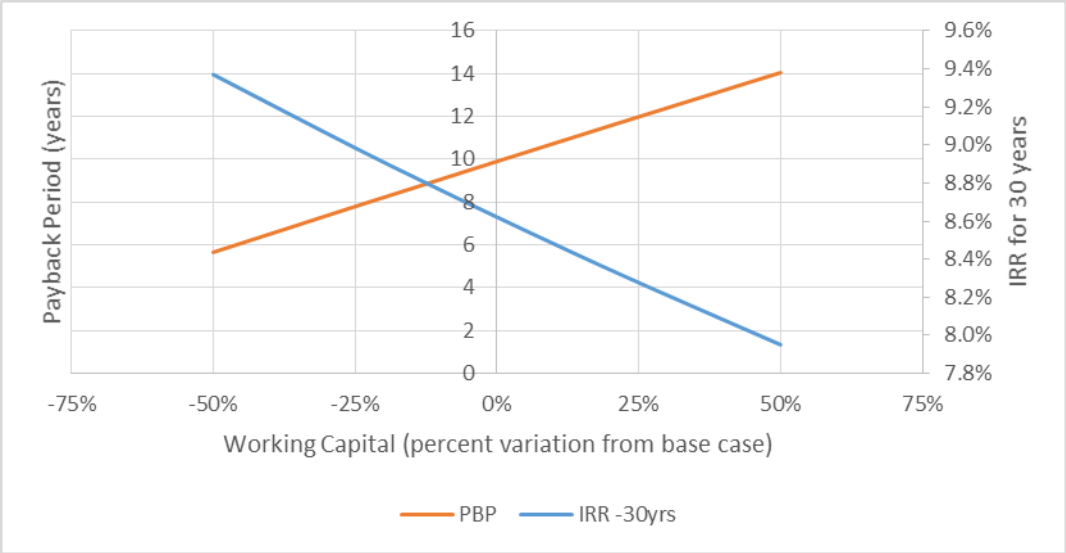

Figure IV-9: Sensitivity analysis for variations in working capital.